



International Committee for Future Accelerators

Sponsored by the Particles and Fields Commission of IUPAP

Beam Dynamics Newsletter

No. 73

Issue Editor:

G. Machicoane and P. N. Ostroumov

Editor in Chief:

Y. H. Chin

April 2018

Contents

1	FOREWORD.....	11
1.1	FROM THE CHAIR	11
1.2	FROM THE EDITOR	12
2	ION SOURCES	14
2.1	RF COUPLING AND MAGNETIC CONFINEMENT ISSUES IN ELECTRON CYCLOTRON RESONANCE ION SOURCES FOR INTENSE HIGHLY CHARGED ION BEAMS PRODUCTION 14	
2.1.1	Introduction	14
2.1.2	Heating models in ECRIS	15
2.1.3	Non-classical scaling with L and influence of collective effects	16
2.1.4	Impact of the microwave coupling to plasma in ECRIS	18
2.1.5	Beyond the ECR Heating Paradigm	20
2.1.6	Conclusions and Perspectives.....	22
2.1.7	References	23
2.2	CHALLENGES OF OPERATING ECR IONS SOURCE AT HIGH FREQUENCY AND HIGH RF POWER.....	25
2.2.1	Introduction	25
2.2.2	ECRIS Frequency scaling law and magnetic confinement	25
2.2.2.1	<i>Frequency scaling law</i>	25
2.2.2.1	<i>Empirical Magnetic confinement</i>	27
2.2.3	Challenges of operation at higher frequency	27
2.2.3.1	<i>Plasma chamber wall burning</i>	28
2.2.3.1	<i>High energy x-ray flux</i>	31
2.2.3.2	<i>Ion beam management</i>	32
2.2.4	Acknowledgement	33
2.2.5	References	33
2.3	DEVELOPMENT OF SUPERCONDUCTING MAGNET USING Nb ₃ Sn.....	33
2.3.1	Introduction	34
2.3.2	General Requirements of This Magnet.....	35
2.3.2.1	Magnet Parameters	35
2.3.2.2	Magnet Structure and Operation	36
2.3.3	Coil Fabrication	36
2.3.3.1	Solenoid Coils Fabrication	37
2.3.3.2	Sextupole Fabrication.....	37
2.3.4	Cold Mass Structure	38
2.3.5	Quench Protection	40
2.3.6	Cryogenic Solution.....	42
2.3.7	Conclusions	44

2.3.8	Acknowledgements.....	44
2.3.9	References.....	44
2.4	A PROMISING MAGNET FOR THE NEXT GENERATION OF ECR ION SOURCE.....	45
2.4.1	Introduction.....	45
2.4.2	Existing Magnets for ECRIS	46
2.4.3	A Promising New Magnet for Future ECRIS.....	48
2.4.3.1	<i>MARS Concept and Magnet Scheme</i>	48
2.4.3.2	<i>A MARS Demonstration</i>	50
2.4.3.3	<i>MARS Closed-loop-coil Prototyping</i>	53
2.4.4	Discussions and Conclusion	54
2.4.5	References.....	55
2.5	INSTABILITIES IN ECRIS PLASMAS.....	57
2.5.1	Introduction.....	57
2.5.2	Classification of ECRIS plasma instabilities.....	57
2.5.2.1	<i>Kinetic instabilities</i>	57
2.5.3	Electron cyclotron instabilities in ECRIS plasmas.....	58
2.5.3.1	<i>Fingerprints and diagnostics of the electron cyclotron instabilities</i>	59
2.5.3.2	<i>Electron cyclotron instabilities limiting ECRIS performances</i>	60
2.5.3.3	<i>Suppression of ECRIS plasma instabilities</i>	62
2.5.3.4	<i>Open research questions</i>	63
2.5.4	Acknowledgements.....	63
2.5.5	References.....	64
2.6	ECR SIMULATIONS	65
2.6.1	Introduction.....	65
2.6.2	Models	65
2.6.2.1	<i>Approaches of other groups</i>	65
2.6.2.2	<i>NAM-ECRIS</i>	66
2.6.2.2.1	The ion module NAM-ECRIS(i).....	67
2.6.2.2.2	The electron module NAM-ECRIS(e).....	69
2.6.2.3	<i>Effects</i>	71
2.6.2.3.1	Isotope anomaly.....	71
2.6.2.3.2	Wall coating effect	73
2.6.2.3.3	Gas-mixing effect	74
2.6.2.4	<i>Conclusions</i>	75
2.6.3	References.....	75
2.7	PULSED HIGH INTENSITY ECRS	77
2.7.1	Introduction.....	77
2.7.2	Quasi-gasdynamical plasma confinement	78
2.7.3	SMIS 37 experimental facility.....	78
2.7.4	Multi-charged ions production.....	79
2.7.5	Short pulse ion beams	81
2.7.6	Proton and deuteron beams formation	82
2.7.7	Conclusion	84
2.7.8	References.....	84

2.8	CHARGE BREEDING WITH ELECTRON CYCLOTRON RESONANCE ION SOURCES.....	86
2.8.1	Introduction	86
2.8.2	ECR Charge Breeders.....	86
2.8.3	The $1+ \rightarrow n+$ Method	88
2.8.3.1	<i>Relevant parameters</i>	89
2.8.3.1.1	Efficiency versus ΔV	89
2.8.3.1.2	Multiple RF frequencies.....	90
2.8.3.1.3	Operating frequency.....	91
2.8.3.1.4	Operating pressure.....	92
2.8.3.1.5	Grounded tube positioning.....	92
2.8.3.1.6	Magnetic field scheme	93
2.8.4	Results	94
2.8.5	On-going Efforts.....	95
2.8.5.1	<i>Contaminants</i>	95
2.8.5.2	<i>1+ beam as plasma probe</i>	98
2.8.6	Conclusion.....	98
2.8.7	Acknowledgements	99
2.8.8	References	99
2.9	EBIS FOR HIGH INTENSITY STABLE BEAMS	101
2.9.1	Introduction	101
2.9.2	Electron beam generation.....	104
2.9.2.1	<i>Magneto-immersed guns</i>	104
2.9.2.2	<i>Guns with electrostatic compression</i>	105
2.9.2.3	<i>Reflex EBIS</i>	105
2.9.2.4	<i>Electron current limitation and mitigation</i>	106
2.9.3	Electron beam collector.....	106
2.9.4	Drift tubes.....	107
2.9.5	Vacuum	108
2.9.6	Cold bore or warm bore?.....	109
2.9.7	Prospects of EBIS intensity increase.....	109
2.9.8	Conclusion.....	109
2.9.9	Acknowledgement.....	110
2.9.10	References	110
2.10	EBIS/T CHARGE BREEDERS FOR POST-ACCELERATION OF RARE ISOTOPES.....	112
2.10.1	Introduction	112
2.10.2	Post-acceleration concept.....	113
2.10.3	Working principle of an EBIS/T	113
2.10.4	Requirements of charge breeders	115
2.10.5	Ion injection and ejection, and beam properties.....	116
2.10.6	Charge breeding and efficiencies	117
2.10.7	Pulse stretching.....	118
2.10.8	Beam purity	119
2.10.9	High current and high current density.....	120
2.10.10	Conclusion.....	120
2.10.11	Acknowledgments	120
2.10.12	References	120

2.11	PULSED LOW CHARGE STATE ION SOURCES	121
2.11.1	Introduction	121
2.11.2	Overview of most common pulsed low charge state ion sources	121
2.11.3	Boundary conditions for pulsed low charge state ion sources.....	122
2.11.3.1	<i>Why pulsing an ion source?</i>	122
2.11.3.2	<i>Advantages for ion sources in pulsed mode operation</i>	122
2.11.3.3	<i>Disadvantages for ion sources in pulsed mode operation</i>	123
2.11.4	Filament driven volume type ion sources and their Renaissance at GSI	123
2.11.4.1	<i>Excursion on PIG ion source at GSI</i>	123
2.11.4.2	<i>Excursion on CHORDIS and MUCIS 2020 at GSI</i>	124
2.11.5	Vacuum arc driven ion sources and their recent development at GSI	126
2.11.5.1	<i>MEVVA IV ion source</i>	126
2.11.5.2	<i>VARIS ion source</i>	126
2.11.5.3	<i>Highlights on recent development of VARIS</i>	127
2.11.5.3.1	Production of high current beams of heavy elements ..	127
2.11.5.3.2	Increasing the beam brilliance for intense $^{238}\text{U}^{4+}$ ion beam	129
2.11.5.3.3	Development of the new projectiles in medium heavy region	130
2.11.6	References	133
2.12	MICROWAVE DISCHARGE ION SOURCES (PROTON SOURCES)	134
2.12.1	Introduction	135
2.12.2	Historical notes	135
2.12.3	The CRNL ion source and the successive developments	136
2.12.4	Theoretical Issues	137
2.12.5	Technological Issues.....	139
2.12.6	EM wave to plasma chamber coupling.....	139
2.12.7	Beam formation and transport	140
2.12.8	Perspectives	142
2.12.9	Acknowledgements	143
2.12.10	References	143
2.13	PULSED, HIGH-CURRENT H^- ION SOURCES FOR FUTURE ACCELERATORS	144
2.13.1	Introduction	144
2.13.2	Surface Plasma Production of Negative Hydrogen Ions	145
2.13.3	Magnetron Negative Hydrogen Ion Sources	146
2.13.4	PIG or Penning Negative Hydrogen Ion Sources	147
2.13.5	The Volume Production of H^- Ions.....	148
2.13.6	Surface Production of Negative Hydrogen Ions.....	149
2.13.7	Converter H^- Sources and Filament Driven H^- Sources	150
2.13.8	RF Driven H^- Sources.....	151
2.13.9	Summary and Conclusions	153
2.13.10	Acknowledgments	154
2.13.11	References	154
2.14	A 60 MA DC H^- ION SOURCE WITH A LONG LIFE FILAMENT FOR ACCELERATORS.	157

2.14.1	Introduction	157
2.14.2	H ⁻ physics.....	158
2.14.2.1	<i>H⁻ production</i>	158
2.14.2.2	<i>H⁻ destruction</i>	159
2.14.3	Background electrons	160
2.14.4	Source setup	161
2.14.5	Ion source and extraction system	161
2.14.6	Electron filters	163
2.14.7	Beam line and diagnostics.....	166
2.14.8	Extraction system	166
2.14.9	Vacuum System.....	167
2.14.10	Results and discussions	168
2.14.10.1	<i>H⁻ Beam current studies</i>	168
2.14.11	Filament lifetime studies	170
2.14.12	Conclusion.....	172
2.14.13	Acknowledgment.....	173
2.14.14	References	173
2.15	LASER ION SOURCE.....	173
2.15.1	Introduction	173
2.15.2	Basic principle of LIS.....	174
2.15.3	General Description.....	175
2.15.3.1	<i>Laser System</i>	175
2.15.3.2	<i>Target</i>	176
2.15.3.3	<i>Plasma Drift Length</i>	177
2.15.3.4	<i>Ion Beam Extraction</i>	178
2.15.3.5	<i>Direct Plasma Injection Scheme</i>	179
2.15.3.6	<i>Beam current manipulation</i>	180
2.15.3.7	<i>Summary</i>	181
2.15.4	Acknowledgement.....	181
2.15.5	References	182
2.16	SOURCES FOR LOW CHARGE STATE RADIOACTIVE IONS.....	182
2.16.1	Introduction	182
2.16.2	Surface ion sources.....	183
2.16.2.1	<i>FEBIAD ion sources</i>	184
2.16.3	ECR ion sources	185
2.16.4	Resonance ionization laser ion sources	186
2.16.5	Summary and outlook	187
2.16.6	References	188
2.17	ION SOURCES FOR THERAPY ACCELERATORS.....	190
2.17.1	Introduction	190
2.17.2	Charged particle radiotherapy	191
2.17.2.1	<i>Proton radiotherapy</i>	191
2.17.2.2	<i>Heavy-ion radiotherapy</i>	192
2.17.2.3	<i>Future prospects for charged particle radiotherapy</i>	193
2.17.3	Boron neutron capture therapy.....	194

2.17.4	Targeted radionuclide therapy	194
2.17.5	References	195
3	WORKSHOP AND CONFERENCE REPORTS	197
3.1	7TH LOW EMITTANCE RINGS WORKSHOP	197
3.2	TOPICAL WORKSHOP ON EMITTANCE MEASUREMENTS FOR SYNCHROTRON LIGHT SOURCES AND FELS	198
3.3	ICFA MINI-WORKSHOP ON BEAM-BEAM EFFECTS IN CIRCULAR COLLIDERS.....	201
3.4	ACCELERATOR-INDUSTRY CO-INNOVATION WORKSHOP: TOOLS AND STRATEGIES TO ENHANCE INDUSTRY-ACADEMIA COOPERATION IN THE PARTICLE ACCELERATOR COMMUNITY	203
3.5	THE 1 ST ICFA MINI-WORKSHOP ON MACHINE LEARNING APPLICATIONS FOR PARTICLE ACCELERATORS	206
3.6	THE 60TH ICFA ADVANCED BEAM DYNAMICS WORKSHOP ON FUTURE LIGHT SOURCES, FLS2018	208
4	RECENT DOCTORIAL THESES.....	209
4.1	DEVELOPMENT OF DIRECT MEASUREMENT TECHNIQUES FOR THE IN-SITU INTERNAL ALIGNMENT OF ACCELERATING STRUCTURES	209
4.2	UNDERSTANDING THE PLASMA AND IMPROVING EXTRACTION OF THE ISIS PENNING H- ION SOURCE	209
4.3	FAST LUMINOSITY MONITORING USING DIAMOND SENSORS FOR SUPERKEKB..	210
5	FORTHCOMING BEAM DYNAMICS EVENTS	212
5.1	MECHANICAL ENGINEERING DESIGN OF SYNCHROTRON RADIATION EQUIPMENT AND INSTRUMENTATION (MEDSI).....	212
5.2	INTERNATIONAL BEAM INSTRUMENTATION CONFERENCE (IBIC2018).....	212
5.3	23RD INTERNATIONAL WORKSHOP ON ECR ION SOURCES	213
5.4	EEFACT2018, 24-27 SEPTEMBER 2018.....	214
6	ANNOUNCEMENTS OF THE BEAM DYNAMICS PANEL.....	216
6.1	ICFA BEAM DYNAMICS NEWSLETTER.....	216
9.1.1	Aim of the Newsletter.....	216
9.1.2	Categories of Articles	216
9.1.3	How to Prepare a Manuscript	216
9.1.4	Distribution	217
9.1.5	Regular Correspondents.....	218

6.2	ICFA BEAM DYNAMICS PANEL MEMBERS	219
-----	----------------------------------------	-----

1 Foreword

1.1 From the Chair

Yong Ho Chin, KEK
Mail to: yongho.chin@kek.jp

The 60th ICFA Advanced Beam Dynamics Workshop on Future Light Sources (FLS2018) was held very successfully on March 4-9, 2018, at the Hotel Equatorial Shanghai, China. About 150 participants from all over the world gathered together to exchange ideas and best practices about accelerator based light sources, their new development trend and related key technologies. The proceedings will be published soon on the JACoW website (<http://www.jacow.org/index.php?n=Main.Proceedings>). For more details of FLS2018, the workshop report is available in the Section 3.

This year, we will have other two ICFA Advanced Beam Dynamics Workshops:

1. The 61st ICFA Advanced Beam Dynamics Workshop on High-Intensity and High-Brightness Hadron Beams (HB2018), June 17-22, 2018, in Daejeon, Korea. <http://hb2018.ibs.re.kr>
2. The 62nd ICFA Advanced Beam Dynamics Workshop on High Luminosity Circular e+e- Colliders 2018 (eeFACT2018), September 24-27, 2018 at Institute for Advanced Studies (IAS), Hong Kong University of Science and Technology (HKUST), Hong Kong. <http://eefact2018.ust.hk/>

ICFA has approved another ICFA Advanced Beam Dynamics Workshop next year:

1. The 63rd ICFA Advanced Beam Dynamics Workshop on Energy Recovery Linacs, ERL2019, September 16-20, 2019, at Helmholtz Zentrum Berlin, Germany.

The preparation of all these workshop is under way and this and the next year will be a very productive year for the ICFA Beam Dynamic Panel activities.

Following the endorsement of ILC operating at 250 GeV by ICFA, the Japanese Ministry of Education, Culture, Sports, Science and Technology (MEXT) renewed its activities with the ILC working groups to discuss physical merits of ILC at 250GeV and the technical and cost aspects. This year is a very crucial year for ILC.

The editors of this issue are Drs. Guillaume Machicoane and Peter N. Ostroumov, senior scientists at Michigan State University. The theme is the ion sources. They collected seventeen well-written review articles, and they provide very comprehensive reviews of most recent development work, achievements and challenges in the area of ion sources for charge particle accelerators. I want to thank Guillaume and Peter for editing a valuable and formidable newsletter of high quality for the accelerator community.

1.2 From the Editors

Guillaume Machicoane and Peter. N. Ostroumov, FRIB, MSU, East Lansing, MI, USA
Mail to: machicoane@frib.msu.edu, ostroumov@frib.msu.edu

Modern hadron accelerators require wide variety of ion sources. The performance of ion source is being continuously improved to satisfy ever-growing demand for higher intensity, higher brightness and higher stability ion beams. Most ion sources include a hot plasma. The plasma properties and beam space charge determine ion beam dynamics in the extraction area. Despite of significant advances in computer simulations techniques, the beam formation in most ion sources is poorly predictable. The development of high performance ion sources usually requires significant effort from highly skilled engineers and physicists with hands-on experience. The first high energy accelerators built nearly 70 years ago required pulsed proton sources. With the invention of charge-exchange injection into the synchrotron many proton sources have been replaced with pulsed negative hydrogen ion sources. DC H⁻ sources have been developed for cyclotrons to enable charge-exchange extraction of protons.

Fundamental research in Nuclear Physics prompted development and construction of many heavy ion accelerators worldwide. Effective acceleration of heavy ions requires high charge state of ion beams extracted from the ion source. To date Electron Cyclotron Resonance ion source (ECRIS) remains the best method to produce intense high charge state DC ion beams due to the large electronic density and long confinement times that can be achieved within an ECRIS plasma. Since the development of the first ECR ion source in 1974 by R. Geller, performance of ECR ion sources have improved by several order of magnitude over the last four decades and can routinely achieve several milliamperes for high charge states of light element while on the other end current over a microampere have been demonstrated for very high charge state of heavy element such as Xe 44+ and Bi 55+. New projects to increase the operating frequency beyond 28 GHz are in development that will push the performances of ECR to a new level to support the next generation of heavy ion accelerator.

Injectors to the heavy ion synchrotrons require high current pulsed ion sources that must provide highest possible charge states at required beam intensity. There are variety of pulsed ion sources to meet these specifications as described in this issue.

There is a strong demand for unstable isotopes produced as a result of interaction of stable ion beams with targets. These isotopes must be ionized to deliver them either directly to nuclear physics experiments or re-accelerate them after full stop. To satisfy these needs, new types of ion sources and charge breeders have emerged recently. Most ion sources are based on a confined hot plasma volume where effective ionization takes place. ECR is a typical example of this type of ion source. Several ECRs have been developed to charge-breed singly charged radioactive isotopes. It appears that ECR-based charge breeders can easily contaminate low intensity isotope beams due to hot plasma and relatively low vacuum. Electron beam ion sources (EBIS) are very effective charge breeders with high purity of charge-bred rare isotopes due to the absence of plasma and very high vacuum in the ionization chamber.

The goal of this Newsletter is to describe most recent development work, achievements and challenges in the area of ion sources for charge particle accelerators. The first 8 chapters focus on ECR ion sources and report on ongoing work in the area of RF coupling, magnet design, and magnet technology, plasma stability and high power

operation that will help increase both beam intensity and high charge state. The following 8 chapters review current status of development and operation of proton sources, negative ion sources, laser ion sources, low-charge state high-intensity ion sources, electron beam ion sources for stable and unstable ion beams. The chapter on ion sources for therapy accelerators concludes the issue.

2 Ion Sources

2.1 RF coupling and magnetic confinement issues in Electron Cyclotron Resonance Ion Sources for intense highly charged ion beams production

S. Gammino, D. Mascali, L. Celona

Mail to: davidmascali@lns.infn.it

INFN – LNS, via S. Sofia 62, 95123 Catania, Italy

2.1.1 Introduction

ECRIS (Fig.1) [1,2] are nowadays the most powerful devices able to feed accelerators with highly charged ions in a reliable and efficient way. The ions are extracted from a dense hot plasma ($n_e \sim 10^{10}-10^{13} \text{ cm}^{-3}$, $T_e \sim 0.1-30 \text{ keV}$) generated by means of the Electron Cyclotron Resonance heating. The plasma is excited inside a cylindrical metallic chamber by microwaves (2.45-28 GHz) and there confined by a MHD stable B-min configuration (a hexapole superimposed to a simple mirror), characterized by closed, quasi-ellipsoidal constant B surfaces (Fig.1(b)). Highly charged ion beams can be generated if the vacuum is in the range 10^{-6} to 10^{-8} mbar and the RF power density is in the range of 300 to 800 W/l. By using highly charged ions beams it is possible to increase the energy of the accelerated beams, according to linear or square laws of the charge state q . In modern

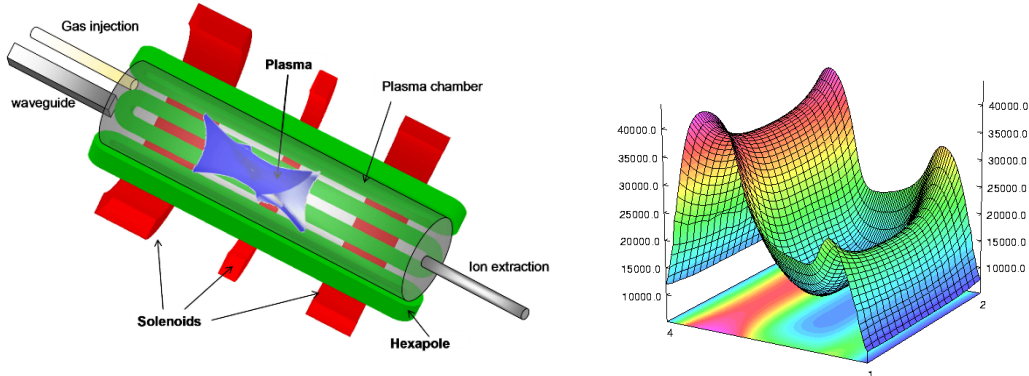


Figure 1: (a) Typical layout of an ECRIS. These sources are also usually equipped with an oven (not shown in the figure) for beam production from metallic elements. (b) Magnetic field B module (in kG): longitudinal trend.

ECRIS the microwaves' frequency is often above 14 GHz, which implies the use of magnets providing 1 to 3 T inside the plasma chamber, sometimes driven by superconducting (SC) technology. To better understand ECRIS principles, atomic physics is needed, which can be summarized in the following equations:

$$n_e \tau_q = \frac{1}{(S_{q,q-1} - S_{q+1,q})} \quad (1) \quad \text{where: } S_{q,q-1} = \frac{1}{n_e} \int_{\epsilon_{q,q-1}}^{\infty} \sigma_{q,q-1} \sqrt{\frac{2\epsilon}{m_e}} F(\epsilon) d\epsilon \quad (2)$$

where τ_q is the lifetime of a q -charged ion, $S_{q,q-l}$ denotes the ionization rate (which in turn depends on the ionization cross section σ), $F(\varepsilon)$ is the energy distribution of the electrons and ε is the ionization threshold of a given charge state [1].

The denominator of Eq. 1 increases for moderate temperatures but it drops above 20-30 keV. With the rates S fixed, a given charge state may be reached only if the product $n_e \tau_q$ is high enough, while the output current is given by the expression:

$$I_q^z \approx \frac{1}{2} \frac{n_q^z q e V_{ex}}{\tau_{q,l}^z} \quad (3)$$

where V_{ex} is the volume of the plasma core and n_q is the density of the given charge state. These formulas demonstrate that large plasma densities and long ion lifetimes are the key for high performance ECRIS. The electron temperature should be adequate for ionization, but overheating should be avoided since suprathermal electrons generate hard bremsstrahlung radiation, with the consequent heat load on the SC magnet's cryostat and the deterioration of the insulators.

The problem of plasma ignition and stability was formerly investigated through semi-empirical laws. The B-min configuration is Magneto-Hydro-Dynamically (MHD) stable when $\beta \ll 1$, being β the magnetic over kinetic pressure ratio. Under the assumption that $n_e = n_c = (m \omega_{RF}^2 \varepsilon_0) / e^2$, the condition for MHD stability is [3]:

$$\left(\frac{B}{B_{ECR}} \right)^2 > 2 \cdot 10^2 kT_e \frac{\mu_0 \varepsilon_0}{m_e} \quad (4)$$

which typically implies $B/B_{ECR} > 2$, where B_{ECR} is the field value that generates the electron cyclotron resonance for the operating frequency (High B mode concept [2,3]). The exhaustive set of magnetic laws were derived in [4]: $B_{rad} \geq 2 B_{ECR}$, $B_{inj} \approx 3 B_{ECR}$ or more, $B_{ext} \approx B_{rad}$, $0.30 < B_{min}/B_{rad} < 0.45$; where B_{inj} , B_{ext} , B_{min} , B_{rad} are the B values at the injection and extraction endplate, the minimum longitudinal value and the maximum radial field respectively. Considering the electromagnetic cutoff, R. Geller proposed two rules for the estimation of I and $\langle q \rangle$ (average charge state) scaling with ω_{RF} [1]:

$$I \propto \frac{\omega_{RF}^2}{M} \quad \text{and} \quad \langle q \rangle \propto \log \omega_{RF}^{3.5} \quad (5)$$

According to these scaling laws, the ECRIS development was based on the general increase of microwave frequency and confining magnetic fields [5]); this trend is now limited by the rising costs and feasibility of magnets and RF generators, and a better comprehension of plasma formation and heating is therefore needed. [6])

2.1.2 Heating models in ECRIS

Lieberman et al. [7] proposed a single particle model based on momentum randomization via stochastic effects in order to explain the collisionless electron heating in ECRIS plasmas. The model assumes that the electrons bounce in a parabolic-like B field: $B = B_{min} (1 + z^2 / L^2)$, where $L = (\nabla B / B)^{-1}$ is the B characteristic scale-length of B. The heating, due to randomness in the particle-wave interaction, stops when the bouncing frequency $\omega_b \cong \omega_c \approx \omega_{RF}$, W_s being the electrons' energy for which this condition holds; the absolute stochastic barrier (ASB) will be:

$$W_b \approx 5W_s = \left[m_e L \left(1 + \frac{l^2}{L^2} \right) \right]^{1/4} l \omega^{1/2} (eE)^{3/4} \quad (6)$$

where l is the distance of the resonance from B_{min} . The scaling with L , RF power and frequency is evident.

A more general description of electron heating can be given assuming a diffusion-like mechanism in velocity space. Employing spherical polar coordinates (v, μ, θ) , where v is the speed, $\arccos \mu$ the pitch angle and θ the angle about the axial magnetic field, the diffusion tensor is formed by the diagonal elements [8]:

$$D_{vv} = \frac{\Delta v^2}{2\Delta t} = \pi \left(\frac{eE}{2m_e} \right)^2 \frac{L}{d\omega} \quad \text{and:} \quad D_{\mu\mu} = \frac{\Delta \mu^2}{2\Delta t} = D_{vv} \left(\frac{v}{v_\phi} \right)^2 \quad (7)$$

where d is the plasma length and v_ϕ the wave's phase velocity (the other parameters assume here the usual meaning).

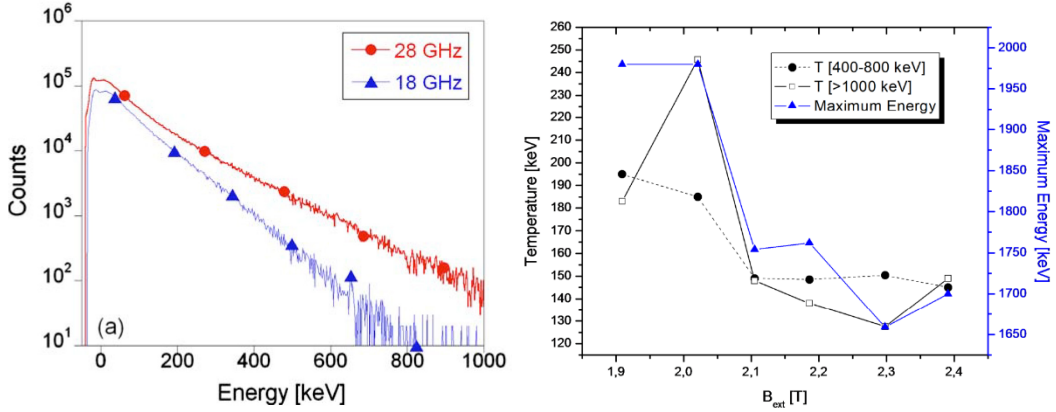


Figure 2: (left) X-ray spectra at different frequency [9]; (right) Trend of the spectral temperature calculated from X-ray spectra collected with the VENUS source at LBNL [10].

The RF term has been written in terms of the diffusion coefficients. The diffusion is anisotropic due to the pitch angle scattering provided by the RF field, which acts along μ . One conclusion coming from this model is that the heating rapidity would grow linearly with L (while the single particle model gives a proportionality to $L^{1/2}$). The impact of the pitch angle scattering on the plasma density is deemed from some authors [8] to be relevant: the RF scattering efficiently injects electrons into the loss cone, and this limits n_e . In [8] a $n_e \propto \omega_{RF}^2$ law was derived only assuming RF-scattering issues; ω_{RF} also fixes the characteristic electron energy: $E_{char} \approx 1/2 m_e v_\phi^2$. This approach is coherent with the "omega squared" law derived by Geller (eq. 5) and it explains the increase of the electrons' average energy with ω_{RF} , as experimentally observed when passing, for example, from 18 to 28 GHz (see Fig.2). The single particle approach predicts the increase of the ASB with $\omega_{RF}^{1/2}$, which however seems to be underestimated.

2.1.3 Non-classical scaling with L and influence of collective effects

Both the models fail when trying to predict the dependence of E_{max} on L , as shown by Koivisto et al. in [11], who made systematic measurements of the EEDF extracted from

X-ray spectra versus L . Results disagreed considerably with the theoretical models. In Fig.2 both the spectral temperature and the energy endpoint of X-ray spectra collected with the VENUS source [8, 9] are reported. The dependence of T^{spectr} and E_{max} on the extraction field (B_{ext}), which in turn modifies L , exhibits a not expected jump even if B_{ext} was changed of few % only. A sort of “phase transition” from a plasma heating regime regulated by single particle interaction to a domain in which collective effects prevail can be postulated [12]

Ivanov et. al [13] correlated the hard-X rays to the plasma emitted electromagnetic and electrostatic spectra. They observed high frequency electrostatic modes and ion acoustic waves in the MHz range, due to non-linear wave – plasma interaction. The signature of activated turbulent heating was the boosting of the hard X-rays production. They verified that the turbulence was enhanced by the magnetic field detuning (few mT) rather than by the RF power (a relatively low threshold in RF power was found).

These results are helpful to explain the "jump" in the plasma heating regimes. The stochastic heating stops when electrons fix their phases with respect to the incoming wave. The spectral broadening was observed either for longitudinal and transversal wave injection, but more evident and with symmetric broadband in the second case. The observed RF power threshold was well below the typical operational values in ECRIS (>300 W). This explains the slight overcoming of ASB observed in ECRIS in any experimental condition. The jump in Fig.2 can be explained only if an additional conversion activates after a given threshold in L . A similar behaviour has been observed even at lower frequency, RF power and B field strength – as shown by Fig.3 – confirming that it is an intrinsic physical process inherently involved in magnetic traps characterized by a given L-parameter.

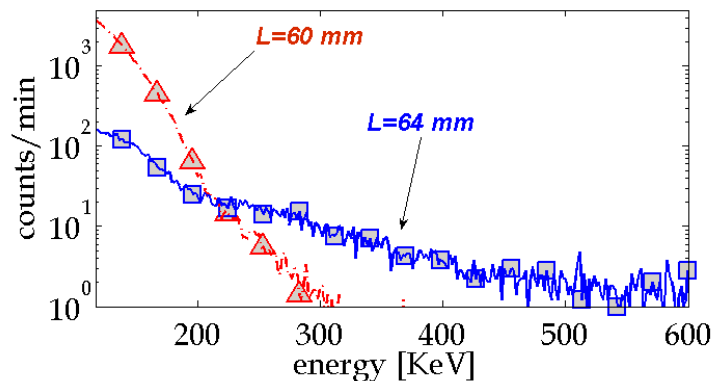


Figure 3: X-ray spectra detected for slightly different magnetic field profiles in the CAESAR ECRIS at INFN-LNS [16].

The non-linear deterioration of ECRIS performances with the mirror ratio (the L parameter), RF power and background pressure has been recently investigated in many details [14]: such non-linear effects have been correlated to the experimental observation of cyclotron instabilities and are detrimental for the confinement of highly charged ions due to plasma perturbations at shorter periodic intervals in comparison with their production time. The occurrence of plasma turbulence is demonstrated to restrict the parameter space available for the optimization of extracted currents of highly charged ions.

2.1.4 Impact of the microwave coupling to plasma in ECRIS

The microwaves play a crucial role in the determination of the ECRIS performances. At the beginning of ECRIS history the design of microwave launching has been not considered relevant to enhance the performances of the ion sources. It has been mainly driven from other considerations, i.e. mechanical ones. Microwave coupling can be seen as a two-step process: coupling of electromagnetic wave with chamber and coupling of forward power to free plasma electrons. Since 1994 the role of frequency has been evident in ECRIS, but the fine structure has been accepted from the community after a breakthrough experiment carried out jointly by INFN-LNS and GSI, demonstrating that changes in the ECRIS performance in terms of the produced current and of the beam shape were obtained by slight variations of the microwave feeding frequency [15, 16]. This phenomenon is usually defined as the “frequency tuning” effect (FTE) and it strongly affects the beam formation dynamics too. Additionally Fig.4 shows a wide fluctuation of the C^{4+} beam current extracted by the Supernanogan source of CNAO, Pavia, as a function of the feeding frequency.

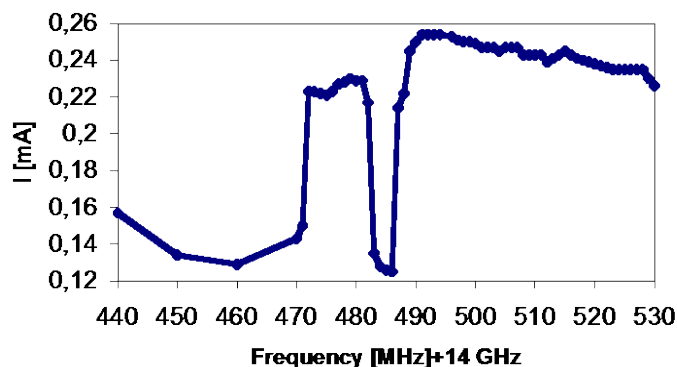


Figure 4: Experimental evidence of Frequency Tuning Effect with the Supernanogan-type ECRIS of CNAO, around 14 GHz.

The strong sensitivity of the plasma dynamics (especially in the warm electron energetic domain 1-30 keV), when tuning the RF frequency, has been confirmed by an experimental campaign aiming to detect X-rays emitted by the plasma of the CAPRICE source – operating at GSI, Darmstadt – carried out in 2013 [17]. Results have shown that the tuning of the pumping frequency considerably modified the plasma density, especially the warm-electron population, i.e. the component responsible of ionization processes, particularly in near-axis regions.

The impact of the wave frequency on the warm electron’ formation and the spatial distribution, including effects on ion dynamics, was investigated in [18] showing that:

- i) the energy absorption is influenced by the electromagnetic field modal distribution inside the cavity, affecting the heating rate;
- ii) the frequency impacts the density distribution, i.e. warm electrons are mostly formed where high field intensity exists;
- iii) The RF heating near the resonance induces the formation of a non-homogeneously distributed plasma. The picture of the FTE impact on plasma dynamics can be reconstructed on the basis of the numerical approach [18, 19].

Effects of the fine frequency tuning, microwave power, axial magnetic confinement onto the spectrally integrated images were evaluated in [18] during measurements jointly performed at ATOMKI-Debrecen (Hungary) by MTA and INFN teams. A summary of the results is here shown in Fig.5: in the upper row, X-ray images of the plasma are shown vs. the pumping wave frequency; in the lower row, images rely to decreasing magnetic field for plasma confinement (the last picture of the lower row is a zoom in the near-axis region). A strong effect of the RF frequency on the plasma images especially in the near axis region was demonstrated and numerically correlated with the $\langle Q \rangle$ of the extracted ion beam. The effect of the axial magnetic confinement on the radial dimensions of the plasma was also highlighted. The maximum strength of the axial B-field was reduced at 80% and 60% of the maximum field strength (the maximum was used for taking the pictures in the upper row of Fig.5, and it corresponds to B_{inj} and $B_{ext}=1.2$ T, $B_{min}=0.2$ T): as decreasing the confining field, the plasma is expanding and it is shifting towards the plasma chamber walls meanwhile the plasma images in the near axis region becomes emptier at each reduction step.

Analysis methods to handle the spectrally resolved images were also presented in [18 and 19]. The multipole trapped ECR plasma is dense in the radial position of the resonant zone, while the near axis region is depleted in density. This hollow structure of the plasma depends on the fine tuning of the pumping wave frequency and it takes to larger beam emittance values.

Therefore, the frequency tuning permits to have an additional degree of freedom, which impacts on the overall plasma density, temperature and even shape. On the other hand, it can be thought as a further “knob” to enhance the matching of microwaves’ field with plasma electrons. This scenario is true for the 2nd generation ECRIS now operating with operational frequency up to 18 GHz where the wavelength is comparable with the density, magnetic field and temperature scales:

$$L_B, L_T, L_n \approx \lambda \quad \text{where} \quad L_B = \left| \frac{B}{\nabla B} \right|, L_T = \left| \frac{T}{\nabla T} \right|, L_n = \left| \frac{n}{\nabla n} \right| \quad (8)$$

In this case, cavity effects are dominant and full wave calculations have to be applied to simulate the wave-plasma interactions, the electromagnetic pattern on ECR surface dominates the heating phenomenon (multi-path absorption) and it is self-determined by the geometrical shape of the plasma chamber, by the wave frequency injected and by the plasma generated inside.

As frequency increases the mode distribution will reach a “continuum” which is related with a certain field distribution on the ECR surface. It is reasonable that at so high frequencies (i.e. for 28 GHz and above) a little variation in a bandwidth of around 1% will be not anymore a valid solution for source tuning. However, as the frequency is increased the optical approximation ($L \gg \lambda$) becomes valid and the cavity effects less evident.

This is the case of the large size fusion reactors, where ray tracing calculations may be used for the simulation of wave propagation. In this case the design of the RF matching is highly predictive and the power deposition may be controlled then maximizing the first-pass absorption efficiency.

Therefore for the 4th generation ECRIS operating at 45 GHz and more (and in lower proportion for the 3rd generation ECRIS working at 28-37 GHz), a “microwave absorption oriented design” may be envisaged from a flexible RF launcher system with the possibility of reduction, increase, redistribution, frequency change, power level,

polarization, power deposition location of the radiated signal. This could be of primary importance for maximizing the power efficiency, improving plasma parameters and source performances.

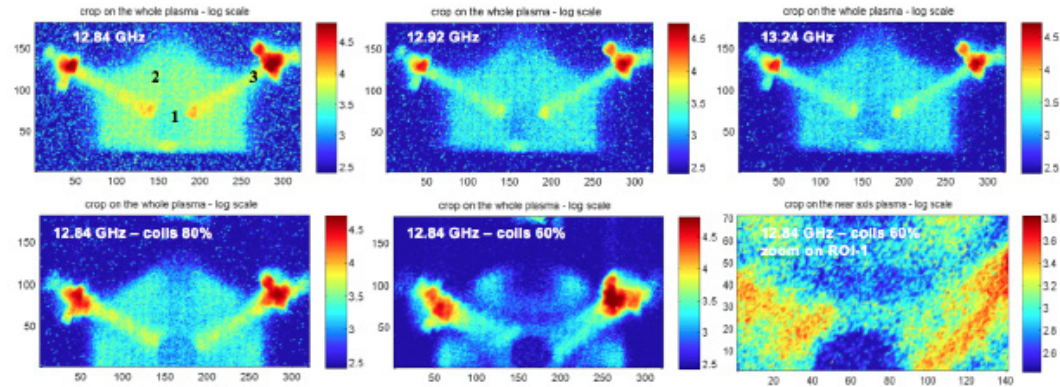


Figure 5: Experimental evidence of Frequency Tuning Effect on the electron dynamics in ECRIS as observed at ATOMKI ECRIS [19].

2.1.5 Beyond the ECR Heating Paradigm

Results coming from 3D simulations are of primary importance to understand the plasma confinement and the beam formation mechanisms. The beam brightness is dominated by physical properties of the plasmas, not only because the extracted current is directly proportional to the plasma density, but also because the EEDF strongly affects the highly charged ion buildup and the emittance formation process, according to partially unknown mechanisms.

An option to overcome this limitation consists in the use of ElectroStatic (ES) waves, experiencing no cut-offs within the plasma. An ES wave is a rarefaction-compression wave whose electric field is parallel to the wave propagation direction. Typically, ES waves do not suffer any resonance within a plasma; however, Electron Bernstein Waves (EBW) [20, 21] can be strongly absorbed by the plasma at cyclotron harmonics. Due to their electrostatic nature, EBWs must be generated inside the plasma from electromagnetic waves.

EBWs have been already generated in large devices for fusion, and the studies have shown that EBW heating could be a valid alternative to the ECR heating. At WEGA stellarator of Greifswald, for example, EBW heating allowed to reach densities up to $10 n_{\text{cut-off}}$ [20]. Three mechanisms have been studied and characterized in plasma fusion devices, as summarized in Fig.6.

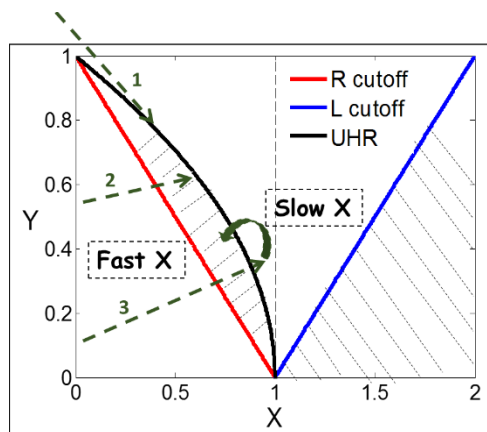


Figure 6: Subplot of the CMA diagram showing the fundamental mechanism of mode-conversion in magnetoplasmas.

In high field side launch (arrow 1 in Fig.6) X waves are launched in regions where $B/B_{\text{ECR}} > 1$. The electron density between injection and absorption must stay lower than the L cut-off.

In directed FX-B conversion (arrow 2 in Fig.6) the fast X-mode (FX) tunnels through the evanescent region between the R-wave cut-off and the Upper Hybrid Resonance (UHR) and couples to the slow X-mode (SX) that, in turn, mode converts to EBWs at UHR. This is the best condition for the establishment of the Budden-type conversion scenario (i.e. a resonator containing mode conversion to EBW as an effective dissipation is formed).

In O-SX-B conversion (arrow 3 in Fig.6) the R cut-off is crossed by the O wave that, if the conditions for O-SX conversion are valid at the O cut-off, is converted into SX waves which are in turns converted into Bernstein waves at UHR.

In the above case, the detection of peculiar signatures of ES waves' formation and their following absorption was observed, such as:

- 1) Overcoming the cut-off density;
- 2) Non-linear heating onset (highlighted by the sudden appearance or increase of the X-ray emission above fixed thresholds of RF power);
- 3) The appearance of ion signal in the EM spectrum, as a signature of interaction between the EM and ES waves;

While in large size fusion machines the efforts for Bernstein wave generation are going towards O-FX-B modal conversion, in compact devices the most straightforward mechanism seems to be the direct SX-B conversion.

A four-times overdense plasma was measured at INFN-LNS in a compact-size plasma reactor [22], corresponding to an electron density of $7 \cdot 10^{11} \text{ cm}^{-3}$.

The conversion of the incoming O-mode, and the following absorption of the X-waves in the vicinity of the UH-resonance layer, should be almost complete in a single "pass" if the proper incidence angle is chosen. If the single pass absorption was not fully exploited, the multiple reflections, from cavity walls may be helpful to increase the overall conversion efficiency.

In order to maximize the conversion efficiency, a dedicated launcher is needed. The Fig.7 shows the irradiated field from a two-waveguides phased array at different phase shifts and a photograph of the launcher already assembled at LNS.

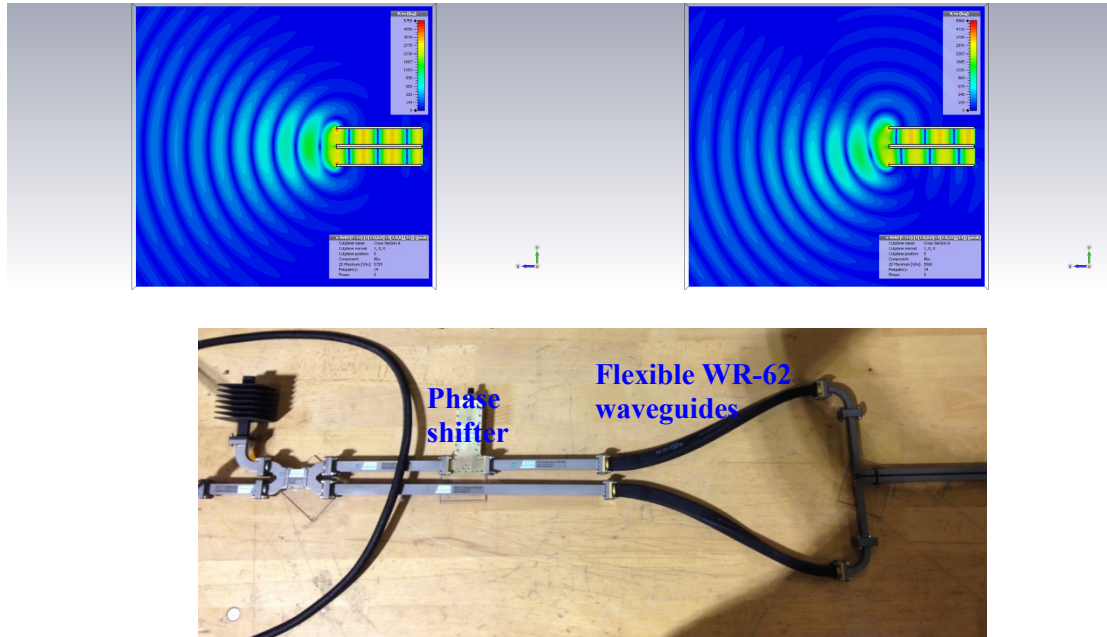


Figure 7: Simulations and assembly about the microwave launcher designed for perpendicular wave launching in Simple Mirror traps.

The maximum achieved tilt-angle is $\theta_{max}=40^\circ$ for a phase difference $\Delta\phi=120^\circ$. By setting up a phase difference $\Delta\phi=48^\circ$ it is possible to rotate the direction of maximum radiation up to 20° with a negligible secondary lobe.

The results of power amplitude measurements are shown in [23].

When $\Delta\phi=120^\circ$ clear peaks arise in the peripheral part of the chamber with respect to the $\Delta\phi=0^\circ$ case, while for $\Delta\phi=180^\circ$ a well-pronounced maximum appears at $z=130$ mm.

Tilt angles have been measured also in cavity and the results are really promising and not far from the free-space ones.

2.1.6 Conclusions and Perspectives

During the last three decades the improvements of ECRIS performances was outstanding but still a great deal of opportunities is available for additional boost of stable currents of highly charged ion beams. The ability to master the microwave coupling and the plasma confinement process is the key to these perspective increases. Different heating schemes have been compared with the experimental results: they qualitatively agree with experiments about the upper energy boundary scaling with the RF power and frequency, explaining correctly the frequency scaling rules on the basis of pitch angle scattering [7,20]. However, they fail when trying to predict how the heating is influenced by the L parameter; a modified diffusion coefficient is needed for large L , which accounts for turbulent heating and kinetic instabilities. For critical L parameters the density profile provides the conditions for mode conversion at the UHR.

On the other hand, a proper handling of the conversion mechanism (avoiding the boosting of stochastic effects) could permit to overcome the ECRIS density limitations (a different magnetic field profile must be designed). Preliminary studies about implementation of O-X-B conversion in ECRIS have been carried out. It can be expected

that the demand of high magnetic field magnets can be relaxed if this mechanism would be advantageous without triggering plasma instabilities and emittance growth.

The impact of the RF heating on the beam formation mechanism has been also outlined: the plasma inhomogeneity generates the hollow beams formation, which is one of the unsolved issues still affecting the ECRIS beams' emittance growth. A different plasma chamber design may help to avoid density depletion in the near axis zone.

A reshaping of both the plasma chamber and related RF launching system - in a plasma microwave absorption oriented scenario - is considered as a possible solution, as well as the design of optimized launchers (taking inspiration from tools adopted in the thermonuclear-fusion) enabling "single-pass" power deposition, i.e. not being affected by cavity walls effects.

The evidence of a saturation of the current increase curve for highly charged ion beams produced by ECR ion sources in the last few years has been compensated by the experimental evidence of "something beyond" the mere scaling of the magnetic field (High-B mode) due to the scaling of the pumping wave frequency. We may now outline some possible future scenarios in the frame of the High-B mode paradigm, or beyond this paradigm, which will permit to satisfy the upcoming requests of mA highly charged heavy ions and multi-milliAmpere of multiply charged light ions:

- a) The "brute technological effort" with some corrections. The extension of the ECRIS standard model (scaling laws plus the High B mode concept) up to the frequency range of 56-60 GHz will be viable in the coming years due to continuous improvement of superconducting magnets; in fact, it is necessary to produce a resonance field above 2 T, so the confining radial field should exceed 4 T and the axial field maxima may range around 5-7 T. The corrections to be done concern the damping of high energy X-rays and RF technology may help either through the change of the phase relation between the incoming microwaves and the plasma within the chamber, and by an appropriate shape of the microwave pulse amplitude;
- b) The contemporary occurrence of ECR and EBW. If we are able to ignite a plasma around the cutoff, then to inject a second set of microwaves with higher frequencies (i.e. 8-18 GHz for the first, 20-35 GHz for the second) we could have in the chamber an ECR-generated plasma volume along with some "shells" of EBW corresponding to an overdense plasma, nested within the ECRIS plasma. This idea will be tested soon with the AISHA source by the end of 2018 at INFN-LNS;
- c) The use of non-linear effects have permitted to generate keV electrons in a small plasma reactor and this track may help to verify the possibility of generating multiply charged light ions with non-B-minimum traps. The effects of UHR crossing and EBW formation in a variable field-variable frequency plasma trap (named Flexible Plasma Trap, FPT [24] is studied at INFN-LNS.

In light of the above studied advances one must drop the prejudice that the development of ion sources for high intensity – highly charged beams is close to saturation. Different solutions are open to the future upgrade of existing Ion Sources and to the design of new injectors for future accelerators.

2.1.7 References

1. R. Geller, Electron cyclotron resonance ion sources and ECR plasmas, Inst. of Phys. Publishing, 1996; Bristol and Philadelphia.

2. S. Gammino, G. Ciavola, The Contribution Of The INFN-LNS To The Development Of Electron Cyclotron Resonance Ion Sources (Invited) Review Of Scientific Instruments, 71, Issue: 2, Pages: 631-636 Part: 2 (2000)
3. S. Gammino, G. Ciavola, R. Harkewicz et al. Effects of frequency and magnetic field scaling on the superconducting electron cyclotron resonance ion source at MSU-NSCL. Review of Scientific Instruments, 67, Issue: 12, Pages: 4109-4113
4. T. Antaya and S. Gammino, Rev. Sci. Instr. **65**(5), (1994) 1723-1727;
5. S. Gammino, G. Ciavola, L. Celona et al. 18 GHz upgrading of the superconducting electron cyclotron resonance ion source SERSE. Review of Scientific Instruments, 71, Issue 9, Pages: 3577-3582 (1999)
6. M. A. Lieberman and A. J. Lichtenberg, Plasma Phys. **15** 125 (1973);
7. D. Mascali, S. Gammino, L. Celona *et al.* Towards a better comprehension of plasma formation and heating in high performances electron cyclotron resonance ion sources (invited). Review of Scientific Instruments, 83, Issue:2. Article Number: 02A336 Part: 2 (2012).
8. A. Girard et al., Phys. Rev. E, 62(1), (2000) 1182;
9. D. Leitner et al., Rev. Sci. Instrum. **79**, (2008) 033302;
10. S. Gammino et al., Plasma Sources Sci. Technol. **18** (2009) 045016;
11. H. Koivisto et al., Proceedings of the 19th ECRIS Workshop, Grenoble, France, August 2010;
12. S. Gammino, D. Mascali, L. Celona, F. Maimone, G. Ciavola, Considerations on the role of the magnetic field gradient in ECR ion sources and build-up of hot electrons component, Plasma Sources Sci. Technol. 18 (2009) 045016.
13. A. A. Ivanov et al. *Europhys. Lett.*, **59** (6), (2002) 841;
14. O Tarvainen et al 2014 Plasma Sources Sci. Technol. 23 025020
15. L. Celona et al. Rev. Sci. Instrum. 79, (2008) 023305;
16. F. Consoli, et al. Rev. Sci. Instrum. 79, 02A308 (2008);
17. D. Mascali, L. Celona, F. Maimone, J. Maeder, G. Castro, F.P. Romano, A. Musumarra, C. Altana, C. Caliri, G. Torrisci, L. Neri, S. Gammino, K. Tinschert, K. P. Spaedtke, J. Roszbach, R. Lang and G. Ciavola. X-ray spectroscopy of warm and hot electron components in the CAPRICE source plasma at EIS testbench at GSI. Rev. Sci. Instrum. 85, 02A956 (2014) ; <http://dx.doi.org/10.1063/1.4858115>
18. R. Racz et al., May 2017. Plasma Sources Science and Technology 26(7) DOI10.1088/1361-6595/aa758f.
19. D. Mascali, G. Castro, S. Biri et al. Electron cyclotron resonance ion source plasma characterization by X-ray spectroscopy and X-ray imaging, Review of Scientific Instruments 87(2):02A510 · February 2016
20. Laqua H. P. et al., Plasma Phys. Control. Fusion, 41 (1999) A273.
21. J. Preinhaelter, et al., Plasma Physics and Controlled Fusion 51 (2009).
22. G. Castro et al. Overdense plasma generation in a compact ion source. April 2017 Plasma Sources Science and Technology 26(5):055019 DOI10.1088/1361-6595/aa61c4
23. G. Torrisci et al., Innovative launching schemes in ECR ion sources. January 2017 The European Physical Journal Conferences 157(2):03055 DOI10.1051/epjconf/201715703055
24. S. Gammino et al. The Flexible Plasma Trap (FPT) for the production of overdense plasmas. July 2017 Journal of Instrumentation 12(07):P07027-P07027. DOI10.1088/1748-0221/12/07/P07027

2.2 Challenges of operating ECR ions source at high frequency and high RF power

Thomas Thuillier

Mail to: thomas.thuillier@lpsc.in2p3.fr

Université Grenoble-Alpes, CNRS-IN2P3, Grenoble Institute of Engineering (INP),
LPCS, 38000 Grenoble, France

2.2.1 Introduction

Electron Cyclotron Resonance Ion Source (ECRIS) demonstrated dramatic improvement in the last decades when operated at high RF power and high frequency. Pioneer research performed in accelerator physics laboratory (LBNL, IMP CAS, MSU, RIKEN) have shown technological limitations that need to be tackled to grant a safe and reliable operation of high frequency ECRIS. This article discusses the challenges of operating ECRIS at high frequency and high RF power. After a brief introduction on ECRIS, the frequency scaling law and the standard magnetic confinement models are presented. The challenges of high power high frequency operation are then reviewed: plasma chamber burning in continuous working operation, wall sputtering in pulse mode operation, high voltage insulator aging, parasitic cold mass heating, high current and magnetic emittance management.

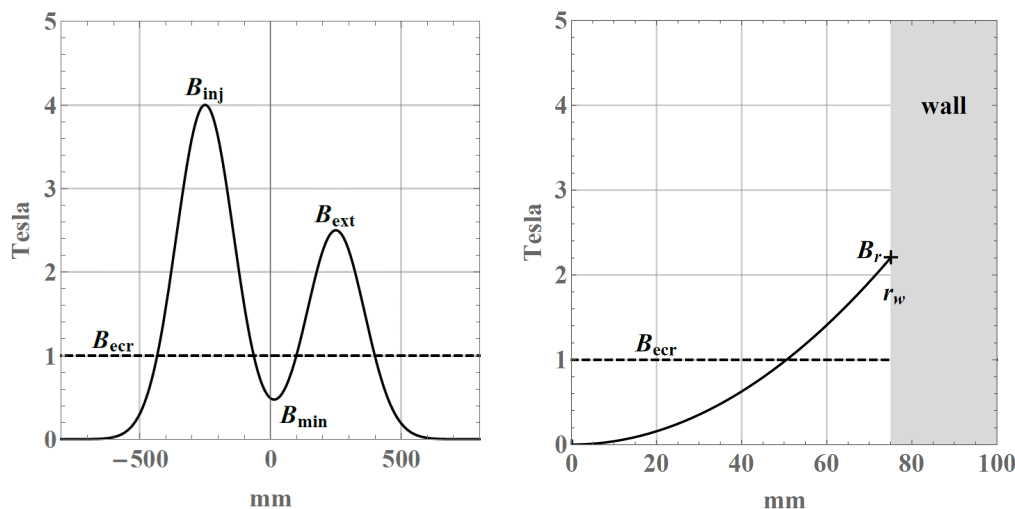


Figure 1: Left: Typical axial magnetic field profile on the ion source axis (RF=28 GHz) displaying the location of B_{min} , B_{med} , B_{ext} and B_{eccr} . Right: Radial magnetic field intensity from the axis to the plasma chamber wall showing the location of B_r and r_w

2.2.2 ECRIS Frequency scaling law and magnetic confinement

2.2.2.1 Frequency scaling law

ECRIS were invented in the 60's by R. Geller [1]. In these instruments, a microwave (RF) maintains a plasma into a cavity featuring a minimum-B magnetic field structure composed of a radial sextupole superimposed to an axial magnetic mirror. An overview of the ECRIS magnetic field confinement is displayed in Fig.1. The axial magnetic mirror

is described by means of two peaks named B_{inj} (injection) and B_{ext} (extraction) and one dip in between: B_{min} . The sextupole confinement is characterized by the radial magnetic field intensity B_r at the plasma chamber wall radius r_w . The radial magnetic field intensity varies quadratically with the radius. Electrons from the plasma are accelerated by the RF when they pass through the closed ECR magnetic surface (characterized by B_{ecr}) displayed in Fig.2, a place where the RF frequency equals the local electron cyclotron frequency:

$$f = f_{ec} = \frac{eB_{ecr}}{2\pi m_e} \quad (1)$$

where e and m_e are respectively the electron electric charge and mass. The mean electrons kinetic energy reaches a few keV, favoring the production of multi-charged ions. On the other hand, ions remain cold with a few eV and can be extracted and accelerated by a high voltage to form an ion beam. An interesting property of ECRIS is that, since the energy coupling is immaterial, there is no direct usable part like in a filament ion source [2]. ECRIS are simple, robust, reliable and are used on many heavy ion CW accelerators. The ion beam current I extractable from an ion source is proportional to the plasma density n , the plasma volume V and inversely proportional to the plasma confinement time τ :

$$I \propto \frac{nV}{\tau} \quad (2)$$

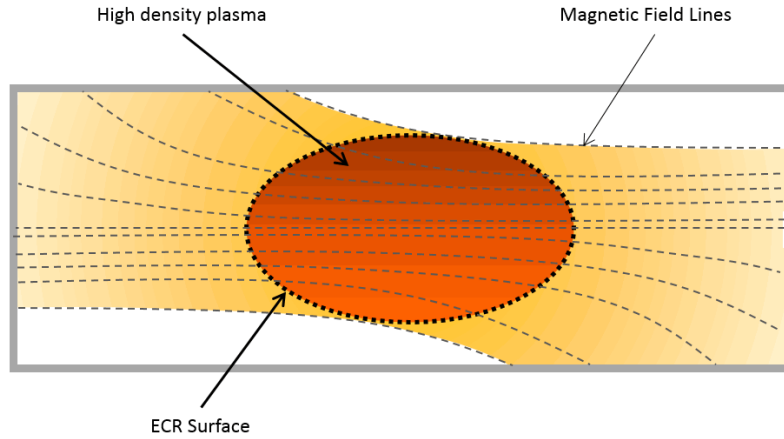


Figure 2: Sectional view of an ECRIS plasma chamber. Dashed grey line: magnetic field lines. Black dotted line: closed ECR surface where $\mathbf{B} = \mathbf{B}_{ecr}$. The high density plasma is located inside the ECR surface. The ion beam extraction hole is visible on the right.

ECR plasma absorbs RF as soon as its frequency is above the plasma frequency:

$$f \geq f_p = \frac{1}{2\pi} \sqrt{\frac{ne^2}{m_e \epsilon_0}} \quad (3)$$

where ϵ_0 is the vacuum permittivity. Therefore, the plasma density is limited for a given ECR frequency [3]:

$$n \propto f^2 \quad (4)$$

Finally, one obtain the ECR plasma frequency scaling law:

$$I \propto \frac{f^2 V}{\tau} \quad (5)$$

This frequency scaling has been experimentally verified from $f=6$ to 28 GHz [4] and has no known limitation. Increasing the ECR microwave frequency is the main driver to improve the ion source intensity. The plasma volume increase is also a way to improve

the ion beam intensity. Table 1 shows the dramatic increase of plasma performance from 2.4 GHz to 60 GHz thanks to the frequency scaling law.

Table 1: Characteristic ECR ion source parameter as a function of the RF frequency (in unit of GHz). Data with * is extrapolated.

Parameter	Unit	2.45	14	28	45	60
B_{ecr}	T	0.087	0.5	1	1.6	2.1
B_{inj}	T	0.3	1.7	3.5	5.5	7.5
B_{min}	T	0.06	0.35	0.7	1.1	1.45
B_{ext}	T	0.2	1.2	2.5	4	5
B_r	T	0.17	1	2	3.2	4.2
Plasma cut-off density	cm ⁻³	7.4×10^{10}	2.4×10^{12}	$\sim 10^{13}$	2.5×10^{13}	4.4×10^{13}
O ⁶⁺ beam current	emA	0.05	1.5	6	15*	25*

2.2.2.1 Empirical Magnetic confinement

The ion source group at INFN-LNS in Italy showed that optimum high charge state ion production in ECRIS is obtained when $B_{inj} \sim 3 - 4 B_{ecr}$, $B_{min} \sim 0.5 - 0.7 B_{ecr}$ and $B_r \sim 2 B_{ecr}$ [5,6]. Because $f \propto B_{ecr}$, an increase of the RF frequency requires a linear increase of the magnetic field confinement to keep the high charge state ion production. Table 1 includes axial and radial peak magnetic field intensities necessary to an appropriate operation of the ion source vs the ECR frequency. Up to ~ 22 GHz, the magnetic confinement can be built with room temperature coils, permanent magnets and soft iron yokes. Above, it is advantageous to generate the magnetic field using superconducting technologies. Such high performance ion sources are under operation on accelerator with frequencies within the 24-28 GHz range [7, 8, 9, 10]. Their magnetic field is generated by means of NbTi coils set into a 4K liquid helium bath. The limitation of NbTi use is the maximum achievable peak field of ~ 7 T on coils at 4K. A possibility to use a 1K pumped liquid helium bath would extend this limit to 9T, but no laboratory tried this option so far. When the peak field is above 7T (@4K), it is necessary to switch to Nb3Sn wire technology with a maximum peak field on coil of ~ 15 T at 4K. IMP CAS team is currently developing a challenging 45 GHz ion source in collaboration with the LBNL superconducting group [11]. The difficulty with this technology is that, once winded, the Nb3Sn coil requires a heat treatment after which it becomes brittle and vulnerable to irreversible damage until it has been epoxy impregnated. LBNL is currently developing an original magnetic structure based on an Ioffe bar sextupole enabling the use of NbTi wire to build a 45 GHz ECRIS [12]. Further discussion on this topic is proposed in the part 1.e.

2.2.3 Challenges of operation at higher frequency

LBNL, then IMP CAS have pioneered the ECRIS operation at 28 and 24 GHz respectively [7, 8]. MSU and RIKEN followed shortly afterward [9, 10]. These superconducting ion sources feature a denser plasma (factor 2 to 4) and a larger plasma volume (factor 3 to 10) than the former room temperature 14-18 GHz ECRIS generation. Thus, for a given plasma electron temperature (optimized for high charge state ion production), the energy stored in those new high performance ECRIS can be as high as 6

to 40 times the one of a compact 14 GHz ECRIS. An important phenomenon observed at higher frequency comes from an enhanced plasma flux to the wall. Indeed, the electron scattering time is inversely proportional to the plasma density. Therefore, the mean electron confinement time should decrease with the frequency, favoring electron loss to the wall. Consequently, high performance plasma sustainability at higher frequency requires more RF power to compensate this enhanced loss rate. The larger plasma volume also implies the use of a larger RF power. As 1 kW RF was typically required to reach the optimum source performance at 14 GHz, 10 kW RF is today injected in modern 28 GHz ECRIS, showing no performance limitation [13]. Apart from the difficulty to design and build a high magnetic field min-B structure, the main challenge of high frequency and high RF power operation of ECRIS is the management of the higher plasma flux to the wall and its consequences. The main energy loss to the wall is brought by the hot electron population; but in unstable operation, ions accelerated by a transient high plasma potential voltage can also trigger sputtering (see part 1.f). Other challenges at higher frequency operation are the need to use a higher voltage to grant an appropriate ion beam current extraction and to manage a larger beam emittance. In the following text, the main challenges of high RF power high frequency operation are reviewed in detail.

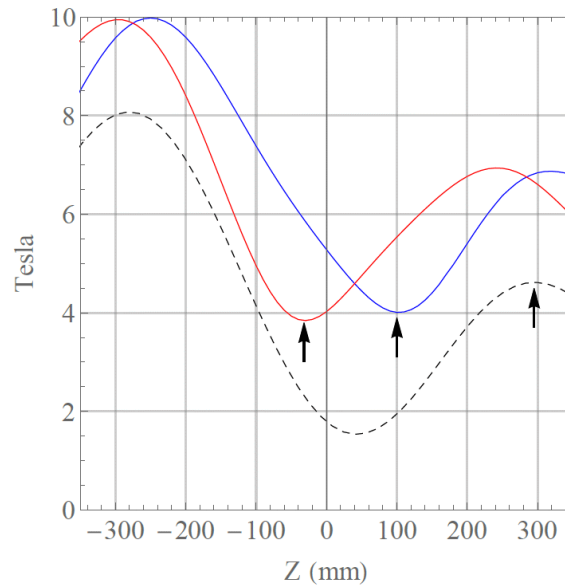


Figure 3: Magnetic field intensity along the ECRIS axis direction of a 60 GHz ECRIS design (LPSC). Dashed black: on the ECRIS axis of revolution ($r = 0$). Solid red: at the plasma chamber wall along a magnetic pole ($r = r_w, \theta = 0$). Solid Blue: at the plasma chamber wall along the next magnetic pole ($r = r_w, \theta = 60^\circ$). Arrows indicate the location of the weakest magnetic field intensity, where plasma predominantly leaks.

2.2.3.1 Plasma chamber wall burning

Charged particles in ECRIS are magnetically confined by mirror effect. The particles are lost to the wall when their velocity eventually scatter into the magnetic loss cone after a collision. In ECRIS, the magnetic field lines feature a strong curvature and a large magnetic gradient: charged particles undergo fast magnetic drifts that make particles jump from one field line to another and eventually explore the whole plasma chamber volume. Hot electrons population, holding the plasma energy, weakly interact with the

plasma and scatter via Coulomb collision [14] and RF [15] scattering with a time scale much larger than the magnetic drift time [16]. Thus, hot electrons will predominantly leak at the place where the magnetic loss cone is the largest, *i.e.* where the magnetic field intensity is the weakest on the plasma chamber walls. Fig.3 shows characteristic magnetic field intensities along the source axis direction. See legend for detail. The weakest magnetic fields positions are indicated by arrows on Fig.3. Such weak magnetic points at wall are unavoidable in a minimum-B: the axial coils generate a radial magnetic component that adds or subtracts to the local sextupole radial magnetic field direction. Hence, 3 weak spots are located at the wall on the injection side (red curve) and 3 others are located at the wall on the extraction side (blue curve). Because the injection solenoid field is higher than the extraction one, the absolute magnetic minimum is located on the injection side. The unavoidable misalignment of the plasma chamber axis with respect to the sextupole axis even makes the situation worst as one specific injection weak point will necessary be weaker than the others and will attract further the electron flux to the wall. Another weak magnetic point is located on the plasma extraction electrode on the source axis (arrow on the black dashed line on Fig.3). This electrode is usually placed close to the B_{ext} peak position. LBNL and IMP CAS ion sources both experienced plasma chamber burn after long term operation at high power (6-10 kW RF) and high frequency (28 GHz). Fig.4 presents photos of holes in the VENUS (right) and IMP CAS (left) aluminum plasma chambers. Aluminum is commonly used as a plasma chamber material because of its high thermal conductivity and high secondary electron emission

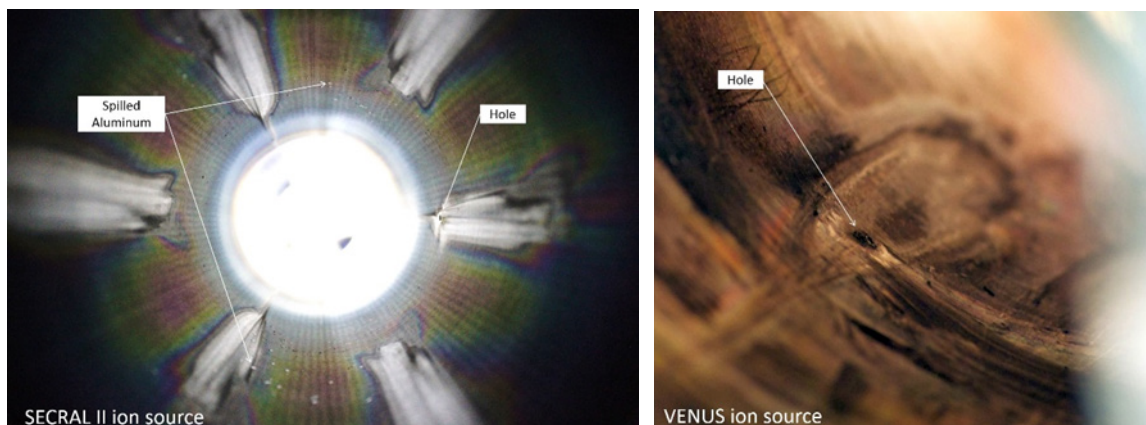


Figure 4: photos of a plasma chamber hole on the SECRALII ion source (IMP CAS, left) and VENUS ion source (LBNL, right).

yield, favorable to sustain a dense plasma. The drawback of aluminum is its low melting point ($\sim 660^{\circ}\text{C}$). The hole formation in VENUS was investigated and shown that the metal suffered recrystallization occurring above 250°C [16]. The metal wall became porous and eventually pressurized water (from the cooling channel located behind the plasma chamber wall) percolated toward the vacuum. In the case of SECRALII, liquid aluminum drops were ejected indicating the hole formation happened at a high surface temperature. In both cases, the origin of the wall degradation is due to the so-called critical heat flux (CHF) limitation. The heat power density P exchanged with the turbulent water flow per unit surface is $P = h\Delta T$, where $h \leq h_{CHF}$ is the forced convection coefficient for water and ΔT the temperature difference between the metal and the water. When P increases, the metal temperature increases and may overshoot the water boiling temperature. The

vapor bubbles stick to the wall, reducing the local heat exchange and resulting in a further increase of the wall temperature to reach a new power equilibrium. Depending on its temperature of equilibrium, the wall stays still, recrystallizes or possibly melts. The wall damage occurs when the local power flux to the wall is above 1 MW/m^2 . An investigation by simulation was carried on the VENUS source to study where hot electrons were leaking to the wall. Results showed that hot electrons favorably leak toward the place where the magnetic field is minimum, and that the flux is concentrated on a sub-millimeter scale inducing local power much higher than 1 MW/m^2 [16]. Simulation results showing the power density at wall are displayed on Fig.5 on the plasma electrode plane (left) and the chamber wall (right). On Fig.5 left, one can note three hot spots located right around the plasma electrode extraction hole. These spots concentrate the drift of the electron flux trapped on the source axis between the high intensity B_{inj} peak on one side and the ion extraction electric field on the other side. ATOMKI group has investigated the x-ray emission from electrons impinging the wall in ECRIS using a pinhole camera [17]. Recent measurement from this group reproduced on Fig.6 left shows the presence of 3 hot spots on the plasma electrode, along with the classical hot spots at the chamber wall [18]. This confirms and explains the melting mechanism of the plasma electrode observed at LBNL visible on Fig. 6 right.

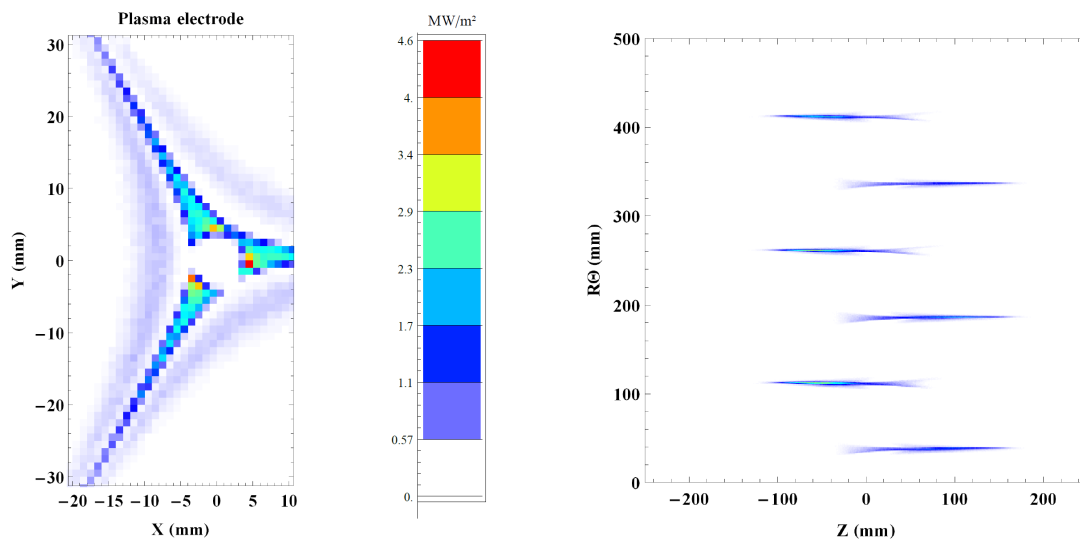


Figure 5: Results of the electron power flux to the wall as simulated in the VENUS ion source [15]. Left: zoom on the plasma electrode plane. Center: Color scale in MW/m^2 . Right: overall hot electron impact along the cylindrical plasma chamber wall surface (Z : source axis, $R\theta$: cylinder azimuthal coordinate).

A possibility to improve the plasma chamber reliability of future ion source design would consist in including a hypervapotron cooling circuit [19] around the plasma chamber. Such system uses an effective diphasic water heat exchange to dissipate up to 20 MW/m^2 of local heating power. However, this system is thicker than a usual plasma chamber and cannot be easily retrofitted on existing ECRIS. Another possibility to mitigate plasma chamber burns would consist in replacing the usual aluminum alloy (or stainless steel) wall by a refractory metal such as tantalum or wolfram.

CERN reported another type of plasma chamber aging specifically observed in pulse mode operation: after a long operation afterglow run with argon beam, the 14.5 GHz GTS ECRIS plasma chamber showed the appearance of grooves at the plasma chamber wall

along the sextupole pole lines [20]. In the afterglow regime, the RF is pulsed and an intense ion beam pulse is extracted from the source when the RF is stopped. When RF is stopped, the plasma electrons are rapidly de-confined, resulting in a transient high voltage plasma potential accelerating ions to the wall and inducing sputtering. CERN team reported that the wall sputtering was not observed after long afterglow lead beam operation. The condensable lead atoms, produced by an oven, have a high probability to stick to the chamber wall where they accumulate. So the afterglow induced sputtering may mainly expel adsorbed atomic lead layers rather than the wall material itself. The afterglow induced sputtering effect will be a challenge for the intense pulse mode operation of next generation accelerator like HIAF [21] requiring high RF power high frequency ECRIS, as the sputtering rate will scale with f^2 .

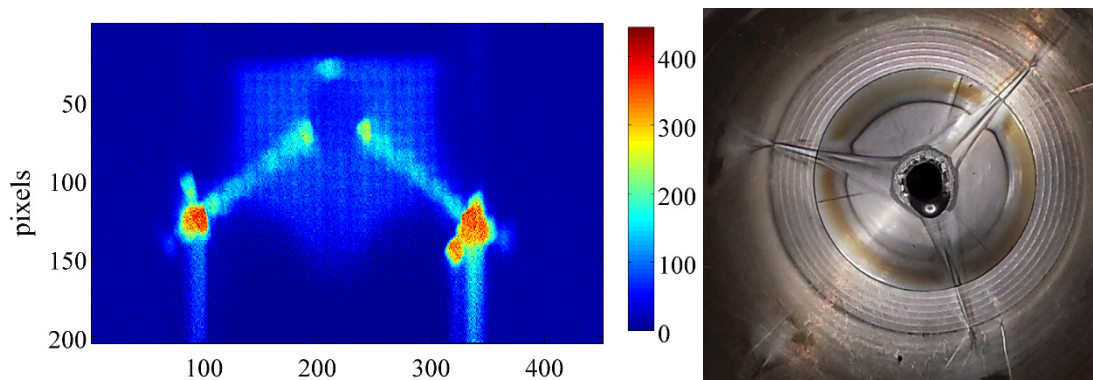


Figure 6: (left) Experimental x-ray measured at ATOMKI with a pinhole camera showing x-ray hot spots at the wall [17]. (Right) plasma electrode melted during operation at LBNL (Courtesy of D. Xie).

2.2.3.1 *High energy x-ray flux*

The hot electron flux impinging the ion source wall is converted into an intense bremsstrahlung x-ray flux radiating outwardly. The x-ray emission is concentrated on the places where the magnetic field intensity is minimum (see 1.1.3.1). While low energy x-rays are easily stopped by a few mm of metal, high energy x-rays weakly interact with matter and can propagate through several cm of metal. The high-energy flux passes through the high voltage insulator located around the plasma chamber, then through the superconducting magnet cryostat, the source soft iron yoke and finally outward in the ion source hall. Therefore high frequency high RF power ECRIS must be placed in controlled access areas to prevent radiation hazard for the accelerator workers. The presence of this continuous radiating x-ray flux has several consequences. The first is the slow degradation of the high voltage insulator surrounding the plasma chamber. Despite the use of a tantalum shield wrapped around the plasma chamber [22], the high voltage insulator accumulates a destructive radiation dose on a few year time scale. Fig.7 left shows a photo of a radiation stained Mylar foil wrapped around the VENUS source. X-ray hot spots on the chamber wall are clearly visible on the injection (upper marks) and extraction side (less visible marks below). When unwrapped, the Mylar foil broke as the material lost its elasticity. Fig.7-right shows both an x-ray induced damage on the Mylar and a dramatic thermal meltdown induced by the inner plasma chamber wall meltdown.

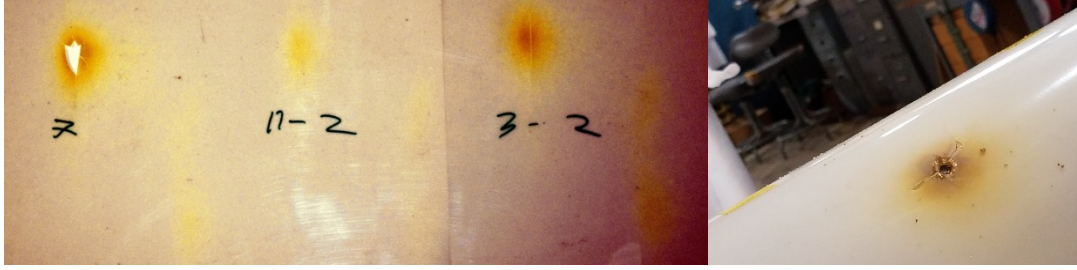


Figure 7: photo showing x-ray irradiation damage on the VENUS high voltage insulator roll (left, color enhanced) and a fast insulator meltdown triggered by a high plasma chamber temperature.

The second consequence of the intense x-ray flux is the continuous deposition of heat into the superconducting coil cold mass. The cold mass is composed of niobium, titanium, copper, aluminum and iron stacked over a thickness of several centimeters. The x-ray stopping power is sufficient to heat the cold mass by several watts. This effect was not considered at the time the first superconducting ECRIS were conceived which only included liquid helium cooling power of the order of 1 watt [23]. Initially, high RF power operation lead to an unbalanced helium evaporation rate, requiring a frequent and costly helium refill. Today, upgraded superconducting ECRIS design include oversized helium cooling capacity of ~ 10 watt to compensate the extra loss of liquid helium bath during operation. Technically, the helium vapor directly re-condenses on heat exchangers attached to a set of cryocooler cold heads located above the cold mass helium bath. The LBNL ECR ion source group recently demonstrated that the x-ray spectral temperature was driven by the B_{min} intensity [24]. Thus tuning the source with a low B_{min} allows a dramatic reduction of the cold mass heating effect and a safer cryostat margin of operation.

2.2.3.2 Ion beam management

Space charge effect becomes dominant above a few emA of ion beam intensity extracted from an ECRIS. The new generation ECRIS daily produce ~ 10 emA of total ionic current. The management of such beam requires an appropriate high voltage extraction to grant a high efficiency transport up to the first accelerating cavity. High frequency ECRIS should use a high voltage at least equal to $V=30-40$ kV when the use of a high voltage platform is not directly required. A special care must also be given to the electromagnetic compatibility of the ion source instrumentation to prevent damages caused by high voltage breakdowns, as the energy dissipated in sparks is proportional to V^2 . Another challenge of high frequency ECRIS operation is the increase of the magnetic beam emittance. Indeed, the ion beam is extracted in a high axial magnetic field intensity ($B \sim 2B_{ECR} \propto f$). The low transverse thermal ion beam emittance is completed by a predominant magnetic term [25]:

$$\epsilon_B^{xx'-rms-norm.} = \frac{qBr^2}{2mc} \quad (5)$$

where r is the mean beam radius, m and q the ion mass and electrical charge. The remaining free parameter to control the beam emittance at high RF frequency is then the mean ion extraction radius. Such emittance must be carefully handled in a dedicated low energy beam line transfer with a large pipe and a UHV level vacuum to prevent charge exchange process and breakdown in the extraction area where a high magnetic field and an electric field are present.

2.2.4 Acknowledgement

The author is indebted to Dan Xie (LBNL), LiangTing Sun (IMP CAS) and Sandor Biri (ATOMKI) for the fruitful discussions and the procurement of original data to complete this article.

2.2.5 References

1. R. Geller, *Electron Cyclotron Resonance Ion Sources and ECR plasmas*, 1996, CRC Press.
2. D. Faircloth, *Negative Ion Sources : Magnetron and Penning*, <https://arxiv.org/pdf/1404.0944>
3. R. Geller et al., *Proc. of the 8th Workshop on ECRIS, East Lansing (1987)* 1.
4. C. Lyneis, *Scaling laws in electron cyclotron resonance ion sources*, *Proc. ECRIS'2016, Busan, South Korea*, paper MOAO01, pp.1-4.
5. S. Gammino, L. Ciavola, *ECR ion sources and scaling laws*, *Proc. 14th International Conference on Cyclotrons and their applications*, 1995, Cape town, South Africa, p. 377.
6. D. Hitz, et al., *Rev. Sci. Instrum.* 73, 509 (2002).
7. C. M. Lyneis, et al., *Rev. of Sci. Instrum.* 75, 1389 (2004).
8. H. W. Zhao et al., *Rev. of Sci. Instrum.* 77, 03A333 (2006).
9. P. A. Závodszy et al., *Rev. Sci. Instrum.* 79, 02A302 (2008).
10. T. Nakagawa et al., *Rev. Sci. Instrum.* 81, 02A320 (2010)
11. M. Juchno et al., *MT-25 Proc.*, Aug. 23 - Sept. 1 2017, Amsterdam, Netherland, to be published in *IEEE Trans Appl. Supercond.*, 2017.
12. D. Xie et al., *Rev. Sci. Instrum.* 87, 02A702 (2016).
13. L. Sun et al., *Rev. Sci. Instrum.* 87, 02A707 (2016).
14. F. F. Chen, *Introduction to Plasma Physics and Controlled Fusion* (Plenum, 1984).
15. A. Girard, C. Perret, G. Melin, and C. Lécot, *Rev. Sci. Instrum.* 69, 1100 (1998).
16. T. Thuillier et al., *Rev. Sci. Instrum.* 87, 02A736 (2016)
17. S. Biri, A. Valek, and T. Suta, *Rev. of Sci. Instrum.* 75, 1420 (2004).
18. R. Racz et al., *Plasma Sources Sci. Technol.* 26 (2017) 075011.
19. G. Cattadori et al., *Exp. Therm. Fluid Sci.* 7, 230–240 (1993).
20. D. K uchler, J. Ferreira Somoza, A. Michet, V. Toivanen, *Proc. ECRIS2016, Busan, Korea WEPP03*, pp.89-91.
21. J.C. Yang et al., *Nucl. Instrum. Phys. Res. B*, Vol. 317, Part B, 2013, pp. 63-265.
22. C. Lyneis, et al., *Rev. Sci. Instrum.* 77, 03A342 (2006).
23. C.E. Taylor, C. Abott and D. Leitner, *An efficient cooling loop for connecting cryocooler to a helium reservoir*, <https://escholarship.org/uc/item/701673cx>
24. J. Benitez et al., *IEEE Trans. Plasma Sci.*, 45, no. 7, july 2017.
25. M. Reiser, *Theory and Design of Charged Particle Beams*, (NY, Wiley, 2008).

2.3 Development of Superconducting Magnet Using Nb₃Sn

Liangting Sun

Mail to: sunlt@impcas.ac.cn

Institute of Modern Physics, CAS 509 Nanchang Road, Lanzhou 730000, China

2.3.1 Introduction

Electron Cyclotron Resonance (ECR) ion source has been developed over four decades. Up to now, three generations of this type of machine have been developed successively and been put in operation. The first and second generation ECR ion sources were mostly ECR physics dominant machines built with the concepts on how the physicists understood this type of machine as the ECR ion source researchers were still developing a better understanding on how these powerful machine work. Based on the 20 to 30 years efforts amongst the ECR community, semi-empirical laws have been developed that have become the main guideline for subsequent high performance ECR ion source development [1]. As a consequence the main challenge, during the development of the 3rd generation ECR ion source did not lie so much in the physics principle used to design the ECR ion source but rather in the techniques that were adopted during the development, primarily characterized by the use of fully superconducting NbTi structure. Because of the added complexity, the successful development of a 3rd generation ECR ion source also resulted in much higher cost and longer completion time. Several high performance 3rd generation ECR ion sources have been developed in different laboratories, such as VENUS, SECAL, SECAL-II, RIKEN SC-ECRIS, SuSI [2, 3, 4, 5, 6, 7], and with their contributions, ECR ion source performances have improved quite often in last 15 years as shown in Fig.1. However, these progresses mostly stemmed from higher microwave frequency and power contribution, as well as larger plasma volume. There is no notable physics advancement that could bring about higher performance with the same ion source.

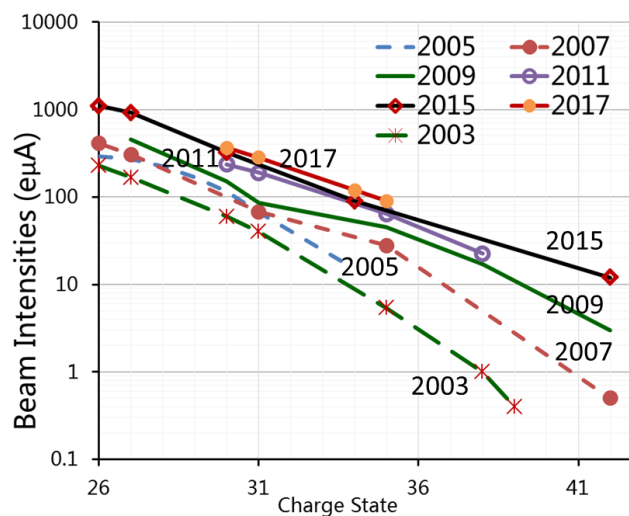


Figure 1: Xenon ion beams intensity evolution in the last 15 years with the contributions of worldwide high performance ECR ion source development.

Nevertheless, new heavy ion accelerator facilities need more intense highly charged ion beams that need more powerful machines to produce, beyond the state of the art 3rd generation ECR ion sources. Since no obvious physics advancement can help with higher beam intensity production, the only path for higher beam intensity production might be still to increase the microwave frequency. For the High Intensity heavy ion Accelerator Facility (HIAF) project for example [8], the injector linac ultimately needs 20 pμA CW and 50 pμA pulsed U³⁵⁺ beam from the ion source, which is two times and five times respectively the recorded beam intensities that had been made with 28 GHz VENUS in

2011 [9]. Based on frequency scaling laws, an ECR ion source working at a frequency above 40 GHz, might have the potential to produce such high intensity high charge state ion beam. Around 2007, there had been quite some investigation and research on a 56 GHz ECR ions source magnet design that features Nb₃Sn Rutherford cable wound coils clamped with an external aluminum shell pretensioned with water-pressurized bladders [10]. In this paper, we will discuss a fully Nb₃Sn magnet for a 4th generation ECR ion source called FECR (the First 4th generation ECR ion source), which is optimally designed for 45 GHz operation.

2.3.2 General Requirements of This Magnet

2.3.2.1 Magnet Parameters

The 3rd generation ECR ion source magnets are already at the performance limits of NbTi superconductor. A next generation or the 4th generation ECR ion source will be typically operated at the frequency of 40~60 GHz which requires significant increase in the ECR magnet fields. Table 1 summarizes the typical magnet parameters for the 45 GHz FECR source in comparison with a typical 3rd generation ECR source. FECR will serve as the injector ion source for a Low Energy heavy ion Accelerator Facility (LEAF) at IMP/Lanzhou, and will also be the prototype for the high performance ion source planned for the HIAF project. As indicated in Table 1, to provide such high fields for the working region, a peak field up to 12 T will be built up in the superconductor that will be possibly energized to a current density of ~1400 A/mm² (with necessary operation safety margin, coil packing factor, and non-Cu ratio~50% considered). Obviously this requirement is far beyond the performance of a NbTi wire. According to the advancement of superconductor materials, Nb₃Sn or Bi-2212 might be the candidate superconducting materials to be used in such a high field magnet design. However, with regards to technical maturity and cost, Nb₃Sn superconductor is a more viable choice.

Table 1: Typical magnet parameters of 45 GHz FECR ion source.

<i>Parameter</i>	<i>Unit</i>	<i>3rd generation ECR</i>	<i>FECR</i>
Frequency	GHz	24~28	45
B _{ecr}	T	0.86~1.0	1.6
B _r	T	1.8~2.2	≥3.2
B _{inj}	T	3.4~4.0	≥6.4
B _{min}	T	0.5~0.7	0.5~1.1
B _{ext}	T	1.8~2.2	≥3.4
Warm bore ID	mm	120~170	≥160
Mirror Length	mm	420~500	~500
Stored Energy	MJ	~0.7	~1.6

B_{ecr} is the field for the ECR resonance. B_r is the maximum radial field on the plasma chamber inner wall contributed by the sextupole. B_{inj}, B_{min} and B_{ext} are the injection peak field, minimum axial field and extraction peak field on the axis respectively.

2.3.2.2 Magnet Structure and Operation

Up to now, only two types of magnetic structures have been technically tested and used for superconducting ECR ion sources, i.e. the conventional structure and the reversed structure as shown in Fig. 2, represented by VENUS and SECRAI respectively. To minimize project risk, it has been advised to take either of the two structures. However, after detailed analysis, even with a high end performance Nb₃Sn wire (for instance OST RRP wire), the reversed structure coils have to be energized at more than 90% of the short sample current to achieve 45 GHz fields. Ultimately, conventional structure is the decision made for FEER magnet. A next generation ECR ion source will be more likely to be used as the heavy ion injector for a linac. Typically, to meet the injection energy requirement, the ion source has to be installed on a high voltage platform. For LEAF, the high performance ECR ion source will be required of producing more than 1 emA of U³⁵⁺ at an energy of 14 keV/u for downstream injection into the accelerator. For such high intensity ion beam, the high extraction energy will help mitigate the influence of strong space charge during transport and will require to use a high voltage platform for initial acceleration. Since the cold mass of the superconducting magnet will be immersed in a 4.2 K liquid helium environment, with an estimated heat load exceeding 10 W a good cryogenic solution need to be developed. Connection of the liquid helium reservoir to a cryo-plant is a very efficient solution but not compatible with a high voltage platform as a consequence of high voltage breakdown in the return helium gas line. Alternatively, placing a cryo-plant on the high voltage platform is a very expensive and non-practical plan. LHe recirculation with several cryo-coolers is widely used with 3rd generation ECR magnets, however it only provides very limited cooling power. Consequently, high excitation currents (typically several kA to 10 kA depending on the cable design) when the ECR magnet coils are wound with cables, result in very high heat load to the cryogenics system, which is not feasible for a 4th generation ECR magnet with cryo-coolers. Therefore, FEER magnet coils are all wound with single wire. Nevertheless, single wire design also has many other challenges, such as quench protection, coil winding and wire joints.

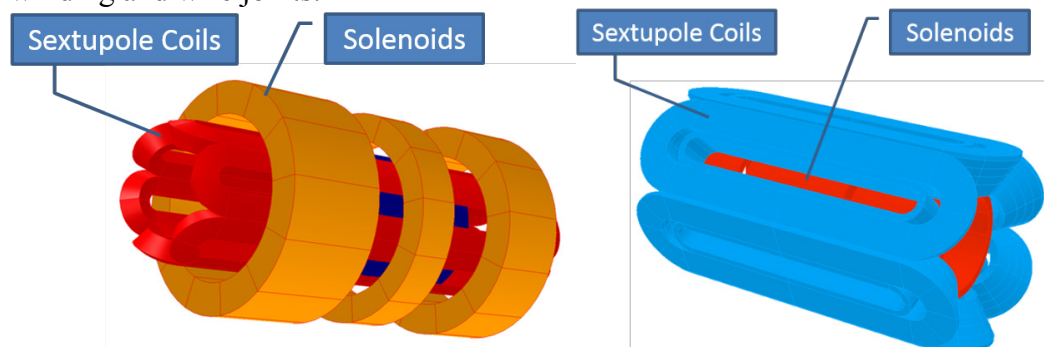


Figure 2: Conventional ECR magnet structure (left plot) and reversed ECR magnet structure (right plot).

2.3.3 Coil Fabrication

2.3.3.1 Solenoid Coils Fabrication

There are not many examples in the superconducting community using single Nb₃Sn wire to fabricate coils. Most of the experience is from Nb₃Sn magnet fabrication with cables, for instance the Large Hadron Collider (LHC) Accelerator Research Program (LARP) High Gradient Quadrupoles (HQ) models for the LHC luminosity upgrades uses 15.35 mm wide Nb₃Sn cable [11]. Nb₃Sn wire is very fragile and non-ductile, therefore, wind and cure strategy is widely adopted in Nb₃Sn coil fabrication. As a result, coil winding must be done with dry winding, i.e. no epoxy resin is allowed and the usage of non-organic glue also needs to be minimized to avoid any possible contamination that might degrade Nb₃Sn wire performance during heat treatment process. For solenoid fabrication, the winding on a cylindrical form is quite similar to dry winding a NbTi coil. The difference is that after coil winding aluminum strip can't be used for pretension when transferring from the winding fixture to the heat treatment tooling as aluminum material can't withstand the high temperature during heat treatment. Typically stainless steel strip or shell is used to keep the coil windings in position. After the heat reaction, Nb₃Sn solenoid will be potted with epoxy resin, and eventually the solenoids will be pre-stressed with aluminum strip of the designed thickness. There will be 4 solenoid coils for FECR, i.e. 2 injection solenoids, one middle solenoid and one extraction solenoid. For the needs of quench detection, every solenoid has been intentionally split into inner and outer halves and connected through a resistive joint as is shown in Fig. 3.

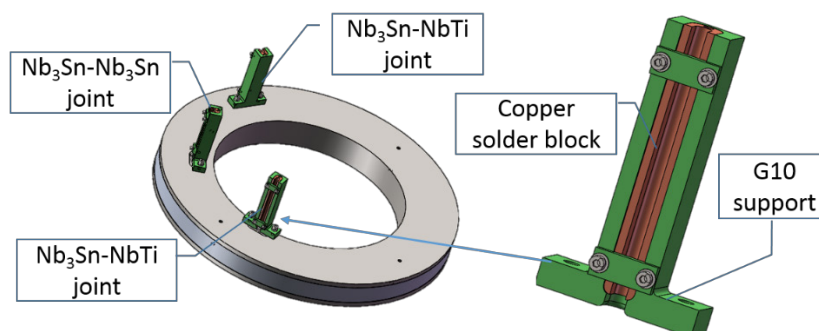


Figure 3: Structure of one of the FECR solenoids with an intermediate split for quench detection (left plot) and the joints designed for Nb₃Sn-NbTi or Nb₃Sn-Nb₃Sn (right plot).

2.3.3.2 Sextupole Fabrication

Compared to solenoids, sextupole coils fabrication is more challengeable that makes them the critical part in the coldmass fabrication. Different from circular contour solenoid coil, it is almost impossible to maintain the winding tension everywhere on the winding strand surrounding a sextupole coil as shown in Fig. 4. The highest forces will be applied to the ends, but there is barely any forces at the straight section. Therefore, specially designed winding tooling is very important and useful to keep every turns of winding in position. Conventional superconducting ECR magnet sextupole coils are mostly wound using wet winding method that relies on epoxy resin to glue every layers during winding, which makes it easy to keep each strand of the coil in position as designed during the winding process, but overall the mechanical conformance of the coil is not perfect and results in lower packing factor. Recently, the ECR ion source magnet developed for the Facility for Rare Isotope Beams (FRIB) has utilized dry winding together with vacuum

impregnation potting method that gives very neat and reliable sextupole coils. Compared to NbTi, one more process has been included in Nb₃Sn sextupole coil fabrication, i.e. heat reaction in furnace, which adds big challenges to the fabrication process. There has been very successful practice using Nb₃Sn cable to make dipole and quadrupole magnets [12, 13]. However, for FECR magnet, single wire scheme will be adopted for the sextupole coil preparation, and totally more than 800 turns of wire will be wound for every coil, which is more challengeable than previous references.

2.3.4 Cold Mass Structure

To make superconducting magnet work at the designed fields, proper magnet pretension and clamping is mandatory to avoid any physical movement of the superconducting coils during field ramping and avoid too high stresses stemmed from magnet cool-down from room temperature and lorentz forces during excitation of the coil. For ECR superconducting magnets, the situation is even more complicated as a result of

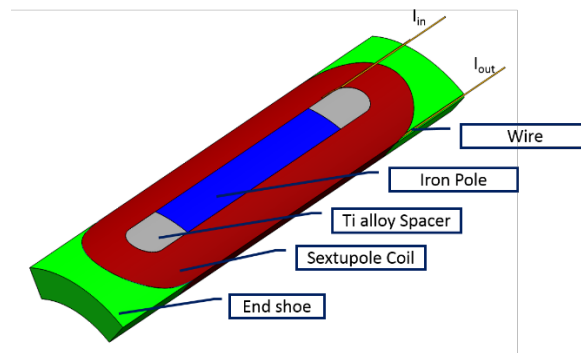


Figure 4: Schematic drawing of the sextupole coil for FECR magnet.

the mutual forces between the axial fields and sextupole radial fields. For conventional structure ECR magnet, represented by VENUS, whose cold mass was clamped with aluminum ring pre-tensioned with liquid bladders and aluminum tapes [14]. For reversed structure ECR magnet, represented by SECRAL, it had used properly designed negative tolerance aluminum rings to do shrink fitting installation on the coils so as to provide sufficient coil clamping and preloading [15]. Both the aforementioned solutions have worked successfully with the 3rd generation ECR magnets. However, unlike NbTi that is ductile and can withstand high compressive force, Nb₃Sn is brittle and strain sensitive. As a result, the current carrying capability of Nb₃Sn coils is affected by mechanical stresses in the windings. The actual behavior depends on several factors, such as the wire design and the fabrication process. However, reversible degradation is generally observed above 150 MPa with severe and permanent degradation occurring above 200 MPa [16]. In addition to high stresses, electromagnetic forces can cause local motion of the conductor leading to frictional energy dissipation and premature transitions quenches to the normal resistive state. Same as the 3rd generation NbTi ECR magnet, Nb₃Sn ECR magnet has complex electromagnetic force distributions and much higher in magnitude. It is therefore mandatory to carefully analyze the strain in the superconductor, and devise a support structure capable of minimizing the stress and motions in the coils from assembly to cool down and excitation.

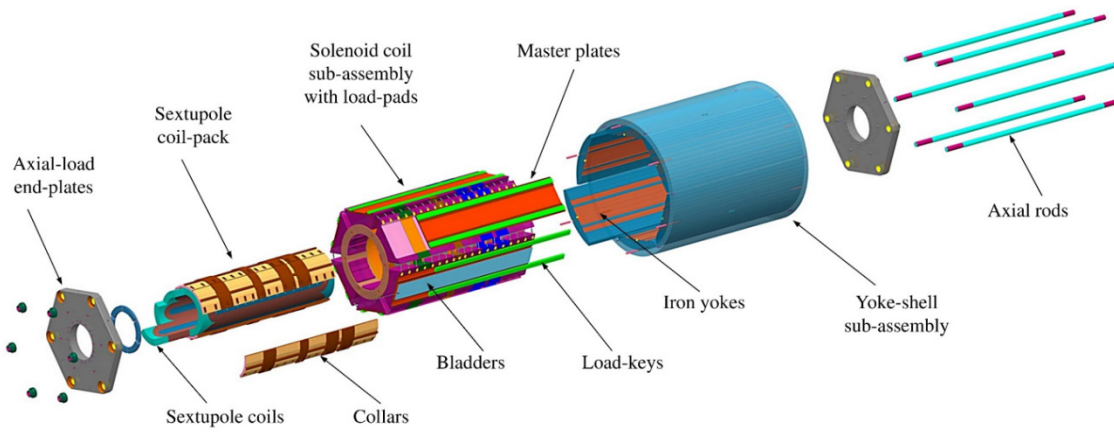


Figure 5: Exploded plot of FECR cold mass.

The significant increase of the confinement magnetic field as given in Table 1 and mechanic properties of Nb_3Sn wire bring fundamental challenges in the magnet design. For FECR magnet design, a structure based on an aluminum shell surrounding the coils and iron yoke, pre-tensioned with water-pressurized bladders and interference keys has been conceived. Previous conceptual design of a 56 GHz ECR magnet was reported 10 years ago [10]. For 45 GHz FECR magnet, an alternative approach has been made to have better control of the cold mass installation and clamping. In this design, aluminum shell supports the sextupole through longitudinal segmented loading pads placed in-between solenoids, and a thin continuous collar placed above the coil. This approach required splitting the injection solenoid in two sub-coils with an axial gap, in order to reduce the longitudinal span between sextupole pads. The solenoids are encased in a stainless steel forms and radially supported by a tensioned aluminum wire, with the aluminum shell providing additional support and alignment through a second set of loading pads interleaved with the first set. Axial support is provided to both sextupole and solenoid subassemblies by aluminum rods and end plates. The exploded view of the magnet structure is given in Fig. 5. More details have been presented in [16].

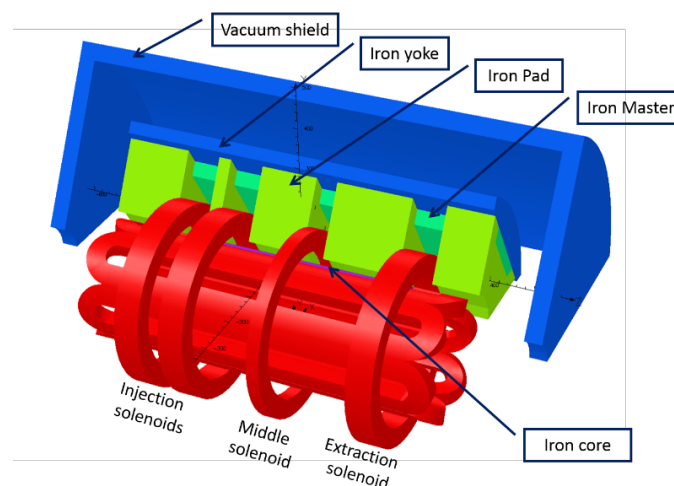


Figure 6: FECR magnet structure and the key components contributed to the magnetic fields.

To evaluate the effectiveness of the structure design, both 2D and 3D Ansys models have been built to give systematic analysis. Several types of materials have been

implemented in the design to minimize the stresses on the coils and provide robust clamping forces and tensions. Except for those key parts that have strict requirement of material yield strength or thermal expansion coefficient at 4.2 K are utilizing special materials, most of the other parts such as the yokes, sextupole center core, and sextupole load-pads and so on are all using iron material, so as to lower the stray fields and increase field efficiency inside the warm bore. A schematic magnetic structure of FECR is given in Fig. 6. Structure analysis has all the material choices included and the choices have also been optimized based on the simulation results. The simulation takes into account the stresses evolution from room temperature to cold-down, and then with magnetic forces when magnet being energized to full currents. Fig. 7 shows the distribution of Von Mises stress in the sextupole coil. While the calculated stress during bladder operation with all six bladders is approximately 116 MPa, the experience shows that when using one or two bladders at the time the stress value drops to a similar value as with load-keys inserted, which is 67 MPa [17]. The stresses after cool-down and with magnetic forces are below 155 MPa and the peak is located in the coil-ends. The radial pre-load is applied to solenoid coils using a 30 mm thick layer of pre-tensioned aluminum strip and stainless steel pads assembled around the banding in order to couple the solenoid system with the support structure. The maximum stress in solenoid coils after cool-down is 100 MPa and 126 MPa when magnetic forces are applied. Results of the analysis shows that, when magnetic forces are applied, coils remain radially compressed and most of their inner radius surface is in contact with their formers.

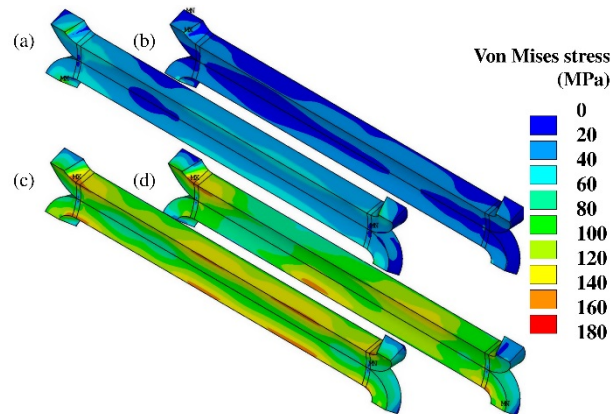


Figure 7: Von Mises stress in the sextupole during (a) the bladder operation, (b) the room temperature pre-load, (c) cool-down and (d) excitation.

2.3.5 Quench Protection

Quench protection is very essential to a superconducting magnet. Conventional 3rd generation ECR magnet built with NbTi wire are all using self-protection scheme that typically employs cold resistor and back-to-back diodes across the protected coil to reduce the hot spot temperature and the voltages to ground during the quench process. While for a Nb₃Sn ECR magnet like FECR, the protection of the magnet is more complicated and challenging for several reasons. First, the higher energy density stored in the conductor due to the higher magnetic field increases the potential for damage. Second, the normal-zone propagation velocities in the low-field regions are reduced due to higher thermal margin to quench. Third, the stabilizer fraction in Nb₃Sn internal tin wire is limited to lower range than NbTi wire, which increases the stabilizer current

density. Fourth, the choice of wire instead of cable as a conductor, in order to avoid the cabling process and to limit the operating current, significantly increases the magnets' self-inductances and decreases the turn-to-turn normal-zone propagation speed. Fig. 8 gives the simulation results of the quench process of one of the FEER injection solenoid. As is indicated, the quench does not propagate quickly enough to safely discharge the magnet around 700 A current excitation. Therefore, quick and efficient energy extraction is required. An active quench protection system based system consists of power supply unit, quench detection unit, and energy extraction unit, as shown in Fig. 9. Upon quench detection, the energy extraction switch is opened and the current is discharged due to the energy extraction resistance R_{EE} [Ω] and coil resistance R_C [Ω]. R_{EE} is selected for each coil as a compromise between a quick current discharge, calling for high resistance, and a low voltage to ground, calling for low resistance.

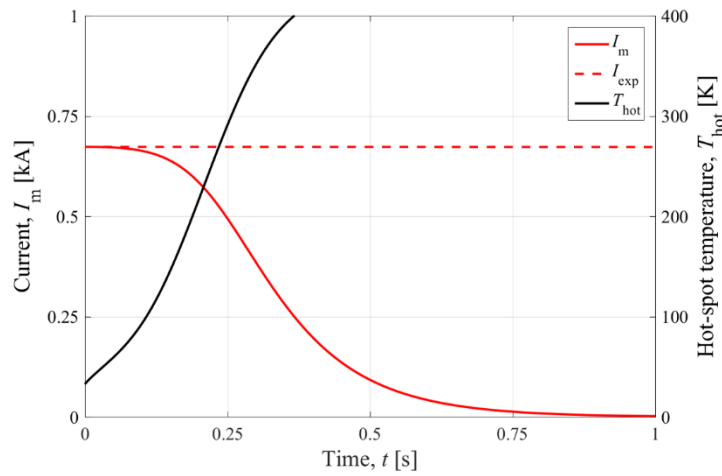


Figure 8: Quench simulation result of one of the injection solenoids with self-protection strategy.

The peak voltage across the EE resistor, reached just after EE triggering, is $U_{EE}=R_{EE}I_0$, with I_0 [A] the initial magnet current. This is the peak voltage to ground reached in the circuit during the quench transient, $U_g=U_{EE}$. However, it is possible to halve U_g by symmetrically grounding the circuit at the middle point of the EE resistor, as shown in Fig. 9b, hence obtaining $U_g \approx U_{EE}/2$. With this concept, Table 2 summarizes the energy extraction system performance for all FEER magnet coils. The quench protection of the sextupole magnet can be achieved with a 2 Ω EE system. However, in the case of SCR (Silicon controlled rectifier) failure $T_{hot}=337$ K, close to the maximum allowed temperature. Given the uncertainties on the model assumptions, wire parameters, and material properties, this margin is unsatisfactory. Furthermore, as FEER will be floated on a high voltage platform, the symmetric grounding scheme might be not applicable since any high voltage sparking can trigger a false quench signal according to the operation experience with several existing NbTi superconducting ECR ion sources. In that case, symmetric grounding design can't be implemented, and thus the 1 kV limit on U_g is exceeded. Therefore, protection of the sextupole magnet with energy-extraction is marginal. Powering and protecting separately sections of the sextupole magnet is not a viable option. However, an alternative approach to quench protection, based on Coupling-Loss Induced Quench system (CLIQ) [18], is feasible. CLIQ can improve the system redundancy and reduce the peak voltages to ground without the need of doubling the

powering and energy-extraction circuits. This possible solution is under investigation and a conceptual design has been made in [19].

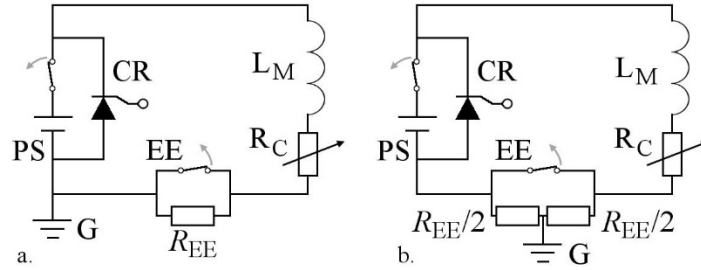


Figure 9: Simplified electrical schematic of one of the FEER coil circuits, including a power supply (PS), its crowbar (CR), the coil (LM), its resistance developing during a quench (R_c), an energy extraction system (EE), and the grounding (G). a. Standard grounding. b. Symmetric grounding.

Table 2: Performance of FEER magnet coils' energy extraction during quench.

<i>Parameter</i>	<i>Unit</i>	<i>Sextupole</i>	<i>Injection</i>	<i>Middle</i>	<i>Extraction</i>
EE resistor R_{EE}	Ω	2.0	0.5	1.5	4.3
Peak voltage to ground, U_g	V	654	95	470	1488
Hot-spot temperature, T_{hot}	K	260	64	249	315
T_{hot} in case of SCR failure	K	337	70	318	410

Note: in case of symmetric grounding not applicable, all values of U_g double.

2.3.6 Cryogenic Solution

FEER cold mass is designed to be immersed and working in a 4.2 K liquid helium bath. HTS leads will be used to minimize the heat load to 4.2 K stage. The current leads will share a common return loop so as to minimize the numbers of current leads. The baseline for FEER magnet is using 4 power supplies, i.e 3 for solenoids and 1 for the sextupole respectively. Thus, there will be totally 5 current leads needed. As FEER will be floated on a high voltage platform, it is not an applicable solution to connect the cryogenic system to liquid helium supply tubes from cryogen plant. Stand-alone operation cryogenic system integrated with cryocoolers will be a more viable technical approach that has been widely applied with most of the 3rd generation ECR ion sources. Experiences with the existing 3rd generation ion sources indicate that the 4.2 K cryocoolers should not only take away the static heat load from the cryogenic system, but also the dynamic heat load induced by the strong bremsstrahlung radiation from the hot dense ECR plasma. It is evident that the dynamic heat load to the 4.2 K cryogenic region has a ratio of ~ 1 w per kW of 24~28 GHz microwave power, which also varies with the B_{min} . ECR ion source operating with lower B_{min} see the heat load at 4.2 K reduced significantly [20]. Nevertheless, a 45 GHz ECR ion source will definitely be working at stronger magnetic field confinement that possibly needs much higher B_{min} . Additionally, the 45 GHz next generation ECR ion source will be working at higher microwave power to reach the performance limit, i.e. 20 kW or higher, which means more dynamic heat

load to the cryogenic system. Consequently, the 45 GHz FECR source magnet needs a total 4.2 K cooling capacity as high as possible, typically higher than 10 W.

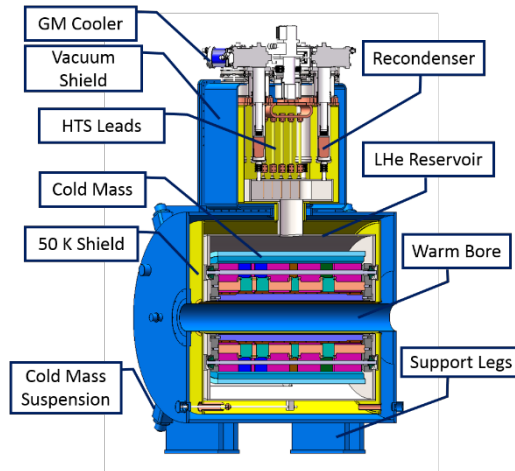


Figure 10: Sectional plot of FECR magnet and the typical components.

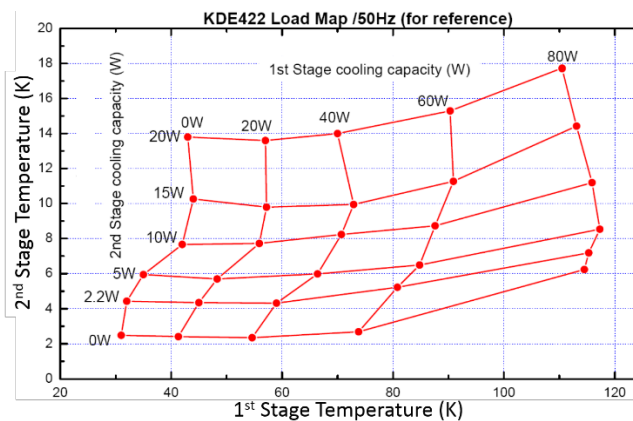


Figure 11: Typical load map of KDE422 GM cryocooler from Easycool.

For FECR magnet, as shown in Fig. 10, two stages design will be adopted for the cryogenic system, i.e. the ~ 50 K shield and 4.2 K liquid helium environment. As high excitation current will be needed for the Nb_3Sn coils, high ohmic heat will be created in the copper leads and therefore induces high heat load to the first stage. To minimize the heat radiation to the 4.2 K region, and also to maintain high enough temperature safety operation margin for the HTS leads, it is advantageous to design the first stage as ~ 50 K. Calculations indicate that a total of 201 W@50 K is needed for FECR magnet shield. Several options are available for the cryogenic solution with cryocooler scheme. For instance, 2 Gifford-McMahon/Joule-Thomson (GM-JT) coolers, one 2-stage Sumitomo RDK-415D and one single stage Sumitomo CH-110 will totally provide maximum 11.5 W@4.2 K, and ~ 205 W@50 K. As GM-JT coolers are not very technically matured, and sometimes not available in all commercial market around the world, this combination is not very feasible. Then, a combination of seven 2-stage 4.2 K GM coolers + 1 CH-110 cooler will also provide maximum 10.5 W@4.2 K and 345 W@50 K. Recently several product upgrade on 1.5 W@4.2 K 2-stage GM coolers have been made and will be soon released to be available in market, such as upgraded Sumitomo RDK-415 D with 30

W@50 K & ≥ 1.8 W@4.2 K, and Easycool KDE422 from a Chinese company with 24 W@44 K & 2.2 W@4.2 K (Fig. 11), which provide flexible combinations of cryocoolers to meet FECR magnet needs. For instance, 6 KDE-422 coolers + 1 Sumitomo RDK500B single stage cooler will give a solution of 13.2 W@4.2 K and ~ 280 W@50 K.

2.3.7 Conclusions

Compared to a NbTi magnet for the 3rd generation ECR ion source, a Nb₃Sn ECR magnet has more challenges to build. It is not just simply to replace the wire in the coils with another kind of material. As the goal of the 4th generation ECR ion source is more ambitious, the requirement to the magnet is stricter and more challenging, which makes the magnet harder to construct with the difficulties from not only the Nb₃Sn magnet characteristics but also the integration of such a magnet with an operating ECR ion source. This paper has summarized typical aspects in developing a 45 GHz ECR ion source magnet with Nb₃Sn wire. The challenges and key issues have been briefly presented and discussed. Institute of Modern Physics (IMP) in collaboration with the ATAP division in LBNL has finished the design of a Nb₃Sn based superconducting magnet system for a 45 GHz ECR ion source, as a injector ion source for LEAF facility at IMP and also the prototyping high performance ECR ion source for HIAF in Huizhou, China. The engineering design of the 45 GHz ECR ion source has been completed and the construction has been recently started. It is also worth mentioning here that the construction of a Nb₃Sn magnet is just one of the challenges in 45 GHz FECR source development [21]. 45 GHz microwave power transmission and coupling with and ECR plasma, strong bremsstrahlung radiation issues, intense beam extraction and transmission with high quality, and so on, are still open questions to be answered. The nominal completion time of the 45 GHz ECR ion source FECR is by the end of 2019.

2.3.8 Acknowledgements

This work took advantage of the great contributions from GianLuca Sabbi, M. Juchno, E. Ravaioli, D. Xie, A. Hafalia from LBNL, and H. W. Zhao, W. Wu, B. M. Wu, W. Lu and etc. from IMP. This work is also supported by NSFC (National Nature Science Foundation of China) research program with contract No.11427904 and the 973 Program of China (No. 2014CB845500).

2.3.9 References

1. R. Geller, *Rev. Sci. Instrum.* **69**, 1302 (1998).
2. D. Leitner, M. L. Galloway, T. J. Loew, C. M. Lyneis, I. Castro Rodriguez, and D. S. Todd, *Rev. Sci. Instrum.* **79**, 02C710 (2008).
3. H. W. Zhao, et al., *Rev. Sci. Instrum.* **83**, 02A320 (2012).
4. L. Sun, et al., *Rev. Sci. Instrum.* **87**, 02A707 (2016).
5. L. Sun, et al., in *Proc. of ECRIS2016*, Busan, Korea (2016), JACoW Archives, 43.
6. Y. Higurashi, J. Ohnishi, H. Haba, M. Kidera, K. Ozeki and T. Nakagawa, in *Proc. of ECRIS2016*, Busan, Korea (2016), JACoW Archives, 10.
7. Guillaume Machicoane, Dallas Cole, Kent Holland, Daniela Leitner, Dan Morris, Derek Neben and Larry Tobos, in *Proc. of ECRIS2014*, Nizhny Novgorod, Russia (2014), JACoW Archives, 1.

8. J. C. Yang, and et al., Nucl. Instr. Meth. B **317**, 263 (2013).
9. J. Benitez, K. Y. Franzen, C. Lyneis, L. Phair, M. Strohmeier, G. Machicoane, L.T. Sun, in Proc. of ECRIS2012, Sydney, Australia (2012), JACoW Archives, 153.
10. P. Ferracin, S. Caspi, H. Felice, D. Leitner, C. M. Lyneis, S. Prestemon, G. L. Sabbi, and D. S. Todd, Rev. Sci. Instrum. **81**, 02A309 (2010).
11. H. Felice, et al., IEEE Trans. Appl. Supercond. **19**, 1235 (2009).
12. S. Gourlay, et al., IEEE Trans. Appl. Supercond. **10**, 294 (2000).
13. G. Sabbi, IEEE Trans. Appl. Supercond. Vol. 23, No. 3, Art. 4000707, June 2013.
14. C. Taylor, et al., IEEE Trans. Appl. Supercond. **10**, 224 (2000).
15. L. Sun, W. Lu, E. M. Mei, GL. Sabbi, W. Wu, D. Xie and H. W. Zhao, “Superconducting Magnets for High Performance ECR Ion Sources”, IEEE Trans. Appl. Supercond., to be published as proceedings of 25th International Conference on Magnet Technology, RAI-Amsterdam, the Netherlands, Sept. 2017.
16. M. Juchno et al., “Mechanical design of a Nb₃Sn superconducting magnet system for a 45 GHz ECR ion source”, IEEE Trans. Appl. Supercond., to be published as proceedings of 25th International Conference on Magnet Technology, RAI-Amsterdam, the Netherlands, Sept. 2017.
17. M. Juchno et al., IEEE Trans. Appl. Supercond. Vol. 26, No. 4, Art. 4005506, June 2016.
18. E. Ravaioli, V. I. Datskov, C. Giloux, G. Kirby, H. H. J. ten Kate, and A. P. Verweij, IEEE Trans. Appl. Supercond., vol. 24, no. 3, Art. 0500905, June 2014.
19. E. Ravaioli et al., “Quench Protection of a Nb₃Sn Superconducting Magnet System for a 45 GHz ECR Ion Source”, IEEE Trans. Appl. Supercond., to be published as proceedings of 25th International Conference on Magnet Technology, RAI-Amsterdam, the Netherlands, Sept. 2017.
20. D. Z. Xie, W. Lu, J. Y. Benitez, C. M. Lyneis, D. S. Todd, in Proc. of ECRIS2016, Busan, Korea (2016), JACoW Archives, 141.
21. L. Sun, H. W. Zhao, J. W. Guo, Y. Yang, W. Lu, W. Wu, and L. Z. Ma, in Proc. of HIAT2015, Yokohama, Japan (2015), JACoW Archives, 268.

2.4 A Promising Magnet for the Next Generation of ECR Ion Source

Daniel Z. Xie

Mail to: zqxie@lbl.gov

Lawrence Berkeley National Laboratory
1 Cyclotron Road, Berkeley, CA 94720, USA

2.4.1 Introduction

A high strength minimum-B field is the prerequisite for an Electron Cyclotron Resonance Ion Source (ECRIS) with production of intense highly-charged heavy ion beams. Geller's scaling law predicts that ECRIS performance will improve with higher magnetic fields and heating frequencies [1]. This has been demonstrated by the successful

ECRIS developments in the past decades, especially by the performance of the 3rd generation NbTi-magnet-based ECRIS [2-7]. Next generation ECRIS operating with even higher magnetic fields will require superconducting magnets capable of producing minimum-B fields greater than 4 T for operation at frequency above 28 GHz. The production of these magnetic fields is out of the reach for magnets using NbTi conductor with the presently employed magnet schemes. While it appears feasible to achieve these fields with Nb₃Sn, this presents some major technical challenges. An attractive approach using a new magnet layout with NbTi conductor is being developed at Berkeley to meet the magnetic field requirements for a next generation ECRIS.

A minimum-B field, resulting from the superimposition of axial magnetic mirrors and radial multipole fields, is the key component of an ECRIS for confining the plasma electrons with millisecond-lifetime needed for the production of highly-charged ions. It provides a closed electron resonance heating surface in which the local field strength satisfies the relation:

$$\mathbf{B}_{ECR} = \frac{2\pi f m_e}{e} \quad (1)$$

where f , m_e and e are the incoming microwave frequency, the electron mass and charge, respectively. Based on the empirical ECRIS design criteria [8], the field maxima of a minimum-B configuration should be proportional to \mathbf{B}_{ECR} in the following manner:

$$B_{inj} \sim 3.5 - 4 \mathbf{B}_{ECR} \text{ and } B_{ext} \approx B_{rad} \geq 2 \mathbf{B}_{ECR} \quad (2)$$

where B_{inj} and B_{ext} are the axial peak fields at the injection and extraction regions, B_{rad} is the maximum radial field at the inner surface of the cylindrical plasma chamber commonly used in ECRIS. For microwaves at 28 GHz correspond to a resonance field strength \mathbf{B}_{ECR} of 1 T and therefore the ECRIS design criteria indicate B_{inj} should be $\sim 3.5 - 4$ T while B_{ext} and B_{rad} be at least 2 T.

2.4.2 Existing Magnets for ECRIS

Fig. 1 shows the two superconducting magnets presently employed in ECRIS: (a) Sextupole-In-Solenoids and (b) Solenoids-In-Sextupole. Because of the very strong

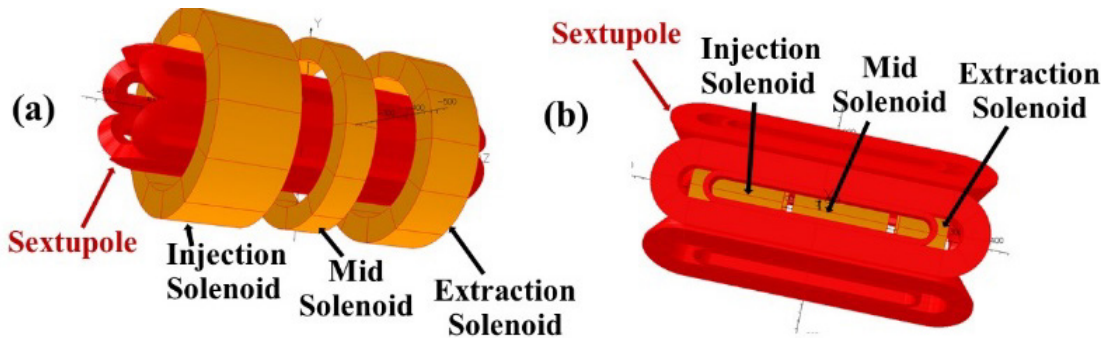


Figure 1: 3D models of the two existing superconducting magnets used in ECRIS: (a) Sextupole-In-Solenoids and (b) Solenoids-In-Sextupole. Each of the magnets has its own advantages and disadvantages.

Lorentz forces, i.e, the attractions and the repulsions resulting from the interactions between the solenoids and the sextupole coil ends, the length of the sextupole coils has to be extended in the Sextupole-In-Solenoids and this requires very elaborate clamping [9]. The Solenoids-In-Sextupole reduces the interaction forces and the magnet fabrication complexities but it does not efficiently utilize the radial fields. Table 1 lists the advantages and disadvantages of these two existing magnets.

Table 1: Comparison of the existing ECRIS magnets

Layout	Sextupole-In-Solenoids	Solenoids-In-Sextupole
Advantages	Better utilization of the radial fields (~50%)*	Lower and simpler interaction forces, slightly smaller magnet and cryostat, simpler fabrication with lower cost
Disadvantages	Longer and bulkier magnet and cryostat; Higher and stronger interaction forces	Inefficient use of the radial fields (~34%)*

*The utilization of radial field is defined as the ratio of the maximum radial field at the source plasma chamber inner surface over the field right at the inner pole tip of the sextupole

The radial field, B_{rad} , in the present superconducting ECRIS is generated by a sextupole consisting of six racetrack or saddle coils as shown in Fig. 2. The end-current of the sextupole coils flows adjacently in opposite direction yielding zero net axial field contribution, thus fairly large solenoids are used to provide all the needed mirror fields of a high field strength minimum-B. Furthermore, the alternative end-current interacts with the injection and extraction solenoids resulting in strong radial inward and outward forces on the sextupole coil ends [10]. This in turn requires an extended distance between the sextupole coil ends and the solenoids so the interaction forces can be managed.

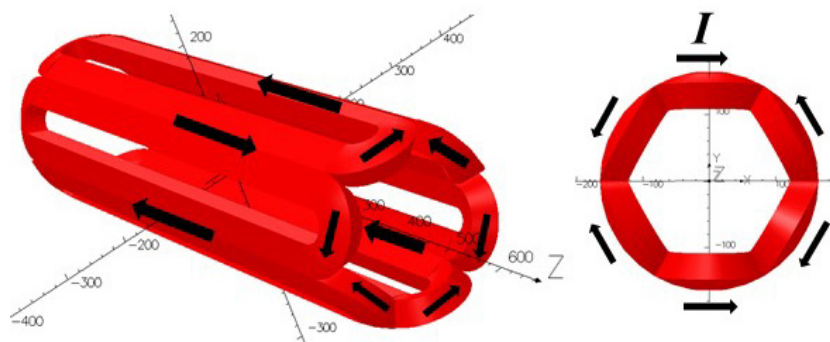


Figure 2: A 3D model of a sextupole consisting of six racetrack coils commonly used in ECRIS, in which the coil end-current I (indicated by the black arrows) flows adjacently in opposite direction yielding zero net axial field contribution to the minimum-B field.

The LBNL VENUS was built with a Sextupole-In-Solenoids NbTi magnet and a cylindrical plasma chamber. It was the first ECRIS to reach 4T on axis and 2.2 T at the plasma chamber inner surface for operation at 28 GHz [3]. The IMP SECAL-I and SECAL-II, built with a Solenoids-In-Sextupole NbTi magnet, reached 3.6T on axis and 2-2.2 T radially for operation at 24 and 28 GHz [4, 11]. These three ion sources have

produced many record ECRIS ion beams [12-14] demonstrating that the ECR plasma is independent of the magnet scheme, as long as a high strength minimum-B is provided. In addition, there are other 3rd generation superconducting ECRIS built using the Sextupole-In-Solenoids NbTi magnets in operation, which are contributing to the advancement of ECRIS technology, such as the SuSI at MSU and SCECR at RIKEN [5-6].

2.4.3 A Promising New Magnet for Future ECRIS

The next generation of ECRIS will operate at substantially higher magnetic fields and higher frequencies to meet the ion beam intensities needed by future heavy ion accelerators, such as the Electron Ion Collider (EIC), and to upgrade the existing facilities. These high magnetic fields, preferably as high strength as possible, will require the use of Nb₃Sn magnets. A straightforward extrapolation of the Sextupole-In-Solenoids magnet employed in present 3rd generation ECRIS indicates that magnetic fields of about 8T on axis and 4 T at the inner surface of the plasma chamber could be achieved with Nb₃Sn coils [15]. However there is still room to further optimize the magnet design and the following sections will focus on a new superconducting magnet for future ECRIS.

2.4.3.1 *MARS Concept and Magnet Scheme*

MARS, a Mixed Axial and Radial field System, is a new magnet scheme aiming to optimize the magnetic field generation and to mitigate the very strong and complex Lorentz interactions occur in the superconducting magnets for ECRIS [16].

Fig. 3 shows the key component of the MARS concept: a closed-loop-coil constructed by combining six straight bars of rectangular cross-section and two tri-segmented-hexagon end solenoids into a single coil. In contrast to the zero axial field contributions of a conventional sextupole, this closed-loop-coil generates both radial and significant axial fields as its end currents all flow in the same direction resulting in a minimum-B field by itself. Fig. 4 (a), (b) and (c) show the axial, the radial, and the resulting minimum-B fields generated by a closed-loop-coil enclosed by a slightly asymmetric iron yoke (not shown in Fig. 3).

While the closed-loop-coil generates a minimum-B field, the axial field mirrors are still required for applications in ECRIS. This can be easily done by taking the advantage of the lack of repulsive forces between the solenoids and the closed-loop-coil ends, i.e., additional solenoids can be located right inside, outside or next to the ends of the closed-loop-coil. Thus a set of auxiliary small solenoids completes MARS for ECRIS.

The sextupole field strength is proportional to the square of the radial distance r :

$$B_r(r) = B_{rm} \left(\frac{r}{R}\right)^2 \quad (3)$$

where B_{rm} is the maximum pole field strength at the inner surface of the chamber of radius R . For optimum utilization of the radial fields generated by MARS, a hexagonal plasma chamber is to be used to match the pole field and the cryostat hexagonal warm-bore housing the closed-loop-coil. As schematically shown in Fig. 5, a hexagonal chamber

more effectively uses the generated radial pole fields and increases the maximum radial field by a factor of $\chi = (R_{\text{maj}}/R_{\text{min}})^2 \approx 1.33$, where R_{maj} and R_{min} are the major and minor radii of a hexagonal chamber, and R_{min} is also the radius of a cylindrical chamber if used in a MARS magnet.

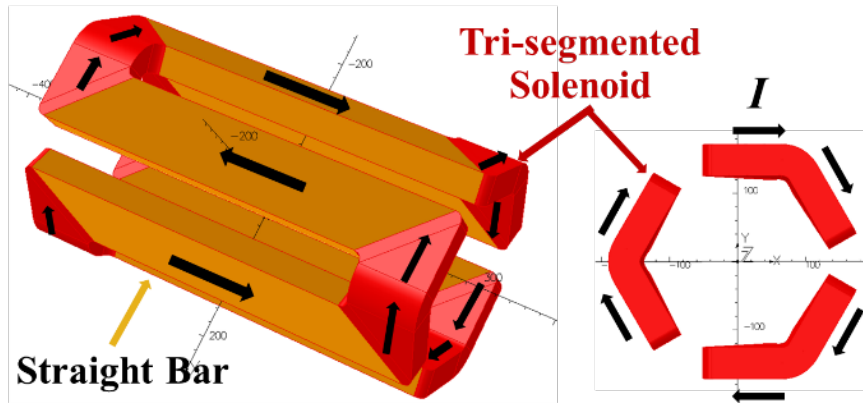


Figure 3: A 3D model of a MARS closed-loop-coil constructed by combining six straight bars with two tri-segmented-hexagon end-solenoids. All the end-currents (indicated by the black arrows) I flow in the same azimuthal direction.

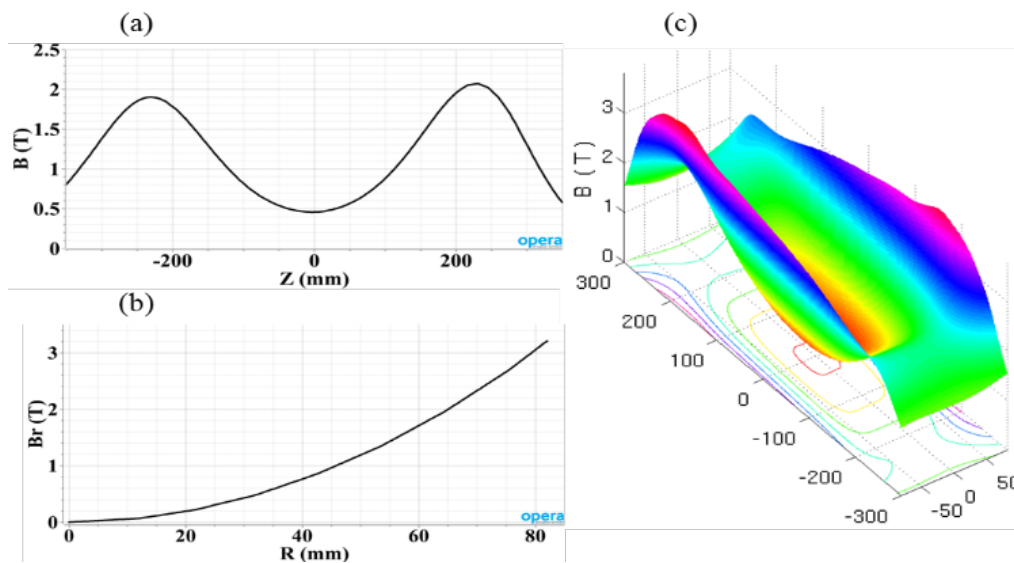


Figure 4: OPERA-3D magnetic field calculations of a MARS closed-loop-coil: (a). Axial field profile in which the slight asymmetry is due to the asymmetric enclosing iron yoke; (b). Radial field profile for an inner chamber radius up to 82 mm; (c). Field contours of the resulted minimum-B field.

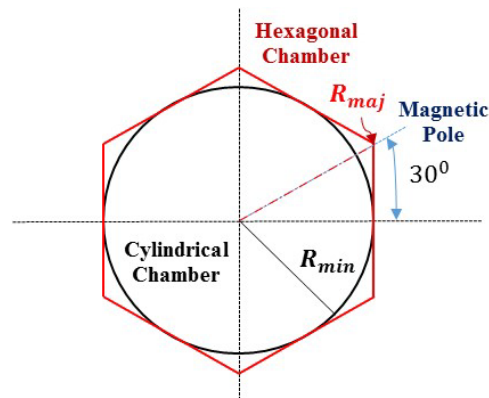


Figure 5: A hexagonal plasma chamber matching the MARS closed-loop-coil has a better geometric form factor than the existing cylindrical designs used in ECRIS. The effective use of the generated radial pole fields can increase the maximum radial field at least 30%.

Compared to the magnets presently used in ECRIS: Sextupole-In-Solenoids and Solenoids-In-Sextupole, a MARS magnet has the following advantages:

- The best utilization of the radial field ($\sim 67\%$ compared to $\sim 50\%$ and 34%);
- The lowest and least complex interaction forces allowing a much simpler coil clamping scheme;
- Uses substantially less conductor which lead to smaller sizes of magnet and cryostat;
- The minimum-B field generated by a NbTi MARS magnet could reach $\sim 5.5\text{-}6\text{T}$ on axis and $\sim 3.0\text{-}3.4\text{ T}$ at the plasma chamber, sufficient to support ECRIS operations at frequency up to $\sim 40\text{-}45\text{ GHz}$, while the existing NbTi magnets are limited to $\sim 28\text{ GHz}$ operations;
- A Nb₃Sn MARS magnet could likely produce $\sim 10\text{T}$ on axis and $\sim 6\text{T}$ at the plasma chamber for supporting ECRIS operations up to $\sim 80\text{-}84\text{ GHz}$. In comparison the existing magnet schemes built with Nb₃Sn can reach fields likely up to only 8T on axis and 4T at the plasma chamber surface for operations at $45\text{-}56\text{ GHz}$.

These advantages of a MARS magnet offset the disadvantages of the increased mechanical complexity in the fabrication of the magnet and the cryostat with hexagonally-shaped warm bore and inner thermal shield.

2.4.3.2 *A MARS Demonstration*

Presently a demonstration ECRIS named MARS-D, based on a NbTi MARS magnet, is under development at Lawrence Berkeley National Laboratory to validate the MARS magnet for applications in ECRIS and to enhance the capabilities of the 56-year-old 88-Inch Cyclotron [17]. Fig. 6 shows the design-in-progress MARS magnet and its cold-mass assembly which has been further optimized by employing a few new features:

- Hexagonally-shaped solenoids in combination with the closed-loop hexagon coil;
- Split solenoids at injection and extraction to reduce the maximum field at the closed-loop-coil so that it could operate at as high current as possible;

- Coils and a protection envelop are vacuum epoxy impregnated together as a module for easier magnet assembly and clamping to reduce the macroscopic coil movements.

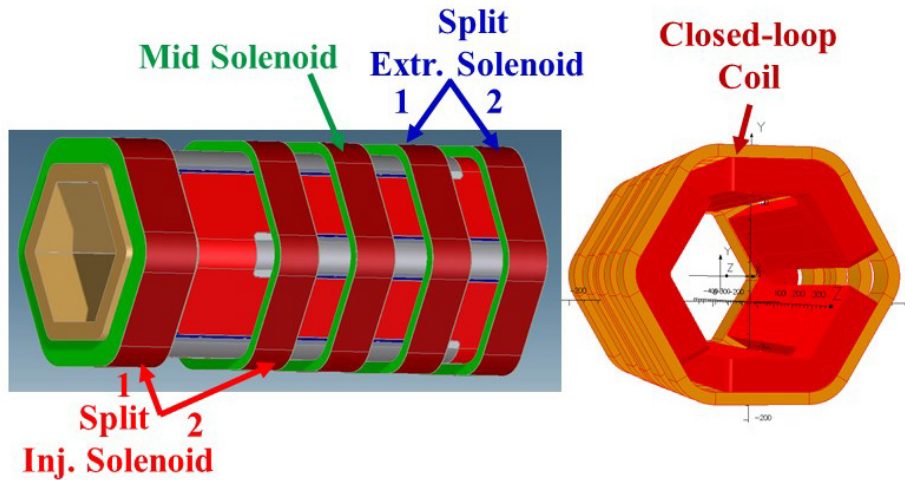


Figure 6: Coil configuration of the optimized MARS magnet for MARS-D. All the coils are to be epoxy impregnated together for easier magnet assembly and clamping.

Fig. 7 (a) and (b) show the computed maximum axial field and the resulting minimum-B field, generated by the MARS magnet shown in Fig. 6, in which the maximum radial field is the same as shown in Fig. 4 (b). Within the NbTi conductor constraints, the designed magnet for MARS-D should be able to generate axial peak fields of 5.6 and 3.3 T separated axially 520 mm, and a maximum radial field of 3.2 T at the 82 mm major radius of a hexagonal plasma chamber having about the same chamber volume as in VENUS. These field strengths meet the design criteria for operations up to 40-45 GHz, i.e., a next generation ECRIS. Table 2 lists the major coil parameters for the designed MARS magnet and magnetic fields with various engineering current densities. To generate the field strengths stated above for MARS-D, the peak fields on the coil conductors reach 7.6 T and about 8 T for the closed-loop-coil and the injection solenoid, respectively. These maximum fields on the coils are feasible with the NbTi conductor and therefore a NbTi MARS magnet can likely be built for the MARS-D ECR ion source.

The calculated magnet stored energies, a manifestation of the overall size and the excitations of a magnet system, clearly indicate the merits of the MARS magnet scheme. To generate the same fields for 28 GHz operations, the 212 kJ stored energy in MARS is just ~ 30% of the stored energy in a Sextupole-In-Solenoids for VENUS. As tabulated in Table 2, MARS requires only ~ 8.2 km of a rectangular NbTi wire (1.92 mm x 1.23 mm) to construct the magnet for operations to 45 GHz, while the VENUS' Sextupole-In-Solenoid magnet would need 18.5 km of the same wire and produce fields for operations to only 28 GHz. For operation frequency above 45 GHz, Nb₃Sn magnets would be needed. With the assumptions of 90% wire packing and ~ 85% of short sample wire loading as indicated in Fig. 8, Oxford Instruments' 6867 NbTi wires (1.92 mm x 1.23 mm, Cu/Sc: 1.35) could be used for constructing the magnet for MARS-D. If this magnet design could be built with the OI 2004 RRP Nb₃Sn wires it would generate a minimum-B field of ~ 10.5T on axis and ~ 6 T radially at the 82 mm major radius of a hexagonal plasma chamber for future higher field ECRIS.

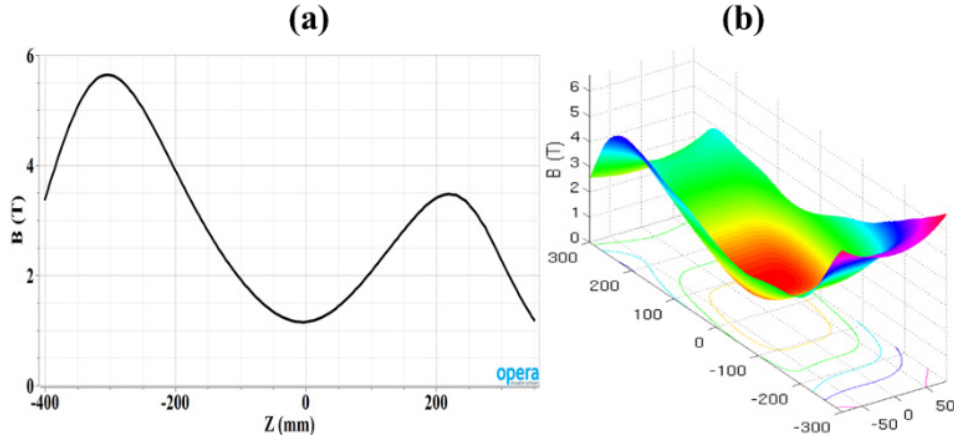


Figure 7: (a). OPERA calculated axial magnetic field profile for MARS-D. (b). Histogram of the resulting minimum-B shows a field minimum at the center. These fields meet the design criteria for ECR operations up to 45 GHz.

Table 2: Major Parameters of the MARS Magnet and Extrapolations

<i>Total magnet length (L = 642 mm)</i>	<i>CIC^a</i>	<i>Inj. Solenoid (1/2)</i>	<i>Mid Solenoid</i>	<i>Extr. Solenoid (1/2)</i>
Axial center (mm)	0	-322/-120	0	120/240
Mini. ID (mm)	200	200/282	282	282/282
Thickness (mm)	41	56/15	15	15/15
Width (mm)	92	90/60	60	60/60
At eng. current density j_e (A/mm ²)				
28 GHz	135	115	-150	270
45 GHz	195	160	-60	210
56 GHz	255	240	-150	270
84 GHz	375	310	-150	370
B (T) radial^b/axial				
28 GHz	2.2	4.1	0.7	3.0
45 GHz	3.2	5.6	1.1	3.5
56 GHz	4.1	8.0	1.3	4.4
84 GHz	5.9	10.5	2.1	6.2
B_{max} (T) at coil^c (at designed j_e)				
28 GHz	5.8	5.9	4.2	5.6
45 GHz	7.6 (0.7)	7.95 (1.4)	4.9	5.9
56 GHz	10.0 (1.1)	11.5 (1.9)	6.7	7.7
84 GHz	14.3 (1.5)	14.7 (2.7)	8.8	10.5
Magnetic stored energy E (kJ) at designed j_e		In comparison:		
28 GHz	212	715 (VENUS@28GHz, [9])		
45 GHz	420			
56 GHz	707	2900 (VENUS56, [15])		
84 GHz	1346			
Total wire ^d usage (km)	8.2	18.5 (VENUS@28GHz)		

^aCIC = Closed-loop-coil.

^bAt major radii of 82 mm of the hexagonal plasma chamber.

^cThe fields quoted in the parentheses are the maximum fields contributed from other coils while the noted coil itself is at zero excitation.

^dOI 6867 rectangular NbTi wire (1.92 mm x 1.23 mm) and 2.5 mm² assumed in winding.

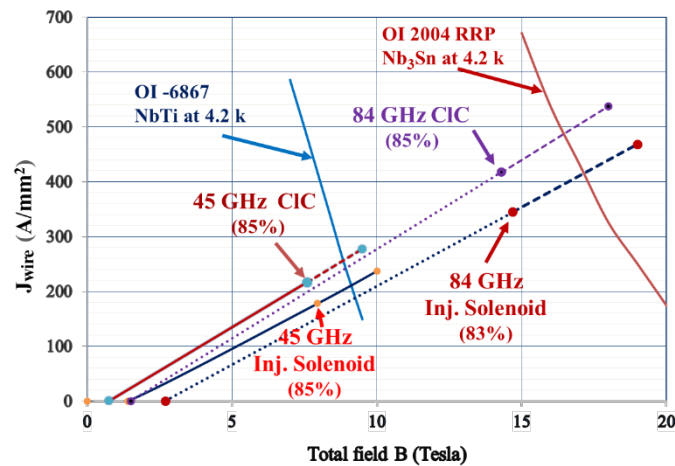


Figure 8: Designed load lines of the closed-loop-coil (CIC) and the injection solenoid of the MARS magnet with the indicated OI NbTi (for MARS-D) and Nb₃Sn wires (for future higher field ECRIS with operations up to ~ 84 GHz).

2.4.3.3 MARS Closed-loop-coil Prototyping

Fabrication of a superconducting closed-loop-coil is the most critical challenge in realizing a MARS magnet. The challenge is to keep the dry tensioned wire in place, in which a set of special winding fixtures and winding procedures need to be developed. To explore the feasibility of such a closed-loop-coil, a test winding has been carried out at LBNL using rectangular copper wire of about the same size as the Oxford Instruments 6867 NbTi wire. The copper closed-loop-coil being prototyped is about the same size as the one designed for MARS-D, except the thickness is about 1/3 of the full design. Shown in Fig. 9 are the wound and epoxy impregnated prototype copper coil and the sliced coil samples indicating satisfactory fabrication quality. Fig. 10a and 10b show the measured axial and radial field profiles at low current and comparisons to the OPERA calculations. The measured field tomography has validated the MARS closed-loop-coil design concept and we are very confident that a NbTi MARS magnet for the demonstration ECRIS: MARS-D, will be fabricated in the near future.

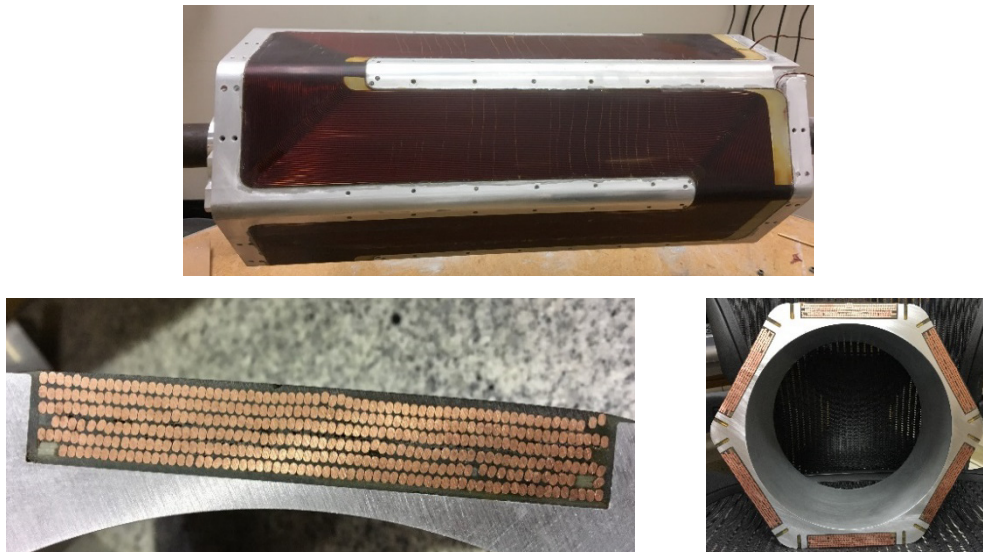


Figure 9: The wound and epoxy impregnated prototype closed-loop copper coil in its winding fixture. The other two photos are the sliced samples showing satisfactory fabrication quality.

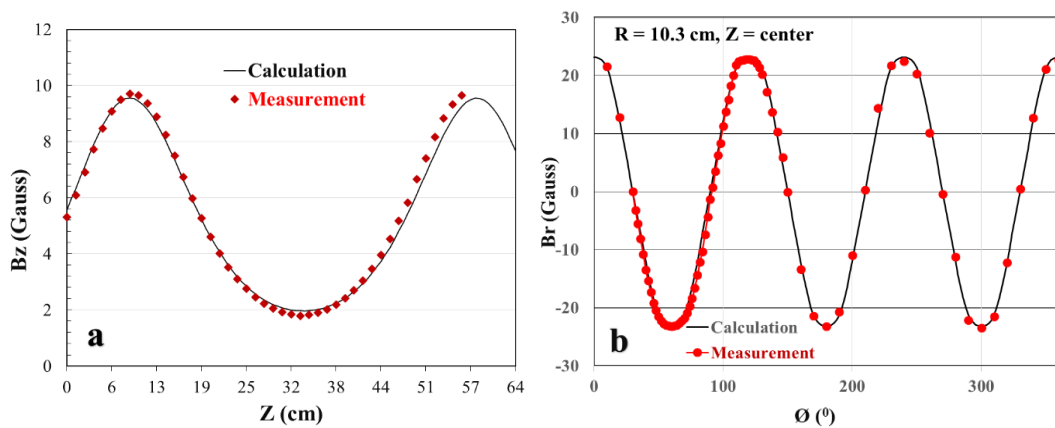


Figure 10: Field tomography of the prototyped copper MARS closed-loop-coil. a. The measured axial field profile (red diamonds) in comparison to the OPERA calculation (black solid line); b. The measured central radial field profile (red dots) at $R = 10.3$ cm against the calculation (black solid line).

2.4.4 Discussions and Conclusion

Beside the MARS magnet, there are a few other possible magnet schemes for future ECRIS, such as a Solenoids-In-Sextupole magnet with a skewed sextupole and a Sextupole-In-Solenoids magnet with a V-bend sextupole [18], and a Canted Cosine Theta (CCT) Structure [19-20]. These possible magnet schemes, which can be further refined, are either an optimization of the existing magnets or a new magnet layout with various advantages over the existing magnets. However, like MARS, none of them has been built and validated in ECRIS. MARS is the most advantageous among all the possible schemes in terms of magnetic field generation, mitigating the interaction forces and usage of conductor, which could be a significant factor in the rather expensive superconductor, such as Nb_3Sn or High Temperature Conductor. That is, MARS will be the best magnet scheme for future ECRIS, once validated.

Constructing a MARS magnet with Nb₃Sn wires would be more challenging than a NbTi one and many issues need to be addressed, such as the Nb₃Sn wire brittleness, the poor ductility, the available length of monolithic wire and the post-heat-react treatments. It would significantly advance the ECRIS technology if a Nb₃Sn MARS magnet can be developed to generate field maxima of ~ 10.5 T on axis and ~ 6 T radially to support ECRIS operations up to ~ 80 GHz. An ECRIS operating at such high frequency is expected to significantly enhance the ECRIS performance on the intensity of multiply-charged ion beams and the charge state of heavy ions as extrapolated in Fig. 11a and 11b.

The development of a MARS magnet for an ECRIS, MARS-D, has achieved a milestone demonstrating the feasible fabrication of at least an NbTi closed-loop-coil. The successful fabrication and operation of MARS-D would substantially advance the ECRIS technology and extend the usefulness of NbTi magnets to the next generation ECRIS. A 45 GHz ECRIS built with a NbTi magnet should result in substantial cost savings and relatively simpler fabrication in comparison to a conventional Nb₃Sn magnet for the next generation ECRIS.

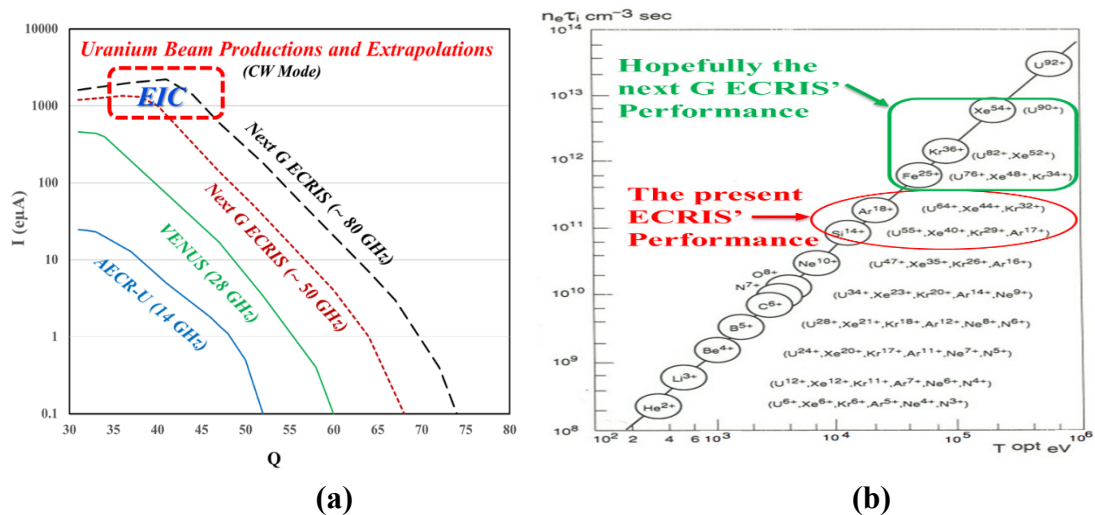


Figure 11: (a). Performance of the AECR-U and VENUS at LBNL and extrapolations of next generation ECRIS. The future ECRIS operating at 50 GHz and 80 GHz should satisfactorily meet the EIC beam demands. (b). The future ECRIS could be capable of producing the highly-charged ion beams, such as bare Kr, Xe and helium-like uranium ion beams, at lower intensities.

2.4.5 References

1. R. Geller *et al.*, "The Grenoble ECRIS Status 1987 and Proposals for ECRIS Scalings," Proc. of the 8th ECR Workshop, NSCL Report: MSUCP-47 (unpublished), E. Lansing, MI, USA, 1987, p1.
2. S. Gammino, G. Ciavola, L. Celona, D. Hitz, A. Girard, and G. Melin, "Operation of the SERSE superconducting electron cyclotron resonance ion source at 28 GHz," Rev. Sci. Instrum. **72**, 4090 (2001).

3. C. M. Lyneis, Z. Xie and C. Taylor, "Development of the third generation electron cyclotron resonance ion source," *Rev. Sci. Instrum.*, vol. 69, no. 2, 1998.
4. H. W. Zhao *et al.*, "Advanced superconducting electron cyclotron resonance ion source SECRAL: Design, construction, and the first test result," *Rev. Sci. Instrum.*, vol. 77, 03A333, 2006.
5. P.A. Zavodszky *et al.*, "Design of SuSI — Superconducting source for ions at NSCL/MSU - I. The magnet system," *AIP Conf. Proc.* 749 (2005) 131.
6. T. Nakagawa *et al.*, "First Results from the New RIKEN Superconducting Electron Cyclotron Resonance Ion Source," *Rev. Sci. Instrum.* **81**, 02A320 (2010).
7. B. S. Lee, S. Choi, J. H. Yoon, J. Y. Park, and M. S. Won, "Manufacturing of a Superconducting Magnet System for 28 GHz Electron Cyclotron Resonance Ion Source at KBSI," *Rev. Sci. Instrum.* **83**, 02A347 (2012).
8. D. Hitz, A. Girard, G. Melin, S. Gammino, G. Ciavola and L. Celona, "Results and interpretation of high frequency experiments at 28 GHz in ECR ion sources, future prospects," *Rev. Sci. Instrum.*, vol. 73, no. 2, 2002.
9. C. E. Taylor *et al.*, "Magnet System for an ECR Ion Source," *IEEE Trans. Appl. Supercond.*, vol. 10, no. 1, March 2000.
10. C. E. Taylor, Internal Design Report (1997, unpublished).
11. L. Sun *et al.*, "Status Report of SECRAL II Ion Source Development," Proceedings of ECRIS-2014, Nizhny Novgorod, Russia (2014).
12. L. Sun *et al.*, "Advancement of highly charged ion beam production by superconducting ECR ion source SECRAL," *Rev. Sci. Instrum.* **87**, 02A707 (2016)
13. D. Z. Xie, W. Lu, J. Y. Benitez, C. M. Lyneis, D. S. Tod, "Recent Production of Intense High Charge Ion Beams with VENUS," Proceedings of ECRIS-2016, Busan, S. Korea Aug 28- Sept 1, 2016 (to be published).
14. H. W. Zhao *et al.*, "Superconducting ECR Ion Sources: From 24-28 GHz SECRAL to 45 GHz FEER," invited talk at ICIS2017, Geneva, Swiss, Oct 15-22, 2017 (to be published).
15. C. Lyneis, P. Ferracin, S. Caspi, A. Hodgkinson and G.L. Sabbi, "Concept for a fourth generation electron cyclotron resonance ion source," *Rev. Sci. Instrum.* **83** 02A301 (2012).
16. D. Z. Xie, "A new structure of superconducting magnetic system for 50 GHz operations," *Rev. Sci. Instrum.*, vol. 83, 02A302, 2012.
17. D. Z. Xie *et al.*, "Development status of a next generation ECRIS: MARS-D at LBNL," *Rev. Sci. Instrum.* **87**, 02A702 (2016).
18. D. Z. Xie, W. Lu, G. Sabbi, D. S. Todd, "Possible Optimizations of Existing Magnet Structures for the Next Generation of ECRIS," Proceedings of ECRIS-2016, Busan, S. Korea Aug 28- Sept 1, 2016 (to be published).
19. L. Sun *et al.*, "Superconducting Magnets for High Performance ECR Ion Sources," Proceedings of 25th International Conf. on Magnet Technology, RAI-Amsterdam, Aug 27-Sept 1, 2017 (to be published).
20. S. Caspi *et al.*, "A superconducting magnet mandrel with minimum symmetry laminations for proton therapy," *Nucl. Inst. Methods*, vol. 719, no. 11, pp. 44–49, Aug. 2013

2.5 Instabilities in ECRIS plasmas

Olli Tarvainen

Mail to: olli.tarvainen@jyu.fi

Department of Physics, University of Jyväskylä, 40500 Jyväskylä, Finland

2.5.1 Introduction

The performance of an Electron Cyclotron Resonance Ion Source (ECRIS) is traditionally quantified by measuring the beam current and quality of the extracted ion beams of different charge state ions. The stability of the extracted ion beam currents has drawn more attention recently as the technology is pushing its limits towards higher ion charge states and beam intensities. The stability of the ion beams extracted from ECR ion sources is affected by two factors. The long-term stability is often related to conditioning (outgassing, oxidation) and accumulation of contaminants on the surfaces of the plasma chamber as well as technical solutions related to the injections of the ionized material, e.g. ovens and sputter samples, which can gradually, i.e. over hours or days, affect the plasma properties and intensities of the extracted beams. The short-term stability is determined by plasma instabilities manifesting themselves as rapid oscillations of the beam currents in millisecond scale [1]. Such fluctuations are often periodic and pose problems for applications such as carbon therapy tumor treatment where utmost short-term stability is required to accurately control the dose received by the patient [2].

In the following we will focus on the fast oscillations of the beam current driven by kinetic plasma instabilities in cw operation mode of ECRIS. The physical reasons for the appearance of the instabilities are introduced and their impact on the ECRIS performances including charge breeders is presented. Finally, we discuss the suppression of the beam current fluctuations by two frequency heating and list open research questions related to ECRIS plasma instabilities.

2.5.2 Classification of ECRIS plasma instabilities

Plasma instabilities can be divided into two general groups; (i) magnetohydrodynamic (MHD) instabilities driven by the topology of the magnetic field and (ii) kinetic instabilities stemming from the “free energy” associated to the electron velocity distribution (EVD) of the plasma. The mathematical description of the two instability categories differs significantly; MHD phenomena are typically treated with fluid models while the instabilities related to the EVD require kinetic plasma description. Although both types of instabilities can lead to observable fluctuation of particle losses (beam current), only kinetic instabilities are believed to affect the performances of minimum-B ECR ion sources as the MHD-instabilities are suppressed by the magnetic field topology and magnetic pressure exceeding the particle pressure, i.e. $n_e k T_e < B^2 / 2\mu_0$, in so-called high-B operation mode [3,4] being the standard for state-of-the-art ECR ion sources.

2.5.2.1 *Kinetic instabilities*

The electron velocity distribution (EVD) of ECRIS plasmas is strongly anisotropic. This is due to the stochastic nature of the resonant electron heating mechanism, which

favors velocity space diffusion in v_{\perp} direction resulting in $\langle v_{\perp} \rangle \gg \langle v_{\parallel} \rangle$, where the subscripts refer to the direction of the external magnetic field. Furthermore, it is commonly accepted that at least three electron populations with average energies (order of magnitude) of $\langle E_{e,cold} \rangle = 10 \dots 100$ eV, $\langle E_{e,warm} \rangle = 1 \dots 10$ keV and $\langle E_{e,hot} \rangle > 10$ keV can be identified [5]. The warm electrons contribute to the ionization and excitation processes of highly charge ions while the hot electron component carries most of the plasma energy content [6]. The anisotropic electron velocity distribution with a significant “free energy” associated with the hot electron population is prone to kinetic (electron cyclotron) instabilities as witnessed by ECRIS researchers and discussed here.

2.5.3 Electron cyclotron instabilities in ECRIS plasmas

Electron cyclotron instabilities are driven by hot electrons interacting resonantly with electromagnetic plasma waves. A characteristic feature of the electron cyclotron plasma instabilities (independent on the mode) is the emission of microwaves. The energy of the microwave emission E_{μ} can be described by mode-dependent [7] growth and damping rates γ and δ as

$$\frac{dE_{\mu}}{dt} \approx \langle \gamma - \delta \rangle E_{\mu} \quad (1)$$

i.e. the intensity of the microwave emission is an exponential function of the difference of the growth and damping rates, which depend on the mode of the microwave emission. Since the instabilities are triggered by the anisotropy of the EVD their (volumetric) growth rate is proportional to the ratio of hot and cold electron densities. The damping rate is determined by volumetric absorption of the wave energy by the collisional background plasma and external (wall) losses.

The balance equation [7] of the hot electron (number) density $N_{e,hot}$ can be written as

$$\frac{dN_{e,hot}}{dt} \approx -\kappa N_{e,hot} E_{\mu} + S(t) - L(t) \quad (2)$$

where κ is a coefficient describing the amplification of the electromagnetic wave and corresponding decrease in the hot electron component due to direct energy loss, $S(t)$ is the source term of hot electrons, i.e. stochastic heating, and $L(t)$ is their loss term due to collisional velocity space diffusion, inelastic collisions and rf-induced pitch angle scattering. In quiescent steady-state ECRIS plasma the damping rate exceeds the growth rate and the source and loss terms of hot electrons cancel out. In unstable operation conditions $S(t) > L(t)$, which causes the anisotropy of the EVD to increase until the condition $\gamma > \delta$ is met and the instability grows exponentially in time.

The transition from stable to unstable ECRIS plasma regime is affected by the magnetic field strength, microwave power, neutral gas pressure and gas species as demonstrated in Fig. 1 showing the instability threshold value of B_{min}/B_{ECR} as a function of microwave power for different gaseous elements (He, Ar, Xe). The most critical tuning parameter affecting the occurrence of the cyclotron instabilities is the (solenoid) magnetic field strength quantified here by the ratio of the minimum field to the resonance field i.e. B_{min}/B_{ECR} . Increasing the magnetic field strength above the given threshold results in

periodic onsets of the instabilities thereby suggesting that the magnetic field largely determines the electron velocity distribution in ECRIS plasmas. The shift of the instability threshold towards higher B_{min}/B_{ECR} -ratio with increasing ion mass is presumably due to increased electron energy loss in inelastic collisions.

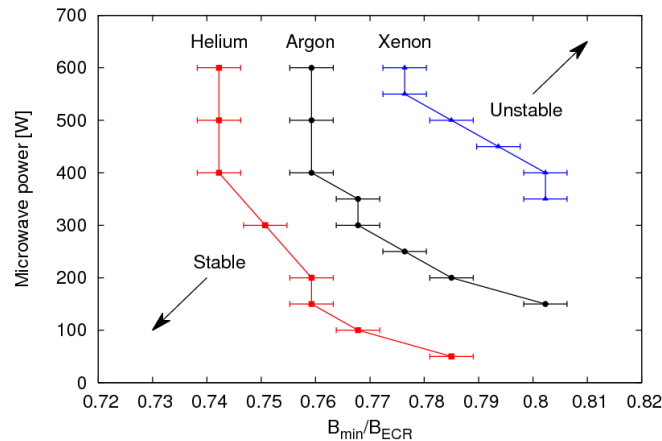


Figure 1: The instability threshold B_{min}/B_{ECR} -ratio as a function of incident microwave power in helium, argon and xenon plasmas. The data were taken with the JYFL 14 GHz ECRIS.

2.5.3.1 Fingerprints and diagnostics of the electron cyclotron instabilities

The transition from stable to unstable plasma regime can be detected since each instability onset is associated with a sequence of fingerprint events. First, hot electrons interacting with the resulting plasma wave emit microwave radiation [8] and are expelled into the loss cone. The increased flux of electrons from the trap results in a burst of wall bremsstrahlung. The abrupt loss of electrons leads to a significant increase of the plasma potential, which in turn repels the positive ions and leads to oscillations of the extracted ion currents. The described chain of events can be detected with appropriate diagnostics as demonstrated in Figs. 2 and 3 and discussed in [1].

Figure 2 shows (i) the microwave signal emitted from the ECRIS plasma and detected with a microwave sensitive diode (0.01 - 50 GHz, 10 ns resolution) connected to the WR 75 waveguide port of the JYFL 14 GHz ECRIS, (ii) the x-ray power flux measured with a bismuth germinate (BGO) scintillator coupled with a Na-doped CsI (300–600 nm) current-mode photomultiplier tube (PMT) and (iii) the currents of O^{2+} (low charge state) and O^{7+} (high charge state) ion beams measured from a Faraday cup. The signals are plotted on logarithmic scale to highlight the difference in their temporal response to the instability. The duration of the microwave emission is on the order of 10-100 ns, the electrons escape and emit bremsstrahlung (x-rays) for 10-100 μ s and, finally, ions react to the loss of electrons with their beam currents dropping approximately 0.1-1 ms after the onset of the instability and then entering a slow recovery phase of 10-100 ms. The duration of the recovery phase depends on the charge state and reflects the step-wise nature of the ionization process.

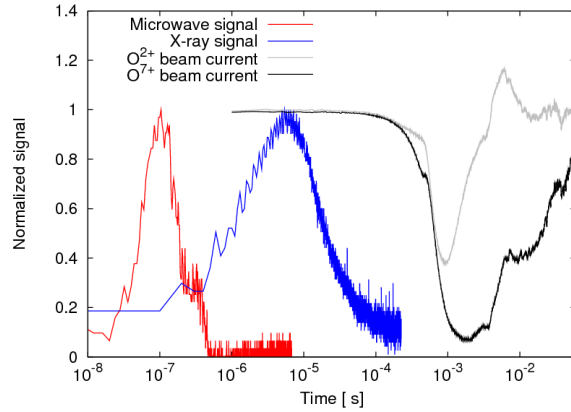


Figure 2: The diagnostics signals associated to instability onset (JYFL 14 GHz ECRIS).

The instabilities expel a significant fraction of the hot and warm electrons, which results to drastic increase of the plasma potential balancing the electron and ion losses. This is demonstrated in Fig. 3 showing the current measured from the biased disc of the ion source, i.e. the charged particle flux escaping the confinement, of the JYFL 14 GHz ECRIS and the temporal energy spread ($\Delta E/E$) of the extracted ion beams (O^{6+} used as a reference ion) during the instability-induced transient. The energy spread of the ion beams was obtained by sweeping the 90 degree m/q -analyzing magnet and recording the corresponding beam current signals. The onset of the instability is associated with a burst of electrons followed by an equal (in terms of expelled charge) burst of positive ions. The burst of positive ions can be observed in the oxygen beam currents as well. This is contrary to Fig. 2 where the temporal resolution is not adequate to resolve the momentary increase of the beam currents. Immediately following the instability the O^{6+} peak of the m/q -spectrum stretches in energy and overlaps with the adjacent N^{5+} and C^{4+} impurity peaks for few μs . This corresponds to $\Delta E/E$ of 10-15 % and implies that the plasma potential reaches values of 1-1.5 kV during the ion transient.

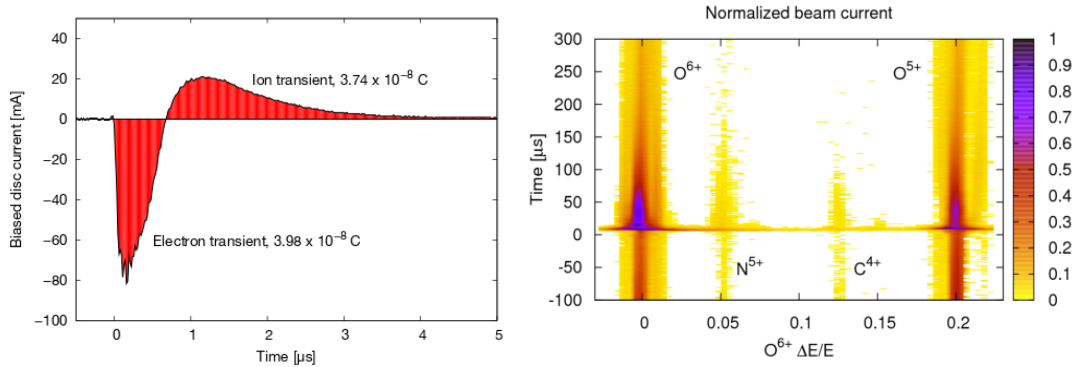


Figure 3: Biased disc current (left) and ion beam energy spread (right) transients associated with the onset of the instability. Data was taken with the JYFL 14 GHz ECRIS.

2.5.3.2 *Electron cyclotron instabilities limiting ECRIS performances*

So far we have concentrated on the physics of a single onset of the instability, which is not sufficient to explain why ECRIS performances are often limited by the instabilities.

This is due to periodic instabilities causing abrupt fluctuations of the plasma properties and beam currents at 10^2 - 10^3 Hz rate. The temporal interval between consecutive instability events is typically shorter than the ionization time of the high charge state ions, which suppresses their currents. This is demonstrated in Fig. 4 (left) showing the O^{6+} current extracted from the JYFL 14 GHz ECRIS at stable and unstable plasma regimes. In stable regime the fluctuation of the beam current is $< 3\%$ while in unstable regime the amplitude of the oscillation is several tens of percent and the temporally averaged beam current is lower. In this particular example the transition across the instability threshold was imposed by increasing the B_{min}/B_{ECR} -value from 0.68 to 0.75. The decrease of the beam current above an optimum B_{min}/B_{ECR} -value is characteristic to all ECR ion sources as demonstrated in Fig. 4 (right) showcasing some examples reported in the literature. The trend is most likely contributed by the appearance of kinetic instabilities at strong magnetic field as witnessed by the author for the JYFL 6.4 GHz ECRIS, JYFL 14 GHz ECRIS, PHOENIX 14.5 GHz charge breeder, VENUS and HIISI ion sources. Fig.5 demonstrates that the effect of the periodic instabilities on temporally averaged beam currents depends strongly on the charge state, i.e. the ion distribution is shifted towards lower charge states in the unstable regime.

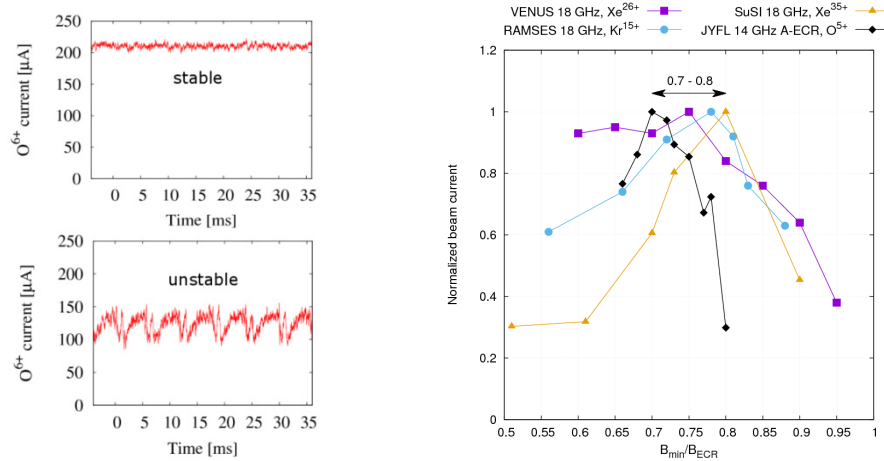


Figure 4: (left) The effect of the instabilities on the beam current of O^{6+} (JYFL 14 GHz ECRIS) and (right) the performance of ECR ion sources as a function of the B_{min}/B_{ECR} [9].

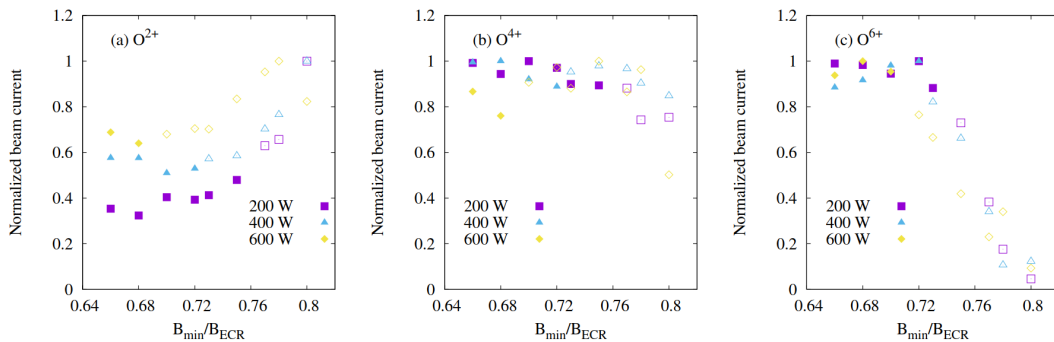


Figure 5: Normalized currents of O^{2+} , O^{4+} and O^{6+} ion beams as a function of B_{min}/B_{ECR} -ratio of the JYFL 14 GHz ECRIS. Solid / open symbols correspond to stable / unstable operating regime.

The described periodic fluctuations of current and energy spread of the extracted beams are limiting ECRIS performances and can be detrimental for their applications. Furthermore, the instabilities cause a significant increase of contaminants (impurities) in

the extracted beams, which is especially problematic for charge breeder ECR ion sources as described in Ref. [10]. Fig.6 shows an example of an m/q-spectrum recorded with the 14.5 GHz PHOENIX charge breeder under stable and unstable plasma conditions. The transition to unstable regime increases the currents of certain impurity ions by an order of magnitude. The effect is caused by the fluctuation of the plasma potential and subsequent sputtering of the plasma chamber surfaces.

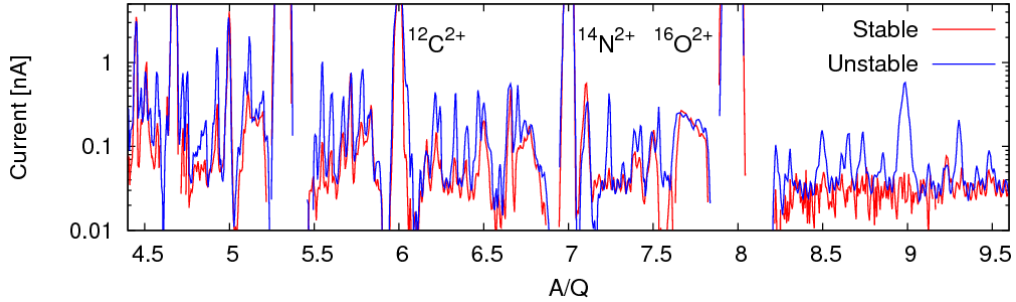


Figure 6: Temporally averaged m/q-resolved spectra at high sensitivity/low current scale in stable and unstable operating regimes. The contaminant peaks appearing / increasing in magnitude in unstable mode are due to sputtering of the plasma chamber material.

2.5.3.3 *Suppression of ECRIS plasma instabilities*

In previous subsections we have shown that kinetic instabilities limit the parameter space of ECRIS optimization by reducing the extracted currents of high charge state ions, increasing the energy spread of the ion beams and releasing contaminants from the plasma chamber walls. Thus, the motivation for suppressing the instabilities is apparent. Multiple frequency heating is one of the most effective techniques to improve the performance of ECR ion sources. It has been recently discovered that the beneficial effect of two-frequency heating is connected to enhanced plasma stability and suppression of kinetic instabilities [11]. The effect is demonstrated in Fig.7 showing data from two ion sources: (left) the O^{6+} beam current and x-ray power flux recorded with the JYFL 14 GHz ECRIS with 430 W of total power in single and double frequency heating modes and (right) O^{6+} beam current and reflected 18 GHz microwave power of VENUS operating with 2 kW at 28 GHz + pulsed 2 kW at 18 GHz. In both cases the periodic ripple observed in single frequency heating mode disappears and the beam current of O^{6+} increases when the secondary microwave source is turned on. Furthermore, the fluctuations of x-ray power flux as well as the microwave bursts, detected as peaks of reflected power from the 18 GHz waveguide of VENUS, disappear in two frequency operation mode.

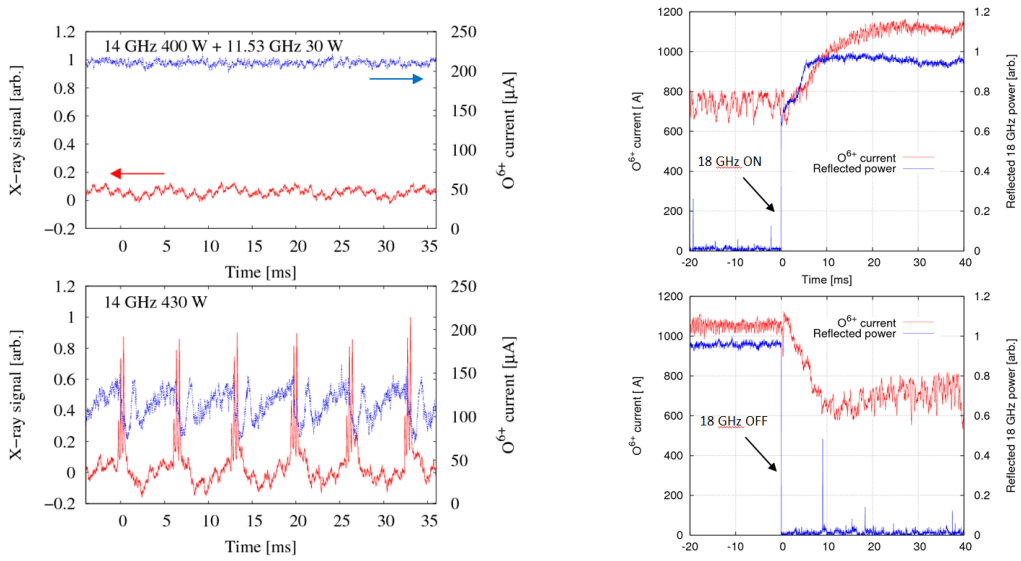


Figure 7: The stabilizing effect of two frequency heating. (left) O⁶⁺ beam current and x-ray power flux of the JYFL 14 GHz ECRIS and (right) O⁶⁺ beam current and reflected microwave signal in the 18 GHz waveguide of VENUS with 2 kW at 28 GHz + 2 kW pulsed at 18 GHz.

2.5.3.4 *Open research questions*

Despite of the advances in research of ECRIS plasmas instabilities, some open questions still remain. It has been observed that the transition from stable to unstable operation regime depends primarily on the magnetic field configuration of the ion source. However, it remains unsolved whether the transition is primarily affected by the field strength or the field gradient at the resonance. Recent experiments [12] with the VENUS ECRIS have revealed that the “spectral temperature” of the bremsstrahlung spectrum depends only on the minimum magnetic field strength (B_{\min}), which indicates that the absolute field strength determines the EVD and therefore drives the instabilities. On the other hand, the gradient at the resonance presumably affects the single-pass energy gain of the electrons, which affects the maximum energy anisotropy of the EVD [13]. Further experiments resolving the effect of absolute field strength vs. magnetic field gradient *averaged over the resonance surface* are required to define the primary cause for the transition to unstable regime. Such work can be carried out best with superconducting ECR ion source allowing independent adjustment of the solenoid and sextupole fields. Also, the exact mechanism underlying the suppression of the instabilities by two frequency heating remains unknown in both, theoretical and experimental levels. Nevertheless, it is evident that the technique is important for future ion sources operating at high frequencies and powers as well as for charge breeders suffering from background impurities.

2.5.4 **Acknowledgements**

This work was supported by the Academy of Finland under the Finnish Centre of Excellence Programme 2012-2017 (Project No. 213503, Nuclear and Accelerator-Based Physics Research at JYFL). The author acknowledges contributions by IAP-RAS and LBNL ion source teams for their support in collecting the data.

2.5.5 References

1. O. Tarvainen, I. Izotov, D. Mansfeld, V. Skalyga, S. Golubev, T. Kalvas, H. Koivisto, J. Komppula, R. Kronholm, J. Laulainen and V. Toivanen, "Beam current oscillations driven by cyclotron instabilities in a minimum-B ECRIS plasma", *Plasma Sources Sci. Technol.* 23, 025020, (2014).
2. M. Muramatsu, A. Kitagawa, "[A review of ion sources for medical accelerators \(invited\)](#)", *Rev. Sci. Instrum.* 83, (2012), p. 02B909.
3. T. A. Antaya and S. Gammino, "The superconducting electron cyclotron resonance 6.4 GHz high - B mode and frequency scaling in electron cyclotron resonance ion sources", *Rev. Sci. Instrum.* 65, (1994), p. 1723.
4. D. Hitz, A. Girard, G. Melin, S. Gammino, G. Ciavola and L. Celona, "Results and interpretation of high frequency experiments at 28 GHz in ECR ion sources, future prospects" *Rev. Sci. Instrum.* 73, (2002), p. 509.
5. G. Melin, F. Bourg, P. Briand, J. Debernardi, M. Delaunay, R. Geller, B. Jacquot, P. Ludwig, T. K. N'Guyen, L. Pin, M. Pontonnier, J. C. Rocco, and F. Zadworny, "Some particular aspects of the physics of the ECR sources for multicharged ions", *Rev. Sci. Instrum.* 61, 236, (1990).
6. S. A. Hokin, R. S. Post, and D. L. Smatlak, "Electron velocity - space diffusion in a microunstable electron cyclotron resonance heated mirror plasma", *Phys. Fluids B: Plasma Physics* 1, 862 (1989).
 - A. G. Shalashov, S. V. Golubev, E.D. Gospodchikov, D. A. Mansfeld and M. E. Viktorov, "Interpretation of complex patterns observed in the electron-cyclotron instability of a mirror confined plasma produced by an ECR discharge", *Plasma Phys. Control. Fusion* 54, 085023, (2012).
 - B. Izotov, O Tarvainen, D Mansfeld, V Skalyga, H Koivisto, T Kalvas, J Komppula, R Kronholm and J Laulainen, "Microwave emission related to cyclotron instabilities in a minimum-B electron cyclotron resonance ion source plasma", *Plasma Sources Sci. Technol.* 24 045017, (2015).
7. O. Tarvainen, T. Kalvas, H. Koivisto, J. Komppula, R. Kronholm, J. Laulainen, I. Izotov, D. Mansfeld, V. Skalyga, V. Toivanen and G. Machicoane, "Limitation of the ECRIS performance by kinetic plasma instabilities (invited)", *Rev. Sci. Instrum.* 87, 02A703 (2016).
8. O. Tarvainen, J. Angot, I. Izotov, V. Skalyga, H. Koivisto, T. Thuillier, T. Kalvas and T. Lamy, "Plasma instabilities of a charge breeder ECRIS", *Plasma Sources Sci. Technol.* 26, 105002 (2017).
9. V. Skalyga, I. Izotov, T. Kalvas, H. Koivisto, J. Komppula, R. Kronholm, J. Laulainen, D. Mansfeld and O. Tarvainen, "Suppression of cyclotron instability in Electron Cyclotron Resonance ion sources by two-frequency heating", *Phys. Plasmas* 22, 083509 (2015).
10. J. Benitez, C. Lyneis, L. Phair, D. Todd and D. Xie, "Dependence of the Bremsstrahlung Spectral Temperature in Minimum-B Electron Cyclotron Resonance Ion Sources", *IEEE Transactions on Plasma Science*, vol. 45, no. 7, pp. 1746-1754, (2017).
11. S. Gammino, D. Mascali, L. Celona, F. Maimone and G. Ciavola, "Considerations on the role of the magnetic field gradient in ECR ion sources and build-up of hot electron component", *Plasma Sources Sci. Technol.* 18 045016, (2009).

2.6 ECR Simulations

Vladimir Mironov

Mail to: vemironov@jinr.ru

Joint Institute for Nuclear Research, Joliot-Curie 6, Dubna, Moscow Region,
141980, Russia

2.6.1 Introduction

Numerical modelling of ECRIS (Electron Cyclotron Resonance Ion Source) is aimed to shed light on the physical processes in the source plasma and to guide the source designers in their efforts to increase the extracted ion beam intensity and quality. So far, the source development is mainly done on semi-empirical basis, following the scaling laws [1] that suggest optimal magnetic field profiles and predict larger output of the highly charged ions with increased frequency of injected microwaves. Various effects are observed in ECRIS, such as wall-coating, gas-mixing, two-frequency heating, afterglow and preglow transient pulses [2]. No commonly accepted explanations were given to these effects till now, though they greatly affect the source performance. Even such important parameters are disputable as the mean electron energy and mechanisms for ion confinement in the ECRIS plasma.

Fully self-consistent model of ECRIS operation is not possible at the moment due to complexity of involved processes; simulations are done with simplifying assumptions and by varying some free parameters to reach correspondence between numerical results and experiment. Still, the codes used to model ECRIS plasma have become more and more detailed over time, and more accurate results are obtained by taking into account important features of ECRIS plasma.

2.6.2 Models

2.6.2.1 *Approaches of other groups*

In first attempts to model the ECRIS performance, dimensionless (0D) balance equations were constructed and solved for ion and electron production and losses by Shirkov et al. [1]. Elastic and inelastic collision processes for charged particles in ECRIS were modelled by using the Spitzer rates; ions were supposed to be confined in ECR volume by negative potential well (dip in the globally positive plasma potential). Electron and ion confinement times were calculated in the model by using the Pastukhov's equations. Electron energy distribution function was supposed to be a combination of three Maxwellian distributions, with typical temperatures around 100 eV for the cold component, 10 keV for the warm electrons and 100 keV for the hot electron component. Warm electrons were supposed to constitute the major fraction of all electrons and to be responsible for the highly charged ion production. Their temperature was taken as free parameter, as well as the value of ion confining potential. Variations in these parameters allowed reaching the correspondence between the experimentally measured extracted ion currents and simulations. Hot ions were observed in the calculations, with typical ion temperatures in the range of ~ 10 eV. The potential dip values were not reported, but it is reasonable to assume that they were close to the ion temperatures during the calculations.

Gas-mixing effect was explained in the model by evaporative cooling of highly charged ions in the potential trap when low-mass gas is added to the main relatively heavy gas. Mobile light and lowly charged ions are easily leaving the trap, carrying away the excess energy; remaining ions are cooled and better trapped in the plasma. Afterglow effect was explained by abrupt losses of electron out of the plasma upon termination of microwave heating, with decreased life time of the ions as the result.

More elaborated model was developed by Girard et al. [1]. There, electron heating in interaction with microwaves and electron losses out of the source magnetic trap were calculated by solving Fokker-Planck equation. It was obtained that the mean electron energy is at the level of ~ 50 keV, larger than in the model of Shirkov. Ion confinement in the plasma was supposed to be governed by collisional ambipolar diffusion with linear dependence of the confinement time on the ion charge state. Motivation for such selection of ion confining mechanism stems from experimental measurements of ion life times by using the x-ray emission spectroscopy [1]. This approach is questionable; nonetheless, qualitative agreement was obtained between the extracted ion currents and simulations. In the model, afterglow effect was explained as a consequence of increased losses of cold and highly collisional electrons produced in ionizing collisions, if they are not heated after terminating the microwave injection. The increased losses of electrons are accompanied with higher losses of ions to maintain the plasma space charge neutrality. Gas-mixing effect was seen in the simulations, but not as pronounced as it is experimentally observed.

Cluggish et al. [1] develop GEM-1D, 2D and “quasi-3D” models of ECRIS operation by using bounce-averaged Fokker-Planck code for electron dynamics combined with collisional fluid equations for ions. Authors calculated mean electron energies that increase with injected RF power and reach the level of ~ 40 keV for RF power above 100 W. Potential dip is seen in the plasma potential spatial distribution around the volume defined by ECR surface, and the dip value is a few Volts. Strong localization of plasma inside the ECR volume is observed. The code is still not able to reproduce the experimentally measured extracted ion currents, probably because of using inaccurate ionization rates.

Mascali et al. [1] are constructing self-consistent 3D code for ECRIS that solves Vlasov-Maxwell system of equations. Their focus is on calculations of coupling between microwaves and plasma and on complicated spatial distribution of electromagnetic field in the source cavity. As in other models, plasma electrons are seen to be localized inside the ECR volume; ions in the model are supposed to be confined by electric fields in double-layer that separates the dense ECR plasma and dilute peripheral plasma. Calculations of ionization dynamics of highly charged ions have not been done yet.

2.6.2.2 *NAM-ECRIS*

“Numerical Advanced Model of ECRIS” of our group uses Particle-in-Cell Monte-Carlo collisions approach (PIC-MCC) for iterative simulations of ion and electron dynamics in ECRIS [1-4]. The Ionic part of the code, NAM-ECRIS(i), traces movement of a large number of computational particles in 3D magnetic field of the source, combined with movement in externally defined electric field. The electronic part NAM-ECRIS(e) uses the ion spatial distributions prepared by NAM-ECRIS(i) and calculates the electron dynamics with heating by microwaves at ECR surface. Results of calculations of both modules are used in iterative way: the electron mean energy and life time averaged over

the plasma volume from NAM-ECRIS(e) are used as input parameters for NAM-ECRIS(i), which in turn calculates the ion life times and ionic (electron) density, and the process is repeated if needed to reach convergence.

2.6.2.2.1 The ion module NAM-ECRIS(i)

The magnetic field of the source is calculated as a combination of axially-symmetric solenoidal component that is calculated by using POISSON-SUPERFISH code, and analytically defined hexapole component in hard-edge approximation. Boris mover [1] is used for tracing of ions. Calculations are done on a relatively coarse Cartesian mesh, and typically 2×10^5 computational particles are used as defined by compromise between calculation accuracy and time. Particles represent both neutrals and ions, with the statistical weights of $\sim(10^8 \div 10^9)$.

Each step, charged particles are scattered such as to simulate the elastic electron-ion and ion-ion collisions in the plasma. Scattering is done following the Takizuke-Abe procedure [1], which conserves both energy and momentum of collisional partners paired within a computational cell. During calculations, the electron density is calculated from the total ion charge density, keeping in mind the requirement of charge neutrality. Electron temperature is input parameter (50 keV in most cases) for ionic part of the code, as deduced from NAM-ECRIS(e). When calculating electron-ion heating and scattering, gradients in electron density are taken into account by adding small rotation of the scattering angle.

Ionization rates for ions are taken from the fits obtained with FLYCHK code [1]. The rates include contributions from excitation-autoionization processes; data are available for all elements up to Au. Ionization of molecular oxygen and nitrogen is modelled by using the cross-sections from [2,3]; energization of particles after dissociation of molecules and singly charged molecular ions is taken into account. Recombination processes are neglected in our model. Processes of charge-exchange in collisions of ions with atoms are calculated by using the Langevin rate coefficients [2].

Each time as ions hit the source walls, they are reflected back into the source as neutrals with reflection angle selected from the “cosine-law”; energy of the reflected atoms is calculated with taking into account a not-complete energy absorption by the walls. Thermal accommodation coefficient is defined as

$$\alpha = (E_r - E_i) / (E_i - E_w) \quad (1)$$

where E_r and E_i are the energies of the reflected and incident particles respectively, and E_w is the mean energy of the wall atoms. The coefficient depends on ratio between the gas and wall atomic masses ($\mu = M_g / M_w$) and on the angle of incidence (θ) of the projectile as [2]

$$\alpha = 3.6 \sin(\theta) \mu / (1 + \mu^2) \quad (2)$$

We take into account substantial energy gain of ions in plasma sheath ($\sim V_p \times Q$ eV, Q is ion charge state and plasma potential V_p is in the range of (10-50) V and, as the result, presence of supra-thermal atoms in the source chamber.

Ions are supposed to be confined inside the (relativistically broadened) ECR volume by potential barrier, which value $\Delta\phi$ is free parameter for the ion module. Whenever ion crosses the ECR surface, its energy along the local magnetic field line is calculated, and the ion is reflected back into the volume if the energy is less than $Q \times \Delta\phi$; if the ion passes over the barrier, its energy along the field line is decremented by the corresponding value. Outside the ECR volume, ions are assumed to be accelerated in pre-sheath electric field

toward the source walls. The presheath electric field is calculated by approximating the ECR volume with axially-symmetric volume and by calculating the electric field with POISSON-SUPERFISH code. The ECR volume voltage V_{ps} is free parameter, and we set the V_{ps} value equal to 2.5 V in most cases; changes in the presheath voltage do not influence the most important parameters of ECRIS plasma such as the extracted ion currents, plasma density and spatial distribution inside the ECR volume. This voltage is only important for calculations of plasma density outside the ECR volume and close to the extraction aperture of the source, directly influencing the initial energies of ions before they are entering the sheath layer and accelerated in the extraction gap.

Specific run of the ion module starts by selecting the statistical weight of particles and the potential barrier value; simulations continue till all processes converge, which typically takes around (1-5) ms of the physical time and ~5 hours of computational time. Extracted ion currents and total flux of atoms into the source are calculated from flux of particles into the extraction aperture; total current of ions to the source walls and into the extraction is calculated. The electron losses out of the plasma are then calculated to be equal to the ion losses. The total current can be multiplied by mean energy of lost electrons to get the coupled microwave power for the specific conditions of the source; mean electron energy is calculated by NAM-ECRIS(e) as will be discussed later. Globally defined ion/electron loss time is calculated from the current of ions to the walls and total number of charged particles in the ECR volume. Distribution of ion densities on the mesh is also calculated to be exported into NAM-ECRIS(e). Additionally, the array is prepared that consists of positions of ionizing events in the source with a sort (charge state) of ionized particle.

Typical output of the ion module is shown in Fig.1, where charge state distribution of extracted ions is shown for DECRIS-PM source [2].

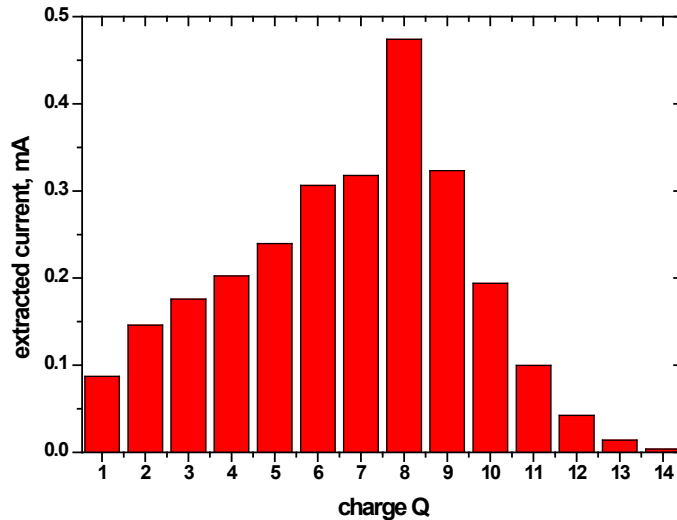


Figure 1: Simulated charge state distribution of the extracted argon ions for DECRIS-PM source.

The distribution is obtained with the potential barrier equal to 0.07 V, for the electron temperature of 50 keV and for the gas flow into the source chamber of 0.65 particle-mA. The ion life time in these conditions is 0.5 msec and power losses out of the plasma are 250 W for mean electron energy of 6 keV. Qualitative agreement is observed between the

simulated charge state distributions and measured extracted ion currents, with excess in the simulated currents of lowly charged ions.

2.6.2.2.2 The electron module NAM-ECRIS(e)

Electron movement in the magnetic field of the source is traced by using the same Boris mover as for ions, but with much smaller time step (10^{-11} sec). Relatively small number of computational particles is used (10^3); simulations are done on the same mesh as for NAM-ECRIS(i). We start simulations by launching the electrons at the positions taken from array of ionizing events from NAM-ECRIS(i); energies of electrons are set to ionization potential of ions that were created at the given positions.

Each computational time step electrons are scattered due to electron-ion and electron-electron collisions by a small angle Θ in random direction through a Gaussian random variable δ related to Θ by $\delta = \tan(\Theta/2)$, where δ has zero mean value and the variance that corresponds to the classical Spitzer rates. For the electron-ion collisions the deflection angle can be calculated [**Error! Bookmark not defined.**] as a single event proportional to the sum of individual contributions of scattering on ions with density n_{iQ} and charge state Q , and the variance of δ -factor is:

$$\langle \delta^2 \rangle \sim \frac{n_s}{v_e^3}, n_s \equiv \sum_Q n_{iQ} Q^2 \quad (3)$$

The deflection angle is decreasing fast with increasing of electron velocities v_e (Eq.3).

Whenever the particle crosses the ECR zone, it experiences random kick in the direction perpendicular to the magnetic field line. The kick value V is calculated according to Lieberman and Lichtenberg [2] as

$$V = \frac{e}{m_e \gamma} E_0 t_e \cos(x) \quad (4)$$

Here, E_0 is the magnitude of the applied microwave field at the resonance field, x is a random number in the range from 0 to 2π giving the phase between the velocity vector and the electric field, e and m_e are the electron charge and mass, and t_e is the effective time the particle spends in resonance. For the effective time we select the minimal of two values, $t_e = \min(t_{e1}, t_{e2})$:

$$t_{e1} \approx 1.13 \left(\frac{2}{|\alpha v_{\parallel}| \omega} \right)^{1/2}; t_{e2} = (0.71/\omega)(2\omega / \alpha v_{\perp})^{2/3} \quad (5)$$

Here, ω is the microwave angular frequency, factor α is the normalized magnetic field gradient along the magnetic field line, v_{\parallel} and v_{\perp} are the velocity components along and perpendicular to the magnetic field line respectively. The first value corresponds to the case when particle passes with constant axial velocity through the resonance zone, while the second expression is applied when the particle begins to turn in the resonance surface.

Magnitude of the microwave electric field is a free parameter in our calculations. In the real conditions, the field depends on the power of the injected microwaves (P) ($E_0 \sim P^{1/2}$ for empty cavities), geometry of chamber and density of the plasma inside the source. Electric field of microwaves has a complicated spatial dependence of magnitude and phase. We omit at the moment all these details and consider the electric field constant over the ECR surface.

Random kicks of electrons at ECR result in diffusion in the velocity space and in heating of the electron component. It is important to note that the heating rate is slowing

down with increasing the electron velocity because the time interval for electrons to resonate with microwaves while passing through ECR zone is decreasing.

The calculated electron energy distribution in ECRIS plasma is shown in Fig.2. Here, amplitude of electric field is set to 250 V/cm and ion densities correspond to the source settings of Figure 1.

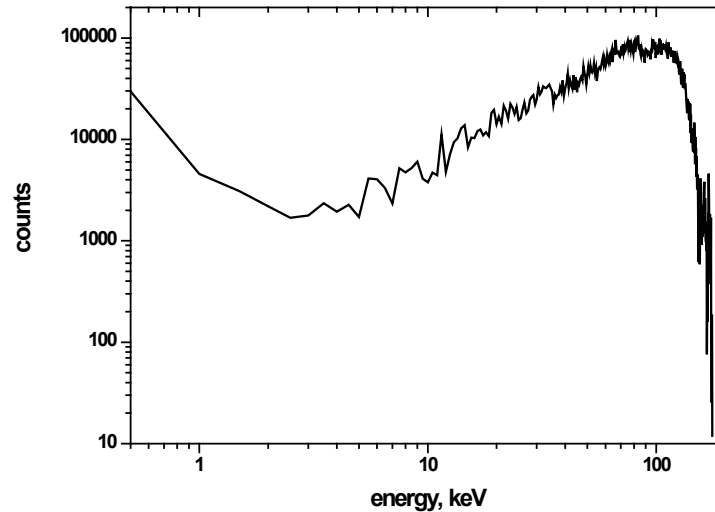


Figure 2: Energy distribution of electrons in the plasma.

The distribution is centered at around 75 keV; small peak at low energies consists of the cold electrons created in the ionizing collisions before they are heated in interaction with microwaves.

Energy distribution of the lost electrons strongly deviates from the distribution for electrons that stays in the plasma. In Fig.3, the distribution is shown for the same settings as in Figs. 1 and 2.

Most of the lost electrons have a rather low energy of less than 1 keV, second peak is around 150 keV close to the sharp right edge of the distribution in Fig.2. The reason for such difference between two distributions is high scattering probability for low energetic electrons, which pushes them fast into the loss cone. Mean energy of the lost electron is ~6 keV in the given conditions, which is an order of magnitude less of the mean energy of electrons inside the plasma. Global electron life time is calculated to be 0.5 msec: electric field amplitude was selected such as to ensure that the electron and ion life times are equal each other.

The higher is the microwave electric field amplitude, the faster the electrons are heated and run away to the low-collisional conditions. The result is larger electron life time, accompanied with increase in the mean energy of lost electrons. Larger ion density increases the electron scattering rates and decreases the electron life time. For the fixed electric field amplitude, mean energy of the lost electron remains almost the same. Small changes in the mean electron energy inside the plasma are seen for varying microwave electric field amplitude.

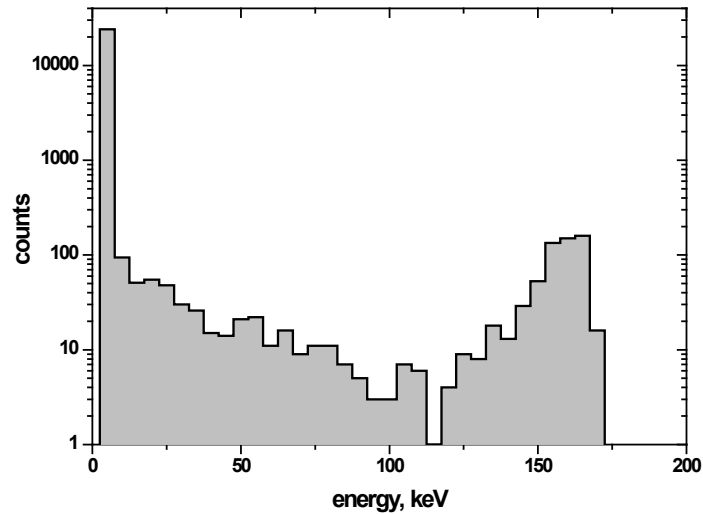


Figure 3: Energy distribution of the lost electrons.

The simulated electron dynamics supports considerations of Girard et al. [**Error! Bookmark not defined.**] concerning the afterglow effect. Indeed, we see that when microwave heating is terminated, newly born secondary electrons are not diffusing in the velocity space toward the long-living non-collisional energies and are lost fast, which in turn increase the ion losses to maintain the charge-neutrality of the plasma and generates peak in the extracted ion currents.

At the moment we are not able to calculate the electric field amplitude for given plasma density, injected microwave power and other parameters of the source; this parameter is free for the model. Still, we can compare the source performances by keeping the amplitude and power losses out of the plasma at some fixed level. Some examples of applying this approach to studies of ECRIS are presented in next section.

2.6.2.3 *Effects*

2.6.2.3.1 Isotope anomaly

It is observed experimentally [2] that when ECRIS is running in a mixture of two isotopes, extracted highly charged ion currents of the heavier isotope are substantially exceeding the currents of the lighter isotope. Several explanations are given to the effect, including selective heating of the ions by low frequency plasma waves [1] as well as ion cooling due to increased rate of lighter ion escape out of the plasma.

We simulated output of ECRIS with mixing two isotopes of argon in the discharge, ^{36}Ar and ^{40}Ar . The source parameters were chosen to be close to the situation presented in Fig.1; we request that the isotope fluxes into the source are equal to each other and compare the charge state distributions of the extracted ion currents (Fig.4). In simulations, ratio between the extracted ^{40}Ar and ^{36}Ar ion currents is increasing with charge state and reaches the level of 1.4 for the highest investigated charge of (15+).

Reasons for such isotope fractionation come from weak dependence of the ion life time on the ion mass, $\tau_i \sim \sqrt{m_i}$ according to the Rognlien-Cutler estimation [**Error!**

Bookmark not defined.] The lighter ions have larger velocity and hit the barrier formed by the potential dip more frequently compared to their heavier counter-partners, taking into account that the ions are in thermal equilibrium in ECRIS plasma. Rates of electron-impact ionization into the higher charge state ($Q+1$) are decreasing with increasing the ion charge Q and only those ions reach the high charge states that stay relatively long in the plasma.

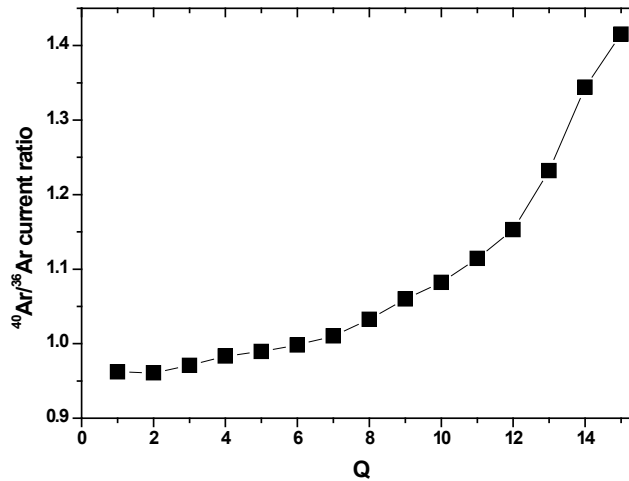


Figure 4: Ratio between the extracted currents of ^{40}Ar and ^{36}Ar ions as a function of their charge state.

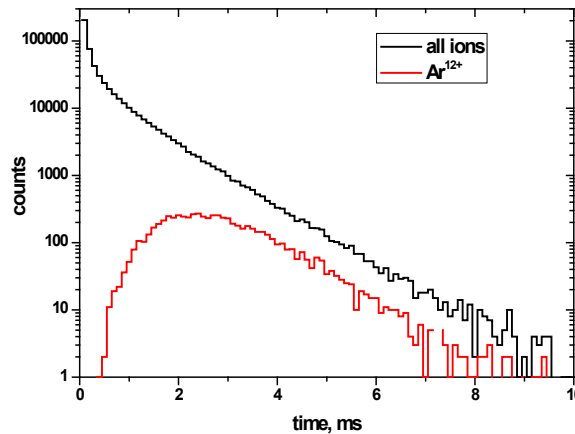


Figure 5: Residence time distributions of all Ar ions (black) and Ar^{12+} ions (red). Time is counted from Ar^{1+} ion creation.

The first passage time distribution of ions in ECRIS plasma is shown in Fig.5. Here residence time distribution of ions ^{40}Ar is calculated starting from the moment of singly charged ion creation and stopping when ion in charge state Q is lost at the source chamber walls or into the extraction aperture. Cumulative distribution for all charge states is shown in black, and charge state resolved distribution for Ar^{12+} ions is shown in red. The

cumulative distribution for the times larger than 1 ms is well fitted with the exponential decay curve with characteristic time τ_{40} of 2.2 ms for ^{40}Ar and τ_{36} of 2.0 ms for ^{36}Ar ions, $\tau_{40} / \tau_{36} \approx \sqrt{40/36}$. Highest charge states of argon ions form the tail in cumulative time distribution; small variations in the decay time constant result in substantial variations in these ion production, with the ratio between distributions of heavy and light isotopes

$$e^{-T/\tau_1} / e^{-T/\tau_2} \sim e^{\frac{\sqrt{m_1} - \sqrt{m_2}}{\sqrt{m_1 m_2}} T} \quad (6)$$

increasing with the residence time T , which in turn results in the enhanced output of heavier isotopes from ECRIS and explains the isotope anomaly.

2.6.2.3.2 Wall coating effect

It is observed experimentally that ECRIS performance strongly depends on the chamber wall conditions [**Error! Bookmark not defined.**]. In particular, when the walls are covered by thin layers of such oxides as Al_2O_3 or SiO_2 , output of highly charged ions increases; the effect is explained in terms of high secondary electron coefficients of the oxidized surfaces and increased flux of electrons from the walls into the plasma, which increases the plasma density.

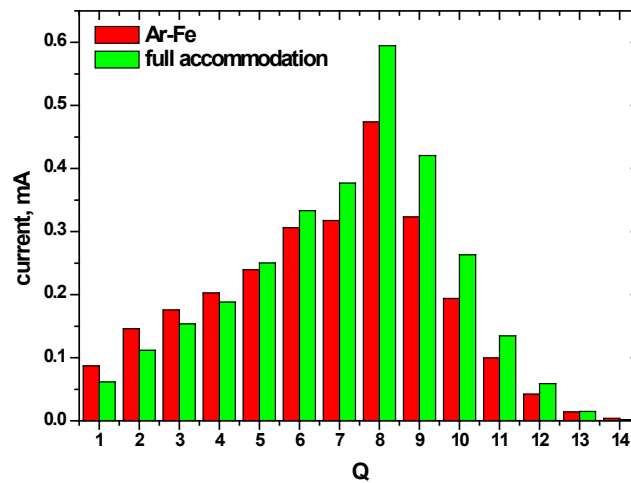


Figure 6: Charge state distribution of the extracted Ar ion currents with thermal accommodation coefficient for Ar-Fe collisions (red) and with full thermal accommodation (green).

We notice that changes in the wall conditions can influence the source by modifying the thermal accommodation coefficient, thus changing the energies of recycling atoms. It is known that oxidized surfaces typically have larger accommodation coefficients compared to the clean surfaces [3]; reduced gas temperature in the source leads to the lower temperatures of lowly charged ions in ECRIS and increases their lifetimes. In Fig.6, we compare charge state distributions of the extracted argon ions for stainless steel chamber (designated as “Ar-Fe” spectrum in the Fig.6) and for the chamber walls with thermal accommodation coefficient equal to 1 (“full accommodation”). Increase in the accommodation coefficient results in cooling of the argon atoms in the

source chamber down to 0.03 eV close to the wall's temperature, compared to the mean atom temperature of 0.14 eV for the stainless steel chamber. For the “cool” gas, potential dip should be set to 0.038 V, much less than the default 0.07 V for the “warm” gas, to maintain the ion and electron losses equal each other (we keep the heating microwave amplitude at the same level of 250 V/cm for both cases). Prominent increase of the extracted currents of the highly charged ions is seen for the chamber walls with high accommodation coefficient, suggesting that wall coating effect can be at least partially explained as the result of gas cooling in the source chamber.

It is worth to note here that spectra in Fig.6 were obtained with setting the plasma potential to 20 V; it was seen in our model that increase in the plasma potential for the stainless steel chamber decreases the highly charged ion output strongly due to increase in energies of the recycling atoms. This shows an importance of reducing the plasma potential for better source performance.

2.6.2.3.3 Gas-mixing effect

Output of highly charged ions from ECRIS can be increased with adding lighter gas to the discharge [3]. Oxygen is considered to be the best choice for mixing gas in many cases. The effect is often explained in terms of the evaporative ion-cooling process [Error! Bookmark not defined.], with conjecturing that fast escaping lowly charged light ions cool the heavy ions by taking away excess energy out of the ion population; the cooled ions are better trapped inside the plasma.

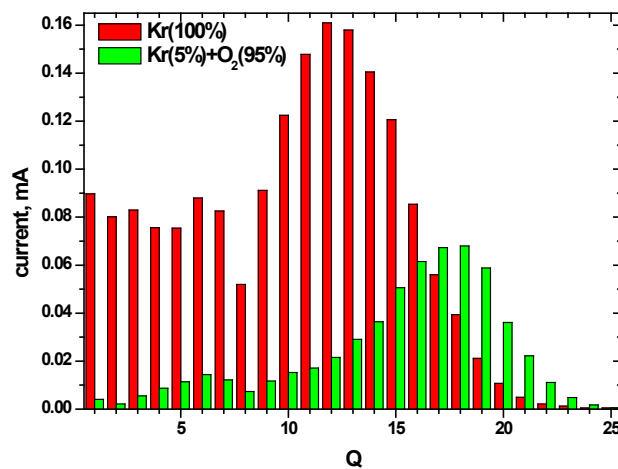


Figure 7: Charge state distribution of the extracted Kr ions for Kr discharge (red) and for mixture of Kr (5%) and O₂ (95%).

We are able to reproduce the gas-mixing effect when compare the charge state distributions of the extracted krypton ions for the clean krypton discharge and in mixture of krypton and oxygen. The distributions are shown in Fig.7 for the case of full thermal accommodation of krypton ions at the walls. Output of the highest charge states of krypton ions ($Q > 18+$) can be substantially increased if ECRIS plasma is mainly composed of the oxygen ions, with krypton content of around (5-10)% of total number of particles. Oxygen dynamics is calculated with taking into account the oxygen ion energization after dissociation of molecular oxygen. The results with oxygen show much hotter ion temperatures in the dense parts of ECRIS plasma, with the resulting large

values of the plasma potential dip that is needed to equilibrate the ion and electron losses. For the krypton discharge, the potential dip is 0.016 V compared to 0.26 V for the Kr-O₂ plasma with optimized content. In the gas-mixed plasmas, ion life time for the highly charged heavy ions is increased even if the ion temperature is much higher than in clean discharge; the better ion confinement stems from the fact that the ratio between dip value and ion temperature is higher in the mixed plasmas for the heavy elements.

We also notice that in the gas-mixed plasmas, the plasma potential is typically lowered, especially for the mixtures with oxygen. Decrease in plasma potential for oxygen plasmas is measured experimentally [3] and is probably connected both to negative ion production and to high energies of the oxygen ions. Decrease in the plasma potential results in cooling of the heavy gas in the source and in the longer ion lifetimes, as for the wall coating effect.

2.6.2.4 *Conclusions*

Our numerical model of processes in Electron Cyclotron Resonance Ion Sources allows accurately reproducing the source output with using a minimal set of free parameters. Various effects that are experimentally observed in the sources can be explained with the model; there are possibilities for systematic studies of the source response to variations of such parameters as magnetic field profile, microwave power, gas flow etc. Calculations of the microwave power coupling to the plasma are missed, and more effort is needed to take it into account and to make the simulations more reliable. Results of the simulations can be used for predicting the optical properties of the extracted ion beams.

2.6.3 **References**

1. R. Geller, *Electron Cyclotron Resonance Ion Sources and ECR Plasma* (Institute of Physics, Bristol, 1996)
2. Denis Hitz, Gérard Melin, and Alain Girard, “Fundamental aspects of electron cyclotron resonance ion sources: From classical to large superconducting devices”, *Rev. Sci. Instrum.* **71**, 839 (2000) <http://dx.doi.org/10.1063/1.1150308>
3. G. Shirkov, “Multicomponent consideration of electron fraction of electron-cyclotron resonance source plasma”, *Rev. Sci. Instrum.* **71**, 850 (2000) <http://dx.doi.org/10.1063/1.1150310>
4. Girard, D. Hitz, G. Melin, and K. Serebrennikov, “Electron cyclotron resonance plasmas and electron cyclotron resonance ion sources: Physics and technology”, *Review of Scientific Instruments* **75**, 1381 (2004); doi: 10.1063/1.1675926
5. G. Douysset, H. Khodja, A. Girard, and J. P. Briand, “Highly charged ion densities and ion confinement properties in an electron-cyclotron-resonance ion source“, *Phys. Rev. E* **61**, 3015 (2000) <https://doi.org/10.1103/PhysRevE.61.3015>
6. [Cluggish](#), [L. Zhao](#), and [J.S. Kim](#), “Simulation of parameter scaling in electron cyclotron resonance ion source plasmas using the GEM code”, *Rev. Sci. Instrum.* **81**, 02A301 (2010); doi: <http://dx.doi.org/10.1063/1.3259166>
7. David Mascali, Giuseppe Torrasi, Lorenzo Neri, Gino Sorbello, Giuseppe Castro, Luigi Celona, and Santo Gammino, “3D-full wave and kinetics numerical

- modelling of electron cyclotron resonance ion sources plasma: steps towards self-consistency”, *Eur. Phys. J. D* **69**, 27 (2015); DOI: 10.1140/epjd/e2014-50168-5
8. V. Mironov and J.P.M. Beijers, “Three-dimensional simulations of ion dynamics in the plasma of an electron cyclotron resonance ion source”, *Phys. Rev. ST Accel. Beams* **12**, 073501 (2009).
 9. V. Mironov, S. Bogomolov, A. Bondarchenko, A. Efremov, and V. Loginov, “Numerical model of electron cyclotron resonance ion source”, *Phys. Rev. ST Accel. Beams* **18**, 123401 (2015).
 10. V. Mironov, S. Bogomolov, A. Bondarchenko, A. Efremov, and V. Loginov, “Numerical simulations of gas mixing effect in electron cyclotron resonance ion sources”, *Phys. Rev. Accel. Beams* **20**, 013402 (2017).
 11. V. Mironov, S. Bogomolov, A. Bondarchenko, A. Efremov and V. Loginov, “Some aspects of electron dynamics in electron cyclotron resonance ion sources”, *Plasma Sources Science and Technology* **26**, 075002 (2017) <https://doi.org/10.1088/1361-6595/aa7296>
 12. C.K. Birdsall, A.B Langdon, “Plasma Physics via Computer Simulation”, Series in Plasma Physics and Fluid Dynamics, CRC Press, 2004. <https://books.google.ru/books?id=S2lqgDTm6a4C>
 13. T. Takizuka and H. Abe, “A binary collision model for plasma simulation with a particle code”, *J. Comput. Phys.* **25**, 205 (1977); [http://doi:10.1016/0021-9991\(77\)90099-7](http://doi:10.1016/0021-9991(77)90099-7)
 14. H.-K. Chung, M.H. Chen, W.L. Morgan, Y. Ralchenko and R.W. Lee , “FLYCHK: Generalized population kinetics and spectral model for rapid spectroscopic analysis for all elements”, *High Energy Density Physics*, **1**, 3 (2005); <https://doi.org/10.1016/j.hedp.2005.07.001>
 15. Yukikazu Itikawa, “Cross Sections for Electron Collisions with Oxygen Molecules”, *Journal of Physical and Chemical Reference Data* **38**, 1 (2009); <http://dx.doi.org/10.1063/1.3025886>
 16. Cechan Tian and C. R. Vidal, “Electron impact ionization of N₂ and O₂: contributions from different dissociation channels of multiply ionized molecules”, *J. Phys. B: At. Mol. Opt. Phys.* **31**, 5369 (1998); <http://dx.doi.org/10.1088/0953-4075/31/24/018>
 17. A. Dalgarno, “The mobilities of ions in their parent gases“, *Philos. Trans. R. Soc. London, Ser. A*, **250**, 426 (1958); DOI: 10.1098/rsta.1958.0003
 18. Frank O. Goodman, “Thermal accommodation coefficients”, *J. Phys. Chem.*, **84**, 1431 (1980); <http://10.1021/j100449a002>
 19. G.G. Gulbekian, B.N. Gikal, V.V. Bekhterev, S.L. Bogomolov, A.A. Efremov, I.A. Ivanenko, N.Yu. Kazarinov, I.V. Kalagin, V.N. Melnikov, N.F. Osipov, S. V. Prokhorov, A.V. Tikhomirov, and M.V. Khabarov, “Proposed design of axial injection system for the DC-280 cyclotron”, *Phys. Part. Nuclei Lett.*, **11**, 763 (2014); DOI: 10.1134/S1547477114060028
 20. M.A. Lieberman and A.J. Lichtenberg, “Theory of electron cyclotron resonance heating. II. Long time and stochastic effects”, *Plasma Phys.* **15**, 125 (1973); <http://dx.doi.org/10.1088/0032-1028/15/2/006>
 21. A.G. Drentje, “Anomalous charge state distribution in ECRIS for oxygen isotopes”, *Review of Scientific Instruments* **63**, 2875 (1992); <http://dx.doi.org/10.1063/1.1142783>

22. Y. Kawai, D. Meyer, A. Nadzeyka, U. Wolters and K. Wiesemann, "Isotope effects in an electron cyclotron resonance ion source in mixtures of $^{15}\text{N}/^{14}\text{N}$ ", *Plasma Sources Sci. Technol.* **10** (2001) 451–458
23. S. Song and M.M. Yovanovich, "*Correlation of Thermal Accommodation Coefficient for Engineering Surfaces*", ASME HTD **69**, Fundamentals of Conduction and Recent Developments in Contact Resistance, edited by M. Imber, G.P. Peterson and M.M. Yovanovich, 107-116 (1987)
24. [G. Melin](#), [A.G. Drentje](#), [A. Girard](#), and [D. Hitz](#), "Ion behavior and gas mixing in electron cyclotron resonance plasmas as sources of highly charged ions", *Journal of Applied Physics* **86**, 4772 (1999); <http://dx.doi.org/10.1063/1.371442>
25. ¹. O. Tarvainen, P. Suominen, T. Ropponen, H. Koivisto, R.C. Vondrasek, and R.H. Scott, "Plasma potential measurements with a new instrument", *AIP Conf. Proc.* **749**, 61 (2005); <http://dx.doi.org/10.1063/1.1893367>

2.7 Pulsed high intensity ECRs

V.A. Skalyga

Mail to: skalyga.vadim@gmail.com

Federal Research Center "Institute of Applied Physics of the Russian Academy of Sciences" 46 Ul'yanova St., 603950 Nizhny Novgorod, Russian Federation

2.7.1 Introduction

Production of high intensity ion beams from an ECR discharge could be realized in a pulsed mode when microwave power level coupled into a plasma is much higher than it is used in continuous wave (CW) operation. Basic principle is rather simple: a high current density ion beam could be produced in case of dense plasma flux from a magnetic trap caused by fast losses; fast losses mean high heating power required for electron temperature sustaining at the level necessary for efficient ionization. Investigations of pulsed ECR discharge in an open magnetic trap under conditions of powerful ECR heating with gyrotron mm-waveband radiation were carried out over the last 20 years at the Institute of Applied Physics (IAP RAS, Nizhniy Novgorod, Russia) [1-5] and continued at Laboratoire de Physique Subatomique & Cosmologie (LPSC, Grenoble France) [6, 7]. In the beginning the work was devoted to development of a high frequency ECR source of multi-charged ions with outstanding parameters of plasma heating (37.5 GHz, 100 kW). According to Geller's scaling laws [8] such increase in frequency and power in comparison to conventional ECRIS was expected to boost the ion source performance and provide a significant progress in ECRIS development. However, due to short pulse operation mode and low repetition rate of the used gyrotrons (pulse duration < 1 ms, 0.1 Hz) breakdown and discharge conditions similar to a conventional ECRIS were unreachable. The minimum neutral gas pressure was two orders higher (10^{-4} mbar) and the plasma parameters differed significantly from conventional ECRIS. After years this work resulted in development of a new type of ion source – high current gasdynamic ion source.

2.7.2 Quasi-gasdynamic plasma confinement

The use of powerful mm-band radiation allows to increase the plasma density in the discharge significantly (proportional to the square of the radiation frequency [4-9]) in comparison to conventional ECRISs, which utilize microwave radiation with frequencies on the order of 10 GHz [8]. In experiments with gyrotrons frequency range 37.5 – 75 GHz the plasma density reaches values of 10^{13} - 10^{14} cm⁻³[10, 11]. Significant increase of the plasma density leads to a change of the confinement mode. A so-called quasi-gasdynamic confinement [4, 5] was realized in the presented experiments instead of the collision-less confinement [12], which is typical for modern ECRISs. The transition from collision-less to quasi-gasdynamic confinement occurs when the plasma density is high enough for the scattering rate of electrons into the loss-cone to be higher than the maximum possible electron loss rate caused by the ion-sound flux through the magnetic mirrors [13]. In such situation the loss-cone in the velocity space is populated, and the plasma lifetime does not depend on the collisional electron scattering rate into the loss-cone i.e. on the plasma density, but is determined by the trap size, magnetic field structure and ion sound velocity [13]. The plasma lifetime, which is much shorter than in conventional classical ECRISs, can be expressed as $\tau=(L \cdot R)/(2V_{is})$, where L is the magnetic trap length, R the trap mirror ratio (ratio between magnetic field in the magnetic mirror and in the trap center) and V_{is} the ion sound velocity. Short plasma lifetime provides high plasma flux density from the trap. The flux is proportional to the plasma density and ion lifetime i.e. $I \sim N / \tau$, where N is the plasma density. Due to the high plasma density, the confinement parameter $Ne \cdot \tau$, which determines the ionization degree and average ion charge, can be as high as $10^8 - 10^9$ s·cm⁻³, which is enough for efficient ionization. The main advantages of quasi-gasdynamic confinement are the following. The plasma lifetime does not depend on its density and, therefore increase of the density would lead to rising of confinement parameter and average ion charge. In addition, the plasma lifetime is proportional to the magnetic trap length and the source performance could be improved by adjusting the trap length. In case of extremely high frequency heating and accordingly higher plasma density multiple ionization is possible even in a small plasma volumes. ECR sources running under conditions of such plasma confinement are called gasdynamic ECRISs.

Possibilities and prospects of the gasdynamic confinement were demonstrated at SMIS 37 facility [4, 5] and at SEISM Prototype [6, 7]. It was shown that the described peculiarities of quasi-gasdynamic ECR discharge sustained by mm-waveband radiation, namely, short lifetime and high density, provide unprecedented ion current densities up to 800 emA/cm².

2.7.3 SMIS 37 experimental facility

The main part of the experiments devoted to the topic was conducted at SMIS 37 facility. During the years its configuration has been changing slightly, the latest one being schematically depicted in Fig.1. The plasma is created and sustained inside a d=4 cm vacuum chamber (placed in a magnetic trap) by pulsed (1 ms) 37.5 GHz or 75 GHz linearly polarized gyrotron radiation with power up to 100 kW. The simple mirror magnetic field (or a cups trap for some experiments) is created by means of pulsed solenoids positioned at a distance of 15 cm from each other, providing a mirror ratio of 5. The magnetic field strength could be varied in a range of 1-4 T at mirror plugs, whereas

the resonant field strength is 1.34 T for 37.5 GHz and 2.7 T for 75 GHz. The microwave radiation is coupled to the chamber quasi-optically through a quartz window and a special coupling system, which protects the window from the plasma flux. Quasi-optical coupling appears to be the best choice for high power microwave radiation transport into an ion source especially because air gaps additionally could be used as a DC-break between high voltage plasma chamber and microwave source. At SMIS 37 the pulsed gas feeding is used and gas line is incorporated into the coupling system i.e. the neutral gas is injected axially.

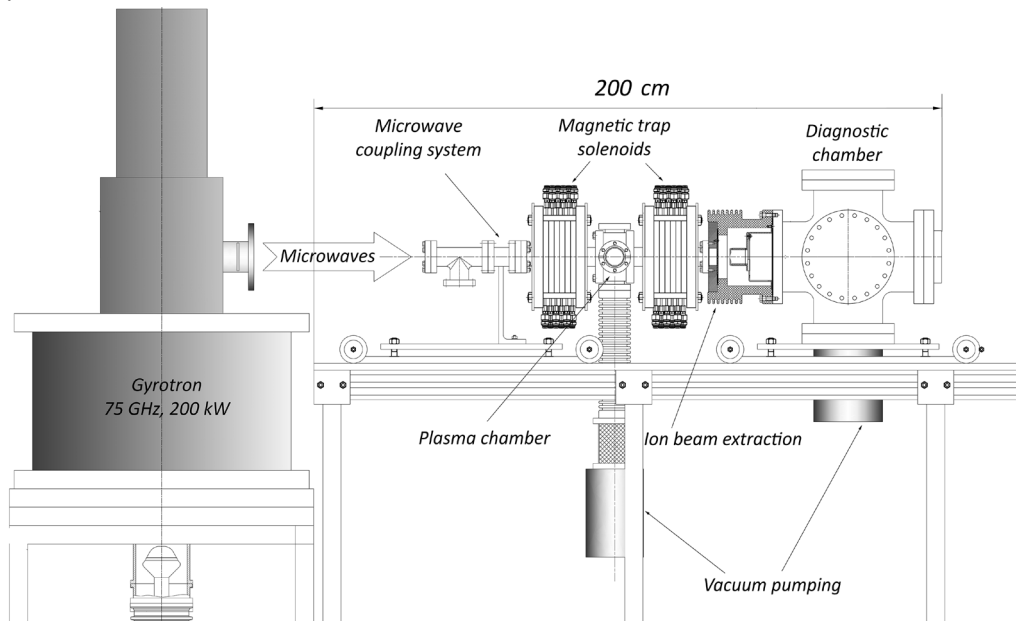


Figure1: Schematic view of SMIS 37 experimental facility.

The ion extraction and beam formation is realized by a two-electrode (diode) system consisting of a plasma electrode and a puller. The diameter of the extraction aperture is varied from 1 to 10 mm. The distance between the extraction system and the magnetic plug at the center of the solenoid magnet was designed to be variable, which allows tuning the plasma flux density at the plasma electrode. The maximum applied extraction voltage is up to 100 kV. A Faraday cup with an aperture of 85 mm is placed right behind the puller (grounded hollow electrode) to capture the whole beam. The cup is equipped with an electrostatic secondary electron suppression. A 42° bending magnet is installed downstream in the beam line for measuring extracted beam spectrum.

2.7.4 Multi-charged ions production

A number of papers were devoted to multi-charged beam production at SMIS 37 [1-5]. In this paper the main results obtained some years ago are shown to demonstrate the typical source performance. In Fig.2 two ion spectra with nitrogen and argon are presented in the case of 37.5 GHz, 100 kW plasma heating.

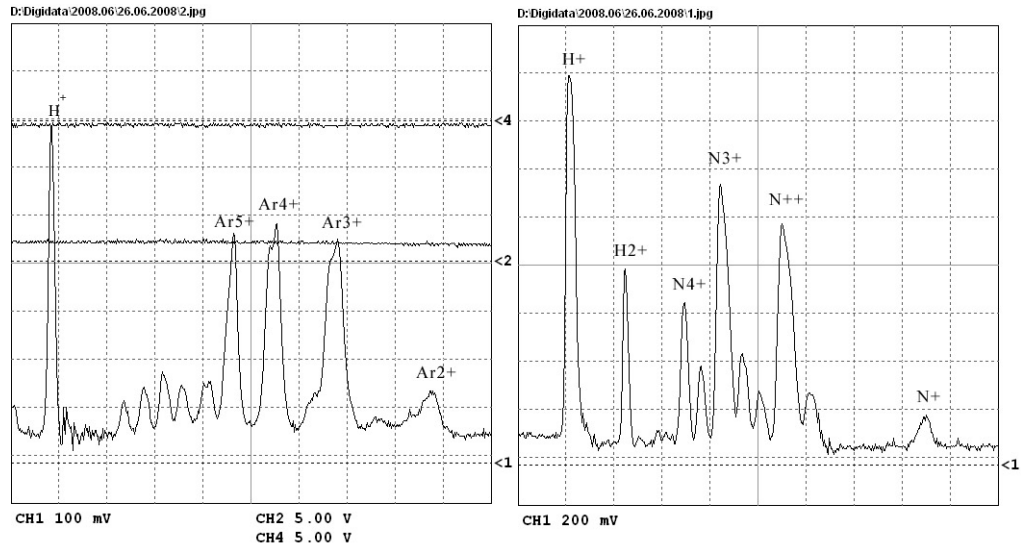


Figure 2: Argon and Nitrogen spectra. ECR plasma heating with 37.5 GHz, 100 kW gyrotron radiation in a simple mirror trap.

The effect of plasma density increase within gasdynamic confinement with increase of microwave frequency is shown in Fig.3. Helium ion spectra for 37.5 and 75 GHz, 100 kW and 200 kW heating correspondingly demonstrate a great improvement in average ion charge.

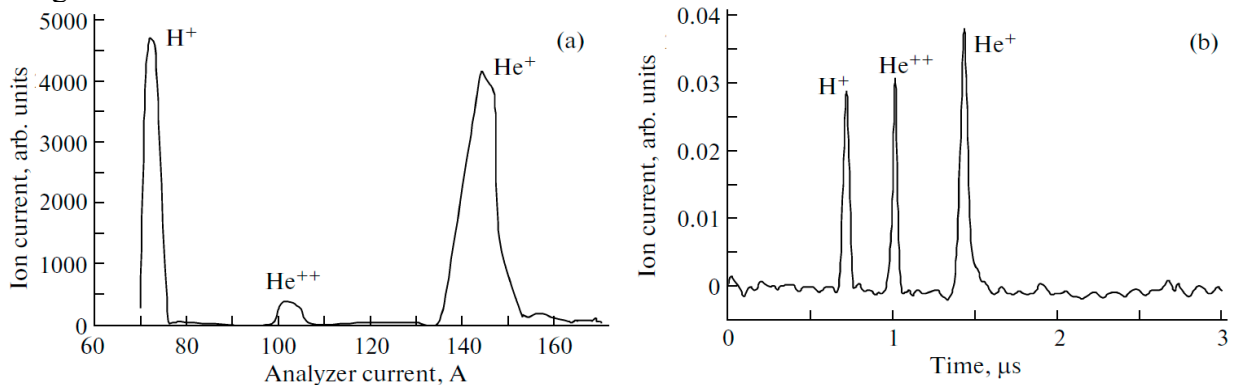


Figure. 3: Helium spectra. 37.5, 100kW ECR heating (left) and 75 GHz, 200 kW ECR heating (right). Plasma is confined in a cusp trap with an effective length of 28 cm, the gas pressure is 10^{-4} Torr.

In these experiments a single aperture two electrode extraction system with 1 mm hole was used for beam formation providing total ion current up to 10 mA [2]. Normalized beam emittance measured with pepper-pot method was of the order of $0.01 \pi \cdot \text{mm} \cdot \text{mrad}$. The experiments were repeated later with multi-aperture extraction systems. Extracted ion current dependence on the accelerating voltage in case of 13-hole (each 3 mm in diameter) plasma electrode is shown in Fig.4.

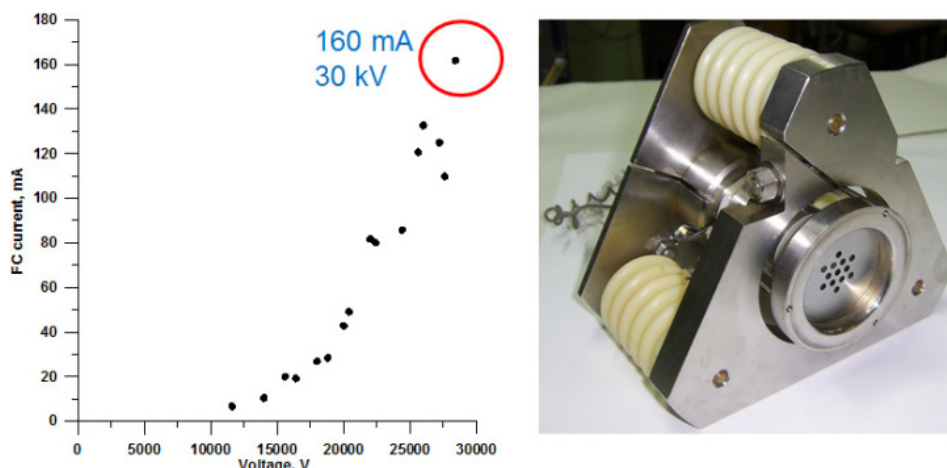


Figure 4: Faraday cup current dependence on extraction voltage (left) obtained with multi-aperture extraction system (right).

Presented results demonstrate that gasdynamic ion source is able to produce hundreds of emA of moderately charged (Q up to $6+$) beams. Low emittance and high current of such beams may allow using them together with charge-breeding or stripping techniques. Further increase of the microwave frequency is promising for the production of high current heavy ion beams with the average charge about $+10$ and their injection into accelerators with strippers after first acceleration stage.

The state of the art ion source of this type called SEISM Prototype have been built recently in Grenoble in the framework of international collaboration between LPSC, IAP RAS and LNCMI (CNRS). It is the first ECRIS with a topologically closed 60 GHz ECR resonance zone, using radially cooled polyhelices. Unique ion beam intensities have been extracted from this prototype, like 1.1 mA of O^{3+} through a 1mm hole representing a current density of 140 mA/cm^2 [7]. In first experiments a significant currents of highly charged ions like O^{5+} were also observed. Further investigation at this experimental facility should demonstrate the ultimate performance of gasdynamic ECR ion sources.

2.7.5 Short pulse ion beams

Many of the modern technologies and basic research facilities require the creation of an ion source capable of generating short-pulse ($20 - 100 \mu\text{s}$), high current (tens or hundreds of milliamps) heavy gases ion beams with a fairly high average charge and low emittance. Gasdynamic ECR sources of multi-charged ions seem to be the most promising in this respect. In this case, the plasma confinement in a magnetic trap is quasigasdynamic and has a typical lifetime of 10 to $20 \mu\text{s}$. Under these conditions, there are two modes of generating high-current ion pulses of short duration, namely, quasi-stationary and non-stationary. The possibility of quasi-stationary generation of short-pulse multi-charged ion beams is related to a short plasma lifetime in the trap of a gasdynamic ECR source, which ensures that the plasma density can reach a steady-state level within a short time. To obtain short pulses in the non-stationary generation mode, one can use the well-known preglow effect [14 - 17], in which a peak current of extracted multiply charged ion beam with amplitude exceeding several steady-state values is observed at the initial stage of a discharge. In addition, it was found in [18] that in the case the gyrotron pulse duration is less than or of the order of the typical time of the preglow peak formation the beam current occurs predominantly after the end of the microwave pumping in the

form of an intense short burst. Apparently a similar effect was observed earlier in [19] and was named “the micropulsed mode”.

In experiments conducted at SMIS 37 it was demonstrated that gasdynamic ECR ion source running in such “micropulsed mode” is able to produce multi-charged ion beams with duration less than 100 μs . Waveforms of the full beam current and for Ar^{4+} and Ar^{5+} currents are shown in Fig.5.

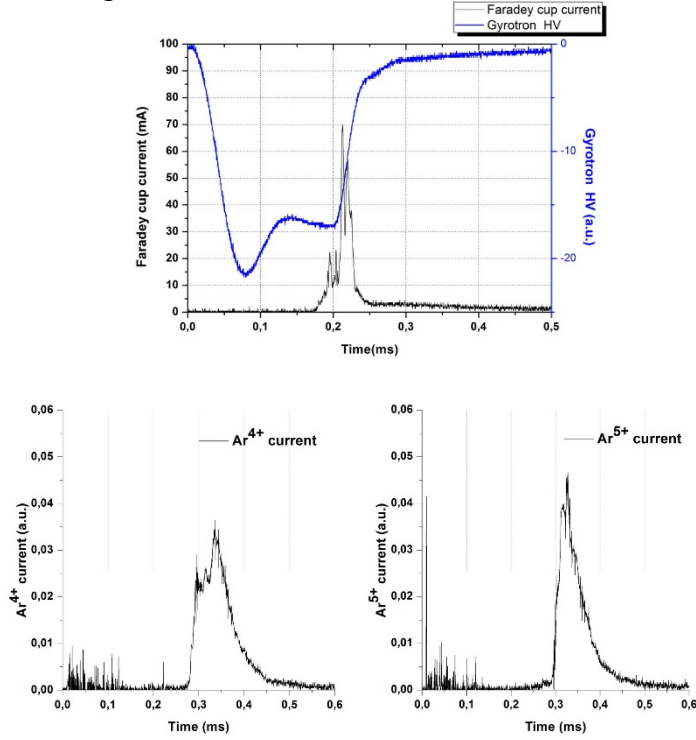


Figure 5: Oscillogram of the argon ion beam current (Faraday cup current) for an extraction voltage of 23 kV is on the left. High-voltage pulse of the gyrotron cathode (which duration is close to the one of microwave power pulse) is shown. Corresponding currents of separate beam species (Ar^{4+} and Ar^{5+}) are on the right.

The total beam current extracted with multi-aperture extraction system described above was at the level of 100 mA.

Later some theoretical work showing a possibility of high ionization efficiency in case of short-living radioactive isotopes beams production was reported in [20]. For the needs of Beta Beam project [21] it was shown that gasdynamic ECR source in the short pulse mode could provide up to 50% utilization of ${}^6\text{He}$ in fully stripped ions.

2.7.6 Proton and deuteron beams formation

Operation of modern high power accelerators often requires production of intense proton and deuterium beams. H^+ beams are utilized or envisioned for use in linear accelerators e.g. the future European Spallation Source under design [22, 23]; some special applications such as neutron generators or the IFMIF project, require D^+ (deuteron) ion beams. Requirements for the brightness of such beams grow together with the demand of accelerator development and arising experimental needs. New facilities aiming at outperforming the previous generation accelerators are usually designed for higher beam currents. Enhancing the beam intensity and maintaining low transverse

emittance at the same time is, however, quite a challenging task. The most modern accelerators require H⁺/D⁺ ion beams with currents up to hundreds of mA (pulsed or CW), and normalized emittance less than $0.2 \pi \cdot \text{mm} \cdot \text{mrad}$ [22, 24] to keep the beam losses at high energy sections of the linacs below commonly imposed 1 W/m limit. Previous experiments on heavy multi-charged ion production demonstrated that gasdynamic ion source is able to produce ion beams with record beam current density and moderate ion charge. The average electron energy in plasma of ECR discharge with quasi-gasdynamic confinement sustained by gyrotron radiation varies from 50 to 300 eV and it is optimal for efficient hydrogen ionization. Due to this coincidence it was decided to test the gasdynamic ECR source performance for proton and deuteron beams formation. In previous papers [25, 26] it was demonstrated that proton beams with current of hundreds of mA could be produced. The latest results are presented below.

A single-aperture extraction system was used for beam formation in the presented experiments. As only two fixed puller holes were available (i.e. 10 and 22 mm in diameter), the optimization of extraction electrode configuration was done varying the gap between the electrodes. The biggest hole diameter in plasma electrode was 10 mm. In this case the optimal gap between electrodes for 10 mm plasma electrode aperture appeared to be 6 mm, while the puller hole diameter was 22 mm. The Faraday cup and puller currents are shown in Fig.6(a). The total beam current remains relatively stable at the level of 450 mA through 70% of the microwave pulse. Accelerating voltage of 41.5 kV was used. Transversal emittance diagram is presented in Fig.6(b), showing an RMS value of $0.07 \pi \cdot \text{mm} \cdot \text{mrad}$.

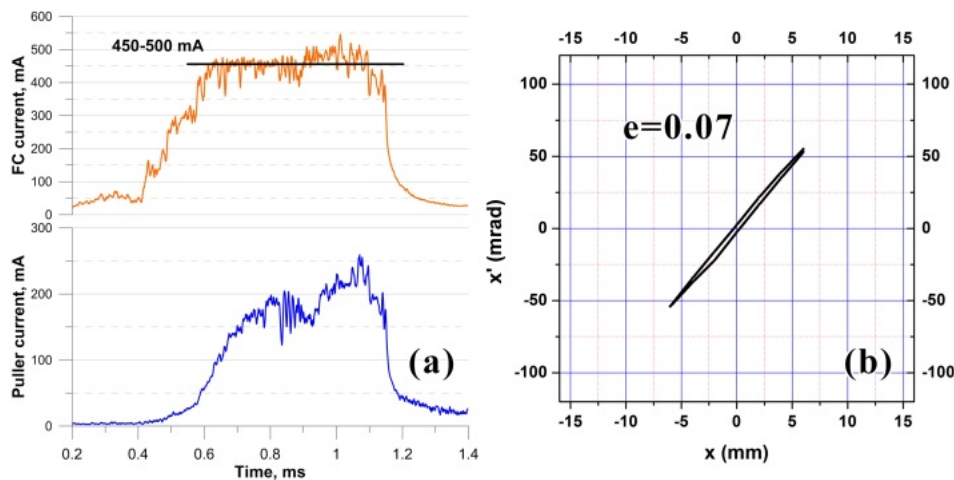


Figure 6: Hydrogen, 10 mm plasma electrode hole (a) Faraday cup and puller currents, (b) RMS emittance diagram.

The experiments with deuterium were performed under similar conditions. Source settings were adjusted slightly from the optimal ones for proton beam to maximize the total current. It was observed that the total beam current rapidly reached a value of 400 mA, then slowly increased to 500 mA and remain there till the end of the microwave pulse. Accelerating voltage of 42 kV was used. Transversal emittance had the same RMS value of $0.07 \pi \cdot \text{mm} \cdot \text{mrad}$.

The presented results demonstrate the prospects of the high current gasdynamic ECR source for light ion beams production. The maximum RMS brightness of extracted beam reached $100 \text{ A}/(\pi \cdot \text{mm} \cdot \text{mrad})^2$. The proton (deuteron) fraction in extracted beams was about 94 % as it was shown in [25].

The extracted beam current could be further enhanced by moving the plasma electrode closer to the magnetic mirror and scaling the extraction voltage and geometry appropriately. According to simulations, the extracted current may eventually exceed 1 A while maintaining the low emittance. Such result would outperform the conventional ECRISs by a great margin.

2.7.7 Conclusion

The presented results demonstrate the main prospects of the gasdynamic ECRIS. This type of ECRIS has already demonstrated its benefits for light ion beam production. Further studies could significantly increase its performance in multi-charged beam formation. One of the most promising new ion sources which may demonstrate all capabilities of gasdynamic confinement is the SEISM, 60 GHz ECRIS at LPSC, Grenoble. The Grenoble facility has a number of advantages in comparison with SMIS 37. The first is a high repetition rate (up to 2 Hz) which allows better control of plasma parameters due to satisfactory wall conditioning. The second is the cusp magnetic field of high intensity (up to 7 T) with closed ECR surface. It is the first ion source which can operate effectively in gasdynamic mode having a closed-ECR field, which is of great importance for trapping of energetic electrons. Therefore, interesting results are foreseen from SEISM source, as it may be the first ECRIS able to operate in-between of gasdynamic and traditional collision-less confinement, thus producing high currents and charges.

Another direction of gasdynamic sources evolution is to apply them to CW operation to produce CW high current beams for different applications. First results on such studies with CW discharge sustained with 24 GHz gyrotron are presented in [27]. It was shown that dense ECR discharge can be sustained in CW mode producing plasma fluxes with 1 eA/cm² density.

2.7.8 References

1. S.V Golubev, S.V. Razin, A.V. Sidorov, V.A. Skalyga, A.V. Vodopyanov, V.G. Zorin, “ High Current Density Ion Beam Formation from Plasma of ECR Discharge ”, *Review of Scientific Instruments*. v.75, n5, p. 1675-1677, 2004.
2. S.V. Golubev, I.V. Izotov, S.V. Razin, V.A. Skalyga, A.V. Vodopyanov, V.G. Zorin. Multicharged Ion Generation in Plasma Created by Millimeter Waves and Confined in a CUSP Magnetic Trap. *Transactions of Fusion Science and Technology*, v. 47, n. 1T , fuste8, p. 345-347, 2005.
3. A. Sidorov, I. Izotov, S. Razin, V. Skalyga, V. Zorin, A. Balabaev, S. Kondrashev, A. Bokhanov. Beam Formation from Dense Plasma of ECR Discharge. *Review of Scientific Instruments*. v.77, n3, p. 03A341-1 – 03A341-4, 2006.
4. V. Skalyga, V. Zorin, I. Izotov, S. Razin, A. Sidorov, A. Bohanov. Gasdynamic ECR Source of Multicharged Ions Based on a Cusp Magnetic Trap. *Plasma Sources Science and Technology* 15 (2006) 727-734.
5. S. Golubev, I. Izotov, S. Razin, A. Sidorov, V. Skalyga, A. Vodopyanov, V. Zorin, A. Bokhanov. High Current ECR Source of Multicharged Ion Beams. *Nuclear Instruments and Methods in Physics Research B*, v. 256, p. 537 – 542, 2007.

6. M. Marie-Jeanne et al., “Status of the SEISM experiment”, proceedings of the 20th International Workshop on Electron Cyclotron Resonance Ion Sources ECRIS2012, Sydney, Australia, pp. 111-113,
7. Lamy, T. et al Proceedings of the 13th International Conference on Heavy Ion Accelerator Technology. P. THM2101.
8. Geller R. Electron cyclotron resonance ion sources and ECR plasmas. Institute of Physics. Bristol. 1996.
9. M.A. Dorf, V.G. Zorin, A.V. Sidorov, A.F. Bokhanov, I.V. Izotov, S.V. Razin, V.A. Skalyga. Generation of Multi-Charged High Current Ion Beams using the SMIS 37 Gas-dynamic Electron Cyclotron Resonance (ECR) Ion Source. // Nuclear Instruments and Methods in Physics Research (section A: Accelerators, Spectrometers, Detectors and Associated Equipment), v. 733, p. 107-111, 2014.
10. Golubev S V et al 2000 Rev. Sci. Instrum. 71, 2, pt. 2, 669
11. Vodopyanov A V et al 2007 High Energy Phys. and Nucl. Phys. 31(S1), 152
12. Pastukhov V 1984 Voprosy teorii plasma 13, 160.
13. Mirnov V.V., Ryutov D.D. 1979 *Pisma v Zhurnal Tekhnicheskoi Fiziki* 5, 678
14. V.G. Zorin, V.A. Skalyga, I.V. Izotov, S.V. Razin, A.V. Sidorov, T. Lamy, T. Thuillier, Trans. Fusion Sci. Technol. **59**, 140 (2011)
15. T. Thuillier, T. Lamy, L. Latrasse, I.V. Izotov, A.V. Sidorov, V.A. Skalyga, V.G. Zorin, M. Marie-Jeanne, Rev. Sci. Instrum. **79**, 02A314 (2008)
16. I.V. Izotov, A.V. Sidorov, V.A. Skalyga, V.G. Zorin, T. Lamy, L. Latrasse, T. Thuillier, IEEE Trans. Plasma Sci. **36**, 1494 (2008).
17. V. Skalyga, I. Izotov, V. Zorin, and A. Sidorov. Physical principles of the preglow effect and scaling of its basic parameters for electron cyclotron resonance sources of multicharged ions. Physics of Plasmas, 19, 023509 (2012).
18. V. Skalyga, I. Izotov, S. Razin, A. Sidorov, V. Zorin, Proceedings of the 8-th International workshop «Strong microwaves and terahertz waves: sources and applications». Nizhny Novgorod - St. Petersburg, Russia, July 9-16, 2011, p. 200-201.
19. L. Maunoury, L. Adoui, J.P. Grandin, F. Noury, B.A. Huber, E. Lamour, C. Prigent, J.P. Rozet, D. Vernhet, P. Leherissier, J.Y. Pacquet, Rev. Sci. Instrum. **79**, 02A313 (2008).
20. I. V. Izotov, V. A. Skalyga, V. G. Zorin. Optimization of gas utilization efficiency for short-pulsed electron cyclotron resonance ion source. Rev. Sci. Instrum. **83**, 02A342 (2012).
21. beta-beam.web.cern.ch
22. Gammino S et al, LINAC2010, Tsukuba, Japan, THP116, (2010). <http://www.JACoW.org>
23. Lindroos M et al. 2011 Nucl. Instrum. Methods B 269, 3258
24. Gobin R et al 2012 Rev. Sci. Instrum. 83, 02A345
25. V. Skalyga, I. Izotov, S. Razin, A. Sidorov, S. Golubev, T. Kalvas, H. Koivisto, and O. Tarvainen. “High current proton beams production at Simple Mirror Ion Source 37”. // Review of Scientific Instruments, v. 85, no. 2, 2014, p. 02A702-1 – 02A702-3.
26. V. Skalyga, I. Izotov, A. Sidorov, S. Razin, V. Zorin, O. Tarvainen, H. Koivisto, T. Kalvas. High current proton source based on ECR discharge sustained by 37.5 GHz gyrotron radiation. JINST, v.7, P10010 (2012).

27. Skalyga, V., Izotov, I., Golubev, S., Vodopyanov, A., & Tarvainen, O. (2016). First experiments with gasdynamic ion source in CW mode. *Review of Scientific Instruments*, 87(2), 02A715.

2.8 Charge Breeding with Electron Cyclotron Resonance Ion Sources

Richard Vondrasek

Mail to: Vondrasek@ANL.GOV

Argonne National Laboratory, 9700 South Cass Ave, Lemont, IL 60439 USA

2.8.1 Introduction

The efficient and rapid production of a high-quality, pure beam of highly charged ions is at the heart of any radioactive ion beam facility. The electron cyclotron resonance (ECR) charge breeding ion source was developed to produce such a beam. With their ability to accept a large influx of low charge state ions, rapidly and efficiently raise their charge state, and extract a high quality beam for post-acceleration, ECR charge breeding technology has been adopted at radioactive ion beam (RIB) facilities worldwide. Since the development of the original technology at the Laboratoire de Physique Subatomique & Cosmologie (LPSC) in 1995 [1], an ever improving understanding of the charge breeding dynamics has led to a rapid advance in breeding efficiency as well as the development of pathways to address the omnipresent stable background thus far inherent to ECR charge breeders.

2.8.2 ECR Charge Breeders

The technology of ECR ion sources is established and has been well described elsewhere [2]. ECR charge breeders (ECRCB), such as the LPSC PHOENIX ion source [3] shown in Fig. 1, are an evolution of this technology, and it is useful to highlight some of the key parameters which determine their performance: the operating frequency (RF), the magnetic field profile, and the operating pressure. With regard to the RF, a higher operating frequency used in conjunction with higher magnetic fields results in a higher electron density n_e producing higher beam intensities and a shift to higher charge states. This principle is embodied in the third generation superconducting sources where a shift to higher operating frequency and stronger fields has resulted in substantially higher beam intensities and achievable charge states [4-7]. However, total extracted beam intensity is not necessarily an indicator of optimum single charge state breeding efficiency. Most ECRCBs run with a low-density plasma which is poor for total extracted beam intensity but is beneficial for breeding efficiency. As charge breeding investigations with superconducting sources have not yet been performed, it is an open question if the higher operating frequencies of these sources will improve the single charge state efficiency and breeding time.

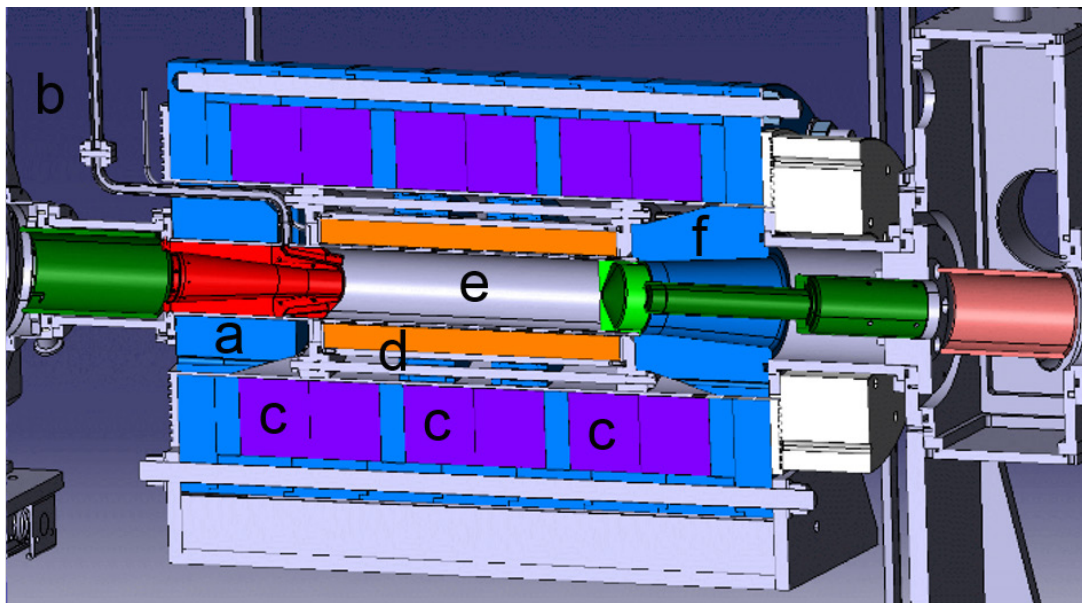


Figure 1: The LPSC PHOENIX source which has versions installed at the LPSC test bench, TRIUMF, SPIRAL1, and SPES. The various parts are the a) soft iron plug, b) RF waveguide, c) solenoid coils for axial magnetic field, d) permanent magnet hexapole for radial magnetic field, e) the plasma chamber, f) the extraction region. (Figure courtesy of J. Angot)

The magnetic field profile of an ECR is a minimum-B structure created by two to three solenoid coils surrounding a permanent magnet hexapole. The minimum-B structure stabilizes the plasma and creates a closed surface at which the resonant electron cyclotron motion excitation is fulfilled by the condition $f_{rf} = eB_{res}/m_e$. This can be conveniently reduced to $f_{rf} = 2.8B_{res}$ where f_{rf} is the operating frequency in GHz and B_{res} is the magnitude of the resonant magnetic field in kilogauss. The resonant condition can be fulfilled by other field topologies, but none have been used in connection with charge breeding. Also of importance are the magnitudes of the magnetic fields at the injection and extraction points as well as on the surface of the plasma chamber vessel. These values will affect the overall source performance and are governed by the scaling laws [8]. An overlay of the ANL ECRCB axial magnetic field profile is shown in Fig. 2 with the B_{inj} on the source injection side, the B_{min} located in the central portion of the plasma chamber, and the B_{ext} at the extraction aperture.

From their inception, charge breeding ECR sources typically operated in the pressure regime of 10^{-7} Torr. However, to improve the high charge state performance, a support gas is introduced which serves to cool the heavier ions within the plasma [9]. Since the introduction of any additional components into the ECR plasma can result in a higher level of stable background, the support gas is typically helium or oxygen thus limiting the number of conflicts with any RIB which may have a similar A/Q. Subsequent investigations have found that operating closer to the UHV regime results in higher charge breeding efficiencies as well as enhanced high charge state production [10].

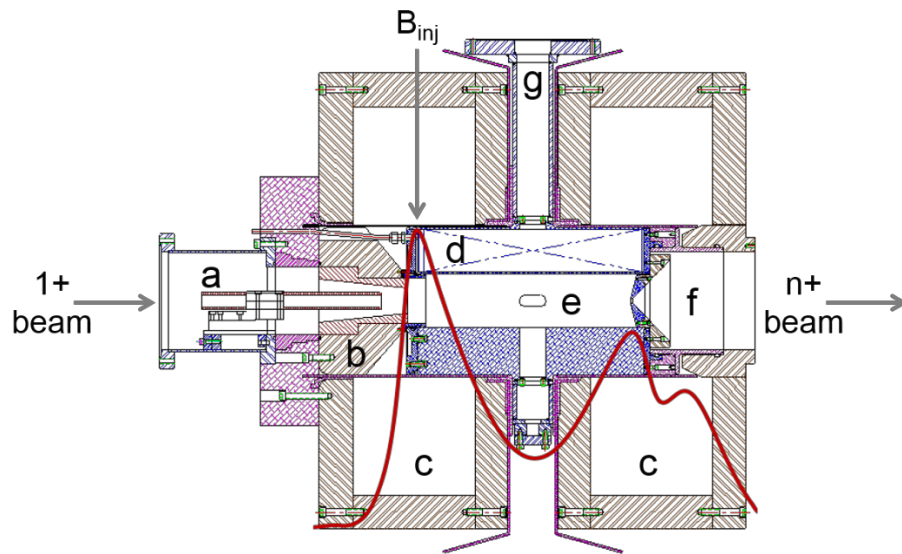


Figure 2: The ANL ECRCB source with an overlay of its axial magnetic field profile showing a maximum value (B_{inj}) near the end of the grounded tube where the $1+$ ions are injected. Shown are the a) grounded tube, b) soft iron plug, c) solenoid coils, d) permanent magnet hexapole, e) plasma chamber with its radial ports, f) extraction region, g) pumping port for plasma volume.

With incident RIB intensities varying between 10^4 Hz and 10^7 Hz, any stable background can obscure RIB detection and limit the accelerator operations envelope. For this reason, the overall plasma chamber cleanliness is crucial in terms of materials of construction as well as materials introduced into the ion source over the course of its operational life. Thus far three facilities - KEK, TRIUMF, and ANL - have reaccelerated RIBs using ECR charge breeders, and each facility has encountered difficulties with the stable background.

2.8.3 The $1+ \rightarrow n+$ Method

Several ECRCBs have been in operation (LPSC [11], ISOLDE [12], KEK [13], TRIUMF [14], GANIL/SPIRAL [15], ANL [16], SPES [17], Texas A&M [18]) with all functioning on the same basic principle. A low-charge state DC beam, typically $1+$, is transported from its point of origin, injected into the ECR ion source, captured in the plasma, and charge bred to $n+$ state. The large trap capacity and acceptance of the ECR permits the injection of large beam currents (up to $2 \mu\text{A}$) with high emittances ($55 \pi \cdot \text{mm} \cdot \text{mrad}$) [19]. The ions are introduced into the source volume via a grounded tube, although it has also been demonstrated that this tube is not a requirement [20]. The capture condition into the ECR plasma is that the final speed of the $1+$ ions is equal to the speed of the plasma ions which is $\sim 2 \text{ eV}$ [21]. This is accomplished with a differential voltage (ΔV) applied between the $1+$ source potential (V) and the ECRCB potential ($V + \Delta V$). With this, the ions decelerate into the plasma region where a sub-set of them undergo long-range ion-ion collisions which serve to thermalize their velocity and capture them in the plasma [22]. The magnitude and width of the ΔV window is dependent upon whether the injected ion is gaseous or metallic as well as the characteristic energy spread of the $1+$ source generating the beam. After capture, the ion charge state is increased stepwise by collisions with energetic electrons. The breeding efficiency of a single charge

state is defined as the ratio $\eta_q = [I(q+)/qI(1+)]$ where q is the desired charge state, $I(q+)$ is the current of that charge state, and $I(1+)$ is the current of the $1+$ beam incident into the plasma. The global efficiency is the sum of efficiencies across all visible charge states $\eta_G = \sum_{i=1 \rightarrow N} \eta_i$.

By pulsing a stable $1+$ beam, the resultant $n+$ beam pulse can be distinguished from any steady-state background constituents which may have a similar A/Q . The various source and beamline parameters available to the operator can then be tuned for maximum $n+$ intensity, and thus efficiency, while remaining decoupled from any changes in the steady state operation of the ion source. The breeding time τ_b of the charge bred beam has been defined as the time between the introduction of the $1+$ ions into the plasma and when the $n+$ beam reaches 90% of its steady-state value. The configuration of the LPSC charge breeding test bench is shown in Fig. 3 and is typical in its components. After production, the stable $1+$ beam is pulsed with an electrostatic deflector, analyzed with a dipole magnet, and the $1+$ intensity measured on a faraday cup. The charge bred $n+$ beam is analyzed with a dipole magnet and detected on another faraday cup thus allowing the breeding efficiency to be calculated. For the detection of RIBs, the $1+$ and $n+$ faraday cups are replaced with aluminum foil covered silicon barrier detectors (SBD). The radioactive beam implants into the foil with the beta decay detected by the SBD. In this case, η_q is simply the ratio of the rates into the two detectors $[N(q+)/N(1+)]$, and the $1+$ beam is not pulsed as any stable beam components with similar A/Q do not trigger a beta decay event.

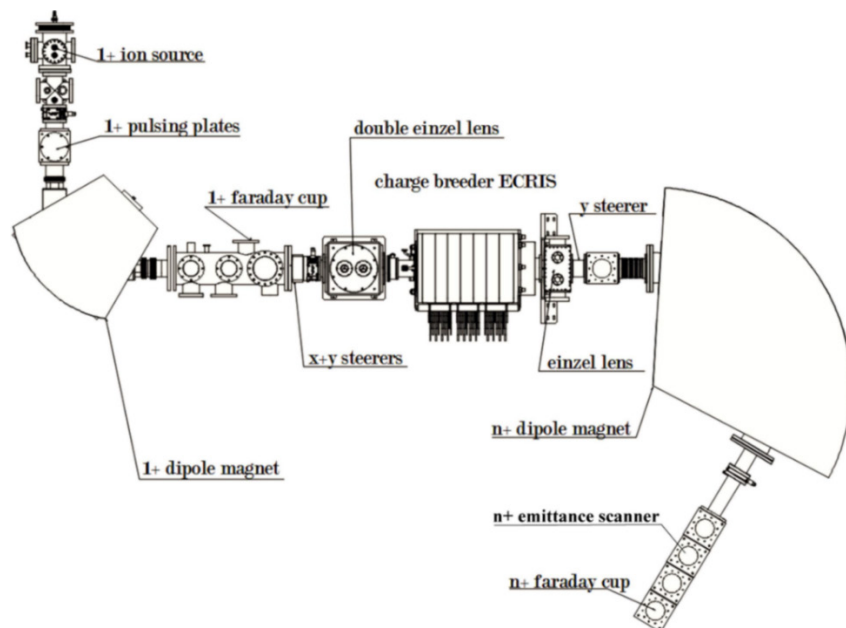


Figure 3: Lay-out of the LPSC ECRCB test bench used with stable beams for the development of charge breeding techniques. (Figure courtesy of LPSC)

2.8.3.1 *Relevant parameters*

2.8.3.1.1 Efficiency versus ΔV

As mentioned earlier, the ΔV voltage applied to the ECRCB serves to compensate for the potential difference between the $1+$ source and the ECR plasma. An example of ΔV tuning is shown in Fig. 4. For the solid elements Na and Cs, the optimum ΔV values were

-4 V and -15 V respectively with acceptance windows of ± 3 V and ± 5 V (FWHM). At the optimum ΔV , the capture condition is fulfilled and the breeding efficiency is maximized. At values below the ΔV window, the ions cannot overcome the plasma potential and are reflected back. At values above the ΔV window, the ions have too much energy and pass through the plasma without being thermalized and captured. The radioactive species Cs-142 demonstrates a ΔV curve similar to stable Cs-133. The elevated tails are due to daughter product build up on the beta detector. The gaseous elements exhibit a different behavior than the solid species. The case for Xe-129 exhibits an optimum ΔV of +10 V and a very large acceptance window. The difference in optimum ΔV is due to the use of an RF discharge source as opposed to the surface ionization source used to produce the Na and Cs. The slope on the negative side is very gradual, attributable to the reflected ions not sticking to the plasma chamber walls as the metallic species do but instead being reemitted into the plasma. The condition of too much energy can still be met, but it also exhibits a more gradual slope. The 1+ beam coupled with ΔV has since been used as a probe of the plasma conditions. It has been observed that even at the optimum ΔV setting $\sim 10\%$ of 1+ ions can pass through the plasma without being captured, and this phenomenon can be exploited to measure various plasma properties [23].

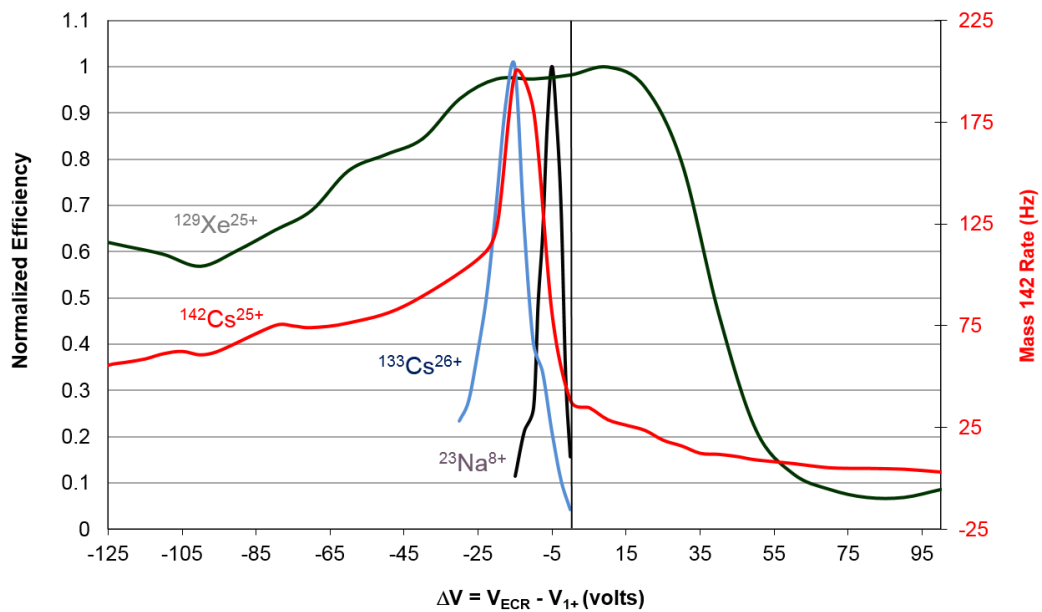


Figure 4: Normalized capture efficiency of stable (Na-23, Xe-129, Cs-133) and radioactive (Cs-142) species as a function of the ΔV between the 1+ source and the ECRCB. The metallic species were produced by a surface ionization source, the gaseous by a RF discharge source, and the Cs-142 was from the CARIBU gas catcher. [24]

2.8.3.1.2 Multiple RF frequencies

The successful use of multiple discrete frequencies to heat the ECR plasma was first explored at Lawrence Berkeley National Laboratory [25]. The general effects are to increase the maximum beam intensity and peak achievable charge state as well as enhance plasma stability. The impact of multiple frequency heating on breeding efficiency was first tested at Argonne National Laboratory [10]. The ECR plasma was excited with a 10.44 GHz klystron and a travelling wave tube amplifier (TWTA) in the 11-13 GHz band.

To serve as a direct comparison of the various RF injection schemes, the total RF power launched into the source was kept constant at 245 W with only the distribution of the power between the two frequencies being varied. With oxygen support gas, a 65 nA beam of $^{129}\text{Xe}^+$ was injected into the ECRCB and the breeding efficiency measured as a function of RF power distribution with the results shown in Fig. 5. For two-frequency heating, the peak of the charge state distribution shifted from 23+ to 25+ accompanied by an increased global efficiency - 42% for 10.44 GHz alone, 46% for 11.90 GHz alone, and 50% for 10.44+11.90 GHz. In the best configuration, with a total of 350 W of RF injected, the global efficiency was 64% with a maximum efficiency of 13.4% into $^{129}\text{Xe}^{25+}$.

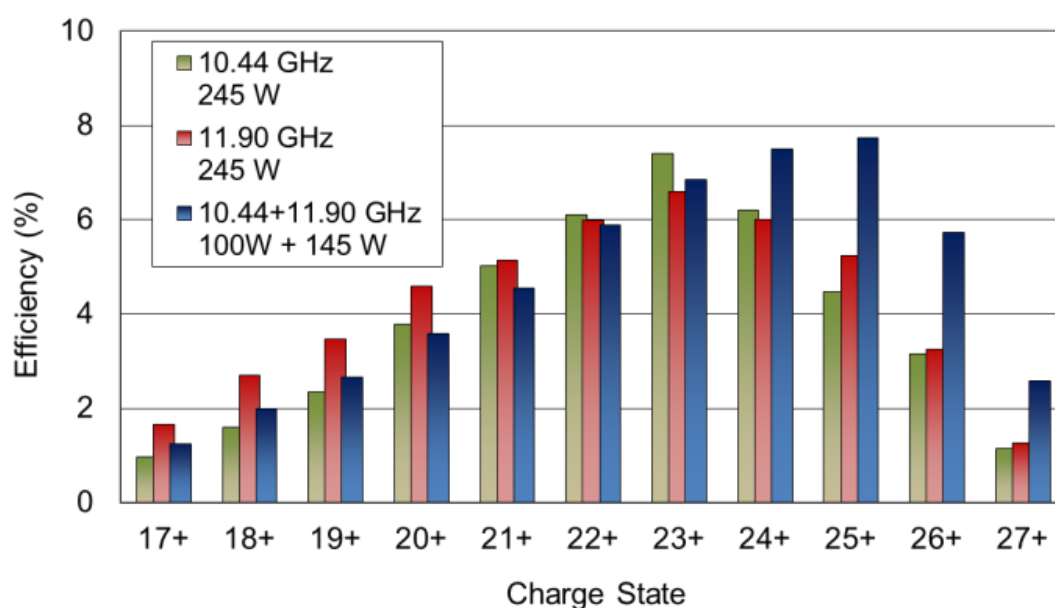


Figure 5: Efficiency of Xe-129 as a function of RF power distribution. The total amount of RF power launched into the source was kept constant. Charge states 18+ and 24+ were obscured by intense background peaks. Their values are interpolated.

2.8.3.1.3 Operating frequency

The charge breeding efficiency as a function of the operating frequency has also been studied [26]. While exciting a plasma with two frequencies provided by a klystron and a TWTA, the operating frequency of the TWTA was scanned at constant power across the 11.5-12.0 GHz range. Numerous operating points were found within this frequency range demonstrating a range of attributes. For $^{133}\text{Cs}^{27+}$, the breeding efficiency varied from 4.6% to 10.0%, the breeding time varied from 250 msec to as long as 500 msec, and the beam stability ranged from excellent ($\pm 0.5\%$) to poor ($\pm 8\%$). The TWTA operating frequencies of 11.77 and 11.88 GHz demonstrated excellent stability though significantly different breeding efficiencies. The measured efficiencies into all of the visible charge states for both cases are shown in Fig. 6. Clearly the choice of operating frequency is just as critical with charge breeding as has been demonstrated in normal ECR operation [27]. The exact mechanism of the operating frequency effect is still being investigated.

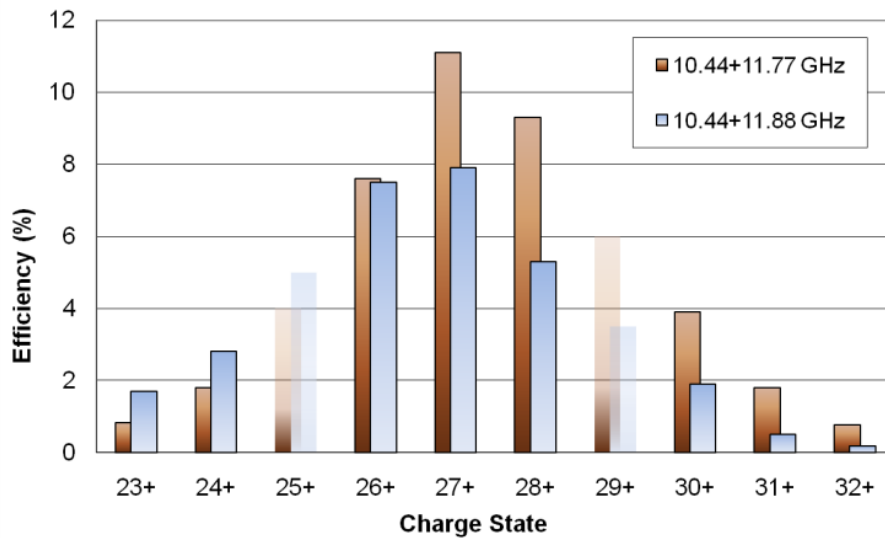


Figure 6: Charge breeding efficiency into the various charge states of Cs-133 as a function of the TWTA operating frequency. Charge states 25+ and 29+ were obscured by intense background peaks. Their values are interpolated

2.8.3.1.4 Operating pressure

The effect of source operating pressure on charge breeder performance was not fully appreciated when the technology was first conceived. It has since been shown with the ANL and LPSC charge breeders that the ECR operating pressure is a critical parameter, and that moving towards UHV-compatible practices results in improvements in charge breeding efficiency, a higher average charge state, and may have an impact on background reduction. The ANL source routinely operated in the $5 \cdot 10^{-8}$ Torr regime, benefitting from its open hexapole structure which allowed direct pumping of the plasma chamber (see Fig. 2). Tests performed during its commissioning phase demonstrated a factor of six improvement in breeding efficiency for $^{85}\text{Rb}^{17+}$ as the base source pressure improved [10]. The LPSC source with its closed hexapole design realized a lower base pressure by improved pumping to the plasma chamber through the enlargement and eventual removal of the grounded tube as well as institution of UHV-compatible materials and practices [20]. Subsequent tests have shown that the total charge breeding efficiency decreases with increasing pressures (from 60% at $2.5 \cdot 10^{-7}$ to 20% at $4.5 \cdot 10^{-7}$ Torr) [11]. The ECRCBs for the SPIRAL1 and SPES facilities have been designed and constructed in accordance with UHV best practices, thus lowering their base operating pressures and improving the breeding efficiencies [28].

2.8.3.1.5 Grounded tube positioning

The metal tube through which the 1+ ions enter the plasma region defines the electrostatic transition between the ground and source potential, and its position is critical to the particle optics in this region. It can also extract ions from the plasma thereby reducing the total amount of beneficially extracted charge bred beam. The ANL breeder placed the tube on a movable stage and found that a position 6 cm outside of the peak injection side magnetic field was the optimum position for breeding efficiency. This position also served to reduce the amount of contaminants entering the plasma region as

the tube was subjected to less ablation by the ECR plasma. The SPIRAL1 breeder has adopted a movable grounded tube scheme [29] with an ultimate goal of complete removal as with the LPSC PHOENIX source. In addition to improving the pumping speed to the plasma chamber volume, the removal of the grounded tube eliminates this as a potential source of contamination.

2.8.3.1.6 Magnetic field scheme

The topography of the minimum-B structure affects the overall source performance. Following the scaling laws, the preferred magnitude of the injection side magnetic field B_{inj} is $4 \cdot B_{res}$. To achieve this goal, a soft iron ring is placed at this location to enhance the magnetic field. For the ECR charge breeders which employ a closed hexapole structure, the RF is introduced into the plasma volume through this ring requiring grooves to be machined into the soft iron. The grooves produce an asymmetric axial magnetic field at the injection region where the $1+$ beam is decelerated resulting in ion steering and reflection effects. These effects reduce the injection efficiency and hence the charge breeding efficiency. The ANL charge breeder's open hexapole structure and radial ports allowed the RF waveguides to be inserted radially, in between the hexapole bars. Hence no grooves were required in the magnetic ring resulting in a symmetric magnetic field on the injection side of the source where the $1+$ ions enter the chamber, as shown in Fig. 7.

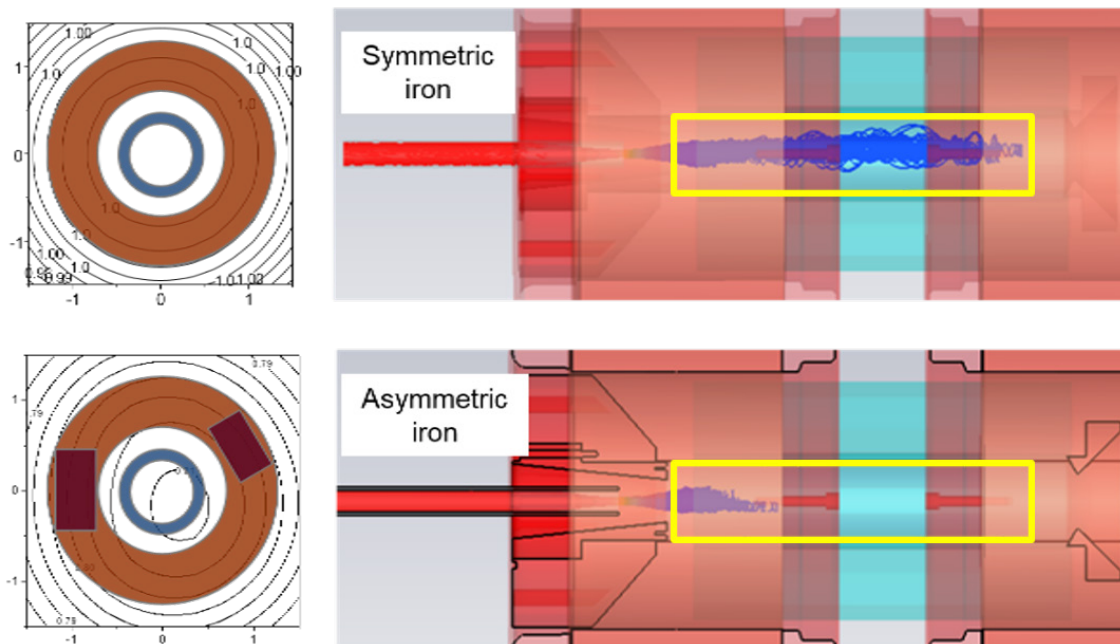


Figure 7: Effect of the magnetic field on $1+$ ion injection trajectories for the ANL ECRCB. The symmetric case, without any iron cut-outs, has the magnetic equipotential lines centered on the grounded tube. The asymmetric case shows an offset in the magnetic field. The ion trajectories are shown in blue and the plasma chamber volume is outlined in yellow.

Several 3D simulations of the ANL charge breeder were performed comparing the asymmetric and symmetric iron cases [24, 30]. Using the operational values for the magnetic and electric fields, the trajectories for Na^+ , K^+ , and Cs^+ were traced as they entered the plasma volume, defined in Fig. 7 by the yellow outline. In the asymmetric iron case, the $1+$ ions had limited penetration into the plasma volume with none of the $1+$ ions reaching the mid-point of the plasma volume. In the symmetric iron case, between

60 and 90% of the 1+ ions reached the mid-point and 40 to 55% penetrated the entire plasma volume. It is believed that this enhanced penetration into the plasma region aids the capture of the 1+ ions and results in higher breeding efficiencies. Recent results with the LPSC and SPIRAL1 PHOENIX charge breeders appear to support this conclusion [11, 31]. For both of these sources, the injection iron configuration was modified to eliminate field asymmetries where the 1+ ions enter the plasma chamber. The sources have since demonstrated uniformly high breeding efficiencies including for the low-mass species such as sodium. These low-mass species had previously been more difficult to charge breed than the mid-mass species limiting single charge state efficiencies to ~4%.

2.8.4 Results

The charge breeding results from the various labs is summarized in Table 1. It is noted that the ANL, ISOLDE, and KEK charge breeders are no longer in operation.

Table 1: Summary of charge breeding results reported by the various labs. Ions listed in red are radioactive species.

<i>Ion</i>	<i>ANL</i>	<i>ISOLDE</i>	<i>KEK</i>	<i>LPSC</i>	<i>SPES</i>	<i>SPIRAL</i>	<i>TRIUMF</i>
$^{20}\text{Ne}^{4+}$				7.5			
$^{23}\text{Na}^{6+}$				3.7			
$^{23}\text{Na}^{7+}$	10.1			3.8		6	
$^{23}\text{Na}^{8+}$	8.6			12.9		5.3	
$^{40}\text{Ar}^{8+}$		13.5		24.2	15.2	18.9	5.5
$^{40}\text{Ar}^{9+}$			13.5	12			
$^{40}\text{Ar}^{11+}$				8.4		12.9	
$^{40}\text{Ar}^{12+}$				14.2			
$^{39}\text{K}^{6+}$				6.5			
$^{39}\text{K}^{9+}$	15.6			8		13	2.1
$^{39}\text{K}^{10+}$	17.9	1.8		11.7		8	
$^{55}\text{Mn}^{14+}$		4					
$^{56}\text{Fe}^{10+}$				2.4			
$^{74}\text{Kr}^{15+}$							6.2
$^{84}\text{Kr}^{12+}$			10.4				6.3
$^{84}\text{Kr}^{13+}$		6.8					
$^{84}\text{Kr}^{15+}$	10.7	4		10			
$^{84}\text{Kr}^{17+}$	15.6			12			
$^{86}\text{Kr}^{15+}$				11		8.3	
$^{86}\text{Kr}^{18+}$				11.3			
$^{91}\text{Kr}^{12+}$			8.2				
$^{76}\text{Rb}^{15+}$							1.7
$^{85}\text{Rb}^{13+}$							3
$^{85}\text{Rb}^{17+}$	11.5			7.5			
$^{85}\text{Rb}^{19+}$	13.7			10.4	7.8	8.4	
$^{96}\text{Sr}^{14+}$		3.5					
$^{98}\text{Y}^{20+}$	10						
$^{98}\text{Zr}^{21+}$	8.4						
$^{100}\text{Zr}^{21+}$	7.9						
$^{106}\text{Mo}^{21+}$	9.7						
$^{110}\text{Ru}^{22+}$	11.8						

$^{107}\text{Ag}^{17+}$				3			
$^{116}\text{Sn}^{22+}$		6					
$^{120}\text{Sn}^{22+}$				3.9			
$^{135}\text{Te}^{26+}$	5						
$^{123}\text{In}^{16+}$			2.3				
$^{129}\text{Xe}^{17+}$							4.8
$^{129}\text{Xe}^{20+}$					11.2		
$^{129}\text{Xe}^{25+}$	13.4						
$^{132}\text{Xe}^{20+}$			7.4	10.9			
$^{132}\text{Xe}^{21+}$		6.2					
$^{132}\text{Xe}^{26+}$				13.3			
$^{132}\text{Xe}^{27+}$	14.1						
$^{124}\text{Cs}^{20+}$							1.4
$^{133}\text{Cs}^{20+}$							3.5
$^{133}\text{Cs}^{26+}$		1.7		13	11.7		
$^{133}\text{Cs}^{27+}$	13			9.5			
$^{141}\text{Cs}^{27+}$	12.3						
$^{143}\text{Cs}^{27+}$	11.7						
$^{138}\text{Ba}^{22+}$			2.4				
$^{143}\text{Ba}^{27+}$	14.7						
$^{144}\text{Ba}^{28+}$	14.3						
$^{146}\text{Ba}^{28+}$	13.3						
$^{139}\text{La}^{23+}$		2.4					
$^{208}\text{Pb}^{25+}$		3.4					
$^{209}\text{Bi}^{28+}$		2.3					
$^{238}\text{U}^{28+}$		2.5					

2.8.5 On-going Efforts

2.8.5.1 Contaminants

The major limitation to ECR charge breeder operations is the ubiquitous stable background. Studies at several labs have highlighted the vast array of stable background species produced by an ECR and their tendency to interfere with the RIB of interest. An example of this is shown in Fig. 8, a silicon barrier detector spectrum taken after acceleration of charge bred Ba-146. The radioactive Ba-146 is present at a rate of 10^4 pps but only accounts for 3% of the total beam current. The spectrum highlights the diversity of contaminants present in an ECR source and their ability to rapidly obscure the beam of interest. Many of the contaminants are due to the plasma chamber itself whose surfaces undergo sputtering by escaping high energy electrons. The chamber is constructed of 6061 aluminum alloy which has components of magnesium, silicon, titanium, chromium, manganese, iron, copper, and zinc – some of which are seen in Fig. 8. The source of the molybdenum, tin, iridium, and mercury is less understood as none of these elements were introduced into the ECR at any point during its operation, but it is assumed they originate as trace impurities from the 6061 aluminum.

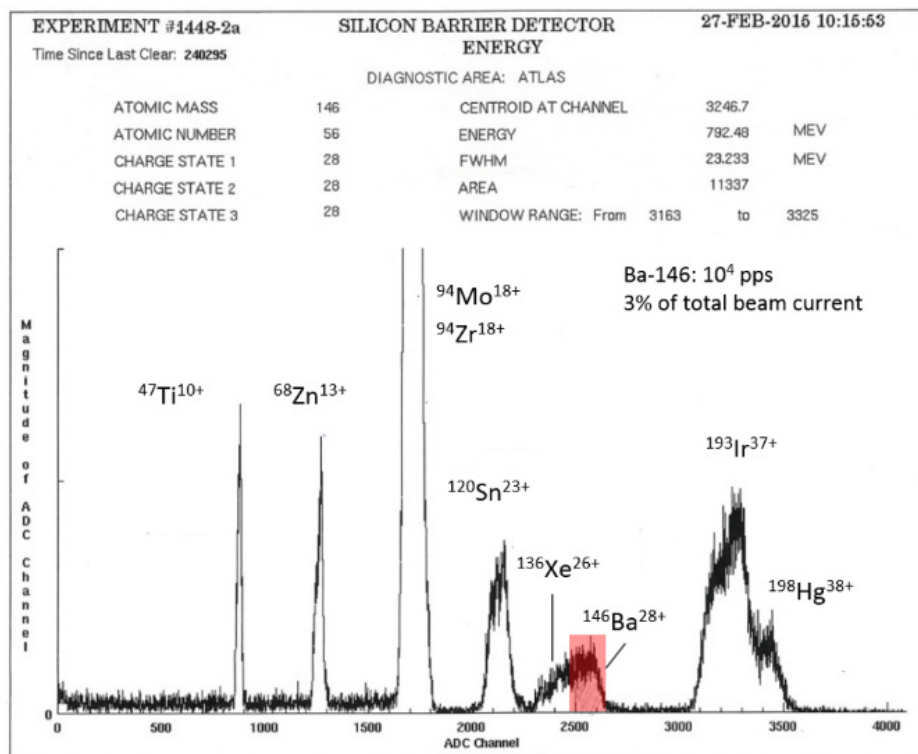


Figure 8: Contaminant load from the ANL ECRCB. Shown are the beam constituents after acceleration to 4 MeV/u and detected on a silicon barrier detector. The radioactive component Ba-146 is highlighted in red with the stable contaminants identified. The Ba-146 rate at the detector was 10^4 pps and accounted for 3% of the total beam current.

A spectrum of Sr-94 from TRIUMF (Fig. 9a) presents a similar situation. The primary RIB is accompanied by a number of stable background elements. To reduce the background level, a stripping foil was inserted increasing the rubidium charge state from 15+ to 22+. This had the effect of shifting the A/Q ratio and enhancing the discrimination of many of the original contaminants [32]. While this technique is effective, it has the drawback of a reduction in RIB intensity due to the stripping fraction.

Attempts have also been made to eliminate the source of the contaminants through cleaning and coating techniques. At KEK, efforts were made to reduce the background introduced by surface contamination. The plasma chamber surfaces were sand blasted, pressure washed, and cleaned in an ultrasonic bath thereby reducing the contaminant load to 600 particles/s in some regions of interest [13]. In ANL's case, the plasma chamber surfaces were cleaned in situ with high-pressure CO₂ snow thereby reducing three major contaminants – a factor of 20 reduction for fluorine, a factor of 4 for chlorine, and a factor of 50 for iron. Following the cleaning, the plasma chamber was coated with ultra-pure aluminum which led to further reductions – a factor of 160 for fluorine, a factor of 17 for chlorine, and iron was no longer detectable. However, large contaminants of tantalum and tungsten were now present due to the heating coil used for the aluminum evaporation [33]. TRIUMF has also coated their plasma chamber and electroplated aluminum onto components exposed to the plasma leading to a reduction in background [14].

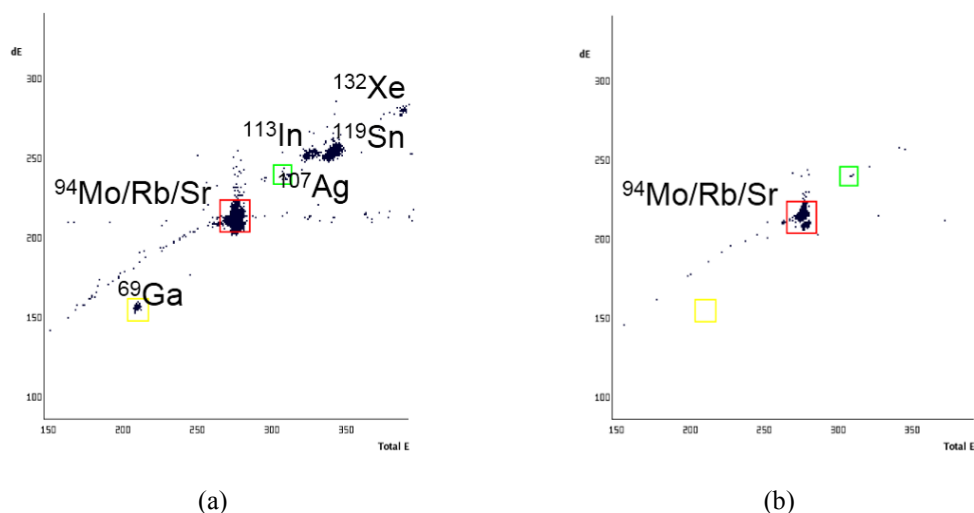


Figure 9: Contaminant load from the TRIUMF ECRCB. (a) The beam constituents as extracted from the ECRCB and before additional stripping. (b) The beam constituents after stripping at 1.5 MeV/u and using the linac as a mass filter. [14]

The group at SPES has adopted a multi-pronged approach. While they have adopted UHV practices for the construction of their PHOENIX source, they anticipate that this will not fully eliminate the contaminant load. To address this concern, they constructed a medium-resolution spectrometer with a resolving power of 1:1000 placed on a 160 kV platform after the charge breeder [34]. This will discriminate a large portion of beams which have conflicting A/Q ratios and ease the identification of clean RIB charge states.

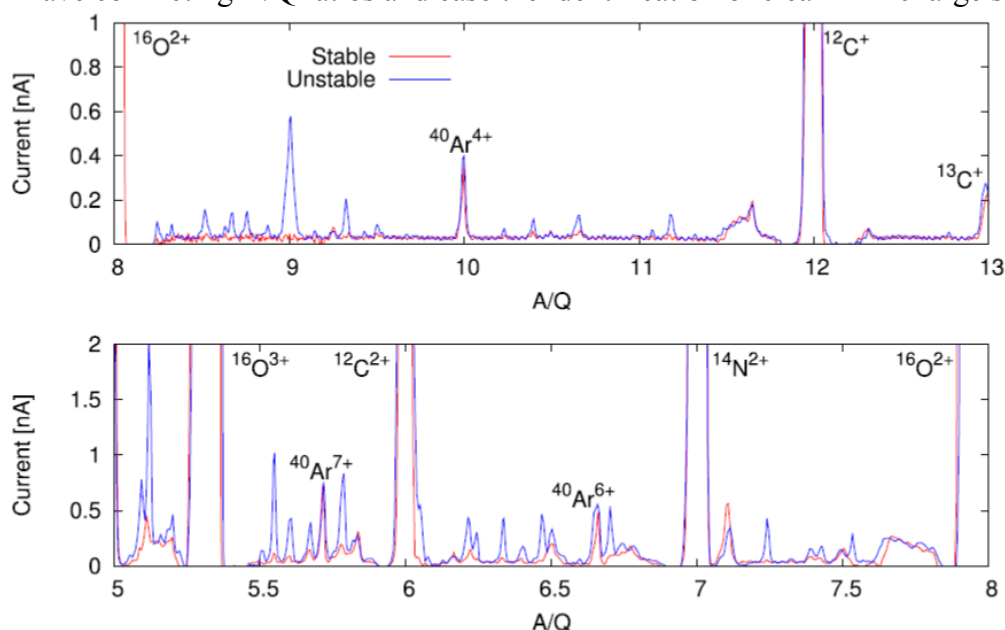


Figure 10: Temporally averaged m/q -resolved spectra at high sensitivity/low current in the ranges of 8-13 (top) and 5-8 (bottom). Carbon, nitrogen, oxygen and argon ions are indicated for convenience. [35]

While the above groups have been pursuing techniques to clean, cover, or filter out the contamination, the ion source group at the University of Jyväskylä (JYFL) has been investigating how the contaminants enter the plasma. They concluded that a transition

from a stable to unstable plasma regime, created by the gradual accumulation and ionization of the injected 1+ beam, leads to loss of ion confinement which sputters the plasma chamber surface. They observed up to an order of magnitude increase of impurity currents in the extracted n+ ion beam due to these instabilities, as shown in Fig.10. By operating in stable regimes, the influx of contaminants was reduced [35].

2.8.5.2 1+ beam as plasma probe

The 1+ beam itself is becoming an important tool for advancing the understanding of the charge breeding process. The JYFL group has demonstrated that the interaction of the 1+ beam with the charge breeder plasma can trigger instabilities (as shown in Fig. 10), and that the instability is not prompt but instead results from a buildup of charge (Fig. 11). The JYFL group has also explored using the 1+ beam to estimate the mean free path, the ion-ion collision frequency, and the plasma density. The lower limits of ion-ion collision frequency and plasma density in the ECRIS plasma can be estimated by measuring the uncaptured fraction of the 1+ ion beam, which propagates through the charge breeder plasma without being ionized [23].

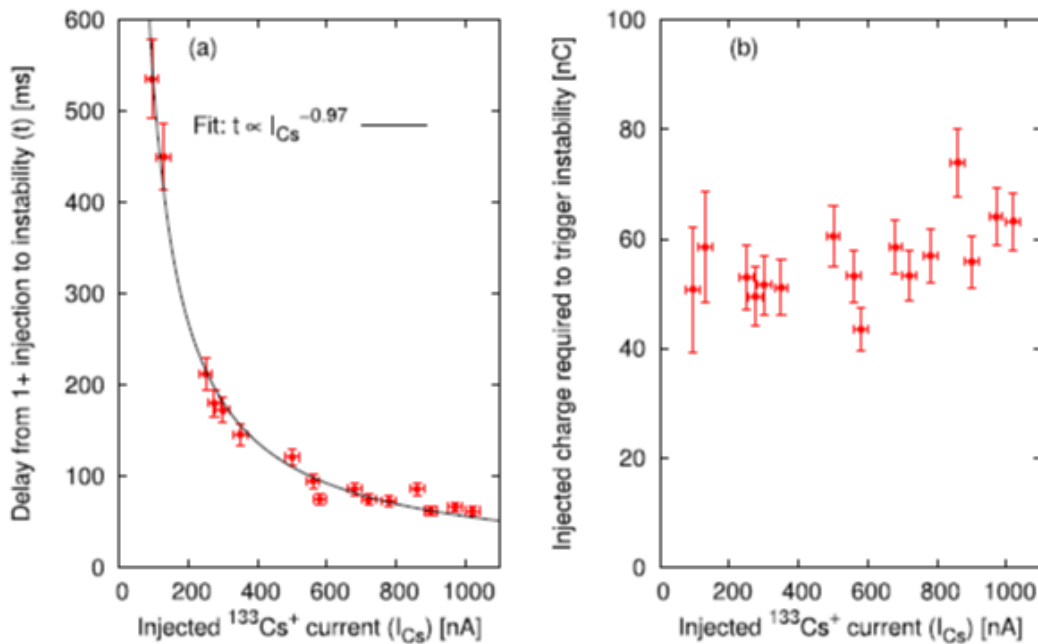


Figure 11: (a) The measured delay between the leading edge of the Cs+ injection pulse and the appearance of the first instability event as a function of the injected beam current. (b) The (total) injected charge required to trigger the instability as a function of the injected beam current. [35]

2.8.6 Conclusion

The ECR charge breeding field is rapidly expanding with a lively community pursuing multiple developmental paths in a quest to provide the highest intensity pure radioactive ion beams. The understanding of the charge breeding process and the available parameter space has advanced, leading to improved breeding efficiencies with single charge state efficiencies reaching 24%. The work at various labs on contamination reduction has shown promise with the stable background reduced to a level which allows

direct observation of 10^3 pps radioactive beams. At the same time, as future radioactive beam facilities push the RIB intensity envelope, the high charge capacity of ECR ion sources will be critical.

2.8.7 Acknowledgements

The author would like to thank the numerous members of the ion source community for many fruitful discussions and who have generously shared their research. This work was supported by the U.S. Department of Energy, Office of Nuclear Physics, under Contract No. DE-AC02-06CH11357 and used resources of ANL's ATLAS facility, an Office of Science User Facility.

2.8.8 References

1. R. Geller, C. Tamburella, and J. L. Belmont, "The ISOL–MAFIOS Source", *Review of Scientific Instruments* **67**, 1281 (1996)
2. R. Geller, "Electron Cyclotron Resonance Ion Sources and ECR Plasmas", Institute of Physics Publishing (1996)
3. P. Sortais, J.L. Bouly, N. Chauvin, J.C. Curdy, R. Geller, T. Lamy, P.Sole,J.L.Vieux-Rochaz, "ECRIS as ion source and charge breeder", *Nuclear Physics A* 701 (2002) 537c–549c
4. J. Benitez et al., "Production of high intensity ^{48}Ca for the 88-Inch Cyclotron and other updates", *Review of Scientific Instruments* **85**, 02A961 (2014)
5. L. Sun et al., "Advancement of highly charged ion beam production by superconducting ECR ion source SECRAL (invited)", *Review of Scientific Instruments*, vol. 87, 02A707, Feb. 2016
6. G. Machicoane et al., "First results at 24 GHz with the superconducting source for ions (SUSI)", 21st International Workshop on ECR Ion Sources (2014)
7. Y. Higurashi et al., "Recent development of RIKEN 28 GHz superconducting electron cyclotron resonance ion source", *Review of Scientific Instruments* **85**, 02A953 (2014)
8. S. Gammino, G. Ciavola, R. Harkewicz, K. Harrison, A. Srivastava, and P. Briand, "Effects of frequency and magnetic field scaling on the superconducting electron cyclotron resonance ion source at MSU-NSCL", *Review of Scientific Instruments* **67**, 4109 (1996)
9. G. Melin, A. G. Drentje, A. Girard, and D. Hitz, "Ion behavior and gas mixing in electron cyclotron resonance plasmas as sources of highly charged ions", *Journal of Applied Physics* **86**, 4772 (1999)
10. R. Vondrasek, S. Kondrashev, R. Pardo, R. Scott, and G. P. Zinkann, "Results with the electron cyclotron resonance charge breeder for the fission source project (Californium Rare Ion Breeder Upgrade) at Argonne Tandem Linac Accelerator System", *Review of Scientific Instruments* **81**, 02A907 (2010)
11. T. Lamy, J. Angot, T. Thuillier, P. Delahaye, L. Maunoury, J. Choinski, L. Standylo, A. Galatà, G. Patti, H. Koivisto, and O. Tarvainen, "Experimental Activities with the LPSC Charge Breeder in the European Context", in *Proceedings of ECRIS-2014, WEOBMH01, Nizhny Novgorod, Russia*
12. P. Delahaye, C. J. Barton, K. Connell, T. Fritioff, O. Kester, T. Lamy, M. Lindroos, P. Sortais, G. Tranströmer, and F. Wenander, "Recent results with the Phoenix

- booster at ISOLDE”, *Review of Scientific Instruments* **77**, 03B105 (2006)
13. N. Imai, S. C. Jeong, M. Oyaizu, S. Arai, Y. Fuchi, Y. Hirayama, H. Ishiyama, H. Miyatake, M. H. Tanaka, M. Okada, and Y. X. Watanabe, S. Ichikawa, H. Kabumoto, A. Osa, Y. Otokawa, and T. K. Sato, “KEKCB electron cyclotron resonance charge breeder at TRIAC”, *Review of Scientific Instruments* **79**, 02A906 (2008)
 14. F. Ames, R. Baartman, P. Bricault, K. Jayamann, “Charge state breeding of radioactive isotopes for ISAC”, *Hyperfine Interact* (2014) 225:63–67
 15. L. Maunoury, P. Delahaye, M. Dubois, J. Angot, P. Sole, O. Bajeat, C. Barton, R. Frigot, A. Jeanne, P. Jardin, O. Kamalou, P. Lecomte, B. Osmond, G. Peschard, T. Lamy, and A. Savalle, “Charge breeder for the SPIRAL1 upgrade: Preliminary results”, *Review of Scientific Instruments* **87**, 02B508 (2016)
 16. R. Vondrasek, J. Clark, A. Levand, T. Palchan, R. Pardo, G. Savard, and R. Scott, “Operational experience with the Argonne National Laboratory Californium Rare Ion Breeder Upgrade facility and electron cyclotron resonance charge breeder”, *Review of Scientific Instruments* **85**, 02B903 (2014)
 - A. Galatà, G. Patti, C. Roncolato, J. Angot, and T. Lamy, “The new ECR charge breeder for the Selective Production of Exotic Species project at INFN—Laboratori Nazionali di Legnaro”, *Review of Scientific Instruments* **87**, 02B503 (2016)
 17. D. P. May, G. Tabacaru, F. P. Abegglen, and W. D. Cornelius, “First operation of the charge-breeder electron-cyclotron-resonance ion source at the Texas A&M Cyclotron Institute”, *Review of Scientific Instruments* **81**, 02A901 (2010)
 18. T. Lamy, J. L. Bouly, J. C. Curdy, R. Geller, A. Lacoste, P. Sole, P. Sortais, T. Thuillier, J. L. Vieux-Rochaz, K. Jayamanna, M. Olivo, P. Schmor, and D. Yuan, “Charge state breeding applications with the ECR PHOENIX source: From low to high current production”, *Review of Scientific Instruments* **73**, 717 (2002)
 19. T. Lamy, J. Angot, P. Sortais, T. Thuillier, and A. Galatà, “Beam injection improvement for electron cyclotron resonance charge breeders”, *Review of Scientific Instruments* **83**, 02A909 (2012)
 20. M. Cavenago, “Thermal equilibrium among ion species into ECR plasma”, *Review of Scientific Instruments* **73**, 555 (2002)
 21. R. Geller, *Review of Scientific Instruments* **71**, 612 (2000)
 22. O. Tarvainen, H. Koivisto, A. Galatà, J. Angot, T. Lamy, T. Thuillier, P. Delahaye, L. Maunoury, D. Mascali, and L. Neri, “Diagnostics of a charge breeder electron cyclotron resonance ion source helium plasma with the injection of $^{23}\text{Na}^{1+}$ ions”, *Physical Review of Accelerators and Beams* **19**, 053402 (2016)
 23. R. Vondrasek, A. Kolomiets, A. Levand, R. Pardo, G. Savard, and R. Scott, “Performance of the Argonne National Laboratory electron cyclotron resonance charge breeder”, *Review of Scientific Instruments* **82**, 053301 (2011)
 24. Z. Q. Xie and C. M. Lyneis, *Review of Scientific Instruments* **66**, 4218-4221 (1995)
 25. R. Vondrasek, A. Levand, R. Pardo, G. Savard, and R. Scott, “Charge breeding results and future prospects with electron cyclotron resonance ion source and electron beam ion source (invited)”, *Review of Scientific Instruments* **83**, 02A913 (2012)
 26. L. Celona, G. Ciavola, F. Consoli, S. Gammino, F. Maimone, D. Mascali, P. Spädtke, K. Tinschert, R. Lang, J. Mäder, J. Roßbach, S. Barbarino, R. S. Catalano, *Review of Scientific Instruments* **79**, 023305 (2008)
 27. P. Delahaye, A. Galatà, J. Angot, J. F. Cam, E. Traykov, G. Ban, L. Celona, J.

- Choinski, P. Gmaj, P. Jardin, H. Koivisto, V. Kolhinen, T. Lamy, L. Maunoury, G. Patti, T. Thuillier, O. Tarvainen, R. Vondrasek, and F. Wenander, “Optimizing charge breeding techniques for ISOL facilities in Europe: Conclusions from the EMILIE project”, *Review of Scientific Instruments* **87**, 02B510 (2016)
28. P. Delahaye, L. Maunoury, and R. Vondrasek, “Charge breeding of light metallic ions: Prospects for SPIRAL”, *Nuclear Instruments and Methods in Physics Research A* **693**, 104–108 (2012)
29. R. Vondrasek, P. Delahaye, Sergey Kutsaev, and L. Maunoury, “Improved charge breeding efficiency of light ions with an electron cyclotron resonance ion source”, *Review of Scientific Instruments* **83**, 113303 (2012)
30. Julien Angot, Thomas Thuillier, Patrick Sole, Josua Jacob, Thierry Lamy, Laurent Bonny, “Recent improvements of the LPSC Charge Breeder”, presented at ICIS2017, Geneva, Switzerland
31. F. Ames, “ECRIS and EBIS charge state breeding at TRIUMF”, presented at Workshop on Applications of Highly Charged Ions (HCI App), National Superconducting Cyclotron Laboratory, Michigan State University, May 22-23, 2014
32. Richard Vondrasek, A. Barcikowski, C.A. Dickerson, P.N. Ostroumov, R. Pardo, A. Perry, G. Savard, R. Scott, S.I. Sharamentov, “Charge Breeding Experiences with ECR and EBIS for CARIBU”, *Proceedings of HIAT2015*, Yokohama, Japan, WEA2I01, (2015)
- A. Galatá, “Status of the SPES-charge breeder (SPES-CB) and its beam line at INFN-LNL”, *Nuclear Instruments and Methods in Physics Research Section B: Beam Interactions with Materials and Atoms*, Volume 376, Pages 329-333, 1 June 2016
33. O. Tarvainen, J. Angot, I. Izotov, V. Skalyga, H. Koivisto, T. Thuillier, T. Kalvas, and T. Lamy, “Plasma instabilities of a charge breeder ECRIS”, *Plasma Sources Sci. Technol.* **26**, 105002 (14pp) (2017)

2.9 EBIS for high intensity stable beams

Alexander Pikin

Mail to: pikin@bnl.gov

Brookhaven National Laboratory, Upton 11973, USA

2.9.1 Introduction

In 1968 [1], Evgeniy Donets proposed a source of highly charged ions based on multistep ionization of ions confined in a closed potential trap within an energetic electron beam. The first observation of ions Au^{19+} injected by pulsed thermal evaporation from a light bulb tungsten filament inside EBIS was decisive confirmation of this method [2].

Since then EBIS technology made significant advances and the EBIS application field expanded greatly.

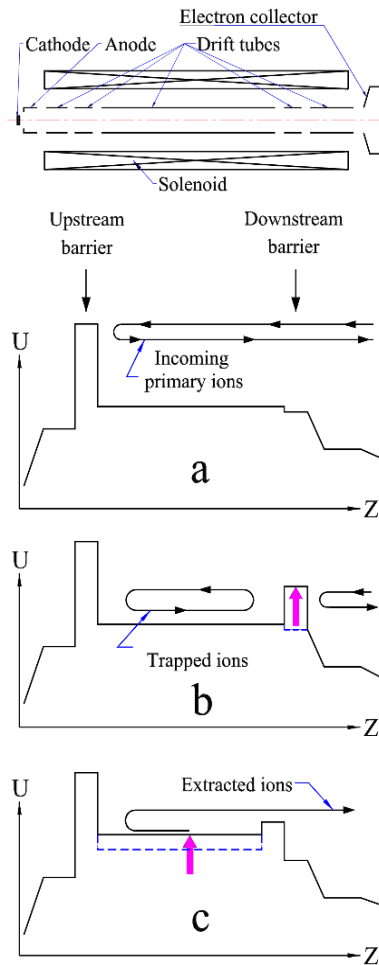


Fig. 1. EBIS ionization cycle

control allows injecting and accumulating ions in a variety of ways, using externally produced ions, internal injection from neutral gas or vapour, or any combination of these methods. By controlling the voltage ramping during the ion extraction one can choose the extraction time and therefore can control the ion current, which makes this kind of ion source unique and very attractive for synchrotrons with a single-turn injection. EBIS can produce high currents of highly charged ions during extraction time of few microseconds. On the other hand, the ion extraction can be made very slow if a slow ramp is used. The accurate ramp control allows one to make an ion pulse “flat” if needed. Even that the capacity of the accumulated total ion charge in EBIS is limited to the electron space within the ion trap, which is $1.4 \cdot 10^{12}$ elementary charges for Relativistic Heavy Ion Collider (RHIC) EBIS, the instantaneous current can reach several mA and exceeds that of its close competitor Cyclotron Resonance Ion Source (ECRIS).

The first applications of EBIS coupled to an accelerator was extraction and acceleration of highly charged light ions (C^{6+} , N^{7+} , O^{8+} and Ne^{10+}) from KRION-1 at Dubna Synchrotron in 1977 [3]. Later in KRION-2 the electron current density was substantially increased by pulling the electron gun into a lower magnetic field [4]. The next application of EBIS at synchrotron was Dione ion source on Saturn II [5]. Unlike

One of the largest advantages of EBIS over other plasma ion sources is separate energy and density distributions of electrons and ions and therefore absence of plasma polarization.

The ability to control the potential distribution inside the ion trap makes possible a flexible control of the ionization cycle in EBIS from ion injection to ion extraction. The electrons are produced by the electron gun and can have independently controlled current and energy.

The principle of EBIS operation can be explained with schematic in Fig. 1. The electrons from the cathode of electron gun propagate inside isolated drift tubes while being compressed and confined with magnetic field of the solenoid. At the exit of the magnetic field the electron beam diverges and its energy dissipates inside the electron collector. A basic ionization cycle with external ion injection is presented in Fig.1. With downstream potential barrier down (a) the low-charged ions from the external source are passing the ion trap region, reflect from the upstream barrier and leave. During this traversing the trap region by ions the downstream barrier is lifted up and it locks the ions within the trap between two potential barriers (b). The trapped ions can be held in the trap for as long as it takes to reach the required charge state distribution. At the end of this confinement time the ions from the trap can be extracted by lifting the bottom of the trap region (c) or bringing the downstream barrier down. Such axial

Dubna EBISes, which used magneto-immersed electron guns, Dione had an electron gun with electrostatic focusing, which was capable of producing Brillouin electron beams with very high current density. It also operated at higher electron current (0.48 A) [6] and remained an EBIS champion until Saturn II was closed down in 1997. Unlike KRIONs with internal gas injection Dione used externally produced singly charged ions, including metals for charge breeding inside the ion trap [7]. This source was a first EBIS for producing polarized ions Li^{3+} injected into the ion trap as singly charged ions from the external ion source [8]. The first French built EBIS CRYEBIS [9], which was discarded as non-usable for Saturn II and replaced by Dione, by an odd twist of fate has been upgraded and used routinely and reliably for highly charged ion injection on CRYISIS accelerator at Manne Siegbahn Institute in Stockholm [10].

At this time the most powerful EBIS providing ion beams to large accelerators is RHIC EBIS, which supplies all required multi-charged ion species with charge to mass ratio $q/M \geq 1/7$ except of hydrogen isotopes for accelerator facility of Brookhaven National Laboratory since September of 2010 [11] with electron current up to 10 A and ion trap length of 1.8 m. RHIC EBIS photo is shown in Fig. 2.



Fig. 2. RHIC EBIS before installation on BNL accelerator facility.

To successfully operate EBIS one needs to have:

- An electron beam with sufficient current and current density,
- High enough magnetic field for the beam compression and transmission with adequate length for a required trap capacity, sufficient transverse correcting coils,
- Good vacuum to retain ions in a trap for sufficiently long time with low contamination from the residual gas,
- A fast and flexible control system with adequate power supplies,
- In the case of using external ion injection, one also needs low-aberration ion optics with fast switching from the injection to extraction regime of ion beam.

The complexity of a powerful EBIS illustrates an interconnection of physical processes which can be effected with sometimes with positive feedback due to: like electron beam losses, electrical discharges and vacuum pressure increase. Perhaps, one of EBIS advantages is the possibility to calculate the charge state distribution in the trap as a function of EBIS parameters, to simulate the evolution of the charge states as a function of charge breeding time. There are several programs capable of such simulations [12, 13, 14]. One thing can be mentioned regarding the model of this charge states evolution. In the process of the electron potential well neutralization the ions tend to spill over the electron beam boundary and spend some time outside of the electron beam. It results in reducing of the ionization efficiency and broadening of the charge state distribution.

Good introduction to EBIS physics one can find in review papers [15, 16, 17].

2.9.2 Electron beam generation

Presently there are two methods of generating the electron beam for EBIS: using a magneto-immersed electron gun and using an electron gun with electrostatic compression and subsequent magnetic compression, which produces a Brillouin electron beam. The first method is simpler and much less critical to matching the electrostatic and magnetic fields.

2.9.2.1 *Magneto-immersed guns.*

For magneto-immersed electron beams the magnetic flux through the beam cross-section conserves, therefore the beam radius at any point with axial coordinate z can be calculated as

$$r(z) = r_{cath} \cdot \sqrt{\frac{B_c}{B(z)}} \quad (1)$$

r_{cath} is the cathode radius

B_c is magnetic field on the cathode

B_z is magnetic field at point with the axial coordinate z .

The beam radius of the magneto immersed beam does not depend on the beam current and energy or the degree of the electron beam neutralization by ions. The electron beam current density is determined by the cathode emission current density and by the magnetic compression. It makes sense to design an electron gun with cathode diameter providing the required current at maximum emission current density for a reasonable lifetime. The typical ion confinement times are in a millisecond range, which are considered “long” pulses for cathodes and one needs to pick a cathode material based on emission current density for DC operation. Of all known to date commercial cathode materials only the high-temperature cathodes operating in temperature range of (1600 – 1800)°C can provide long time operation with continuous emission current density of 10 -18 A/cm². The RHIC EBIS electron gun

generates $I_{el}=10$ A electron beam from the 9.2 mm diameter cathode ($j_{em}=15.0$ A/cm²). This electron beam current density is 500 A/cm² in the ion trap with magnetic field $B_{trap}=5.0$ T. s.

The most popular cathode materials are hexaborides (LaB6 and CeB6) and IrCe, the latter is superior but available from one vendor only.

During the design the electron gun one needs to take into account a Larmor motion at low magnetic field. The best gun should generate a laminar electron beam with nominal parameters at minimum required magnetic field. The electron guns with adiabatic electrostatic field, developed at Budker Institute of Nuclear Physics (BINP) (18, 19) provide a reliable no-thrill approach, but do not allow using it with maximum emission current density at magnetic field on the cathode lower than $B_{\text{cath}} = 0.15$ T due to unacceptably large radial beam oscillations. Using electron guns with non-adiabatic fields allows extending operating range of the gun into much lower magnetic fields [20], which should allow reaching current densities close to 1000 A/cm². On the down side, the operating range of such a gun is smaller than of the adiabatic gun: it has optimum combinations of electron current and magnetic field in the gun, where the beam is laminar.

2.9.2.2 *Guns with electrostatic compression*

Electron guns with electrostatic compression produce electron beams with current density up to $j_{\text{el}} = 5 - 20$ kA/cm² in magnetic field $B_{\text{trap}} = 5$ T. However, it requires careful matching of electric and magnetic field and good axial symmetry of electrodes and the main magnetic field to get a beam with low radial oscillations.

Dione EBIS at Saturn-II was equipped with Brillouin electron gun. It operated with electron current up to 486 mA and with magnetic field in the trap $B_{\text{trap}} = 5$ T. The apparent electron current density varied from 1300 A/cm² at very low electron beam neutralization to 700 A/cm² at 75% neutralization. [5].

At present time, there are no EBIS or Electron Beam Ion Trap (EBIT) devices with Brillouin electron gun, which can generate highly charged ions with effective current density higher than 1000 A/cm² and operating with electron current higher than 0.5 A. The existing EBIT devices have electron current density in the range of 5000 A/cm², but typically operate with lower electron beam current; they have a short ion trap, and are hardly suitable for high-intensity ion beam production. Nevertheless, the efforts to build a high-current EBIS with Brillouin electron gun continue at BNL [21, 22] and at CERN [23].

2.9.2.3 *Reflex EBIS*

In 1996 E. Donets proposed a version of EBIS with electron beam oscillating between the cathode and reflecting electrode in a confining magnetic field [24, 25]. Such oscillating electron system appears to stabilize within a few microseconds after start and E. Donets named it as “electron string”. The electrons are used for ionization and ion confinement many times and such electron string saves substantial electron beam power. The Dubna EBIS KRION-2 was modified for string operation has been successfully used in Nuclotron for accelerating light bare ions and Fe²⁴⁺ [26]. The ion capacity of KRION-6T is still no match to RHIC EBIS but it has a decent current density of several hundred A/cm². This concept of ion source has some advantages over traditional EBIS and has a good potential for future improvements.

2.9.2.4 *Electron current limitation and mitigation*

The maximum attainable current in EBIS and EBIT devices is usually limited by excessively high current loss on the anode of the electron gun and some other electrodes in the transition regions. This loss seems to be caused by the electrons reflected from the magnetic mirror [27, 28, 29] and to less extent, by electrons reflected from the electron collector area. The electrons reflected from partial virtual cathode caused by slow electrons can also cause this loss. The reason of reflecting the electron from the magnetic mirror is an excessive transverse energy, which makes the trajectory angle of this electron larger than the acceptance cone of the magnetic mirror. Electrons reflected from the magnetic mirror oscillate between the cathode and the mirror and can bunch and modulate the primary electron beam when their density exceeds certain threshold [30]. Such bunched electron beam makes operation of EBIS unstable. The main contributing components to the electron transverse energy are optics of the gun, non-coaxiality of the electric and magnetic fields, non-uniform cathode emission.

The gun optics makes a major contribution to the energy of electron Larmor motion. It is advisable to operate the gun with specific current in a magnetic field, where this Larmor motion makes the maximum trajectory angle of the electron beam significantly smaller than the magnetic mirror acceptance cone. The parameters affecting the gun anode load with electron loss are:

- Transverse and axial position of the gun with respect to the main solenoid;
- Transverse correcting magnetic fields in the EBIS transition regions and in the main solenoid;
- Electron energy in the transition region between the gun and the main solenoid.

The ability to move the electron gun axially and transversely together with ability to adjust the transverse magnetic fields are of primary importance for transmitting the maximum electron beam with minimum losses. Independent control of the magnetic field in the gun allows decoupling of the electron beam size in the ion trap from the phase of axial oscillations of the reflected electrons. It would be also advantageous to control the magnetic field distribution in the transition region gun/main solenoid with an independent coil.

2.9.3 **Electron beam collector**

The electron collectors (EC) in EBIS serve a simple purpose: to collect the primary electrons and let the incoming and outgoing ions in and out. However, there are several aspects, which require approaching this simple task carefully.

- **Optics.** The EC should not restrict the EBIS acceptance for the incoming ion beam. Usually its geometrical acceptance is much larger than the EBIS acceptance, but it would be prudent to simulate the ion injection in this region. The ion extractor electrode, which sometimes is called as an electron repeller should not restrict the path of ions extracted from EBIS even for the maximum current and lowest ion energy. Also, it should not collimate the incoming ion beam. The electron beam should be distributed on the water-cooled cylindrical surface of the EC with maximum uniformity and its density in the centre should be minimal to minimize the flow of electrons reflected from the electron repeller back into the EBIS. In most EBIS EC with electron repeller the pattern of electron flux inside EC has a “folding” structure

with two maximum power density regions: one is at the beginning of axial power distribution and the other one is at the end of it. The first one is caused by higher total electron current on the electron beam periphery and the second one is a result of overlap when the beam “folds”. A good solution for magnetic field control in the EC is a magnetic shielding, which helps to expand the electron beam inside EC rapidly. This magnetic shielding also does a good job in trapping the backscattered electrons inside the EC and not letting them out. Without such shielding and with residual magnetic field of few hundred Gauss inside the collector the backscattered electrons can spiral back into EBIS along the magnetic field lines. The most probable energy of electrons backscattered from copper is 80% of their initial energy. It is also possible to limit the backscattered electrons from going back by using a geometrical factor of ratio of the radius of the bombarded cylindrical surface of the electron collector to the radius of the entrance aperture: this ratio should be as large as possible [31].

- **Thermal issues.** This depends on power regime of the EC. It appears, that pulsed operation of EBIS can bring additional complication to the EC design and to the choice of its material, even that the average power is smaller than the peak power. The electron beam power causes temperature gradient and mechanical stress in the EC wall. For safe operation of the EC the deformation caused by this stress should be within elastic margin and this consideration determines a choice of materials with appropriate combination of heat conductance and strength to avoid damage by fatigue. In an powerful EC to prevent collapse of the heat exchange between the wall and cooling water, which can result in a wall melting one needs to perform analysis of the critical heat flux. Since some electron beam power dissipates on the front surface of powerful EC as well, it also should be water cooled. Useful toolbox for analysis of a powerful EC can be found in [32, 33].
- **Vacuum.** High power deposition by the electron beam in the EC determines heavy outgassing of its surfaces, which makes EC a major gas source for EBIS. With strict requirement to the residual gas pressure in the ion trap all efforts should be made to reduce the gas flux from the EC into the EBIS central volume. Apart of standard vacuum treatment of internal surfaces the design of the EC should:
 - ✓ Provide a good vacuum conductance from the internal EC volume to the nearby vacuum pump.
 - ✓ Have vacuum connection of the internal EC volume with the rest of EBIS only through the EC entrance aperture and have this aperture as small as possible, just sufficient for transmission of the electron beam. Magnet coil at the EC entrance can provide the necessary magnetic field for controlling the electron beam size in this area. It would be advantageous to have the EC water-cooled cylindrical surfaces to serve as a vacuum envelope. In this case the EC has to be electrically isolated from the rest of EBIS, from the ion beam line and from the vacuum pump.
 - ✓ Effective vacuum separation between the EC and the central vacuum chamber can reduce the gas flux from the EC by a factor of 10 or more.

2.9.4 Drift tubes

The primary purpose of the EBIS drift tubes (DT) is axial ion control in an ionization cycle. In a classic EBIS the DT system should provide a gun-side potential barrier, a trap

region and an extraction barrier: all of them with individual potential control. There are several aspects to consider when designing the drift tubes.

- **Inner diameter (ID)** of the trap DT should be large enough, so that the ratio of the drift tube radius to the electron beam radius is the largest in the electron beam path. In this case the electron beam components, which constitute the beam loss will be trimmed off on other electrodes, where this ratio is smaller. Apart of direct electron loss the ion loss during confinement should be also considered: small ID is equivalent of insufficient axial potential trapping: ions with energy higher than the potential distance from the beam axis to the wall will be lost. Study of ion loss rate on CRYEBIS with DT ID 5 mm and 10 mm [34] shows that ion loss rate during confinement with ID 10 mm is substantially smaller than for ID 5 mm.
- **Trap length.** If necessary, the ion trap may extend into area with magnetic field beyond traditionally accepted margin of magnetic field non-uniformity of few percent. Experiments demonstrated almost proportional increase in ion intensity with extending the ion trap into low-magnetic field area [35]. It would be prudent to retain the radial potential well created by the electron beam uniform along the drift tube structure by increasing the DT ID in low-magnetic field areas.
- **Shape.** A cylindrical DT structure inside the long ion trap may require several drift tubes if a fast ion extraction is required. R. Becker suggested using for the central DT a system of two interleaving tubes which provide a linear electrostatic gradient in the centre if different potentials are applied to both tubes [36]. This approach can help reduce the number of drift tubes and to provide the necessary uniform axial extraction gradient for fast ion extraction.
- **Material.** There is no consensus on the best material for drift tubes. EBIT devices operate with copper drift tubes. KRION-1 had its first copper DT structure excited by the electron beam and this excitation disappeared after replacing the copper tubes with stainless steel ones, which also had increased capacity between each other.

2.9.5 Vacuum

Vacuum is a key parameter for EBIS: it determines the achievable ion charge state, the intensity of the extracted working ion beam and the stability of EBIS operation. A good target for the residual gas pressure in the ion trap region for “warm” EBIS would be $P=1 \cdot 10^{-11} - 1 \cdot 10^{-10}$ Tor with electron beam running (RHIC EBIS range). It can be even lower for the “cold” EBIS.

The main sources of the gas load are thermal outgassing, electron collector, electron gun and discharges. Thermal outgassing can be reduced with conventional vacuum procedures, like using low-outgassing materials, NEGs [37, 38, 39], vacuum firing and bakeout. For “warm” EBIS it is essential to have vacuum conductance from the ion trap to vacuum pumps as large as possible even if NEG materials in the ion trap region are used. In this case the vacuum pumps can still provide acceptable vacuum when the NEG materials are partially or completely saturated. The gas load from the electron gun and EC can be reduced with vacuum separation.

The electrical discharge can be a dominant source of gas inside EBIS. P. A. Redhead [40] proposed a model for calculating the condition for magnetron discharge. Usually, the most probable areas with magnetron discharge are regions with low magnetic field and high radial electric field. The most efficient method of reducing this kind of discharge

is eliminating the radial electric field by using a grounded drift tube. If this is not possible, adding an axial electric field to drain the carriers away by making the concentric opposite surfaces conical rather than cylindrical may help.

2.9.6 Cold bore or warm bore?

There is a consensus regarding a choice of solenoid for the powerful EBIS: it has to be superconducting to provide magnetic field in the trap region in a range of 5-6 T. A choice of internal drift structure (cold or warm) is debatable with good arguments on both sides. There are good working solutions for both approaches. The main argument against cold structure is the so-called memory effect: the gas molecules, which are condensed on the internal surfaces of the drift tubes can be desorbed by the trap components and contaminate the ion content of the trap. Such contamination normally is not desirable in EBIS, which works as an ion source for the accelerator because the contaminants substitute the working ions and effectively reduce their intensity. First EBISes used for accelerators (KRION, CRYEBIS and Dione) had cold drift structure and the main inconvenience with it was a long turnaround time determined by the warming/cooling cycle of the large mass of solenoid and its cryostat. But the turnaround time for a “warm” EBIS is not shorter because of pumping/baking cycle, which also carries a risk of leak and damage. With “cold” drift structure one can provide vacuum separation between different EBIS regions using cold drift tubes. Availability of cryogenic temperatures allows a pulsed ion injection with continuous gas injection for a broad range of gases. This kind of ion injection is routinely used on all KRION ion sources in Dubna. A good compromise between the “warm” and “cold” bores can be a “warm” bore with drift structure cooled with independent cold head. Such structure is independent on vacuum in the cryostat of the solenoid and its turnaround time can be shorter than for a classic “cold” bore EBIS, or for classic “warm” EBIS.

2.9.7 Prospects of EBIS intensity increase

So far the main progress with EBIS intensity increase has been made primarily by increasing the electron beam current. Presently in RHIC EBIS the electron current is 8-10 A at the beam energy of 22 keV. One way to increase the capacity of the ion trap and therefore the ion beam intensity is to increase the electron beam current using electron gun with larger cathode. One more approach in boosting the ion trap capacity is increasing the length of the ion trap. The first step in increasing the RHIC EBIS ion trap length by 25% has been done by extending the ion trap into area with lower magnetic field (80% of the maximum). The next step will be done by chaining two superconducting solenoids together [41, 42].

2.9.8 Conclusion

Building EBIS is not a simple task, especially building a powerful one. The accumulated experience with the Test EBIS, with RHIC EBIS and with KRION generations found solutions for many aspects of the powerful EBIS design and operation, which seemed unsolvable in the past. At the present stage, EBIS has a good potential for further increase of the intensity of highly charged ions.

2.9.9 Acknowledgement

Work was supported by Brookhaven Science Associates, LLC, under Contract № DE-SC0012704 with the U.S. Department of Energy.

2.9.10 References

1. E. D. Donets, USSR inventor's certificate #248860 16 March 1967, Bul. OI No. 24, 65, 1967
2. E. D. Donets, V. I. Iluschenko, V. A. Alpert, Ultrahigh vacuum electron beam ion source of highly stripped ions, Proc. First International Conference on Ion Sources, Saclay p. 635, (1969)
3. A.M. Baldin, Yu. D. Beznogikh, V. I. Volkov, E. D. Donets, L. P. Zinoviev, I. F. Kolpakov, L. G. Makarov, V. A. Monchinskiy, A. I. Pikin, I. N. Semenyushkin, E. A. Silaev, Light Nuclei Acceleration in LHE JINR Synchrophasotron, Proceedings, 10th International Conference On High Energy Accelerators, **1**, pp. 367-375, Protvino (1977)
4. E. D. Donets, V. P. Ovsyannikov, Cryogenic electron beam ionizer KRION-2, JINR P7-80-515, (1980)
5. J. Faure, P. Antoine, J. C. Ciret, L. Degueurce, P. Gros, A. Courtois, B. Gmstlnesu, R. Gobln, P. Leaux, P. A. Leroy, J. P. Penlcaud, Dione status report, AIP Conf. Proc. **188**, pp. 102-113, (1989)
6. B Visentin, A Courtois, R Gobin, F Harrault and P A Leroy, Metallic ion production with Dione EBIS, Physica Scripta, 1997 **T71**, pp. 204-206, (1997)
7. J. Faure, B. Feinberg, A. Courtois, R. Gobin, External ion injection into CRYEBIS, Nucl. Instrum. Meth. **219**, 3, pp. 449-455, (1984)
8. P. Chamouard, A. Courtois, J. Faure, R. Gobin, J. Lagniel, J. Lemaire, P. Leroy, B. Visentin, P. Zupranski, Polarized Lithium-6 beam at Saturne, Journal de Physique Colloques, **51** (C6), pp. C6-565-C6-568, (1990)
9. Arianer J., Cabrespine A., Goldstein Ch., CRYEBIS, a multipurpose EBIS the synchrotron Saturne II, IEEE Trans. Nucl. Sci., **NS-26**, 3, pp. 3713-3715 (1979)
10. L. Lilieby and A. Engström, Status report on the Stockholm Cryogenic Electron Beam Ion Source, AIP Conference Proceedings **188**, 27, pp. 27-31 (1989)
11. J. Alessi, E. Beebe, S. Bellavia, O. Gould, A. Kponou, R. Lambiase, R. Lockey, D. McCafferty, M. Okamura, A. I. Pikin, D. Raparia, J. Ritter, L. Snydstrup, A high-performance electron beam ion source, Proceedings of 11th International Conference on Heavy Ion Accelerator Technology, Venezia, Italy, WE11T (2009)
12. R Becker, O Kester and Th Stoehlker, Simulation of charge breeding for trapped ions, Martin Stockli, and C. L. Cocks, The physics of electron beam ion sources, Nuclear Instrum. Meth., in Physics Research, **B56/57** pp. 239-245 (1991), J. Phys.: Conf. Ser. 58, pp. 443-446 (2007)
13. B.M. Penetrante, J. N. Bardsley, D. DeWitt, M. Clark, and D. Schneider, Evolution of ion-charge-state distributions in an electron-beam ion trap, Phys. Rev. A, **43**, No. 9, pp. 4861- 4872 (1991)
14. Xiaojun Lu, and F. J. Currell, Numerical simulation of the charge balance and temperature evolution in an electron beam ion trap, Phys. Rev. Special Topics – Accelerators and Beams, **12**, 014401 (2009)

15. Fred Currell and Gerd Fussmann, Physics of electron beam ion traps and sources, *IEEE Transaction on Plasma Science*, **33**, 4, pp. 1763-1777 (2005)
16. Daniela Leitner, Damon Todd, Daniel Winklehner, USPA – Fundamentals of ion sources (16) Electron beam ion sources and traps, http://www-eng.lbl.gov/~dleitner/USPAS_2016_Fundamental_Of_Ion_Sources/4_Thursday_PM_EBIT.pdf
17. Reinard Becker, Electron beam ion sources and traps, *Rev. Sci. Instrum.*, **71**, 2, pp. 816-819 (2000)
18. Gennadi I. Kuznetsov, Marina A. Batazova, and Michael A. Tiunov, Formation and collection of electron beams for EBIS, *AIP Conference Proceedings* **572**, pp. 143-153 (2001)
19. A. Pikin, J. Alessi, E. Beebe, A. Kponou, K. Prelec, G. Kuznetsov, M. Tiunov, EBTS: design and experimental study, 8th Intl. Symp. Electron Beam Ion Sources and Their Applications, in *AIP Conference Proceedings* **572**, pp. 3-19 (2001)
20. Alexander Pikin, James G. Alessi, Edward N. Beebe, Deepak Raparia, and John Ritter, Analysis of magnetically immersed electron guns with non-adiabatic fields, *Review of Scientific Instruments* **87**, 113303 (2016)
21. A. Pikin, E. N. Beebe, and D. Raparia, Simulation and optimization of a 10 A electron gun with electrostatic compression for the electron beam ion source, *Rev. Sci. Instrum.* **84**, 033303 (2013)
22. Alexander Pikin, James G. Alessi, Edward N. Beebe, Andrey Shornikov, Robert Mertzig, Fredrik Wenander, and Richard Scrivens, First test of BNL electron beam ion source with high current density electron beam, in *AIP Conference Proceedings* **1640**, pp. 12-18 (2015)
23. R. Mertzig, M. Breitenfeldt, S. Mathot, J. Pitters, A. Shornikov, F. Wenander, A high-compression electron gun for C6+ production, *Nucl. Instrum. Methods*, **A859**, pp. 102-111 (2016)
24. Evgeniy Donets, Review of recent developments for electron-beam ion sources (EBIS), *Review of Scientific Instruments* **67**, 873-877 (1996)
25. A. Yu. Boytsov, D. E. Donets, E. D. Donets, E. E. Donets, K. Katagiri, K. Noda, D. O. Ponkin, A. Yu. Ramzdorf, V. V. Salnikov and V. B. Shutov, Electron string ion sources for carbon ion cancer therapy accelerators, *Rev. Sci. Instrum.* **86** (8) 083308 (2015)
26. E. D. Donets, D. E. Donets, E. E. Donets, V. V. Salnikov, V. B. Shutov, S. V. Gudkov, Yu. A. Tumanova, and V. P. Vadeev, Use of EBIS in the string mode of operation on the Nuclotron facility in JINR, *Rev. Sci. Instrum.*, **75**, 5, pp. 1543-1545 (2004)
27. Louksha, G.G. Sominski, D.V. Kas'yanenko, Experimental study and numerical simulation of electron beam in gyrotron-type electron-optical system, *Proceedings of International University Conference on "Electronics and Radiophysics of Ultra-High Frequencies,"* St. Petersburg, Russia, 24–28 May p. 130 (1999),
28. Ioannis Gr. Pagonakis, , Bernhard Piosczyk, Jianhua Zhang, Stefan Illy, Tomasz Rzesnicki, Jean-Philippe Hogge, Konstantinos Avramidis, Gerd Gantenbein, Manfred Thumm, and John Jelonnek, Electron trapping mechanisms in magnetron injection guns, *Phys. Plasmas* **23**, 023105 (2016)
29. D. V. Kas'yanenko, O. I. Louksha, B. Piosczyk, G. G. Sominsky, and M. Thumm, Low-Frequency Parasitic Space-Charge Oscillations in the Helical Electron Beam of

- a Gyrotron, *Radiophysics and Quantum Electronics*, **47**, Nos. 5–6, pp. 414-420 (2004)
30. X. Gu & others, RHC electron lenses upgrades, IPAC 2015, THPF059
 31. Z. Fang, S. Fukuda, S. Yamaguchi and S. Anami, Returning Electron Simulation for a Klystron Collector Using EGS4, Proceedings of the Second International Workshop on EGS, 8.-12. August 2000, Tsukuba, Japan, KEK Proceedings 200-20, pp.272-279 (2000)
 32. Alexander Pikin, Ahovi Kponou, Louis Snyderstrup, Optical, Thermal and Stress Simulations of a 300-kwatt Electron Collector, C-A/AP#246 (2006)
 33. A. Pikin, J. G. Alessi, E. N. Beebe, Optics modification of the electron collector for the Relativistic Heavy Ion Collider Electron Beam Ion Source, C-A/AP/#457 (2012)
 34. J. L. Faure, [B. Feinberg](#), [P. Antoine](#), [J.C. Ciret](#), [A. Courtois](#), [L. Degueurce](#), [R. Gobin](#), [P. Leaux](#), [H. Lecroart](#), Status report on CRYEBIS, in the Proceedings of 12th International Conference on High-Energy Accelerators, Batavia, Illinois, 11-16 Aug 1988, pp 206-208 (1988)
 35. A. Pikin, J. Alessi, E. Beebe, A. Kponou, and K. Prelec, Experimental study of ion injection into an extended trap of the Brookhaven National Laboratory EBIS, *Review of Scientific Instruments* 73, pp. 670-672 (2002)
 36. H. Höltermann, R. Becker, M. Kleinod, I. Müller, Fast Ion extraction from the MedEBIS, *Journal of Physics: Conference Series* **2** pp. 94–96 (2004)
 37. F. Wenander¹, B. Jonson¹, L. Liljeby², G. Nyman, REXEBIS the Electron Beam Ion Source for the REX-ISOLDE Project Design and Simulations, Preprint CERN CERN-OPEN-2000-320 (2000)
 38. A. Pikin, J. G. Alessi, E. N. Beebe, A. Kponou, R. Lambiase, R. Lockey, D. Raparia, J. Ritter, L. Snyderstrup, and Y. Tan, RHC EBIS: Basics of design and status of commissioning, *Journal of Instrumentation*, 5, C09003, (2010)
 39. S. Kondrashev, A. Levand, P. N. Ostroumov, R. Vondracek, A. Pikin, G. I. Kuznetsov, M. A. Batazova, Commissioning of CARIBU EBIS charge breeder subsystems, Proceedings of HIAT 2012, Chicago, WEB02 (2012)
 40. P. A. Redhead, The Townsend discharge in a coaxial diode with axial magnetic field, *Canadian Journal of Physics*, 36, 3, pp. 255-269, (1958)
 41. A. Pikin, J. G. Alessi, E. N. Beebe, M. Okamura, D. Raparia, J. Ritter, L. Snyderstrup, Tandem EBIS, Proceedings of HIAT 2012, Chicago, PO18 (2012)
 42. E. Beebe, S. Ikeda, T. Kanesue, S. Kondrashev, M. Musgrave, M. Okamura, A. Pikin, D. Raparia, J. Ritter, A. Zelenski, The extended EBIS Intensity Upgrade at Brookhaven National Laboratory, https://indico.cern.ch/event/628126/contributions/2673105/attachments/1540875/2416334/ICIS2017_Talk_Beebe.pdf

2.10 EBIS/T charge breeders for post-acceleration of rare isotopes

Alain Lapierre

Mail to: lapierre@nscl.msu.edu

National Superconducting Cyclotron Laboratory, Michigan State University,
640 South Shaw Lane, East Lansing, 48824, USA.

2.10.1 Introduction

Charge breeders convert beams of ions of low charge state into multiply charged ion beams. As the energy of ions accelerated through accelerators scaled with their charge, they are employed at accelerator facilities to extend the energy range. At facilities for rare-isotope beams (RIB), the rare isotopes produced by, for instance, fast projectile fragmentation or the ISOL (Isotope Separation On-Line) technique are charge bred for post-acceleration to energies that differ from their energies after production. Stripper targets can be utilized to increase the charge of the ions in a beam. However, efficient production of a specific charge state, needed for post-acceleration, depends on the velocity of the ions impinging on the target. Depending on the required final beam energy, this can necessitate multiple stripping and acceleration stages, reducing the overall efficiency and adding to the construction cost of the accelerator. Due to straggling and scattering, interaction with the target can significantly increase the beam longitudinal and transverse emittances. Electron Cyclotron Resonance Ion Sources (ECRISes) are often used as charge breeders. In an ECRIS, an electron-ion plasma is confined in a minimum magnetic field region. Injected ions are captured by the plasma and further ionized by the plasma electrons. ECRIS breeders have a high charge capacity for efficient capture of intense beams and can operate in a mode of continuous beam injection and extraction. However, ECRISes produce beams of large emittances. Moreover, interaction of electrons and/or ions with the wall of the plasma chamber generates a high stable-isotope background that can strongly contaminate rare-isotope beams of low intensity. Electron-beam ion sources and traps (EBIS/Ts) uses a magnetically compressed electron beam to produce multiply charged ions. EBIS/T breeders can reach high efficiencies within short breeding times, which can be varied to optimize production of specific charge states. The stable-isotope background is significantly lower than in ECRISes. Although they have a small charge capacity, often not a limiting factor with rare-isotope beams, they can provide beams of small emittances. This publication reviews the use of EBIS/T breeders for post-acceleration of rare isotopes with a focus on the ReA EBIS/T [1] and an emphasis on beam dynamics. For exhaustive reviews, see [2, 3].

2.10.2 Post-acceleration concept

All post-accelerator facilities employing EBIS/T breeders are similar in concept, such as the operating REX ISOLDE [4], ReA [1], and CARIBU (ANL) [5], and those under construction as CANREB [6] and RAON/RISP [7]. Although the production method of the rare isotopes differ, they all incorporate a beam buncher, an EBIS/T, a charge-over-mass (Q/A) separator (typically achromatic), and a radio-frequency quadrupole (RFQ) accelerator and a linear accelerator (LINAC). Rare-isotope ions in the $1+$ (typically) charge state are continuously injected and accumulated into the buncher. The ions are ejected as pulses and transported to the EBIS/T for injection. They are then captured and charge bred to $Q+$ within hundreds of milliseconds. After breeding, multiply charged ion pulses are ejected to the Q/A separator for charge-state selection. The ions are subsequently accelerated with the RFQ and the LINAC up to several to tens of MeV/u, and transported to an experiment.

2.10.3 Working principle of an EBIS/T

An EBIS/T produces and confines multiply charged ions with an electron beam compressed by a magnetic field of high flux density [8]. It is composed of an electron

gun, a magnet solenoid (or Helmholtz coils), coaxial cylindrical electrodes, placed in the magnet bore, and a collector. The electrons leaving the gun are accelerated by an electrostatic potential difference between the electrode structure and the gun. The electron beam is then injected (on-axis) into the magnetic field, is focused, and traverses the electrode structure where ions are confined by trapping potentials. After crossing the trapping region, the beam is decelerated and stopped within the collector. The electron-beam size in the focusing magnetic field is well described by Herrmann theory [8].

Injected ions are ionized in the trapping region by the electron beam of high current density. There, the ions are trapped in the axial direction with two potential barriers forming a square-shaped potential well. They are confined in the radial direction by the electron-beam space-charge potential. The electron-beam energy determines the maximum reachable charge state by affecting the electron-impact ionization cross section. Other atomic-physics processes can also occur in the trap, such as electron-capture radiative and resonant multi-electronic recombination with beam electrons as well as charge-exchange recombination with neutral (residual) gas, and contribute to modifying the charge-state balance. The high electron current density is essential for the ionization rate to exceed the charge-exchange rate, particularly for production of high charge states.

In the trap, the ions can gain kinetic energy by collisions with the beam electrons and in accelerating in the space-charge potential during ionization. The interplay between electron-beam heating, exchange of kinetic energy in ion-ion collisions, and cooling resulting from high-energy ions escaping the trapping potential controls the ion temperature. This temperature plays a role in the charge-state balance. The high-temperature ions, as they are less confined, can only partially overlap the electron beam, reducing the electron current density they experience (effective current density). The ion temperature influences the energy spread of ejected ion beams and defines their transverse emittance [4, 9, 10]. The maximum number of trapped positive charges (charge capacity) is equal to the number of beam-electron charges between the two potential barriers. During the breeding process, ions from the residual gas can accumulate and “neutralize” the electron beam, reducing ion confinement by the trapping potentials. This can affect the charge-state balance by decreasing the effective electron current density and increase the transverse emittance of ejected beams. Depending on parameters such as the depth of the trapping potentials and the breeding time, the neutralization ratio can be between 10% and 80%. A high ion temperature and/or a large neutralization ratio often limit production of high charge states that requires high electron current densities and long breeding times.

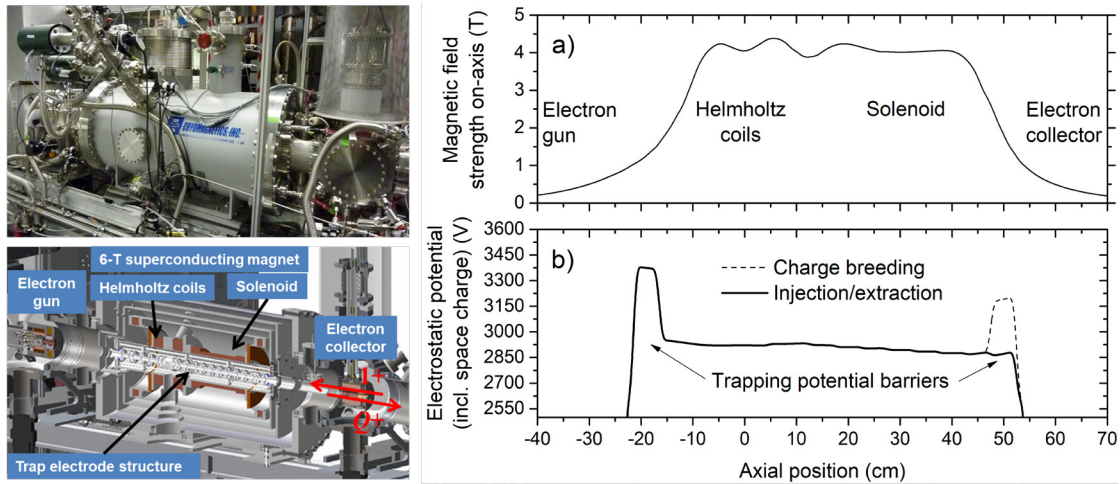


Figure 1: *Left:* Photograph and engineering model of the ReA EBIS/T breeder. *Right:* a) Magnetic field distribution measured on-axis of the ReA EBIS/T's magnet composed of Helmholtz coils and a long solenoid, and b) injection, trapping, and ejection electrostatic potentials, including the space-charge potential (on axis) of a 300-mA electron beam.

2.10.4 Requirements of charge breeders

EBIS/T breeders are mostly designed for high charge capacity and high beam acceptance, needed to efficiently capture ion pulses of long width and large transverse emittance. Compression of high-current electron beams in strong magnetic fields is technically challenging. Moreover, this can reduce the transverse beam acceptance, proportional to the electron-beam size [4]. Hence, EBIS/T breeders have long trapping regions. They can generate high electron currents, but only of moderate current densities, sufficient to breed charge states of $Q/A \geq 1/7$ within less than hundreds of ms. Typical electron-beam currents range between 200 mA and 2 A, and the densities are often less than ~ 750 A/cm². This Q/A range matches the RFQ's injection velocity, of tens of keV/u or less (e.g., 12 keV/u for ReA's RFQ), with reasonable EBIS/T's acceleration (ejection) voltages. The electron energy does not normally exceed 30 keV, and the charge capacity is typically less than 10^{11} C. Figure 1 presents the ReA EBIS/T and its magnetic field distribution along with the axial trapping potential. Table 1 lists typical operational parameters of EBIS/T breeders for post-acceleration of rare isotopes.

Table 1: Operational parameters of EBIS/T breeders for post-acceleration of rare isotopes.

<i>Parameter</i>	<i>Unit</i>	
Q/A range	...	$\geq 1/7$
Electron beam current	A	$\sim 0.2 - 2$
Electron beam energy	keV	5 - 30
Nominal magnetic field	T	≤ 6
Electron beam radius	μm	$\sim 200 - 600$
Electron beam current density	A/cm ²	≤ 750
Breeding time	ms	≤ 500
Charge capacity	C	$\leq 10^{11}$
Length of the trapping region	m	≤ 1

2.10.5 Ion injection and ejection, and beam properties

The most common method of injection of rare-isotope beams into EBIS/T breeders is pulsed injection. Continuous injection is another method that is less common and normally less efficient [12]. In pulsed injection, ions of tens of keV in energy from the ion source are injected as continuous beam into a buncher (such as a Paul or Penning trap) on a high-voltage platform. The ions are decelerated, accumulated, and cooled with a buffer gas (*e.g.*, helium). After accumulation, the buncher ejects a pulse of ions that are then transported at tens of keV to the EBIS/T, placed on a high-voltage platform that is biased near the beam energy. The ions are decelerated to a few keV, pass through the collector, and are decelerated to hundreds of eV by a potential applied to the trap structure before reaching the trapping region. The ion pulse can then enter this region by dynamically lowering the barrier potential, on the collector side, below the beam energy. When the pulse reaches the trap center, this potential is raised (above the beam energy) to capture the pulse (see Fig. 1).

The efficiency of bunchers in operation ranges between 20% and 100% [2]. The properties of beams injected into EBIS/T breeders is presented in Table 2. The width of the ion pulses ejected from bunchers is typically less than tens of μs , shorter than the round trip time of a pulse between the two EBIS/T's potential barriers. The root-mean-square (rms) normalized transverse emittance is less than ~ 0.01 mm mrad, but can vary with the number of ejected ions per pulse. This emittance is preferentially smaller than the EBIS/T's acceptance, defined as the largest emittance of an injected beam fully contained within the electron beam [4]. The (normalized) acceptance of most EBIS/T breeders is ~ 0.01 mm mrad. It is proportional to the electron-beam radius and the square-root of the electron current. The capture efficiency of pulses injected into EBIS/T breeders typically exceeds 80% [2].

After breeding, the ions are ejected by either lowering the collector-side barrier potential or raising the central trap potential. In the first scheme, the entire (thermal) energy distribution of the trapped ions is released within the ejected pulse, which can lead to ion beams of large energy spread. The second scheme is normally preferred as raising the central potential pushes the ions over the potential barrier to exit the trap with a narrower kinetic-energy range. The energy of the ejected beams is matched to the RFQ's injection velocity by adjusting the EBIS/T's platform (acceleration) voltage for the charge state selected for post-acceleration.

Table 2: Properties of beams injected into and ejected from EBIS/T breeders.

<i>Parameter</i>	<i>Unit</i>	
Injection energy	keV	< 60
Injected pulse width	μs	~ 10
Injected normalized emittance	mm mrad	~ 0.01
Ejection energy (RFQ's inj. velocity)	keV/u $\times A$	a few tens
EBIS/T's norm. acceptance (95%)	mm mrad	~ 0.01
Ejected normalized emittance	mm mrad	~ 0.1
Ejected pulse width	ms	$\sim 0.02 - 100$
Injection/ejection repetition frequency	Hz	≤ 100

The width of the ion pulses ejected from EBIS/T breeders by rapidly lowering or raising the ejection potential with a step (square-like) time function is typically tens of μs . This is related to the round trip time of the ions between the two potential barriers. Depending on parameters such as the depth of the trapping potentials, the temperature of the trapped ions is normally in the range of tens of eV/Qe [11]. The EBIS/T's transverse emittance varies in dependence of the size of the cloud of ions orbiting the electron beam and the ion temperature, which both define the ion source size and the transverse velocity of the ejected ions [9, 10]. The rms normalized transverse emittance of multiply charged ion beams is typically less than 0.1 mm mrad. The pulsed injection and ejection repetition frequency, defined by the chosen breeding and ejection times, is less than 100 Hz.

2.10.6 Charge breeding and efficiencies

In EBIS/T breeders, the electron beam of small energy spread produces a narrow charge-state distribution. $j_{\text{eff}} \tau_B$, the product of the effective electron-beam current density and the time the ions are captured in the trap (breeding time) is a key parameter that defines the average charge state of this distribution and, hence, the breeding efficiency in single charge states. Accurate breeding times can be obtained from simulations including various atomic-physics processes and the dynamics of the ions in the trap [8]. However, from low to moderate charge states and in ultra-high vacuum, electron-impact ionization dominates the recombination processes. The time to fully convert an initial population of $1+$ ions to $Q+$ can be estimated as

$$\tau_B(Q+) \approx \frac{e}{j_{\text{eff}}} \sum_{i=2+}^{Q+} \frac{1}{\sigma_{i-1 \rightarrow i}} \quad (1)$$

where e is the elementary charge. Eq. (1) shows that the breeding time is proportional to the inverse of the current density and the sum of the inverse of all successive ($2+$ to $3+$, $3+$ to $4+$, etc.) ionization cross sections ($\sigma_{i-1 \rightarrow i}$) from $2+$ to $Q+$. Operating with a constant density, the abundance of a charge state is often maximized by adjusting the breeding time and the electron energy to maximize the ionization rate. For ionization of a single bound electron, the ionization cross section of a given charge state peaks at an energy ~ 3 times as large as its ionization threshold. A charge state is normally selected for post-acceleration based on the energy of the rare-isotope beam to deliver (high Q for high energy), beam contamination, and its expected breeding efficiency. A simulated charge-state evolution of potassium bred for different times with a current density of 150 A/cm^2 and beam energy of 15.5 keV is presented in Fig. 2. Efficiencies of more than 30% can be expected within less than 100 ms for low to moderate charge states of elements of medium atomic numbers. As long as electron-beam neutralization and heating remain negligible, higher efficiencies exceeding 60% can be anticipated by breeding closed-shell electronic configurations, such as helium-like, for half a second. The charge-state distributions of heavier elements such as rubidium or cesium are broader. Simulations predict lower efficiencies in single charge states in the range of 20%.

Figure 2 shows selected efficiencies in single charge states of EBIS/T breeders currently in operation. These values do not include the efficiencies of the bunchers. The REX EBIS typically breeds moderate charge states. Its efficiencies approaching 30% for

elements of medium atomic numbers agree with the simulation, indicating narrow charge-state distributions and high overall efficiencies of nearly 100% for the sum of all charge states. The REX EBIS and CARIBU (ANL) EBIS can reach efficiencies in single charge states of approximately 20% for heavy elements such as cesium, as expected. The ReA EBIS/T has lower efficiencies as it breeds high charge states (for high post-accelerated energies) with long breeding times. The overall efficiencies of the ReA EBIS/T range between 65% and 89%.

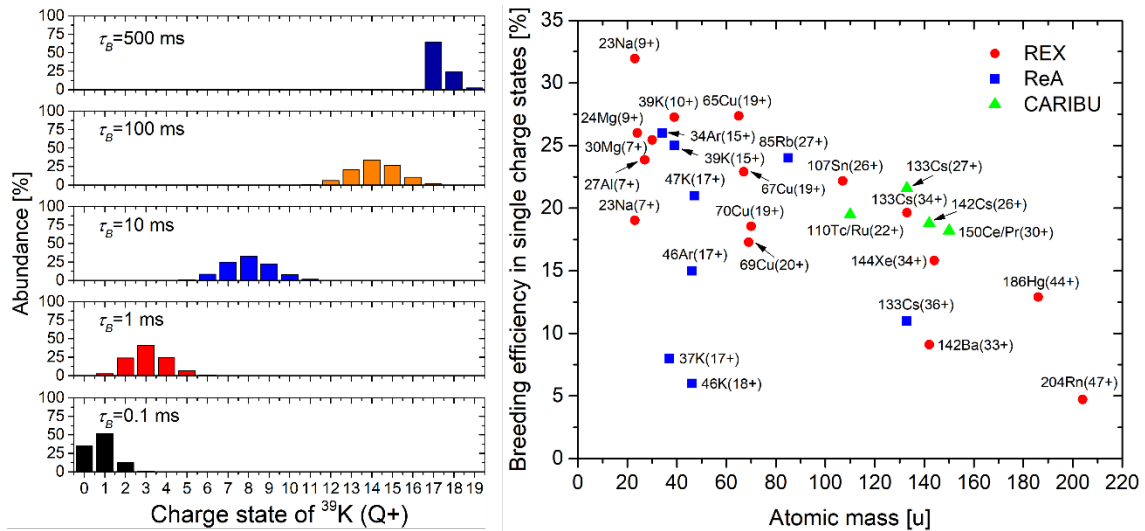


Figure 2: *Left:* Simulated charge-state distributions of potassium ions bred for various times with an electron current density of 150 A/cm² and energy of 15.5 keV. *Right:* Efficiencies in single charge states of EBIS/T breeders in operation.

2.10.7 Pulse stretching

EBIS/T breeders are ion traps and, as such, are pulsed devices. The width of the ion distributions ejected by quickly varying the ejection potential (barrier or central potentials) with a step time function is tens of μs . The instantaneous ion rate (the ratio of the number of ejected ions to this width) of such short pulses accelerated to experiments is often too high for efficient detection of all ions or related events within each pulse. This is caused by the long “dead” time of detection systems. The pulse width can be stretched by slowly varying the ejection potential over an extended time with a continuous time-dependent function [14]. Another approach is to vary the potentials with a series of incremental step functions, fine-tuned to produce a square-like ion time distribution [15].

The ions in the trap can be assumed to have a Maxwell-Boltzmann energy distribution. The position of its maximum in the potential well is governed by the ratio of their charge to their temperature. The ions in high charge states, for instance, are deeply confined in the trapping potential. To maximize the ion spread within an ejection time, the ejection potential has to be first varied rapidly at the beginning of the ejection time. Then, when near the peak of the distribution, the lowering rate has to be reduced to slowly release the ions. Under certain conditions, a logarithmic function is the optimum function to produce a square-like ion time distribution of an ejected Boltzmann energy distribution [14].

Using exponential and logarithmic functions, $^{34}\text{Ar}^{15+}$ and $^{39}\text{K}^{18+}$ pulses ejected from the ReA EBIS/T could be stretched to 40 ms and 70 ms, respectively.

Another technique being developed as part of the EMILIE project is to capture the short pulses ejected from an EBIS/T breeder and spread out their distribution in time with a downstream ion trap [13].

2.10.8 Beam purity

Rare-isotope beams of low rates (*e.g.*, 10,000 particles per second) can easily be obscured by the tail of beams of residual-gas contaminants. In ECRIS breeders, high-energy electrons and/or ions can leave the confinement region and interact with the wall of the plasma chamber. Due to their close proximity, the released contaminants can migrate to the confinement region. In EBIS/T breeders, the (unidirectional) electron beam passes through the trapping region with no or little interaction with the trap structure, located some distance away from the electron gun and collector, which are potential (warm) sources of contamination. Between breeding periods, the electron beam can be pulsed down, improving the vacuum [5]. The contaminating background of EBIS/Ts is typically orders of magnitude lower than in ECRISes. In the ReA EBIS/T, all stable isotopes of C, N, O, and Ar are the strongest contaminants in addition to lesser amounts of the stable isotopes of F, Na, Si, S, and Cl. Several Q/A regions contain contamination of less than thousands of particles, suitable for post-acceleration of rare isotopes [12].

Many experiments prefer lower rates (less statistics) as a trade-off for contaminant-free beams. The first step in producing a high-purity beam is to choose for post-acceleration a charge state of the rare isotope in a Q/A region containing the least contaminants. Purifying the beam can then involve the use of various techniques that differ depending on the charge and mass of the contaminants as well as the beam energy. As a typical example, isobar contaminants of lower atomic numbers can be eliminated by breeding fully stripped or hydrogen-like ions. However, because of their low ionization cross sections demanding long breeding times, doing so can be inefficient. An alternative can be to bred a more efficient charge state, such helium-like, and, following post-acceleration, improve beam purity by selecting a different charge state after a stripper foil. Contaminants can be eliminated by time of flight. When released with a slow ejection function, ions of different charge states, as they experience an axial trapping potential proportional to their charge, can be released at different times. Beam purity can then be improved by preventing post-acceleration of the contaminants with a gating technique. RF excitation of trapped ions during the charge breeding process is also a method that could also be employed to remove contaminants. However, due to magnetic field inhomogeneities, this method has a low Q/A resolving power. Development is still needed for its use as a valuable technique to clean beams [16].

The ReA EBIS/T typically provides rare-isotope beams with a purity better than 80%. The majority of the contaminants are the daughters and grand-daughters (isobars) of the rare isotopes injected from the ion source, where rare isotopes are lost and can decay.

2.10.9 High current and high current density

Future RIB facilities will increase the production yield of rare-isotope beams. Certain beams are expected to reach rates exceeding the space-charge capacity of current bunchers. Such high rates can induce excessive losses in the bunchers and increase the transverse emittance of the bunched beams, larger than the acceptance of current EBIS/T breeders. These high rates can also surpass the charge capacity of present EBIS/Ts. The development of electron guns providing beams of, both, high current (τ 500 mA) and high current density (τ 5,000 A/cm²) will be needed to reduce the breeding times (for pulsed injection at high frequencies) as well as increase the charge capacity and acceptance of next-generation EBIS/T breeders [17, 18]. Significant effort in this direction over the years have yielded only modest results.

2.10.10 Conclusion

Over the past decades, EBIS/Ts have been increasingly employed as charge breeders for post-acceleration of rare isotopes owing to their high efficiencies in single charge states ($> 20\%$), small rms transverse emittances (< 0.1 mm mrad), and high beam purity ($> 80\%$). Future RIB facilities will increase the production yield of rare isotopes, exceeding the charge capacity of present bunchers and EBIS/T breeders. The development of electron guns providing electron beams of higher current and higher current density will be needed to efficiency capture and breed these intense beams. In rare-isotope science, EBIS/T breeders have now become a necessary and valuable tool.

2.10.11 Acknowledgments

The author thanks R. Vondrasek and F. J. C. Wenander for sharing efficiency values. The NSCL is supported by the National Science Foundation, Grant No. PHY-1565546.

2.10.12 References

1. A. Lapierre, S. Schwarz, K. Kittimanapun, *et al.*, AIP Conf. Proc. **1525** 497 (2013)
2. F. J. C. Wenander, JINST, **5** C10004 (2010)
3. F. J. C. Wenander, CAS-CERN Accelerator School: Ion Sources, Senec, Slovakia, 2012, edited by R. Bailey, CERN-2013-007 (arXiv:1404.0945)
4. F. Wenander, B. Jonson, L. Liljeby, G. Nyman, *REX EBIS, the electron beam ion source for the REX-ISOLDE project, design and simulations*, CERN (1999)
5. P. N. Ostroumov, A. Barcikowski, C. A. Dickerson, *et al.*, RSI, **86** 083311 (2015)
6. F. Ames, M. Marchetto, A. Mjøs, and A. C. Morton, RSI, **87** 02B501 (2016)
7. J. Kim, J. E. Han, H. J. Son, *et al.*, AIP Conf. Proc., **1640** 38 (2015)
8. F. J. Currell and G. Fussmann, IEEE Trans. on Plasma Science, **33** 6 (2005)
9. R. E. Marrs, NIM B **149** 182 (1999)
10. C. Dickerson, B. Mustapha, A. Pikin, *et al.*, PR AB, **16** 024201 (2013)
11. T. M. Baumann, A. Lapierre, S. Schwarz, *et al.*, AIP Conf. Proc., **1640** 80 (2015)
12. A. Lapierre, S. Schwarz, T. M. Baumann, *et al.*, RSI, **85** 02B701 (2014)
13. P. Delahaye, A. Galatà, J. Angot, *et al.*, RSI, **87** 02B510 (2016)
14. A. Lapierre, Can. J. Phys., **95** 361 (2017)
15. F. Ullman, A. Schwan, G. Zschornack, *et al.*, IPAC 2011, San Sebastián, Spain.

16. A. Lapiere, M. Brodeur, T. Brunner, *et al.*, NIM A, **624** 54 (2010)
 17. R. Mertzig, M. Breitenfeldt, S. Mathot, *et al.*, NIM A, **859** 102 (2017)
 18. S. Schwarz and A. Lapiere, RSI, **87** 02A910 (2016)

2.11 Pulsed Low Charge State Ion Sources

Ralph Hollinger and Aleksey Adonin

Mail to: R.Hollinger@gsi.de

GSI-Helmholtzzentrum, Planckstrasse 1, 64291 Darmstadt, Germany

2.11.1 Introduction

This article presents an overview on pulsed low charge state ion sources for particle accelerator applications, as for synchrotron machines or other low duty factor accelerators. There is also a huge area of applications in the industry, such as coating for semiconductors, ion implantation or medical applications. In addition there are some special applications like plasma generation for Tokamaks or thrusters for aerospace.

In the following we define low charge state as maximum four-fold ionized (1-4+) ions, while medium charge state is in the range of 5 to 10+, and high charge state beyond of 10+. A special focus lies on high current ion sources. This means we are talking about beam current where space charge is a not negligible effect during the formation of the beam in the extraction system. In general this is the effect when the extracted ion beam current overcomes the [mA] limit.

A special emphasize is on two types of ion sources, which serve the UNILAC (Universal Linear Accelerator) [1] of the GSI accelerator facility with high current heavy ion beams very successfully nowadays and in the future when the FAIR facility [2] (Facility for Antiproton and Ion Research) will be in operation: Filament driven Multi Cusp Ion Sources (MUCIS and MUCIS 2020) and the MeVVA type ion source VARIS, all developed at GSI [3, 4, 5, 6, 7].

2.11.2 Overview of most common pulsed low charge state ion sources

- **Filament driven volume type ion sources [8]:** This ion sources are the eldest (from 1930s) and includes numerous types, such as PIG (Penning Ionization Gauge), CHORDIS (Cold or Hot Reflex Discharge Ion Source), MUCIS, HIEFS (High Efficiency Ion Source), Duoplasmatron, DuopIGatron, and others. This ion sources are all favorable to produce low charge states and high emission current densities and most of it can operate in cw and in pulsed mode.
- **MeVVA ion sources:** MeVVA (Metal Vapor Vacuum Arc) developed for accelerator applications in the 1980s at Berkeley by I. G. Brown [24] are originally pulsed low charge state ion sources with high emission current densities. Later on GSI developed a new version called VARIS (Vacuum Arc Ion Source) for four fold high current uranium beams [9].
- **RF driven volume type ion sources [8, 10, 11, 12]:** This kind of ion sources were developed in the 1960s as thrusters for space propulsion. Since the 1970s they were commercially used and since the 1990s they were used as neutral beam injectors. The RF ion source is able to produce low charge states with high emission current densities. Currently this ion source is used usually for

H⁻ production for accelerators (DESY at Hamburg, LINAC 4 at CERN, SNS at Oak Ridge) and operates with duty factors of up to 25 %.

- **Special ion sources:** Nier and Bernas type ion sources, Nielsen ion source, hollow cathode ion source, Wilson ion source, Metal ion source of Wilbur and Wei, Freeman ion source, Magnetrons. These ion sources are used e.g. for ion implantation, mass spectroscopy and mass separation, ion beam analysis or isotope separation. Originally, they do not have their application in the field of accelerators. A detailed overview is given in [8].

2.11.3 Boundary conditions for pulsed low charge state ion sources

2.11.3.1 *Why pulsing an ion source?*

One reason for pulsing an ion source could be that it is required by the accelerator itself. This is the case for synchrotrons where a linear accelerator serves as an injector. In fact it would be possible to operate the ion source in cw mode but in case of high beam power one reaches easily the limits e.g. for beam diagnostics. A 100 emA at 100 kV beam (10 kW beam power), as it is foreseen for FAIR proton injector, is a cost driver for cooling and beam diagnostic. Therefore, it is more sufficient to pulse the ion source itself and not using only a beam chopper. Beam choppers are generally used to select the filet part out of the ion beam in front of the rf accelerator.

Another reason, and this is in most cases the main reason, is to improve the performance of the ion source in lifetime or beam quality. Some ion sources operate in pulsed mode by implication, such as vacuum arc ion sources (MeVVA) or laser ion sources.

2.11.3.2 *Advantages for ion sources in pulsed mode operation*

For a filament driven ion source we simply can increase the lifetime by pulsing the arc discharge. In general the arc discharge is pulsed and not the filament due to thermodynamic reasons. Obviously, we do not pulse the extraction power supply. In this case we would have a pulsed beam but no advantage for the ion source itself. In this case it is better to use a beam chopper in front of the following rf accelerator as mentioned above.

It is possible to increase the arc current and therefore the plasma density by pulsing the arc discharge. This results in a higher emission current density. One can increase the arc current by a factor of 2 or 3 without any improvement of the cooling system. The arc current is anyway limited for cw ion sources by something like 100-150 A, because the cooling capacity is limited to ~10-20 kW per liter ion source volume. This depends strongly on the type of plasma confinement and in special cases one can overcome this limit, especially for very small ion source volumes.

By pulsing the ion source it is possible to increase the maximum field strength in the extraction system which results in a higher emission current density and therefore in a higher ion beam current. The reason for this is the following: The temperature rise of the ion source is reduced by pulsing the arc discharge as well as the temperature rise in the extraction system, especially on the surface of the electrodes. This results in a lower risk of a voltage breakdown and therefore in a higher electrical field strength. In addition, it is possible to increase the plasma confinement if it is accomplished e.g. with a magnetic

coil. In this case one can also pulse the current in the coil, which results in a higher magnetic flux density.

2.11.3.3 *Disadvantages for ion sources in pulsed mode operation*

Generally, in pulse operation the system becomes more complicated and expensive: One has to control the stability of the extraction voltage to get a stable beam. While the electrical load is pulsed, one has to use more complicated electronics: a fast pulser or switcher is needed, a trigger device is needed, the synchronization to the accelerator gets more complicated. The operational experience shows in addition that ~20 % of operational failures are connected to the timing system (hardware and software).

The lower temperature of the ion source by use of pulsed mode operation could also be a disadvantage. For some applications a high temperature inside the plasma chamber is required. This is the case when condensation processes to the walls are not wanted, especially when evaporation processes of metals (e.g. using an oven or sputtering) occurs. Possible solution to counteract is to use a hot screen.

By pulsing the arc discharge the magnetic field of the arc is also pulsed. This effect brings in additionally mechanical stress to filigree parts of the ion source (e.g. filament) and therefore could reduce the lifetime.

Another fact has to be mentioned as well: when we pulse the arc discharge the plasma itself is pulsed. This means, that the plasma is completely build up at the beginning of the pulse and completely disappears at the end. This process takes a dedicated time in both cases. If everything is optimized (enough electrical capacity, low impedance of the wiring, fast pulser, etc.), this process finishes after several tens of μs . As a consequence, in pulse mode the ion source operates in series in two completely different modes. This has a strong influence on beam performance. For each pulse the ion beam extraction is performed in so called not matched case (matched case is when the ion beam is extracted with a minimum divergence angle). The extraction system is driven at the full perveance limit. This causes secondary particle emission from the walls and electrodes inside the extraction system caused by ion bombardment with a high risk of voltage break downs. However, pulsing the ion source reduces the temperature inside the extraction system as mentioned before. Taking this strong benefit into account, a much higher maximum field strengths for pulsed mode operation can be achieved, which is very favorable.

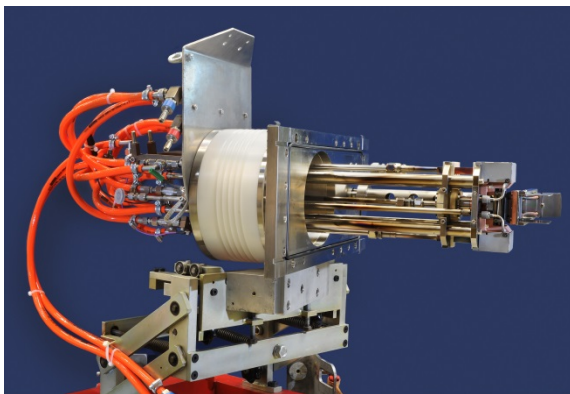
2.11.4 **Filament driven volume type ion sources and their Renaissance at GSI**

As mentioned before, two types of filament driven ion sources are in operation at GSI: PIG ion source which is the working horse for high duty factor experiments for a various kind of elements and multi cusp-type ion sources like CHORDIS and MUCIS which serve the heavy ion synchrotron SIS18 mostly.

2.11.4.1 *Excursion on PIG ion source at GSI*

For low energy experiments (3.6-11.4 MeV/u) with high duty factor beams the Penning ion source is used. With this kind of ion source we are able to offer a variety of ion species in a large range of different mass over charge ratio: Bi^{4+} is feasible as well as Bi^{10+} . Fig. 1 shows the ion source and the most important operational parameter. For more details see the following references [8, 13, 14]. In the 1970s the ion source has been overtaken from ITEP/Russia and is being improved till today. Up to 18 PIG sources are

in operation at GSI for gaseous or metal ion beam production. The relatively short beam times of only several days up to 3 or 4 weeks make this kind of source very attractive. The lifetime is limited either by the filament or by the sputter target and takes for high duty factor experiments (25 %) only one day, but exchange of the ion source lasts only 30 min. up to 1 hour till the beam is back on the target. During last decade this ion source has been optimized in terms of current density and reliability. It was successfully in operation for different high-level experiments [15, 16, 17, 18], as the ^{50}Ti beam time for SHE production experiments (search for Super Heavy Elements 119 and 120). For this long-time experiment over 3 month an average ion beam intensity (including all failures) of $0.8 \mu\text{A}@25\%$ duty factor at the target has been reached, which is an outstanding record. The limited lifetime of this ion source, compared e.g. to ECR ion sources, is not really a showstopper, because the simpler ion source exchange is very short. Using enriched material, especially for ^{50}Ti operation, is possible. By mixing with natural material we reached a quote of 10 % ^{50}Ti and then had the same consumption (10 mg/day) compared to the ECR, using an oven. Finally, we reached the same reliability compared to ECR. The daily PIG exchange took approx. 1 hour, but the lifetime of the ECR oven is also limited to 4 days and it took 4 hours to exchange.



Max. A/q for RFQ*	65
Injection energy	2.2 keV/u
Repetition rate	10-50 Hz
Pulse length	1-5 ms
Charge state	1-10+
Arc current	≤ 10 A
Arc voltage	≤ 2.5 kV
Extraction voltage	$\leq \xi 22$ kV
Emission current	≤ 50 mA
Elements	Gases and metals

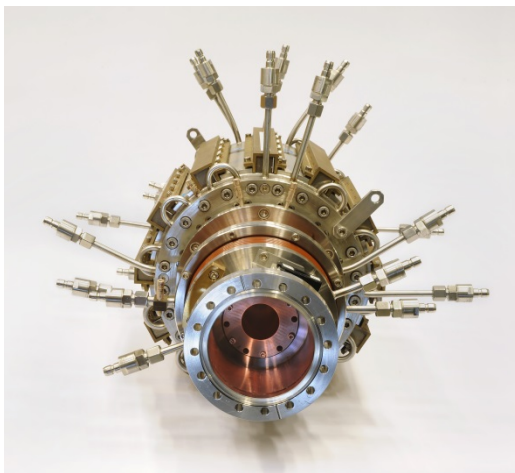
Figure 1: Photo of the Penning ion source and its operational parameter. *RFQ = Radio Frequency Quadrupole

2.11.4.2 *Excursion on CHORDIS and MUCIS 2020 at GSI*

For injection into the synchrotron SIS18 delivering ion beams for high energy experiments with energies of up to 4 GeV/u the ion sources MUCIS, MUCIS 2020 and CHORDIS are used generally at low duty factor. Due to the higher plasma density these ion sources have their maximum of intensity in a charge state of 1+ or 2+. The very low ion and electron temperature of such cold plasma sources and the sharpness of the energy distribution [19] together with the boundary condition of surface emission of the ions allows to reach small emittance values, which cannot be achieved with other ion source types at high emission current densities. Additionally, there is no emittance increase due to magnetic fields in the extraction region. The price to pay for the brilliant beam is to live with low charge states. Using a gas and/or solid target stripper increases the charge state but particle losses occur. However, at the target we reach much higher intensity (factor of 100), compared to the ECR while beam stripping is not necessary.

CHORDIS and MUCIS, developed at GSI by R. Keller are in operation since more than 30 years, although they are equipped with “old-fashion” filaments: The specialty of

GSI is to provide an enormous variety of elements. On the other hand the experiment time for a single experiment is pretty short: a few days up to 2 or 3 weeks. With this boundary condition it is not really a disadvantage to use filaments as an electron emitter, especially when the filament exchange takes only 15 min. The CHORDIS is mainly used for nitrogen beam because we get the best result producing N_2 molecule ions. MUCIS is used for all the other gaseous ions (see Tab. 1). The development of the MUCIS is still ongoing. Recently, the third generation called MUCIS 2020 is in operation. It is equipped with a new filament setup and a new type of plasma confinement, using a Halbach-type multi cusp and solenoidal magnetic arrangement. By pulsing the solenoid it is possible to reach much higher magnetic flux densities. Special emphasis went into the development of heavy gases like kryptonite or xenon where we have to generate $2+$ or even $3+$, because of the limited mass over charge ratio of 65 for the RFQ. For kryptonite it was possible to shift the mean charge state to $2+$. With such an improved spectrum we reach enough intensity for the accelerator to serve the experiments satisfactorily. The most recent development was dedicated to ion production of C and H rich molecules, like CH_4 or C_3H_7 . With CH_3^+ for example we overcame easily the space charge limit of $0.25 \text{ mA} \cdot A/q$ for the RFQ (0.25 mA for protons) and have in addition a higher acceleration voltage of 33 kV or 95 kV , resp. (2.2 keV/u). As a consequence we produce an intense particle beam for C and H in parallel: In the gas stripper the CH_3^+ ion is cracked and stripped into C^{6+} and H^+ with an intensity more than 20 times higher compared to H_3^+ ion beam produced earlier. Due to the fact, that the accelerator is operated in pulsed mode with different so called virtual accelerators, we are able to produce with one ion beam (CH_3^+) two different kinds of high intensity ions (C^{6+} and H^+) in parallel to serve different experiments.



Max. A/q for RFQ	65
Injection energy	2.2 keV/u
Repetition rate	1-5 Hz
Pulse length	0.2-1 ms
Charge state	1-3+
Arc current	$\leq 300 \text{ A}$
Arc voltage	$\leq 550 \text{ V}$
Extraction voltage	$\leq 40 \text{ kV}$
Emission current	$\leq 200 \text{ mA}$
Extraction system	Multi aperture, triode, $13 \times 3 \text{ mm}$
Elements	Gases (H_2 to Xe)

Figure 2: Photo of the MUCIS 2020 and its operational parameter.

Fig. 2 shows the MUCIS 2020 and the most important operational data. For more information please see reference [13, 14, 19, 20]. Tab. 1 summarizes the data for CHORDIS and MUCIS 2020.

It is well known that GSI is on the way to build up a new accelerator facility named FAIR. One goal is to deliver up to 1000 times higher primary intensities with energies of several GeV (depending on the ion and its charge state) for various kind of ion species. For a lot of ion species we will still use filament driven ion sources, where no other ion source is able to deliver such a high brilliant ion beam. The beam brilliance for a filament

driven ion source using a single aperture extraction system can reach values of about $2000 \text{ A}/(\text{m}\cdot\text{rad})^2$, which is unachievable for ECR ion sources [21].

2.11.5 Vacuum arc driven ion sources and their recent development at GSI

The history of the vacuum ion sources extends back to the middle of the last century. First ion sources driven by vacuum discharge arc had been developed in the late 1950s in the former Soviet Union [22]. The primary application of this type of source was an ion implantation for material surface modification. Also they have been evolved for ion beam production and injection in particle accelerators. The distinctive feature of the vacuum arc ion sources (compare with other types) is the production of high current metal ion beams. A detailed review on this kind of ion sources, as well as on their applications, is given in [23]. At GSI two types of ion sources based on the vacuum discharge arc principle are in use: MEVVA IV and VARIS.

2.11.5.1 *MEVVA IV ion source*

The MEVVA [24] ion source is used at GSI since 1980s. It was the main ion source for generating high current metal ion beams for SIS18-synchrotron operation until 2010. It provided eight different metallic elements in a wide range of masses from ^{24}Mg to ^{181}Ta . The MEVVA is operated in pulsed mode with a maximum duty cycle of 1 Hz and 1 ms pulse duration, providing ions with a mean charge state between 1+ and 3+ depending on the element. This ion source has two solenoids for 0.1 and 0.2 T, owing to this it is possible to increase the plasma density and to achieve high emission current densities (up to $150 \text{ mA}/\text{cm}^2$) in the extraction system. The MEVVA is equipped with a revolver system for 17 cathodes that allows switching between cathodes for a few seconds. One could install the cathodes made of various elements into the revolver, so it is possible to change the ion species without changing the ion source. The average lifetime of one cathode operating at 1 Hz / 1 ms is about 8 hours. The operation lifetime of the source (time between services) is about 1 week. However, fast ion source exchange time: 30 min to 1 hour (of beam interruption for experiments) provides high availability of MEVVA ion beam for experiments. For MEVVA the same extraction system as for CHORDIS and MUCIS is used, namely, triode multi-aperture with 13 holes $\varnothing 3 \text{ mm}$, allowing to apply an extraction voltage up to 35 kV. More technical characteristics of MEVVA as well as its operation specificity and features are described in [6, 7].

2.11.5.2 *VARIS ion source*

The vacuum arc ion source VARIS, has been developed at GSI in 2004 based on the MEVVA IV ion source [23]. The main purpose was the production of high current $^{238}\text{U}^{4+}$ ion beams for synchrotron operation [9]. VARIS has a number of differences in construction compared to MEVVA: enhanced geometry of the plasma chamber and anode, optimized position of magnetic coils and filtering grids, more compact setup of the extraction system and improved isolating materials. Due to these construction features the VARIS has a number of improved characteristics compared to the MEVVA IV ion source: higher emission current density, better vacuum conditions, better pulse-to-pulse stability, reduced intensity fluctuations during the beam pulse, higher U^{4+} fraction in the plasma, reduced power consumption and therefore higher efficiency, reduced service time, faster start of operation after ion source replacement at the injector, better

availability and higher cost efficiency [9]. For operation with duty cycles up to 2 Hz / 1 ms no water cooling of the VARIS is necessary.



Max. A/q for RFQ	65
Injection energy	2.2 keV/u
Repetition rate	≤ 2 Hz
Pulse length	0.1-1 ms
Charge state	1-4+
Arc current	≤ 1200 A
Arc voltage	≤ 550 V
Extraction voltage	≤ 45 kV
Emission current	≤ 200 mA
Extraction system	Multi aperture, triode, 13x3mm
Elements	Metals (Mg to U)

Figure 3: Photo of the VARIS and its operational parameter.

The VARIS has been optimized for production of high intensity U^{4+} beam. With this ion source it was possible for the first time to achieve an ion charge state distribution maximum at 4+ (up to 67 %), providing up to 15 mA of U^{4+} in front of the RFQ. Besides performance optimization the physical processes inside the plasma, as: ignition of the arc, self-confinement of the plasma plume, anode spot phenomena, etc. as well as the main plasma parameters, as ion and electron energy distribution have been investigated using a high resolution 127° electrostatic cylinder spectrometer and a high resolution gated CCD-camera [9].

Since 2004 VARIS is established as a “standard” source for production of high intensity uranium beams at GSI. Since 2010 VARIS had fully replaced MEVVA IV the previous generation of vacuum arc ion sources. At the moment there are 12 VARIS sources at GSI, some of them are dedicated to certain elements in order to have optimized performance and maximum beam availability.

2.11.5.3 *Highlights on recent development of VARIS*

The upcoming FAIR facility [25] that will be recently built at GSI will provide wide opportunities for investigations and research in different branches of science including antiproton physics, bio and material research, nuclear astrophysics and many others. The requirements to the primary ion beams in the sense of beam intensity, beam brilliance, repetition rate and availability of various ion species will be significantly increased [2]. Oriented on recent and future requirements the development of VARIS for the last five years went on three main directions [26]: production of high current beams of heavy elements (Au, Pb and Bi), increasing the beam brilliance for U-beam and extending the list of available projectiles for the experiments.

2.11.5.3.1 Production of high current beams of heavy elements

A significant part of the future research programs at FAIR will require high intensity primary beams of heavy ions: ^{197}Au , ^{208}Pb and ^{209}Bi . The main limiting factor for operation with these heavy elements is given by injection requirements of the HSI (high

current injector) RFQ. The mass-over-charge ratio (A/Q) is limited 65, that gives the requested charge state (Q) for considered elements of $4+$. Another important aspect is the temporal structure of the ion beam pulse. It should have a flat top of more than $120 \mu\text{s}$ in length in order to realize a multi-turn injection scheme for SIS18 for the most efficient beam accumulation.

By operation of the vacuum arc ion source with low discharge current (below 400 A), the typical ion charge state distribution in the plasma is the following: more than 90 % of $1+$, less than 10 % of $2+$, and a very small fraction of $3+$ (depending on the element, surface quality, confining magnetic field, etc.). In order to shift the ion spectrum to higher charge states, it is necessary to increase the discharge current of vacuum arc. Particular difficulties with considered elements (Au, Pb and Bi) are caused by their physical properties. These are soft and fusible metals with relatively low melting point. Therefore, increasing of arc discharge current above 500 A (keeping the same pulse length and duty cycle) can cause melting of the cathode material and unrecoverable failure of the cathode. Another important aspect is the metal vapors pressure at the cathode surface that indicates flux of the neutrals to the plasma and it strongly depends on surface temperature [27]. Operation of vacuum arc ion source with high discharge current causes a significant increase of the cathode surface temperature near the cathode spots during the discharge pulse. As a result, the increasing neutrals flux from the cathode surface dramatically reduces the average charge state of ions in the plasma [28]. However, the situation could be drastically improved by changing the physical properties of the cathode material (i.e., increasing the melting point and reducing vapor pressure on the surface at certain temperature). This can be achieved by using composite materials in the cathode: an alloy or a mixture of the desired material with a more refractory metal. Detailed analysis and selection of possible admixed materials for all three elements (Au, Pb and Bi) are presented in the following works: [26, 27, 29].

First tests have been performed with Bi-Cu composite cathodes with Cu content between 8 and 15 % in weight. The tests have shown excellent results. It was possible to produce a stable high current Bi^{4+} ion beam providing up to 10 mA in front of the RFQ [27]. However, it was noted a significant difference in operation performance between same type of cathodes. And all composite cathodes in general have required long conditioning time, during which they showed slow, but continual increasing of performance. In order to understand this peculiarity some of the Bi-Cu cathodes have been analyzed after the tests using an optical and a scanning electron microscopes. It was investigated not only the working surface of the cathodes but also a material structure and a distribution of the composed elements in the cathode material [27, 29]. Similar tests and investigations have been performed with other two elements: Au and Pb. The Cu seemed to be a quite appropriate material to be mixed with Bi and Pb. The best operation performance was achieved with Bi-Cu (40 % Wt.) and Pb-Cu (40 % Wt.) compositions. To find a proper admixing material for Au five different metals have been tested: Cr, Pd, Ta, Ti and Zr, with in total nine various compositions [26]. The most promising results have been achieved with Au-Cr (50 % Wt.).

Thus, the using of composite materials in the cathodes has allowed us to develop three new high intensity heavy projectile beams for existing synchrotron and future FAIR experiments. A stable operation with a good pulse-to-pulse repetition was achieved providing the following ion beam parameters in front of the RFQ: up to 6 mA of Au^{4+} with duty cycle of 0.5 Hz / 0.25 ms (pulse length), 6 mA of Pb^{4+} with 0.5 Hz / 0.3 ms and 12 mA of Bi^{4+} with 0.5 Hz / 0.4 ms. This development resulted in several successful

beamtimes for a number of research programs on the synchrotron SIS18 and high energy experimental area [13, 30, 31].

2.11.5.3.2 Increasing the beam brilliance for intense $^{238}\text{U}^{4+}$ ion beam

To fulfill the FAIR requirements for $^{238}\text{U}^{4+}$ beam in front of the gas stripper (15 mA, 1 μm horizontal beam emittance) it is necessary to essentially increase the current and the beam brilliance of U-beam from the ion source.

With the VARIS we produce U-beam intensity of more than 150 mA (total extracted beam current), containing about 100 mA of U^{4+} ions [9]. Behind post-acceleration system we have 90 mA of total beam containing about 60 mA of U^{4+} ions. However about 75 % of the beam intensity is lost in LEBT (Low Energy Beam Transport line) between ion source terminal and the RFQ mostly due to the high divergence and relative big transversal emittance of the ion beam [32]. Initially the LEBT was designed for a pencil beam from Penning ion source with an emittance of up to $138\pi \text{ mm}\cdot\text{mrad}$. As the consequence, the beam brilliance at the exit of the ion source operation terminal has to be increased by reducing the beam brilliance.

The first step to reduce the emittance of the ion beam is an optimization of the extraction system of ion source. A standard extraction system of VARIS (multi-aperture triode system with 13-holes $\varnothing 3 \text{ mm}$) has been replaced by a new system with 7-holes $\varnothing 4 \text{ mm}$. The emission area of the new system is about 4.5 % smaller compare to standard, that will course a proportional reduction of extracted beam current. However, with the new extraction system the outer aperture of the ion beam is reduced by 20 % [26]. Moreover, to keep the optimum aspect ratio of 0.5 [7] the distance between plasma and screening electrodes has been increased from 3 to 4 mm, allowing to apply higher extraction voltage (up to 45 kV). The higher ions energy behind the extraction system, the less ion beam losses between extraction and post-acceleration gap could be achieved.

The implementation of the new extraction system to the VARIS allows to reduce the beam emittance in front of the RFQ, keeping the same U^{4+} beam current of 15 mA which is slightly exceed a space-charge limit of the RFQ [9]. Due to this, a significantly improved beam transmission through RFQ and further sections of high current injector of UNILAC has been achieved. In combination with recently developed pulsed H_2 -gas stripper [33] this resulted in a new intensity record for U^{28+} ions of 11.1 emA and horizontal beam brilliance of 20 mA/ μm at 1.4 MeV/u of UNILAC [34]. That amounts 74 % of the FAIR intensity requirements for U^{28+} beam [2, 33, 34].

Another option that could help in providing for a more brilliant ion beam core is electrostatic beam compression in the post-acceleration gap. This possibility has been demonstrated with high intensity Ta-beam from the VARIS on high current test injector (HOSTI) at GSI [35]. The post acceleration gap of operation terminal consists of unmovable HV (High Voltage) electrode and movable set of 3 electrodes (ground-screening-ground) allowing to change the distance between HV and first ground electrodes from 25 to 90 mm with precision of 0.1 mm. By varying the aperture of the HV electrode from $\varnothing 60 \text{ mm}$ to $\varnothing 40 \text{ mm}$ it was possible to reduced transversal beam emittance on more than 30 % keeping the same ion beam current behind the post acceleration gap (Fig. 4). The work in this direction is still ongoing.

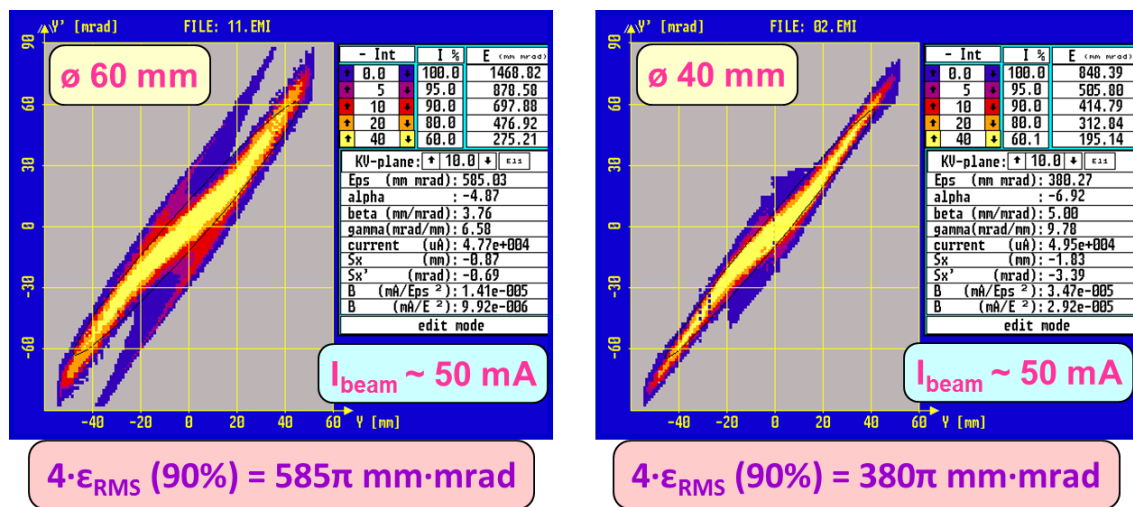


Figure 4: Transversal emittance of 50 mA Ta beam behind the post acceleration gap with $\phi 60$ mm HV electrode (left) and $\phi 40$ mm HV electrode (right).

2.11.5.3.3 Development of the new projectiles in medium heavy region

A number of key experiments at the future FAIR facility will require for an improved quality and intensity of ion beams for certain ion species, as well as for new primary ion beams to be developed. To fulfil these requirements tests at operation terminal with VARIS have been performed recently.

Nine new elements have been tested in various operation modes and under different conditions. For four elements (O_2 , Mg, Mo and Ag) the goal was to improve the performance. Another five elements (Al, V, Fe, Zr and Ru) have never been performed from high current vacuum arc ion sources at GSI before. For medium heavy elements (V, Zr, Mo and Ru) the performance has been tested for various ion charge states optimizing for highest particle current and stability of operation.

Plasma generation processes in vacuum arc ion source define a certain distribution of ion charge states in plasma and in extracted beam, respectively. This distribution depends mainly on plasma density and could be changed by tuning the ion source parameters or by changing the operation duty cycle. Normally, the ion source is optimized for maximum production efficiency and the distribution maximum is situated on the desired ion charge state. However, during the ion source optimization for highest beam current in front of the RFQ the maximum of this distribution could be shifted to higher charge states reducing the production efficiency. The performance could be improved by adding to the plasma a small amount of proper auxiliary gas. Due to varied energy- and charge-exchange schemes in ion source plasma the maximum of the distribution could be returned to the desired ion charge state further increasing the beam intensity (Fig.5). Moreover admixture of the auxiliary gas in most of the cases leads to a more stable vacuum arc discharge and results in noise reduction of the beam pulse and improved pulse-to-pulse repetition stability. In Fig.5 the influence of auxiliary gas on charge state distribution as well as on the production efficiency for Ru^{2+} ions is depicted.

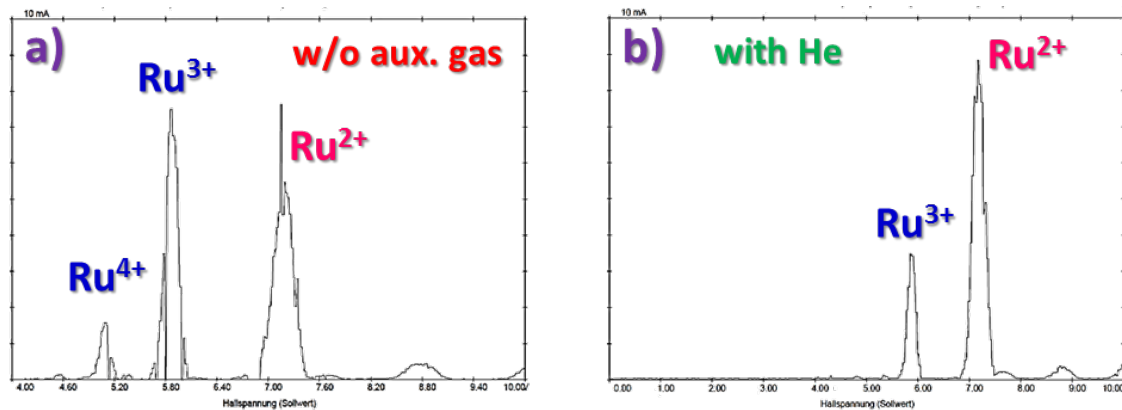


Figure 5: Mass spectrum of Ru beam without (a) and with (b) auxiliary gas.

Summarizing the results, the production of O_2^+ ions was most efficient using V-cathodes. It showed very good performance also with 2 Hz repetition rate, achieving 3.5 mA in front of the RFQ. Mg has shown very good pulse-to-pulse stability, providing 3.5 mA of Mg^+ beam current. The production efficiency was optimal using He as auxiliary gas. Al showed average performance with noisy beam pulses and pulse-to-pulse instabilities even with auxiliary gases. Situation became worse by increasing the duty cycle. 2 mA of Al^+ ions have been reached with 2 Hz repetition rate. In contrast to Al, V showed extremely good performance also with 2.7 Hz (maximum requested for FAIR experiments) operation, providing 2.3 mA of V^+ ions with O_2 as an auxiliary gas. As a possible option for accelerator one could tune the VARIS for production of V^{2+} ions. In this case no auxiliary gas is necessary. Operation was very stable with the same particle current as for V^+ . The highest particle current for Zr of 8 mA has been achieved with Zr^{2+} ion beam. However the stable operation was possible only with 1 Hz. Switching to charge state of 3+ notably improved pulse-to-pulse stability and allowed higher repetition rates but at the cost of particle current that reached 6 mA. The similar situation was with Ru. It was possible to achieve 9 mA of Ru^{2+} and 5 mA of Ru^{3+} with 2 Hz repetition rate. Mo in 2 Hz-mode has shown much better stability and higher particle current (up to 5 mA) with 3+ charge state compare to 2+. Operation with Fe^{2+} ions has shown extremely good stability in the sense of pulse-to-pulse repetition and very low noisiness of the beam pulse (intensity fluctuations during the pulse) even without any auxiliary gas. The beam current of 8 mA in front of the RFQ has been reached with duty cycle of 1 Hz. The highest particle current over all tests of 10 mA and relatively good operation stability has been achieved with Ag^{2+} ions also with 1 Hz operation. Thus, five new projectiles for future experiments have been established for standard operation from high current VARIS source and for another four projectiles the operation performance was notably improved [36].

Table 1: Overview of produced ions from high current ion sources at GSI and their most important parameter.

ions	I_{FC}^a [mA/kV]	I_{ACC}^b [mA]	I_{RFQ}^c [mA]	duty factor [Hz/ms]	$\epsilon_{IS}/\epsilon_{RFQ}^d$ [π mmrad]	life time [d] ^e	current fraction [%] 1+/2+/3+/4+/...	sputter, aux. gas	type of IS
$^1H_3^+$	40/6.6	15	1	5/1	~320/~110	>7	H_1^+ : 37, H_2^+ : 8, H_3^+ : 55		MUCIS
$^2H_3^+$	90/13.2	50	2	5/1	~320/~110	>7	D_1^+ : 30, D_2^+ : 5, D_3^+ : 65,		MUCIS
$^{12}C^+$	15/6	9	0.5	5/1	~320/~110	2	divers (C, H, CH, ...)	CH ₄	MUCIS
$^{14}N^+$	20/10	12	2.5	5/1	~320/~110	7	N_2^+ : 31, N^+ : 69		MUCIS
$^{12}CH_3^+$	30/8	12	1.2	5/1	~320/~110	2	divers (C, H, CH, ...)	CH ₄	MUCIS
$^{12}CH_3^+$	50/8	17	2.8	2/0.5	~320/~110	2	divers (C, H, CH, ...)	CH ₄	MUCIS
$^{12}C_3H_7^+$	30/9	16	1.1	1/0.4	~320/~110	2	divers (C, H, CH, ...)	C ₄ H ₁₀	MUCIS
$^{14}N_2^+$	35/13	25	5.5	5/1	~320/~110	3	N_2^+ : 50, N^+ : 50		CHORDIS
$^{16}O_2^+$	70/20	35	3.5	2/0.5	~650/~150	7	O_2^+ : 40	V	VARIS
$^{20}Ne^+$		0.15	0.09	50/6	<500/~90	5			PIG
$^{20}Ne^{3+}$		0.035	0.02	50/5.5	<500/~90	2			PIG
$^{22}Ne^+$		0.4	0.2	50/6	<500/~90	3			PIG
$^{24}Mg^+$	80/15	30	3.5	2/1.2	~650/~150	7	46/54	He	VARIS
$^{27}Al^+$	80/17	15	2	2/0.5	~650/~150	7	36/64	O ₂	VARIS
$^{40}Ar^+$	50/19	33	22	5/1	~320/~110		90/10		CHORDIS
$^{40}Ar^{2+}$	8/10	0.8	0.25	50/5	<500/~90	6	23/77		PIG
$^{40}Ar^{2+}$	50/16	16	1.5	5/1	~320/~110	5	65/35		MUCIS
$^{40}Ca^{2+}$		0.3	0.1	50/5	<500/~90	2		Xe	PIG
$^{50}Ti^{2+}$		0.35	0.07	50/6	<500/~90	3	9/46/45	Ar	PIG
$^{51}V^+$	70/24	35	2.3	3/0.6	~650/~150	7	9/47/16 (28% rest)	O ₂	VARIS
$^{51}V^{2+}$	70/24	35	4.5	3/0.6	~650/~150	7	20/77/3		VARIS
$^{51}V^{2+}$		0.02	0.02	50/6	<500/~90	5		Ar	PIG
$^{52}Cr^{2+}$	11/11	0.2	0.07	50/5	<500/~90	2		Ar	PIG
$^{56}Fe^{2+}$	80/19	26	9	1/1	~650/~150	7	5/87/8		VARIS
$^{56}Fe^{3+}$	10/14	0.15	0.06	50/5	<500/~90	2		Ar	PIG
$^{58}Ni^+$	60/22	40	8	1/0.6	~650/~150	4	72/22/5	N ₂ , O ₂	MEVVA
$^{58}Ni^{2+}$	60/18	17	5	1/0.6	~650/~150	4	8/76/16		MEVVA
$^{58}Ni^{3+}$	16/15	0.6	0.2	50/5.5	<500/~90	2		Ar	PIG
$^{74}Ge^{4+}$		0.25	0.02	10/2.5	<500/~90	1		Ar	PIG
$^{80}Kr^{2+}$	60/22	28	0.15	5/1	~320/~110	3	17/53/29		MUCIS
$^{86}Kr^{2+}$	80/19	33	9.5	2/1	~320/~110	3	48/45/7	$^{86}Kr^f$	MUCIS
$^{86}Kr^{3+}$		0.4	0.2	50/6	<500/~90	3		$^{86}Kr^f$	PIG
$^{90}Zr^{2+}$	90/28	40	8	1/0.4	~650/~150	>5	5/77/18	N ₂	VARIS
$^{98}Mo^{3+}$	100/24	35	5	2/0.4	~650/~150	>5	2/21/77	He	VARIS
$^{102}Ru^{2+}$	100/31	40	9	2/0.5	~650/~150	>5	5/68/27	He	VARIS
$^{107}Ag^{2+}$	120/30	55	10	1/1	~650/~150	>5	>5/75/20		VARIS
$^{124}Sn^{5+}$	14/15	0.2	0.008	20/2	<500/~90		7/20/62/11	Ar	PIG
$^{132}Xe^{3+}$	80/24	40	6.5	5/1	~320/~110		-/48/33/15/4	$^{132}Xe^f$	MUCIS
$^{136}Xe^{3+}$	20/15	0.3	0.25	25/3	<500/~90	2	1/9/24/29/25/12	$^{136}Xe^f$	PIG
$^{142}Nd^{3+}$	80/28	32	1.5	1/0.4	~650/~150	10	0/4/87/9 or 0/55/45		MEVVA
$^{152}Sm^{3+}$	20/12	0.2	0.06	10/4	<500/~90	3		Ar	PIG
$^{181}Ta^{3+}$	75/24	31	7	1/0.6	~650/~150		0/0/56/35/8	Ar	MEVVA
$^{197}Au^{4+}$	130/31	50	6	0.5/0.3	~650/~150	7	0/3/19/21/3 (54% rest)	Cr ^g	VARIS
$^{197}Au^{8+}$	20/15	0.06	0.05	50/4	<500/~90	3	2/14/19/26/24/12/3/1	Ar	PIG
$^{208}Pb^{4+}$	100/32	40	6	0.5/0.3	~650/~150	7	0/2/13/24/3 (58% rest)	Cu ^g	VARIS
$^{208}Pb^{9+}$	17/12	0.4	0.02	50/5	<500/~90	2	4/24/40/33	Ar	PIG
$^{209}Bi^{4+}$	110/30	40	10	2.8/0.3	~650/~150	7	0/3/15/55/18 (9% rest)	Cu ^g	VARIS
$^{209}Bi^{4+}$		0.3	0.2	10/1	<500/~90	2		Ar	PIG
$^{238}U^{4+}$	110/40	40	15	2/0.5	~650/~150	7	0/0/18/67/15		VARIS

a) full beam current at extraction potential

b) full beam current at 2.2 keV/u

c) ion beam current in front of the RFQ

d) 90 % 4-rms emittance behind extraction / in front of the RFQ

e) life time of the filament for MUCIS, CHORDIS, PIG, and life time of the plasma grids for MEVVA and VARIS

f) enriched material

g) cathodes with composite materials

2.11.6 References

1. U. Ratzinger, "Commissioning of the new GSI high current linac and HIF related RF linac aspects", Nucl. Instrum. and Meth. in Phys. Res. A, 636-645 (2001)
2. FAIR, Baseline Technical Report, ISBN 3-9811298-0-6 (2006), <https://www.gsi.de/en/researchaccelerators/fair.htm>
3. R. Hollinger et al., "Development of a vacuum arc ion source for injection of high current uranium ion beam into the UNILAC at GSI", Rev. Sci. Instrum. 75 (5), p.1595 (2004)
4. R. Keller et al., "Multicharged ion production with MUCIS", GSI Scientific Report 1987, GSI 88-1, p.360 (1988)
5. R. Keller et al., "Recent results with a high-current, heavy-ion source system", Vacuum 36, p.833 (1986)
6. B. H. Wolf et al., "Investigation of MEVVA ion source for metal ion injection into accelerators at GSI", Rev. Sci. Instrum. 65 (10), p.3091 (1994)
7. I. G. Brown, "The Physics and Technology of Ion Sources", 2-d edition, Wiley-VCH Verlag GmbH & Co. KGaA, Weinheim, ISBN 3-527-40410-4 (2004)
8. B. H. Wolf, "Ion Sources", ISBN 0-8493-2502-1 (1995)
9. R. Hollinger and M. Galonska, "Status of vacuum arc ion source development for injection of high current uranium ion beams into the GSI accelerator facility", Nucl. Instr. and Meth. in Phys. Res. B 239, p.227 (2005)
10. S. K. Hahto et al., "Multicusp ion source with external rf antenna for production of protons", Rev. Sci. Instrum. 75 (2), p.355 (2004)
11. P. Beller et al., "The Frankfurt RF-driven ion source", Nucl. Instrum. Meth. A 449, p.16 (2000)
12. K. N. Leung et al., "rf driven multicusp H⁺ ion source", Rev. Sci. Instr. 62, p.100 (1991)
13. R. Hollinger et al., "Ion Source Operation at the GSI", GSI Scientific Report 2015, p.305, Darmstadt (2016)
14. R. Hollinger et al., "Ion source operation at GSI" GSI Scientific Report 2016, p.387, Darmstadt (2017)
15. A. Di Nitto et al., "ALBEGA: A decay spectroscopy setup for chemically separated samples", GSI Scientific Report 2014, p.184, Darmstadt (2015)
16. B. B. Back et al., "Recent developments in heavy-ion fusion reactions", Rev. Mod. Phys. 86, p.317 (2014)
17. Y. T. Oganessian and V. K. Utyonkov, "Super-heavy element research" Rep. Prog. Phys. 78 (3), 036301 (2015)
18. J. Khuyagbaatar et al., Proc. of the TAN15, Urabandai, Japan, 2015
19. R. Hollinger et al., "Basic plasma investigations on the Frankfurt high intensity proton source with an electrostatic 127° cylinder spectrometer", Nucl. Instr. and Meth. in Phys. Res. A 481, p.86 (2002)
20. A. Adonin and R. Hollinger, "Ion source development of H-rich molecular beam operation for production of high-intensity proton beams at the UNILAC", GSI Scientific Report 2014, p.399, Darmstadt (2015)

21. R. Hollinger et al., “Measurement of the beam emittance of the Frankfurt proton source” *Rev. Sci. Instrum.* 73 (2), p.1027 (2002)
22. I. G. Kesaev, *Cathode Processes in Electric Arcs*. Moscow: Nauka, 1968 (in Russian).
23. I. G. Brown and E. Oks, “Vacuum Arc Ion Sources: Recent Developments and Applications”, *IEEE Trans Plasma Sci.* (2005)
24. I.G. Brown, “Vacuum arc ion sources” *Rev. Sci. Instrum.* 65, p.3061 (1994)
25. O. Kester et. al., “Status of FAIR Accelerator Facility”, *Proc. of IPAC, Dresden, Germany*, p.2084 (2014)
26. A. Adonin and R. Hollinger, “Progress on MEVVA source VARIS at GSI”, submitted for publication in *Rev. Sci. Instrum.* (2018)
27. A. Adonin and R. Hollinger, “Development of high current Bi and Au beams for the synchrotron operation at the GSI accelerator facility”, *Rev. Sci. Instrum.* 83, 02A505 (2012)
28. A. Anders and G. Yu. Yushkov, “Puzzling differences in bismuth and lead plasmas: Evidence for the significant role of neutrals in cathodic vacuum arcs”, *Appl. Phys. Lett.* 91, 091502 (2007)
29. A. Adonin and R. Hollinger, “Challenges of Production of High Current four-fold Bi and Au Beams from Vacuum Arc Ion Sources at GSI”, *Accelerator Facility Proc. of ISDEIV, Tomk, Russia*, 6412599 (2012)
30. R. Hollinger et. al., “Ion Source Operation at the GSI Accelerator Facility”, *GSI Scientific Report 2011*, p.285, Darmstadt (2012)
31. R. Hollinger et. al., “Ion Source Operation at the GSI Accelerator Facility”, *GSI Scientific Report 2012*, p.257, Darmstadt (2013)
32. R. Hollinger et. al., “Status of high current ion source operation at the GSI accelerator facility”, *Rev. Sci. Instrum.* 79, 02C703 (2008)
33. W. Barth et.al., “U28+-intensity record applying a H₂-gas stripper cell at GSI-UNILAC”, *Physical Review Special Topics - Accelerators and Beams*, 18 (4), 040101 (2015)
34. W. Barth et.al., “High Brilliance Uranium Beams for FAIR”, *Physical Review Accelerators and Beams*, 20 (5), 050101 (2017)
35. A. Adonin and R. Hollinger, “Beam brilliance investigation of high current ion beams at GSI heavy ion accelerator facility”, *Rev. Sci. Instrum.* 85 (2), 02A727 (2014)
36. A. Adonin and R. Hollinger, “Development of new projectiles for future FAIR experiments”, *GSI Scientific Report 2016*, p.423, Darmstadt (2017)

2.12 Microwave Discharge Ion Sources (Proton Sources)

L. Celona, G. Castro, L. Neri

Mail to: celona@lns.infn.it

INFN – LNS, via S. Sofia 62, 95123 Catania, Italy

Microwave discharge ion sources (MDIS) are the most suitable tools for the production of intense beams for high power accelerators as they produce multimilliampere beams of protons, deuterons, and monocharged ions. Such sources usually must obey to the request of high brightness, stability, and reliability. A description of the technical evolution in the years up to the state of art is given, analyzing their performances with particular care to the quality of the beam, especially in terms of its emittance.

2.12.1 Introduction

The production of high current beams is a key point for different applications and this role is deemed to increase in the coming years, either for industrial applications and for the research projects. High current and high brightness proton beams can be provided by microwave discharge ion sources which present many advantages in terms of compactness, high reliability, ability to operate in continuous wave (CW) mode or in pulsed mode, reproducibility, and low maintenance [1].

Table 1 shows a list of projects (operating and under construction) using high current proton beams with low transversal emittance.

The optimization of the beam formation and of the transport through the LEBT plays a fundamental role to provide a high quality beam to the accelerator. This is a common request of such facilities where rms normalized emittances at the entrance of the radio frequency quadrupole (RFQ) in the order of 0.20 to 0.30 π mm mrad are needed, making essential the design and test of the ion source and low energy beam transport (LEBT) as a whole. The major challenge of the accelerator front-end is therefore the preparation of a high quality beam, with a pulse well defined in time and a small transversal emittance.

Table 1: High power accelerator requirements (all the listed projects require protons except IFMIF that requires deuterons).

	Beam current [mA]	ϵ rms norm. [π mm mrad]	Beam pulse [ms]	Rep. Rate [Hz]	Duty Factor
LEDA	100	0.25	---	---	100%
IPHI	100	0.25	---	---	100%
TRASCO	30	0.2	---	---	100%
ESS	74	0.25	2.84	14	4%
IFMIF (D)	150	0.25	---	---	100%
FAIR	100	0.3	0.035	4	
MYRRHA	30	0.2	---	---	100%

2.12.2 Historical notes

The history of 2.45 GHz MDIS started about 35 years ago with different source designs proposed by Sakudo [2] and by Ishikawa *et al.* [3] especially for industrial applications. The sources produced remarkable results not only for protons, but also for deuterons and monocharged light ions. A simple concept of microwave discharge source was based on a nonconfining magnetic field higher than the resonance field (i.e. 87.5 mT). Sakudo and his collaborators at the Central Research Laboratory of Hitachi Limited pioneered the development of high-current microwave ion sources for ion implantation

[4]. The first Hitachi ion source was composed by a plasma generator that was, essentially, a section of coaxial waveguide with an axial magnetic field supplied by three solenoids. The 2.45 GHz microwaves were introduced via a water cooled antenna connected to the inner conductor of a coaxial-to-rectangular waveguide transition. The magnetic induction was varied along the length of the antenna to match the impedance of the plasma filled chamber to the impedance of the microwave line. The extraction system was a multiaperture triode and it was able to supply 2 mA of As and 15 mA of B and they were successfully adapted to industrial application setups.

A step forward was done by Ishikawa [5], who designed a source able to produce mA beams of any species, finding applications not only in ion implantation device but also for ion deposition. The absence of antennas made this equipment more reliable for long time operations.

2.12.3 The CRNL ion source and the successive developments

In 1991 a simple and robust design was proposed by Taylor and Mouris at Chalk River National Laboratory [6] (CRNL) (see Fig. 1). This source can be considered as the basis for all designs proposed in the following 25 years. The main innovation consisted in the use of a matching unit to adapt the waveguide to plasma impedance, which enhanced the plasma density and finally the current density of the extracted beam. Moreover, two separately fed solenoids, approximately placed at the two extremes of the plasma chamber, permitted to vary the magnetic field profile. The extraction system was based on the accel-decel operation mode performed by means of three electrodes.

The plasma generator was simply a hydrogen filled chamber, with a ceramic rectangular waveguide window, encircled by two solenoids. The extraction system was a 50 kV multiaperture triode.

This design was further improved by J. Sherman and co-workers at Los Alamos National Lab, who modified the extraction system and the LEBT in order to optimize the beam coupling to the RFQ of the LEDA project. The CRNL plasma generator was integrated to a 75 kV accel structure (Fig. 1b) [7] and the first acceleration of 100 mA proton beam through the RFQ have been carried out at Los Alamos.

At the end on 90's a common effort of INFN and CEA permitted a significant improvement of the beam reliability and of the ion beam emittance produced by this sources making them the optimal tool to fed High Intensity Proton Accelerators [8].

In particular, the experiments carried out at CEA-Saclay on the SILHI source [9,10,11] and at INFN-LNS on TRIPS source [12, 13] permitted to improve brightness and reliability.

A step forward in robustness against sparks was given by the Versatile Ion source (VIS) source, developed and built at INFN-LNS in 2006 [14]. In VIS the movable coils have been replaced with permanent magnets, and the extraction geometry and extraction column have been simplified (figure 2a). All these changes decreased the high voltage sparks and increased the source reliability to 99.9% in 1 week run. All the devices were placed at ground potential, thus leaving only the plasma chamber and the permanent magnets at high voltage; the compact dimensions have also helped to get a better and easier maintenance [15].

The high intensity proton source for the European Spallation Source PSESS [16], designed and commissioned at INFN-LNS, represents the current state of art of MDIS (Figure 2b). All the single parts of PSESS have been optimized to produce a stable total

current between 40 and 125 mA through an 8 mm extraction aperture in pulsed operation. The proton fraction of the beam reach 87% and a 99% normalized beam emittance of 0.2π -mm-mrad was obtained. In the best operative conditions, PSESS is able to ensure intra pulse current fluctuation below $\pm 1.5\%$ and long term current fluctuation below $\pm 3\%$. High reliability of the overall system was measured with long duration test and fast beam recovery after vacuum break of 24 hours.

From the first Sakudo and Ishikawa MDIS up to the PS-ESS, more and more efforts have been done to continuously improve the source performances in terms of reliability, stability and low beam ripple. The increasing request of source compactness, reliability and high performances in terms of high proton current with low emittance represent the crux for the development of the future MDIS.

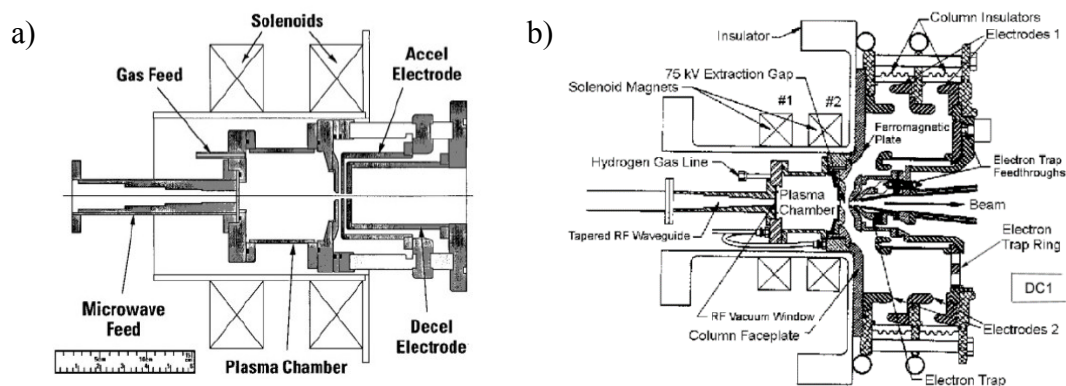


Figure 1: a) The CRNL microwave source. b) Ion source of the Los Alamos National Lab.

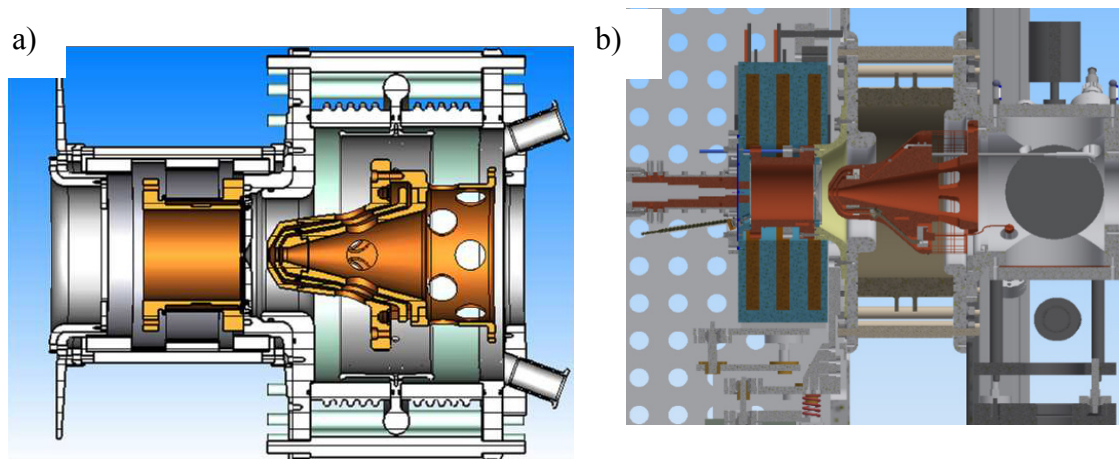


Figure 2: a) The TRIPS ion source on the 100 kV platform. b) the PS-ESS ion source at INFN-LNS

2.12.4 Theoretical Issues

In a plasma source, extracted current $I_{extr.}$, mean charge state $\langle q \rangle$ and normalized emittance ε depend on the plasma parameters as follows:

$$I_{extr.} \propto \frac{n_e}{\tau}$$

$$\langle q \rangle \propto n_e \tau$$

$$\varepsilon = 0.016 \sqrt{\frac{kT_i}{M/Q}} + 0.032r^2 \frac{B_{extr.}}{M/Q}$$

Where n_e is the plasma electron density, τ is ion confinement time, T_i the ion temperature, $B_{extr.}$ is the magnetic field in the extraction region, M/Q is the ratio between the ion mass and charge and r is the extraction hole radius.

Since MDIS generate $q=+1$ charge state ions, ion confinement time should be the minimum one able to ensure generation of a proton-rich plasma according to typical ionization cross sections in a hydrogen plasma [17]. Typical values of τ are in the order of a few hundreds of μs . Electron density should be the maximum as possible to ensure high current beam generation. At the same time, the ion temperature is kept low and therefore small emittance beams are generated even by means of an opportune design of the extraction column oriented to minimize the magnetic field in the extraction region.

Many experiments revealed that electron density could overcome up to a factor 10 the cut-off density, which should be a limit for electromagnetic propagation in plasmas. A comprehensive explanation of MDIS ignition is still not available. Currently, the most persuasive explanation is to consider the coupling of the Electromagnetic (EM) waves to electrostatic waves that can propagate and be absorbed in overdense plasmas.

If the sources operate at magnetic field below the ECR ($B < B_{ECR}$), the Upper Hybrid Resonance can exist somewhere within the plasma chamber, the EM X-wave can be converted into Electrostatic Bernstein Waves (EBW) and ion waves. EBW penetrate in the warm plasma core without any cut-off [18], and they can be absorbed at cyclotron harmonics B_{ECR}/n , where n is an entire number ranging from 1 to ∞ . It is worth to note that the ECR layer is a resonance layer also for EBW. An experiment demonstrating the density optimization by varying B is reported in [19], where clear evidences of energy absorption at cyclotron harmonics are shown. Because of the electrostatic nature of plasma heating, the density rises well above the cut-off. This option is useful but a plasma created in such a way is turbulent and non-uniform (some parts of the plasma chamber remain empty, as observed in [20], because of the peripheral BW absorption). Furthermore, the ion waves generated at UHR together with EBW could lead to an increase of the ion temperature, with detrimental consequences on emittance.

The other case is the off resonance EM wave-plasma interaction when $B > B_{ECR}$. Resonances between the electromagnetic waves and the plasma electrons can occur even for high plasma densities [21, 22]: in particular EM power can be coupled to electrostatic Trivelpiece-Godes modes (a generalization of Langmuir waves in a magnetic field) propagating in off-resonance and overdense magnetic fields. In such a case, a first ignition due to the single particle ECR heating is needed. The presence of ECR regions can be pictured as an ECR 'gas-lighter' which gives a spark, that afterwards is maintained by the 'fuel' ensured by an off-resonance discharge, covering the whole chamber. Indeed, Sakudo [23] demonstrated that the higher plasma density is obtainable when $B_{ECR} < B < 1.3 B_{ECR}$. The results obtained during the TRIPS magnetic profile optimization confirmed that the best performances can be obtained when $B > B_{ECR}$ everywhere, except for the ECR layer placed in injection and extraction regions.

2.12.5 Technological Issues

The microwave ion sources present some technological issues that must be correctly addressed in the design phase. The coupling between microwave generator and plasma chamber is the results of a detailed study carried out with high frequency structures simulation tools permitting to reduce the microwave losses, simultaneously with an adequate matching of the waves to the plasma chamber.

The plasma is usually generated by means of the microwaves provided by a 2.45 GHz Magnetron through a WR 340 (86.4 mm x 43.2 mm) waveguide excited in the TE dominant mode. A tuning unit is needed to adjust the modulus and phase of the incoming wave in order to match the plasma chamber impedance with and without the plasma, and a high directivity directional coupler is used to precisely measure the forward and the reflected power. Matching transformers are used to enhance the electric field on plasma chamber axis, in order to improve the wave to plasma coupling. The magnetic field profile plays an important role not only for plasma heating, but also for the source reliability and for long term operations. On this purpose two independent resistive coils are usually employed, but electronics at high voltage (power supplies and control) is usually needed.

A crucial point to ensure source reliability is certainly the extraction region. Different parameters have to be taken into account: residual magnetic fields, vacuum, extraction system topology. Beam extraction system requires at least a classical three electrode system (accel-decel). The most performing sources have more sophisticated systems with 4 or 5 electrodes [24]. The five electrodes topology allows the on-line optimisation of the extracted beam, permitting to operate on a wide current range by optimising the beam formation for each working condition.

2.12.6 EM wave to plasma chamber coupling

In the off-resonance microwave ion sources, the ECR is not a predominant condition for plasma generation; in fact, in this case higher electron densities can be obtained by means of a microwave discharge at higher magnetic field value and higher pressures. However, differently from the ECR ion sources, the cavity diameter and excitation frequency are chosen to allow only one cavity mode to be excited for a given cavity length. In this case the power coupling into a given mode is usually accomplished by means of tuning stubs in order to achieve the necessary impedance matching. The steady-state microwave discharge is characterized by the equality between the power absorbed by the plasma and the lost power, mainly due to inelastic ionization, excitation collisions, and energy transmission out of the active discharge region. The power absorbed by the plasma is given by one-half the real part of the complex Poynting vector, therefore it depends from the electric field strength in the plasma. In order to optimize the coupling for a given mode it is important to maximize such electric field. The waveguide transformer (usually a maximally flat design) is widely used for such purpose from most of microwave sources in operation nowadays. Such device realizes a progressive matching between the waveguide, normally operating in the dominant mode, and the equivalent impedance of the plasma filled chamber, also concentrating the electric field at its center. Figure 5 shows a comparison of the electric field on plasma chamber axis in the case that no transformer is used or by employing the Trasco intense proton source (TRIPS) or versatile ion source (VIS) one. The excitation frequency is 2.45 GHz in all cases and it can be

observed that an increase in factor of 2 can be obtained, in a frequency range of ca. 400 MHz by appropriately shaping the waveguide ridges as detailed discussed in Ref. [25].

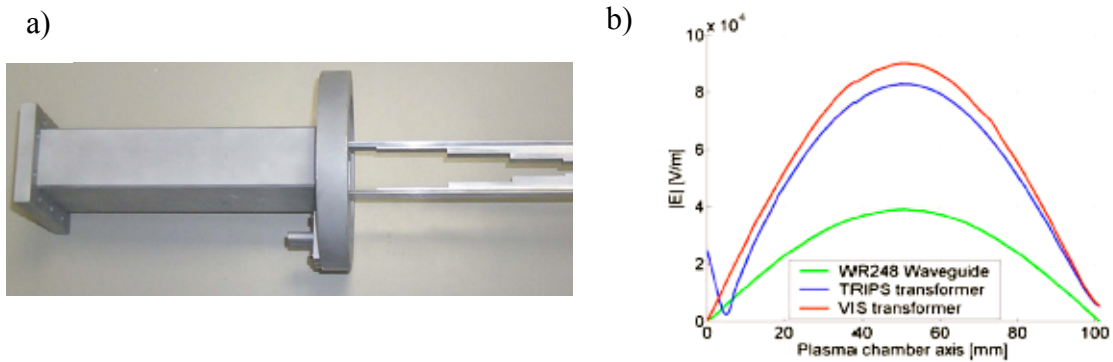


Figure 5: a) The matching transformer coupled to the plasma chamber of the VIS source. b) Comparison of the electric field on plasma chamber axis in different cases.

Therefore, both matching transformers concentrate the electric field around its axis in a smaller region than the original WR284 cross section. Nowadays most of the ion sources for high intensity use automatic tuning units to optimize the power coupling into the operational mode and waveguide transformers similar to those previously described to enhance the plasma density inside the source. The increase in the latter parameter is mandatory for further increase in the produced currents.

2.12.7 Beam formation and transport

The production of a high quality beam has been one of the major challenges for such kind of sources, since the first measurements made at CRL by T. Taylor and J. S. C. Willis, together with the beam reliability. In the years a lot of development have been carried out to improve these aspects and the most important results have been obtained through a deep optimization of the extraction geometry together with an appropriate design of the low energy beam transfer line.

Following the Child-Langmuir law [21] the maximum extracted current density in space-charge-limited flow is:

$$j = 1.72 \left(\frac{q}{A} \right)^{\frac{1}{2}} \frac{V^{\frac{3}{2}}}{d^2}$$

where j is the current density in mA/cm², q/A is the charge to mass ratio of ions, d is the extraction gap in cm and V is the extraction voltage in kV. From a 0.4 cm extraction hole, 1.0 cm extraction gap, $V=75$ kV, considering an effective mass of 1.2 (proton fraction higher than 80%) we can get a theoretical maximum proton current of 125 mA. The real situation is worse because of beam halos, which may decrease the reliability because of outgasing phenomena over the electrodes. This obliges to decrease the electric field in the gap and finally to get less current. Hence the beam formation and handling in the LEBT determines the success of a source design even more than the other components, placed at high voltage.

The relatively low magnetic field gives a low contribution to the emittance, whereas larger contributions come from the aberrations and space charge effects, which are often

more important even in case of high degree of neutralization; a careful study of space charge compensation has to be carried out for any source setup.

The simplest solution [8] is the exploitation of the electrons created by the beam collisions with the residual gas of the beamline; the potential dip created by the beam attracts the electrons that neutralize the ion charge. The main drawback of this method is the possible fluctuation of the level of space charge neutralization that may arise if the beam intensity changes (e.g. for pulsed beams) or if the vacuum inside the beamline is not constant. In transit gaps, where no magnetic nor electric fields influence the particle trajectories, electrons are trapped by the beam's potential well, whilst the positive ions are repelled towards the walls. Inside the solenoids, the electrons are strongly focused around the axis, and the compensation is partially lost. A further contribution to the potential well, with the following compensation of the space charge effects, can be obtained by the electrons emitted by heavy noble gases like Argon, Krypton or Xenon injected in the LEBT [9].

This significant step ahead in the production of higher quality beam have been done in the framework of a collaboration between INFN and CEA where an innovative method based on the controlled injection of a gas into the line has been developed. The idea was based on the fact that the ions obtained from residual gas ionization are expelled from the center of the beam line, where the potential is positive, towards the wall. Electrons from the wall are attracted from the beam, so that the beam is compensated, provided that the pressure is high enough to have an adequate number of electrons (a compromise between beam losses and space charge compensation is to be found experimentally). According to that approach, the most effective gases are the heaviest, which easily release a large number of electrons. If a number N of hydrogen atoms per unit volume is required for the optimum compensation, (i.e. if N electrons neutralize the beam space charge), for species which gives Z electrons when the atoms interact with the 95 keV proton beam, the optimum number of atoms per unit volume is N/Z (this clue neglects the dissociation process, which does not require a large amount of energy).

The experiments have been carried out by injecting different gases (H, N, Kr, and Ar) in the SILHI beam line through a leak valve placed after the LEBT solenoid and comparing the emittance measurements at different pressures with an extracted beam on range of 75-80 A. In all the cases considered, a decrease of beam emittance has been observed with the beam line pressure increase. These results have been explained by a higher space charge compensation degree as confirmed by a series of measurements carried out in collaboration with the Los Alamos National Laboratory [8,9]. As observed the behavior depends upon the atomic mass of the species injected. Emittance values under 0.15π mm mrad have been easily obtained also by using Ar with similar pressures. A lower efficacy is obtained by N and H injection: in particular with the N injection we have measured 0.13π mm mrad at relatively high pressure, while for H the minimum value of emittance obtained is 0.198π mm mrad as shown in Fig. 3.

Fig. 3 a) summarizes the results obtained and in all cases a decrease of beam emittance has been observed with the increase of beam line pressure. Figure 3b summarizes also the losses at the end of the beam line at the different pressures, losses which are less than 5 % for gases heavier than Ar.

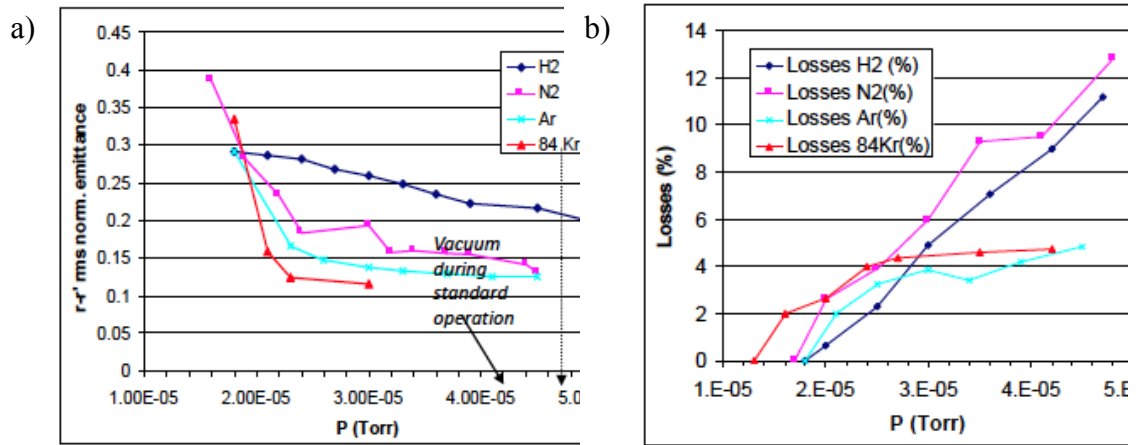


Figure 3: a) Emittance vs H, N, Ar, Kr pressures in the beam line. b) Losses of the beam current.

Recently, an extensive study of the beam emittance produced by the source developed at INFN-LNS for the European Spallation Source has been carried out. Figure 4 shows the typical beam distribution coming out from the most stable configuration of this source [16].

The emittance increases while increasing the extracted current. The figure 4a shows a linear trend that can be addressed to the optimum stability of the configuration found. ESS project requirement was defined by using the 99% normalized beam emittance, so in the next figure this value is reported. The beam transport in the LEBT is very sensitive to the space charge effect for such a big amount of current. Emittance variation for different gas injection is finally presented in figure 4b.

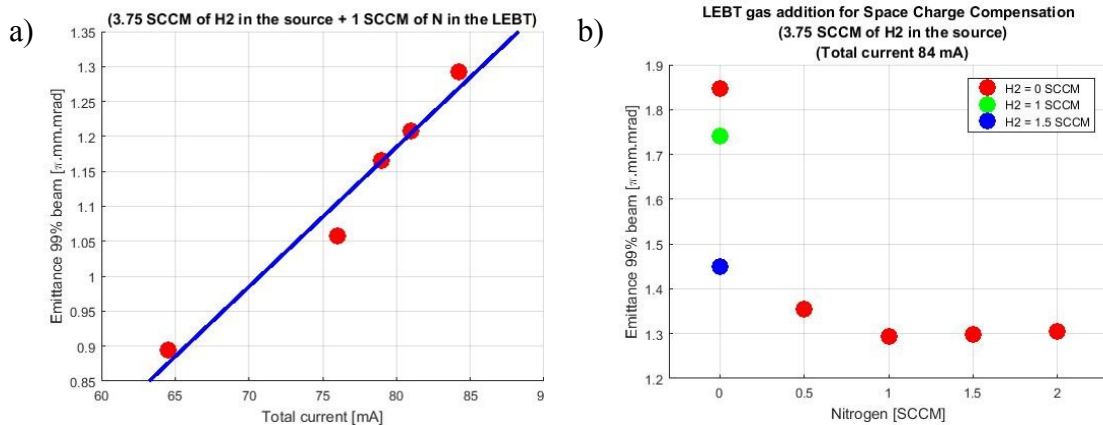


Figure 4 a) Emittance versus extracted current. b) Emittance versus Nitrogen flux (SCCM) for a total extracted current of 84 mA;

2.12.8 Perspectives

Future developments in MDIS are strongly connected with the further development with a better and better improvement of the wave-to-plasma coupling. A more efficient transmission of the energy to the plasma electrons may favour H₂ dissociation and this goal must be obtained with a better comprehension of plasma physics issues and related

technological issues. Studies on EBW generation in plasmas for very high density plasmas generation are currently being performed at INFN-LNS with very encouraging results. Plasma densities 20 times the density cut-off have been produced in small plasma reactor [26]. In order to increase the BW creation efficiency from X-waves, a proper injection angle is needed: this can be achieved by using single cut antennas (waveguides) launching O waves in a proper direction with respect to the magnetic field lines. In this way the O-X-B conversion is possible, as observed in Ref. [19]. More details are discussed in Ref. [20]. The main limitation of EBW plasma generation, as already discussed in the introduction, should be given by a strong increase of emittance induced by an increase of the ion temperature at the plasma meniscus. Beam extraction test are therefore mandatory. First extracted beams by EBW plasmas are foreseen in next months to understand the capability to get higher brightness.

Although the largest part of MDIS is developed and designed for proton and deuteron generation, the request of H_2^+ beam is going to grow in these years. The use of this molecule instead of H^+ may represent a solution of the space charge effects affecting the acceleration of high intensity proton beams. H_2^+ , indeed, allows the decrease of the generalized perveance, the parameter that measures the space charge effect, because of the larger m/q ratio with respect to protons. Generation of a high intensity (25-50 mA) H_2^+ beam is key point of the IsoDAR [27] and DAE δ ALUS [28] experiments. Both these experiments will make use of a MDIS as injector of a new high power cyclotron.

The best performances in terms of H_2^+ extracted current has been currently obtained by the PKU ECR ion source, where up to 40 mA H_2^+ were extracted. However, the optimization of the MDIS for the H_2^+ is still far from being satisfactory because the ionization process in the plasma is quite complicated and many channels are active [29,30].

2.12.9 Acknowledgements

The pioneering work of J. Sherman, J.M. Lagniel, R. Gobin, G. Ciavola and S. Gammino is gratefully acknowledged.

2.12.10 References

1. B. Wolf, Handbook of Ion Sources (CRC Press, Boca Raton, 1995).
2. N. Sakudo, *Rev. Sci. Instrum.* 49, 940 (1978).
3. J. Ishikawa, Y. Takeiri, and T. Takagi, *Rev. Sci. Instrum.* 55, 449 (1984).
4. Ian G. Brown, *The Physics and Technology of Ion Sources*, 2004 WILEY-VCH Verlag GmbH Co. KGaA, Weinheim.
5. J. Ishikawa, Y. Takeiri, and T. Takagi, *Rev. Sci. Instrum.*, 55, 449, (1994).
6. T. Taylor, *High-current cd microwave ion source (invited)* AECL Research, Chalk River Laboratories, Chalk River, Ontario KOJ1J0, Canada (1991).
7. J. Sherman et al., *Rev. Sci. Instrum.* 69, 2, (1998).
8. R. Gobin et al., *Rev. Sci. Instrum.*, 70, 2652 (1999).
9. P.-Y. Beauvais et al., *Rev. Sci. Instrum.*, 71, 1413 (2000).
10. J. M.- Lagniel et al. *Rev. Sci. Instrum.*, 71, 830 (2000).
11. R. Gobin et al., *Rev. Sci. Instrum.* 75 (5), 1414 (2004)
12. L. Celona et al., *Rev. Sci. Instrum.*, 71, 771 (2000).
13. L. Celona et al., *Rev. Sci. Instrum.* 75 (5), 1423, (2004).

14. G. Ciavola et al., *Rev. Sci. Instrum.*, 75 1453 (2004).
15. F. Maimone et al., *Status of the versatile ion source vis*, volume 868, page MOPC151. Proceedings of EPAC08, Genoa, Italy, (2008).
16. L. Celona et al., High intensity proton source and LEBT for the European Spallation Source, Proceedings of 17th Intern. Conf. on Ion Sources, Geneva, (2017)
17. H. Zhang, Ion sources (Springer Science Press, Beijing, 1999).
18. H. P. Laqua, the W7-AS Team, and the ECRH Group, *Plasma Phys. Controlled Fusion* 41, A273 (1999).
19. H. Laqua et al., *Study of the Bernstein wave heating in the WEGA stellarator plasma and possible application to ECRIS*, INFN, Report No. INFN/AE-09/1, (2009).
20. D. Mascali et al., *Rad. Eff. Defects Sol.* 163, 471 (2008)
21. Geller, *Electron Cyclotron Resonance Ion Sources and ECR Plasmas*, 1996 by CRC Press
22. G. Lisitano, M. Fontanesi, and E. Sindoni, *Appl. Phys. Lett.* 16, 122 (1970)
23. N. Sakudo, *Rev. Sci. Instrum.* 71, 1016 (2000)
24. S. Gammino et al., *Rev. Sci. Instrum.* 81, 02B313 (2010)
25. L. Celona et al., *Rev. Sci. Instrum.* 81, 02A333 (2010)
26. G. Castro et al., *Plasma Sources Sci. Technol.* 26, 055019 (2017)
27. J. Alonso et al., (The DAE δ ALUS Collaboration), e-print arXiv:1006.0260 [physics.ins-det].
28. A. Bungau et al., *Phys. Rev. Lett.* 109, 141802 (2012).
29. Neri et al., *Rev. Sci. Instrum.*, 87, 02A505 (2016)
30. G. Castro et al., *Rev. Sci. Instrum.*, 87, 083303 (2016)

2.13 Pulsed, high-current H⁻ Ion Sources for Future Accelerators

Martin P. Stockli

Mail to: stockli@ornl.gov

Spallation Neutron Source, Oak Ridge National Laboratory, Oak Ridge, TN 37830, USA

2.13.1 Introduction

This is a short report on the fall 2017 performance of the high-current negative Hydrogen ion (H⁻) sources that supply the world's top nine pulsed, high-power and high-energy H⁻ accelerators. It includes brief introductions to place the technological achievements in historical perspective. It briefly describes some other H⁻ source developments to explain why they are no longer included in today's top list. It briefly describes the underlying physics to the extent needed to elucidate the working of the following ion source type, whereas any details can be found in the respective references. It recommends the highly successful magnetron and RF H⁻ ion sources for future accelerators, depending on their requirements.

The need for pulsed sources of high-current negative hydrogen ions (H⁻) is growing due to upgrading the power of existing H⁻ accelerators and due to building new, more powerful proton accelerators [1]. Accelerating negative hydrogen ions and stripping the two electrons between two dipole magnets in an accumulator ring allows the resulting

positive ions to join the ions that were previously injected, as shown in Fig. 1. This can drastically increase the beam power of an accelerator. For example, the Spallation Neutron Source (SNS) [2], a pulsed neutron scattering user facility at Oak Ridge National Laboratory (ORNL in Oak Ridge, Tennessee) stacks about 1000 ~35 mA H⁺ beamlets to make one ~30 A proton beam.

The production of high current ion beams requires the generation of powerful plasmas containing many positive ions, electrons, neutral atoms, molecules, and normally very few negative ions [3]. The inefficiency of the negative ion production drastically increases the needed power to produce the required number of negative ions.

To limit the strain on the power supplies and the heat stress of the equipment for high-current negative ion sources, the dominant source of power is switched off when not needed by pulsing the discharge that drives the plasma.

The product of the pulse length and the repetition rate is called the duty factor, the % of time the discharge is on. Other electrical equipment can be left on because they represent a negligible fraction of the heat load, and they normally enhance the stability of the system. The discharge may have to be turned on for stabilization before ion beams can be extracted, leading to plasma duty factors (% of time the discharge is on) that exceed the beam duty factor (% of time ion beam is extracted). The beam duty

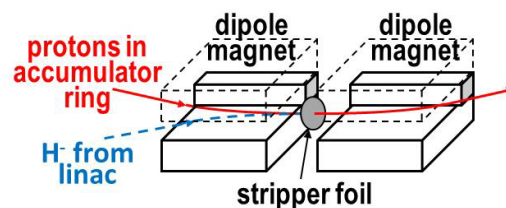


Figure 1: Stacking hydrogen ion beams through charge exchange in an accumulator ring. factor relates to the quantity of the extracted H⁻ ions, while the plasma duty factor relates to the Cesium (Cs) consumption and to the lifetime of sources limited by plasma wear, the so called sputtering [4].

2.13.2 Surface Plasma Production of Negative Hydrogen Ions

In 1965, only tens of μA of H⁻ could be extracted directly from well suited ion sources [5]. A drastic breakthrough was achieved in the early 1970s at the Budker Institute for Nuclear Physics (BINP in Novosibirsk, Siberia, Russia) when G. Dimov, Y. Belchenko and V. Dudnikov added some Cs into their magnetron ion source. As a result, they obtained up to 300 mA of H⁻ beam current [6, 7] and up to 880 mA H⁻ beam current [8] with up to 1% duty factors. How could the addition of the alkali metal Cs so drastically increase the yield of H⁻ ions?

The answer is in the surface plasma production of H⁻ ions. Accelerated by the plasma potential protons and H₂⁺ ions impact on grounded, plasma-containing metal surfaces and neutralize by capturing an electron. When energetic, neutralized or other hyper-thermal hydrogen atoms reflect from such metal surfaces and encounter an electron, the electron will return to the surface because it has a work function in the range of 3 to 5.5 eV. Only in the rarest cases is a fast H atom able to capture the electron through its 0.75 eV affinity.

Kishinevskiy [9] and others [10] have shown the capture probability β^- of a second electron to depend on the metal's work function ϕ and the hydrogen atom's normal escape velocity v_{\perp} . The low-velocity approximation by Rasser is especially illustrating:

$$\beta^-(v_{\perp}) \approx (2/\pi) \cdot \exp[-\pi(\phi - S)/(2 \cdot a \cdot v_{\perp})] \quad (1)$$

where S is the hydrogen atom's electron affinity, and a is the exponential decay constant of the transition rate at large distance [11]. The equation shows that low work functions and high plasma potentials are the keys to enhance the surface production of negative ions, and Cs with a work function of only 2.1 eV is certainly a top player.

2.13.3 Magnetron Negative Hydrogen Ion Sources

Magnetron devices were developed in the 1920s as electric switches before Princeton developed some into proton sources. As seen in Fig. 2, the gap between the anode and cathode forms a race track. The magnetic field B is normal to the race track and therefore forces the electrons to spiral along the race track, yielding long path lengths and accordingly high ionization efficiencies. The cathodes feature dimples opposite to the extraction openings to geometrically focus negative ions produced on the cathode surface into the extractor opening [12].

Today's most successful Magnetron Surface Plasma Sources are listed at the top of Table 1, which evolved from Ref. [13]. The table shows parameters achieved simultaneously in typical production runs, rather than the best values obtained under different conditions. For the same reason the table does not include any results from test runs or test stands. To further reduce ambiguities, both the plasma and the beam duty factors are listed. The average beam pulse current is the average beam current during the extraction phases measured as close to the source output as possible.

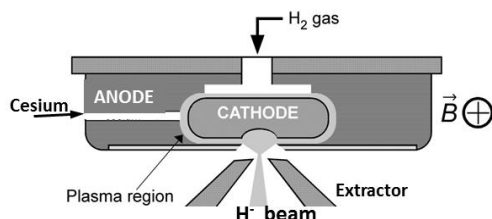


Figure 2: Schematic cross section through the FNAL magnetron H^- source [14].

Table 1: Fall 2017 Pulsed High-Current H^- Ion Sources for Accelerators

The service cycle is the maximum length of time a source can be used without maintenance with acceptable performance degradation and a minimal risk of catastrophic failures. Therefore, the performance can be fully restored within the next prescheduled maintenance period. Service cycles are shorter than lifetimes, which are defined to be the average length of time that a source can be used without maintenance before unacceptable performance degradation or a catastrophic failure causes unplanned downtime requiring the source or some of its components to be replaced to restore acceptable performance. The high user-turnover of successful user-facilities makes the intentional running to failure of equipment unacceptable. Therefore, reliable lifetime data are based on exceptional cases and are accordingly marked with an asterisk. Finally, the last column, the charge of the extracted H^- ions from a single source without any maintenance is simply the service cycle converted into hours multiplied by the beam duty factor and the average beam pulse current converted into Amperes. Asterisks show that the numbers are based on a lifetime rather than on a service cycle.

The top two rows show the Magnetrons surface plasma sources using the highest discharge voltages to produce the highest H^- beam currents. Their lifetimes are limited by sputtering which is aggravated by their higher voltages. However, at their <1% duty

factors, both work flawlessly for their entire yearly accelerator cycles. Brookhaven National Laboratory's (BNL near New York) legendary 2 [15, 2002], and now 3 A·h [15, 2017] of H⁻ ions extracted with a single source without any maintenance held the world record until 2011 when SNS extended its service cycles to 6 weeks [23]. Fermi National Accelerator Laboratory's (FNAL near Chicago) actual lifetime extracted charge is likely twice the listed 1.6 A·h because they often do not have to replace parts during their yearly maintenance period.

There is no data or consensus regarding whether magnetrons can be developed for much higher duty factors without severe reductions of their lifetimes. However, BNL has started an R&D program to expand the range of applicability of their magnetron sources [24].

H ⁻ Source [ref.]	Method	Discharge & Repetition Rate	Plasma & Beam Duty Factors	Average Beam Pulse Current	Extraction Aper- ture	Service Cycle/ Lifetime *	Extracted H ⁻ Charge
BNL [15] Operation	Magnetron Surface	12-14A;130 V @ 7.5 Hz	0.50 % 0.44 %	110-120 mA	2.8 mm ∅	6-8 months	3.0 A·h
FNAL[16] Operation	Magnetron Surface	15 A;180 V @ 15 Hz	0.345 % 0.3 %	80 mA	3.2 mm ∅	9 months	1.6 A·h 3.2 A·h*
ISIS [13] Operation	Penning Surface	55 A; 70 V @ 50 Hz	3.75 % 1.1 %	55 mA	0.6 x 10 mm ² slit	5 weeks*	0.51 A·h*
CSNS[17] Phase I	Penning Surface	~50 A; ~100 V @ 25 Hz	1.5 % 1.25 %	50 mA	0.6 x 10 mm ² slit	1 month*	0.46 A·h*
INR RAS linac [18]	Penning Surface	100A;120V @ 50 Hz	1 % 1 %	20 mA	1.0 x 10 mm ² slit	Intermittent use	
LANSCE Operation [19]	Filament driven converter	30-35A; 180 V @ 120 Hz	10 % 7.6 %	16-18 mA	9.8 mm ∅	4 weeks	0.87 A·h
SNS Operation [20]	Internal RF Antenna	CW 300 W 13 MHz & 60 Hz 60 kW 2 MHz	6 % 5.94 %	>60 mA	7 mm ∅	14 weeks	>7 A·h
J-PARC Operation [21]	Internal RF antenna	CW 50 W 30 MHz & 25 Hz 22 kW 2 MHz	2 % 1.25 %	47 mA	9 mm ∅	11 weeks	1.1 A·h
CERN Linac4 [22]	External RF antenna	0.8 Hz 40 kW 2 MHz Pulsed H ₂	0.07 % 0.05 %	45 mA	5.5 or 6.5 mm ∅	7 weeks	0.026 A·h

2.13.4 PIG or Penning Negative Hydrogen Ion Sources

In 1937 F. Penning at Phillips in Eindhoven, Netherlands, invented the Penning or Phillips ion gauge [25]. Within a few years Penning ion gauges (PIG) started to be used as internal ion sources in cyclotrons. The breakthrough for H⁻, however, came in the 1970s when V. Dudnikov developed a Penning source that could deliver up to 150 mA for up to 1% duty factors, an improvement over the magnetron sources [26]. Since that time Penning sources tend to be used for higher duty factor applications.

Penning ion sources have hollow anodes, which are terminated at both ends with parts of a cathode. As seen in Fig. 3 for the case of the ISIS Penning source, electrons emitted from the cathode are prevented by the magnetic field between the two pole pieces from reaching the anode, and spiral and oscillate between the two parts of the cathode, reaching long path length and accordingly high ionization efficiencies [27].

The most famous Penning H^- ion source is at the ISIS accelerator at the Rutherford Appleton Laboratory near Oxford, England [1, 13]. It operates with a 1.1% beam duty factor which is limited by the ISIS accelerator. 700 to 800 μs plasma pulses are used to achieve very stable plasma yielding a respectable 3.75% plasma duty factor. Despite the high plasma duty factor, it achieves a 5-week lifetime during which $\frac{1}{2} A \cdot h$ of H^- ions are extracted. ISIS researchers continue to explore improvements on their Frontend Test Stand (FETS) and continue to achieve remarkable progress in part by increasing the size of their source [13].

In 2006 the Chinese Spallation Neutron Source (CSNS in Dongguan near Hong Kong) had to decide on an ion source for their 100 kW (Phase 1) and later 500 kW project. They selected the ISIS Penning source because it was the only H^- source with a proven track record that matched their requirements. The ion source and the accelerator for Phase 1 are commissioned and user operations will start in early 2018.

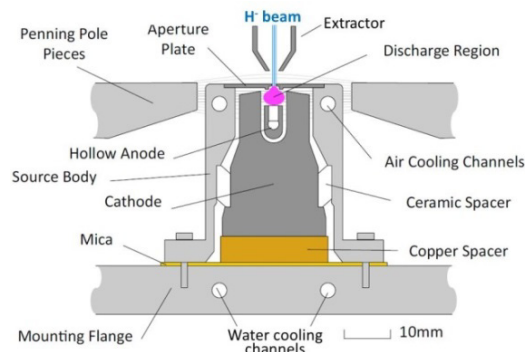


Figure 3: Schematic cross section of the ISIS Penning H^- source [27].

Using half the repetition rate but more than twice the beam pulse length CSNS achieves very similar results to ISIS as seen in Table 1. Unfortunately, their emittance is larger than the acceptance of their RFQ, which is no problem for their 100 kW phase 1 [17]. To reduce maintenance requirements in the future they started to develop an RF H^- source [27], the topic of a later section.

The Institute for Nuclear Research (INR RAS linac, Moscow) operates a linac with multiple injectors, one of which is a Novosibirsk type Penning source [18]. Due to the intermittent use of each injector, reliable service cycles or lifetimes are not available.

2.13.5 The Volume Production of H^- Ions

In 1977 M. Bacal found signals of large negative ion populations in her hydrogen plasma. Years of research and collaborations revealed that negative ions can be populous in cold plasma when highly rovibrationally excited hydrogen molecules collide with slow electrons [4, 10]. Inconveniently the excitation of the molecules requires hot electrons which rapidly destroy the formed negative ions. This dilemma was overcome with Tandem sources [4, 29].

Tandem and other modern ion sources provide magnetic confinement by surrounding the plasma chamber with strong bar magnets, alternating the direction of magnetization to form magnetic cusp fields [30]. The strength of magnetic cusp fields decrease rapidly with the distance from the magnets, and accordingly they form a minimum magnetic field in the center of a plasma chamber. With charged particles drifting towards lower magnetic fields, ions accumulate near the center towards the outlet, which is why multi-cusp sources are also called bucket ion sources [4].

Initially, such sources were powered by filament driven discharges and delivered remarkable H^- currents [31]. However, the H^- currents fell short of the currents obtained for short beam pulses with compact surface plasma sources (CSPS), as the family of Magnetrons and Penning sources is called. The solution was to use large extraction apertures to extract the volume produced H^- ions as seen in the last four entries in Table 1 and to enhance the H^- output with surface plasma produced H^- ions.

2.13.6 Surface Production of Negative Hydrogen Ions

The plasma near the surface provides ions and electrons, and the plasma modifies the potential, essential components for the efficient production of H^- ions. Despite this critical role, many ion source papers omit the plasma term and refer to the H^- surface production in contrast to the H^- volume production.

Molybdenum (Mo) has been very successful in ion sources; in part because of its low sputter rates, in part due to its characteristic as a positive-to-negative hydrogen ion converter. As seen in Fig. 4a the Mo 4.6 eV work function is much too high to produce negative hydrogen ions, and the ~ 2.1 eV work function of one or more monolayers of Cs is much better. Interestingly enough, for ~ 0.6 monolayers of Cs the work function drops to 1.6 eV, a significant enhancement because the work function appears in the exponent of equation (1).

Applying exact doses of Cs is very difficult and routine cesiations normally apply multiple monolayers. The surface coverage can then be reduced by heating the Mo substrate to a certain temperature for a certain length of time as shown in Fig. 4b [32].

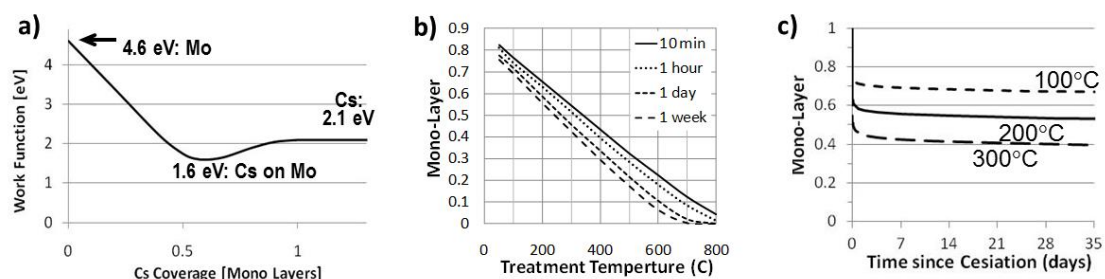


Figure 4: a) The work function of Mo surface partially covered with Cs; b) the remaining fractional monolayer after heating the Mo substrate for a certain time versus its temperature; c) the remaining fractional monolayer for certain Mo substrate temperatures versus time.

Lower temperatures and longer time periods yield larger margin for errors and may allow the optimization of the H^- yield, before stopping the emission by lowering the substrate temperature to $<100^\circ\text{C}$.

Alternatively, one can take advantage of the physics of the system: When adsorbed on Mo, Cs is $\sim 30\%$ larger than the metallic radii of the substrate Mo. This causes the

surface binding energy of the Cs to increase with decreasing surface coverage, which leads to a self-stabilizing thermal emission [33]. After cesiation, one can heat the substrate to a certain temperature so that the Cs surface coverage will approach the ideal coverage within a few hours or days, then, barely change over the next many weeks or months as shown in Fig. 4c. It should be noted that Figs. 4b and 4c are based on a certain model for the surface binding energy [32]. Because this does not exactly apply for the technical multi-crystalline Mo metals used for actual converters, the optimal temperatures have to be determined experimentally.

2.13.7 Converter H⁻ Sources and Filament Driven H⁻ Sources

The Los Alamos Neutron Science Center (LANSCE) at Los Alamos National Laboratory (LANL near Santa Fe, USA) successfully operates a filament-driven converter H⁻ ion source shown in Fig. 5a, which was designed and built by Lawrence Berkeley National Laboratory (LBNL in California, USA). The plasma pulses are started by raising the heated filaments to -200 V so that emitted electrons produce positive hydrogen ions. The partially Cs covered, concave shaped Mo converter at -300 V attracts the positive ions, converts some of the ions to H⁻ and then pushes those towards the source outlet. Having -300 V on the converter enhances the sputtering of the Cs which leads to a less than optimal Cs coverage and lower H⁻ currents [19]. Despite its lower H⁻ beam pulse current, the high duty factor allows for more H⁻ ions to be extracted from this source during its service cycle than from Penning sources with comparable service cycles as seen in Table 1.

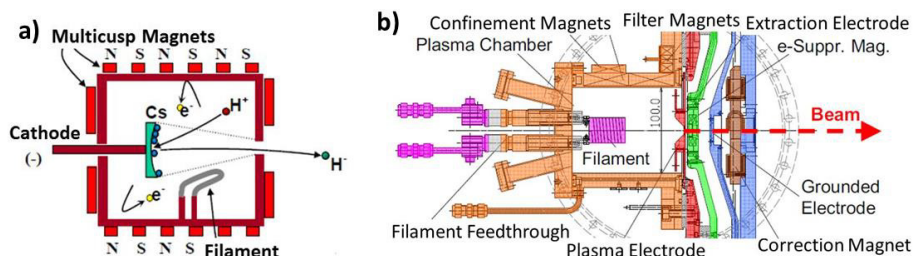


Figure 5: Schematic cross section of a) the LANSCE filament-driven Converter [34] and b) the former J-PARC LaB₆ filament driven [35] H⁻ sources.

In addition, an algorithm was developed to prevent filament failures before the end of the service cycle by slightly reducing the filament current when needed [19]. The facility continues to reliably support numerous users for close to 30 years.

While much effort was put into converting or developing filament-driven ion sources into H⁻ sources, the effort by the Japan Proton Accelerator Research Complex (J-PARC near Mito, Japan) stood out and is shown in Fig. 5b. Their success was due to their filaments which were fabricated from highly-emissive LaB₆, allowing for low operational filament temperatures. While it was never investigated in detail, the J-PARC Mo plasma electrode must have served as a converter, by adsorbing emissive layers of materials evaporated from the filament [35]. While the H⁻ output current met the 36 mA requirement for the first project stage, it fell short of the 60 mA requirement for the 1 MW upgrade goal. Adding Cs produced very impressive H⁻ output currents but only for short time periods. To satisfy their 1 MW requirement J-PARC adapted SNS RF antennas, which will be discussed below.

There is a general consensus that filament vapors gradually cover the Cs layer in Cs enhanced filament driven sources, and that accordingly filament-driven sources are not a good match for high-current H^- sources because of their enhanced Cs consumption.

2.13.8 RF Driven H^- Sources

RF driven ion sources have been around since 1948 [36]; however, they were first introduced to high-current H^- sources when LBNL replaced the filament driver from their multicusp source with a RF antenna and obtained more H^- beam. The source was very successful when operated at low power and/or low duty factor on 9 to 5 test stands [37]; however, testing different versions of this source at 24-hour facilities with high power and/or high duty-factor or heavy ions yielded frequent antenna failures [4, 38, 39]. Observations of only failed antennas were used to erroneously conclude that internal antennas sputter excessively and therefore could never work reliably [39]. Accordingly, a RF source with an external antenna was developed, which again worked well at low duty factors; however, the source could not compete against the CSPS, and it could not support high duty factors [40]. Although several efforts to develop this source for high duty factor failed, one effort succeeds at 6% duty factor after more than ten years of development and fundamental changes [41].

However, SNS at ORNL needed a H^- source that could deliver ~ 50 mA at a $\sim 6\%$ duty factor for ~ 3 weeks by 2009 and lacked the time to see which speculations would pan out. Except for the antenna issues, the LBNL designed and built RF H^- source was promising. Analyzing the antenna failures, it was found that the single-layer porcelain coatings of the antennas were of marginal thickness and questionable composition [42].

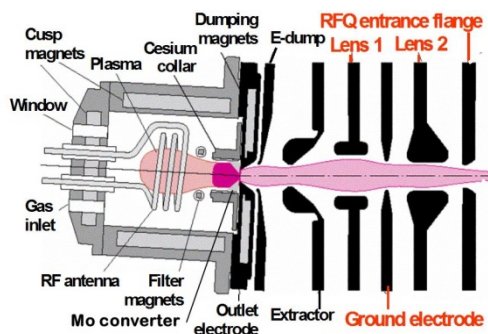


Figure 6: Schematic cross section of the SNS RF H^- ion source and LEBT.

Together with a local porcelain company [43] a TiO_2 -free, 3-4 layer, ~ 0.7 mm thick antenna coating was developed which worked with up to 55 kW of 2 MHz RF power at 5% duty factor. In 2009 this was sufficient to support 1 MW for up to 4 weeks with about two antenna failures per year due to the infant mortality of the antennas introduced with the 10 to 15 source changes requested by management [4].

As shown in Fig. 6, about 30 sccm of H_2 gas (standard cubic centimeter per minute) leaks into the back of the stainless-steel plasma chamber surrounded by water-cooled multi-cusp magnets. The H_2 flow is doubled for about 1-2 s to ignite a dim plasma with 300 W of 13 MHz circulating through the $2\frac{1}{2}$ turn antenna. This plasma starts the 50-65 kW 2 MHz plasma needed for the 50-60 mA H^- beamlets injected into the Radio Frequency Quadrupole accelerator (RFQ) for 1 ms at 60 Hz.

A 200 G filter field returns hot electrons to the hot plasma inside the antenna where cold electrons, ions, and highly excited molecules drift towards the outlet. As the cold electrons collide with the excited molecules, H^- ions form and escape through the outlet.

Many of the positive ions impact on the partly Cs covered Mo converter and some bounce back as H^- ions and again some of them escape through the outlet. In 2009, of those extracted ions about 45 mA were injected into the RFQ, the first location the H^- beam current of the SNS injector can be measured [44, 45], as is widely published since 2009 [44, 45, 46]. The elevated temperature of the low-energy beam transport system (LEBT) shows that a significant amount of the beam is lost in the SNS LEBT. This is why the SNS H^- beam current cannot be compared with other facilities who measure the H^- beam current much closer to their H^- source. Comparisons based on claims that SNS measures the H^- beam current at the source exit are incorrect [47].

However, it took another 5 years to bring the SNS H^- source performance to 55-65 kW of 2 MHz at a full 6% duty factor with >99% availability for the 50-60 mA of H^- injected into the RFQ, the requirement for 1.4 MW. Increasing the duty factor by 6% and the RF power by 9% beyond the 1 MW requirements increased the antenna failures to ~6 per year. Rigorous quality control [48] reduced and later several improvements of the cleanliness in the antenna coating process [43] brought the failures under control with no antenna failure since 1-13-2013. Realizing that the increased power heated the porcelain around highly exposed, porous patches to the melting point, the antenna coating was reduced from ~0.6 to ~0.5 mm [20]. This was another fine-tune of the 2001 increase in thickness to mitigate electrical breakthroughs and sputtering when the coatings were only 0.1-0.2 thick [42]. It was evaporation during the life-terminating melting of the porcelain that was erroneously interpreted as excessive sputtering [39].

In 2011 a start frequency of 1.97 MHz was introduced to enable higher RF powers without encountering plasma outages [33]. However in 2014 the start frequency had to be increased to 1.985 MHz to extend the pulse length from 0.88 to 1.0 ms to avoid plasma outages [49]. This was followed by adding a feedback to the 13 MHz matching network, which allowed detailed characterizations of the 13 MHz plasma. One of the discoveries was that the 2 MHz completely displaces the 13 MHz plasma and that it has to reestablish itself as the 2 MHz plasma decays [50]. As a result a slightly off-resonance tune was found that is more robust against plasma outages [51].

Mitigating the plasma outages enabled operations with lower H_2 pressures, which yields higher H^- beam currents. And finally, it was highly accurate wear measurements [20], which convinced management that it was safe to operate the SNS H^- source for up to ~20 weeks, the expected life time of the SNS targets. So far up to 14 weeks have been demonstrated, during which more than 7 A·h H^- were extracted [20], more than

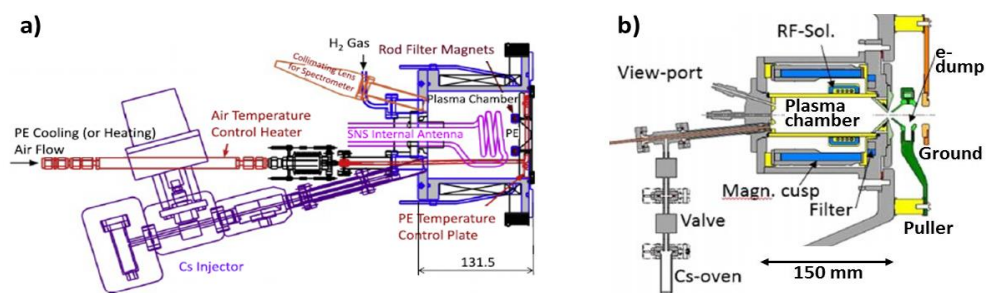


Figure 7: Schematic cross sections of the a) J-PARC RF source with an SNS antenna [21]; b) the CERN RF source with an external antenna [52].

double the amount than any other pulsed H^- source delivered in a service cycle. This has saved numerous hours of ion source maintenance and accelerator retuning. It is these recent achievements that have earned the SNS ion source team the 2017 Brightness Award [53].

As seen in Fig. 5b J-PARC essentially replaced the filament back flange with an SNS antenna back flange, which also contains a Cs injector as seen in Fig. 7a [21]. While they are capable of 60 mA, they currently use only 22 kW to make 47 mA. Because they operate at a lower duty factor than the SNS source they can benefit from thicker antennas [54].

And last but not least Fig. 7b shows the CERN RF driven H^- source with an external antenna, which faces no challenging duty factor, although future upgrades may change that significantly. Its 0.8 Hz repetition rate allows for a pulsed gas valve to ignite the plasma at high pressure before extracting the beam at lower pressures. The CERN H^- source is impressively automated systems with a large team supporting and maintaining it [22].

2.13.9 Summary and Conclusions

This paper gives a rough outline describing the successful pulsed high-current H^- sources for accelerators, with a focus on the very successful SNS RF-source, and the underlying physics which allows the production of very bountiful H^- beams. With the ambitious requirements of the SNS project as well as its planned upgrades being met [55], the high-current H^- sources have reached an excellent state of the art.

For new projects magnetrons are recommended for very high H^- currents (>60 mA) at low duty factors ($<1\%$). High currents (≤ 60 mA) with higher duty factors ($\leq 6\%$) are best served with RF sources. Upgrading H^- sources is a complex undertaking normally followed by significant learning curves, often due to the limited understanding how H^- sources work exactly. Source upgrades need to be planned with utmost caution.

Despite the excellent state of the art, plenty of work remains. Operations would appreciate fewer variations in the performance [56], which likely includes tighter control of the Cs, the temperatures, and other parameters of which some may still remain to be identified.

However, future accelerators will eventually require higher H^- beam currents and/or longer lifetimes. Such goals could be met by increasing the size of magnetron sources, a method that was successful for Penning sources. For higher duty factors such goals could be met by increasing the power of RF sources and fine-tuning the converter geometry and operation. However, higher beam currents will increase the H^- beam emittance and accordingly future accelerators using higher beam currents ought to be designed with higher acceptances, at least in the low beta section.

This space did not allow a discussion of the issue of the co-extracted electrons that can make or break H^- sources. Past experience has shown that all reliable high-current (>40 mA) production H^- sources require Cs, and the consumption varies over orders of magnitude due to sputtering, other subjects that exceed the given space. The emittance of the H^- beam is another important subject that had to be omitted to save space, but can be found in [13].

2.13.10 Acknowledgments

The skillful proofreading by J. Holmes (SNS) is highly appreciated. The proofreading, corrections and updates by M. Bacal (Ecole Polytechnique, Univ. Paris 06), Yu. Belchenko (BINP), A. Belov (INR), D. Bollinger (FNAL), W. Chen (CSNS), V. Dudnikov (Muons, Inc.), D. Faircloth (RAL, ISIS), S. Lawrie (RAL, ISIS), J. Lettry (CERN), S. Liu (CSNS), H. Oguri (J-PARC), D. Raparia (BNL), G. Rouleau (LANL) and A. Zelenski (BNL) were very important to correctly document the present status. This review was performed at Oak Ridge National Laboratory, which is managed by UT-Battelle, LLC, under contract number DE-AC05-00OR22725 for the United States Department of Energy.

2.13.11 References

1. J. R. Alonso, “High-current, negative-ion sources for pulsed spallation neutron sources: LBNL Workshop, October 1994” in *Rev. Sci. Instrum.* **67**, 1308-13 (1996).
2. S. Henderson et al, “The Spallation Neutron Source accelerator system design” in *Nucl. Instrum. Meth.* **A763**, 610-673 (2014).
3. M. P. Stockli and T. Nakagawa, “Ion Injectors for High-Intensity Accelerators”, in *Rev. Acc. Sci & Tech.* (World Scientific Publishing Company), **Vol. 6**, 197-219 (2013).
4. M. P. Stockli, “Volume and Surface-Enhanced Volume Negative Ion Sources” in *Proceedings of CERN Accelerator School on Ion Sources*, Senec, Slovakia, 2012, R. Bailey Edt., Report **CERN-2013-007**, 265-84 (2013).
5. G. P. Lawrence, A. K. Beauchamp and J. L. McKibben, “Direct Extraction of negative ion beams of good intensity from a duoplasmatron” in *Nucl. Instrum. Meth.* **32**, 357-59 (1965).
6. V. G. Dudnikov, “Method of negative ion production”, Russian Patent No. 411542 (1972).
7. Yu. I. Belchenko, G. I. Dimov, and V. G. Dudnikov, and A. A. Ivanov, “On formation of Negative ions in gas-discharge” in *Doklady Akademii Nauk SSSR* (Proceedings of the Academy of Science of the USSR), **233**, 1283-5 (1973).
8. Yu. I. Belchenko, G. I. Dimov, V. G. Dudnikov, “A powerful injector of neutrals with a surface-plasma source of negative ions” in *Nucl. Fusion*, **14**, 113 (1974).
9. M. E. Kishinevskiy, “Novosibirsk Report No. 116-73”; *Sov. J. Tech. Phys.* **48**, **73** (1978).
10. M. Bacal, M. Wada, “Negative hydrogen ion production mechanisms” in *Appl. Phys. Rev.* **2**, 021305-1/30 (2015).
11. B. Rasser, J. N. M. Van Wunnik and J. Los, “Theoretical models of the negative ionization of hydrogen on clean tungsten, cesiated tungsten and cesium surfaces at low energies” in *Sur. Sci.* **118**, 697-710 (1982).
12. Yu. I. Belchenko, V. G. Dudnikov, “Negative ion production surface-plasma sources with unclosed electron drift discharges”, *J. de Physique Colloque C7*, **40**, 501-2 (1979).
13. D. Faircloth and S. Lawrie, “An Overview of Negative Hydrogen Ion Sources for Accelerators”, in *New J. Phys.* **19**, (2017) and private communications (2017).
14. Courtesy from Dan Bollinger, FNAL, with minor adaptations (2017).

15. J. G. Alessi, “Performance of the Magnetron H⁻ Source on the BNL 200 MeV Linac” in American Institute of Physics **CP642**, 279-81 (2002) and D. Raparia, BNL, private communication (2017).
16. P. R. Karns, D. S. Bollinger, A. Sosa, “Recent Operation of the FNAL Magnetron H⁻ Ion Source” in American Institute of Physics **CP1869**, 030055-1/8 (2017) and D. Bollinger, FNAL, private communication (2017) .
17. S. Liu, H. Ouyang, T. Huang, Y. Xiao, X. Cao, Y. Lv, K. Xue, W. Chen, “The modifications at the CSNS ion source” in American Institute of Physics **CP1869**, 030056-1/8 (2017).
18. A. S. Belov, O. T. Frolov, V.S. Klenov, V. P. Yakushev, “Ion Sources for linac of Moscow Institute for Nuclear Research” in Rev. Sci. Instrum. 63, 2622-4 (1992) and O.M. Volodkevich, V. N. Zubets, Yu. V. Kiselev, V. S. Klenov, “Development of Remote Control System for H-minus Ions Source of INR Linac” in Proceedings of RuPAC2014, Obninsk, Kaluga Region, Russia, 423-5 (2014).
19. R. Keller, O. Tarvainen, E. Chacon Golcher, E. G. Geros, K. F. Johnson, G. Rouleau, J. E. Stelzer, T. J. Zaugg, “H⁻ Ion Source Development for the LANCE Accelerator Systems” in American Institute of Physics **CP1097**, 161-70 (2009) and G. Rouleau, LANL, private communication (2017).
20. M. P. Stockli, , B. X. Han, S. N. Murray Jr., T. R. Pennisi, M. Santana, C. M. Stinson, R. F. Welton, “Record Performance of and Extraction Studies with the Spallation Neutron Source H⁻ Injector” in American Institute of Physics **CP1869**, 030010-1/10 (2017).
21. H. Oguri, K. Ohkoshi, K. Ikegami, A. Takagi, H. Asano, T. Shibata, K. Nanmo, A. Ueno, K. Shinto, “Operation Status of the J-PARC RF driven H⁻ Ion Source” in American Institute of Physics **CP1869**, 030053-1/7 (2017) and H. Oguri, J-PARC, private communication (2017).
22. J. Lettry et al., “CERN’s Linac4 Cesium surface H⁻ Source” in American Institute of Physics **CP1869**, 030002-1/8 (2017) and J. Lettry (CERN) private communications (2017).
23. M. P. Stockli, B. X. Han, S. N. Murray, T. R. Pennisi, M. Santana, R. F. Welton, “Recent Performance of the SNS H⁻ Source for 1-MW Neutron Production” in American Institute of Physics **CP1515**, 292-301 (2013).
24. A. Zelenski, BNL, private communications (2017).
25. F. M. Penning, “Ein neues Manometer fuer niedrige Gasdrucke, insbesondere zwischen 10⁻³ und 10⁻⁴ mm”, in Physica, **IV**, 71 (1937).
26. V. G. Dudnikov, “Surface plasma source of negative ions with Penning Geometry” in Proceedings of the 4th All-Union Conference on Charged Particle Accelerators, Moscow, 1974 (Moscow, Nauka, 1975) and Los Alamos Scientific Laboratory translation, **LA-TR-75-4**.
27. D. Faircloth, “Negative Ion Sources: Magnetron and Penning” in Proceedings of CERN Accelerator School on Ion Sources, Senec, Slovakia, 2012, R. Bailey Edt., Report **CERN-2013-007**, 285-310 (2013); adapted from Fig 13.
28. W. Cheng, H. Ouyang, Y. Xiao, S. Liu, Y. Lu, X. Cao, T. Huang, K. Xue, “RF H-minus ion source development in China spallation neutron source” in American Institute of Physics **CP1869**, 030013-1/5 (2017).
29. K. N. Leung, K. W. Ehlers, M. Bacal, “Extraction of volume-produced H⁻ ions from a multi cusp source”, in Rev. Sci. Instrum. **54**, 56-61 (1983).
30. K. W. Ehlers, K. N. Leung, “Characteristics of the Berkeley multicusp ion source”

- in *Rev. Sci. Instrum.* **50** 1353-61, (1979).
31. K. N. Leung, K. W. Ehlers, C. A. Hauck, W. B. Kunkel, A. F. Lietzke, "Small multicusp H⁻ source" in *Rev. Sci. Instrum.* **59** 453-6, (1988).
 32. M. P. Stockli, B. X. Han, S. N. Murray, T. R. Pennisi, M. Santana, R. F. Welton, "Towards Understanding the Cesium Cycle of the Persistent H⁻ Beams at SNS" in *American Institute of Physics CP1390*, 123-33 (2011).
 33. M. P. Stockli, B. X. Han, T. W. Hardek, Y. W. Kang, S. N. Murray, T. R. Pennisi, C. Piller, M. Santana, R. Welton, "Producing persistent, high-current, high-duty-factor H⁻ beams for routine 1 MW operation of the Spallation Neutron Source" in *Rev. Sci. Instrum.* **83**, 02A732-1/7 (2012).
 34. R. F. Welton, "Overview of high-brightness H⁻ ion sources" in *Proceedings of LINAC 2002*, 559-63 (2002); adapted from Fig. 3.
 35. H. Oguri, K. Ikegami, K. Ohkoshi, Y. Namekawa, A. Ueno, "Operation Status of the J-PARC Negative Hydrogen Ion Source" in *American Institute of Physics CP1390*, 235-44 (2011); adapted from Fig. 2.
 36. P. C. Thonemann, J. Moffatt, D. Roaf, J. H. Saunders, "The Performance of a New Radio-Frequency Ion Source" in *Proc. Phys. Soc. London* **61**, 483-5 (1948).
 37. K. N. Leung, G. J. DeVries, W. F. DiVergilio, R. W. Hamm, C. A. Hauck, W. B. Kunkel, D. S. McDonald, M. D. Williams, "RF driven multicusp H⁻ ion source" in *Rev. Sci. Instrum.* **62**, 100-4 (1991).
 38. D. Wutte, J. Burke, B. Fujikawa, P. Fetter, S. J. Freedman, R. A. Gough, C. M. Lyneis, Z. Q. Xie, "Development of a radioactive ion beam test stand at LBNL" in *American Institute of Physics CP473*, 566-77 (1999).
 39. J. Peters, "Internal versus External RF coupling into a volume source" in *Proceedings of EPAC 2002*, 1727-9, (2002).
 40. J. Peters, "The HERA RF-driven multicusp H⁻ ion source" in *Proceedings of LINAC 2006*, 388-90, (2006).
 41. R. F. Welton, A. Aleksandrov, B. X. Han, Y. W. Kang, M. M. Middendorf, S. N. Murray, M. Piller, T. R. Pennisi, V. Peplov, R. Saethre, M. Santana, C. Stinson, M. P. Stockli, "A New 2.5 MeV Injector and Beam Test Facility for the Spallation Neutron Source" in *American Institute of Physics CP1869*, 060002-1/8 (2017).
 42. R. F. Welton, M. P. Stockli, Y. Kang, M. Janney, R. Keller, R. W. Thomae, T. Schenkel, S. Shukla, "Ion source antenna development for the Spallation Neutron Source" in *Rev. Sci. Instrum.* **73**, 1008-12 (2002).
 43. Cherokee Porcelain Enamel Corporation, 2717 Independence Lane, Knoxville, TN 37914, USA.
 44. M. P. Stockli, K. D. Ewald, B. X. Han, S. N. Murray Jr., T. R. Pennisi, C. Piller, M. Santana, J. Tang, R. F. Welton, "Recent performance of the SNS H⁻ ion source and low-energy beam transport system" in *Rev. Sci. Instrum.* **85**, 0B137-1/4 (2014).
 45. B. X. Han, R. F. Welton, S. N. Murray, T. R. Pennisi, M. Santana, C. M. Stinson, M. P. Stockli, "Refined beam measurements on the SNS H⁻ injector", in *American Institute of Physics CP1869*, 030014-1/10 (2017).
 46. M. P. Stockli, B. X. Han, S. N. Murray, D. Newland, T. R. Pennisi, M. Santana, R. F. Welton, "Ramping up the SNS beam power with the LBNL baseline H⁻ source" in *American Institute of Physics CP1097*, 223-35 (2009).
 47. A. Ueno, "Cesium surface H⁻ ion source: optimization studies" in *New J. Phys.*

- 19**, 015004-1/15 (2017).
48. R. F. Welton, V. G. Dudnikov, B. X. Han, S. N. Murray, T. R. Pennisi, C. Piller, M. Santana, M. P. Stockli, M. W. Turvey, “Improvements to the internal and external antenna H^- ion source at the Spallation Neutron Source” in *Rev. Sci. Instrum.* **85**, 02B135-1/5 (2014).
 49. M. P. Stockli, B. X. Han, S. N. Murray, T. R. Pennisi, C. Piller, M. Santana, R. F. Welton, “Recent performance and ignition tests of the pulsed SNS H^- source for 1 MW neutron production” in *American Institute of Physics CP1655*, 030001-1/9 (2015).
 50. M. P. Stockli, B. Han, S. N. Murray, T. R. Pennisi, C. Piller, M. Santana, R. Welton, “Recent performance and plasma outage studies with the SNS H^- source” in *Rev. Sci. Instrum.* **87**, 0B140-1/5 (2016).
 51. B. X. Han, M. P. Stockli, Y. Kang, C. Piller, S. N. Murray Jr., T. R. Pennisi, M. Santana, R. Welton, “Characterization of the CW starter plasma RF matching network for operating the SNS H^- ion source with lower H_2 flows” in *Rev. Sci. Instrum.* **87**, 02B143-1/4 (2016).
 52. Lettry et al., “Linac4 H^- ion sources” in *Rev. Sci. Instrum.* **87**, 02B139-1/3 (2016).
 53. J. R. Alonso, “Brightness Award” in *Rev. Sci. Instrum.* **89** (2018).
 54. A. Ueno, K. Ohkoshi, K. Ikegami, A. Takagi, H. Asano, H. Oguri, “Pre-conditioning procedure suitable for internal-RF-antenna of J-PARC RF-driven H^- ion source”, in *Rev. Sci. Instrum.* **87**, 02B129-1/3 (2016).
 55. M. S. Champion, R. A. Dean, J. D. Galambos, M. P. Howell, M. A. Plum, B. W. Riemer, “Progress on the Proton Power Upgrade of the Spallation Neutron Source”, in *Proceedings of IPAC2017, Copenhagen, Denmark, 2245-8*, (2017).
 56. M. P. Stockli et al., “Workshop on Performance Variations in H^- ion sources 2012: PV H^- 12” in *American Institute of Physics CP1515*, 594-7 (2013).

2.14 A 60 mA DC H^- Ion Source with a long life filament for accelerators

Keerthi Jayamanna

Mail to: keerthi@triumf.ca

TRIUMF, 4004 Wesbrook Mall Vancouver BC Canada V6T2A3

2.14.1 Introduction

This paper describes the latest multi-cusp type external ion source developed at TRIUMF, which is capable of producing a negative hydrogen ion beam (H^-) of up to 60 mA of direct current with 90A and 140V arc. The lifetime of the ion source filament of the TRIUMF 500 MeV cyclotron has also been increased from three weeks to more than six months while continually running at 7 A arc current and 110 V arc voltage. Filament installed in the TR13 cyclotron revealed no measurable degradation after 10 months of operation. This filament lifetime improvement will benefit machines with filament based ion sources. The results achieved to date are discussed.

One of the major components of the accelerators is the ion source. In developing the design of cyclotrons for protons or deuterons, negative ions are favoured over positive ions due to the charge-changing ability of the energetic beam. While going through a

stripping foil placed at the perimeter of the cyclotron, the H^-/D^- change to H^+/D^+ prompts a change in the beam trajectory to shift outwards due to the reverse Lorentz force. This makes extracting the energized beam easy. The change of the beam trajectory outwards simplifies the beam extraction out of the cyclotron, where a strong magnetic field is present and extraction is otherwise very difficult. After the ejection, the beam can be transported further out of the cyclotron through a beam line to irradiate single or multiple targets to produce short-lived and long-lived radioactive isotopes. While low intensity machines use internal type H^- ion sources [1], all high and medium current cyclotrons use external ion sources [2, 3].

Cyclotrons developed by manufacturers like ACSI, BEST, and CYCIAE employ external ion sources; hence, they can deliver over 1 mA to their targets and use TRIUMF-type ion sources. Large hospitals like Vancouver General Hospital [4] (VGH) and radio pharmaceutical producers like Nordion [5, 6] also use the same type of ion source for the injection into cyclotrons.

Beside the application as beam injector to cyclotrons H^- ions are used to provide protons to high power storage rings with multiple injection. An accelerated H^- beam is fed to the storage ring through a stripping foil and a magnetic dipole. The H^- beam bends into the ring in the dipole and electrons of the H^- are stripped by the thin foil. The protons then accumulate in the ring, passing multiple times through the stripping foil unaffected. This allows a large number of protons to be stored in the ring (CERN and Fermilab).

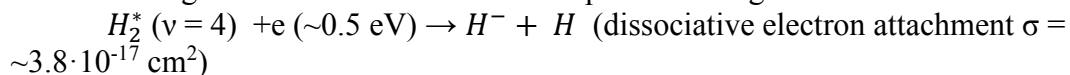
In fusion research, energetic neutral beams are used for plasma generation and heating. They are created by the neutralization of negative ion beams. It is the only viable option because at energies above 100 keV the positive ion neutralization efficiency is too low to create neutral beams of the required densities.

2.14.2 H^- physics

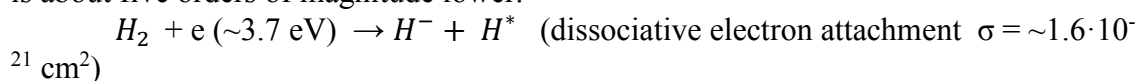
2.14.2.1 H^- production

The most common method to produce H^- ions is volume production via dissociative electron attachment and surface production on a thin coat of alkali metal. Only volume production [7] is discussed here since it is robust, involves less breakdowns and has easy maintenance as well as simple operation and it is chosen for TRIUMF H^- development.

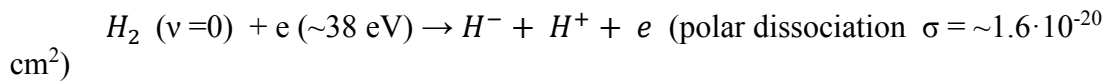
According to the calculations by Wadehra and Bardsley [8] the highest cross section for H^- volume production is from the dissociation of a H_2 molecule in a vibrational state above $v = 4$. Figure 1 shows cross sections values of the most probable production and destruction reactions [9, 10]. Cross section values for the following reactions are given where available and for optimum energies.



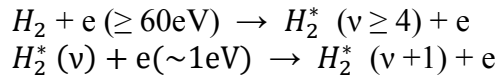
Cross section for dissociative electron attachment from ground state molecules is about five orders of magnitude lower.



H^- ions can also be produced through polar dissociation with energetic electrons but the cross section is still lower.

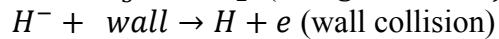
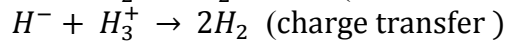
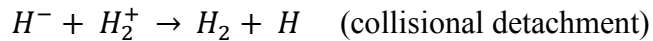
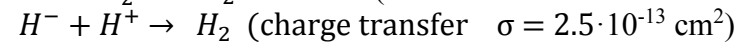
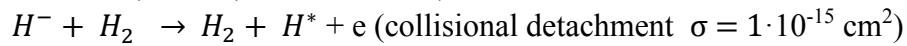


Therefore, the only viable option to enhance H^- ions is to increase the density of the vibrationally excited molecules at higher states. Vibrationally excited molecules are created by hydrogen gas colliding with higher energy electrons in the plasma as well as through recombination processes.



2.14.2.2 H^- destruction

H^- ions recombine while colliding with high energy electrons, neutral atoms, molecules, positive ions as well as plasma chamber walls



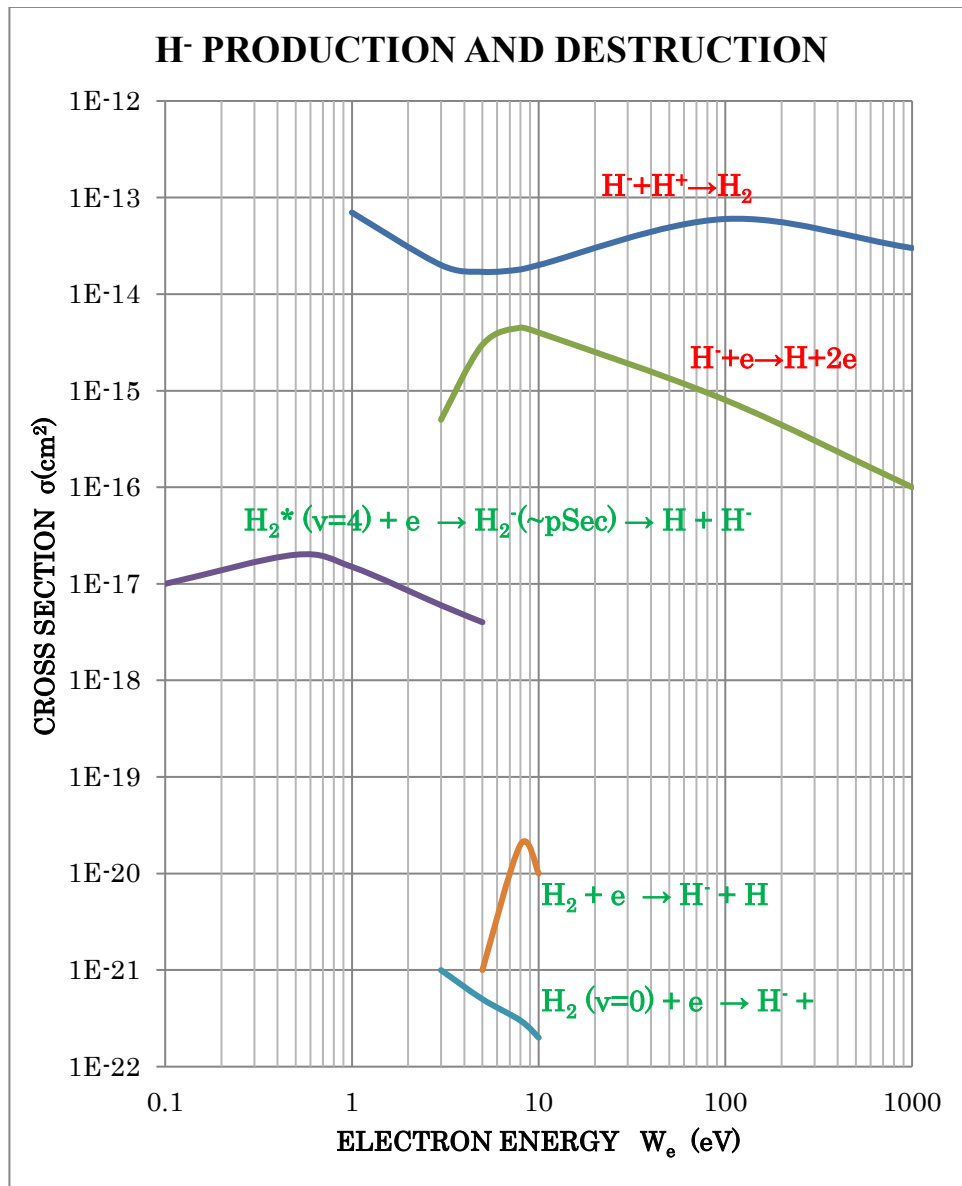


Figure 1. The cross sections of the H^- production processes (Green text) and destruction processes (Red text). Only the reactions with the highest cross section for both processes are shown here for clarity.

2.14.3 Background electrons

It is clear that the high energy electrons are needed to sustain plasma and for producing excited molecules while only low energy electrons should be present near the extraction region where H^- ion production must occur. Hot filament and an arc discharge are common as the electron driver and could produce energetic electrons as high as the arc energy to produce plasma and excited molecules. The fraction of low energy electrons produced in the plasma increases with the gas pressure. It is imperative to filter and stop high energy electrons entering the extraction region where H^- ions are produced and extracted. It was found that creating a simple transverse field can easily filter high energy electrons while letting the low energy electron migrate through the filter due to the

difference in the Larmor radius. Higher energy electron bend away from the center due to large Larmor radius. Low energy electron with small Larmor radius move close to the center known as Bowman diffusion.

2.14.4 Source setup

TRIUMF has been developing arc discharge H^- ion sources based on volume production and multi-cusp magnetic configuration since the mid-eighties. In 1989, 9 mA was reached [11] and 15 mA was achieved [12] in 1995. After a long break, H^- development started again in 2012 in order to improve performance of the main H^- ion source of the TRIUMF 500 MeV cyclotron. The goal was to design a source with a brighter and higher H^- current as well as to develop a long-lasting filament. A state-of-the-art test stand was built for that purpose and 20 mA was achieved [13] soon after commissioning it in 2013. In order to allow operation at higher currents significant improvements had to be done. Detailed source description and improvements mentioned above are described in the following section.

2.14.5 Ion source and extraction system

A schematic of the source set-up can be seen in figure 2a. A water-cooled, 100 mm diameter, 150 mm long and 1.5 mm thick copper tube surrounded by a 10 pole, 20 row Halbach type cusp magnetic configuration (figure 5) serves as the plasma chamber of the ion source. Four poles are also installed and arranged in the back plate where the filament holders are located, so that the cusp confinement continues throughout the plasma volume. The arc is created by applying a voltage of up to 200 V between a hot filament and the plasma chamber.

Two extraction systems, a three electrode (accel-accel - figure 2a and 2b) and a four electrode (accel-accel-decel - figure 3 and 4), were tested. The three-electrode system is simple but optimal only for fixed energy at 30 keV for the fixed gaps between electrodes. The four-electrode system allows the source to run at optimum extraction voltage for a large range of extracted beam energies with minimal impact on the beam properties [13]. With this extraction system, the beam energy can be as low as 1 keV and as high as 60 keV with negligible changes in beam quality.

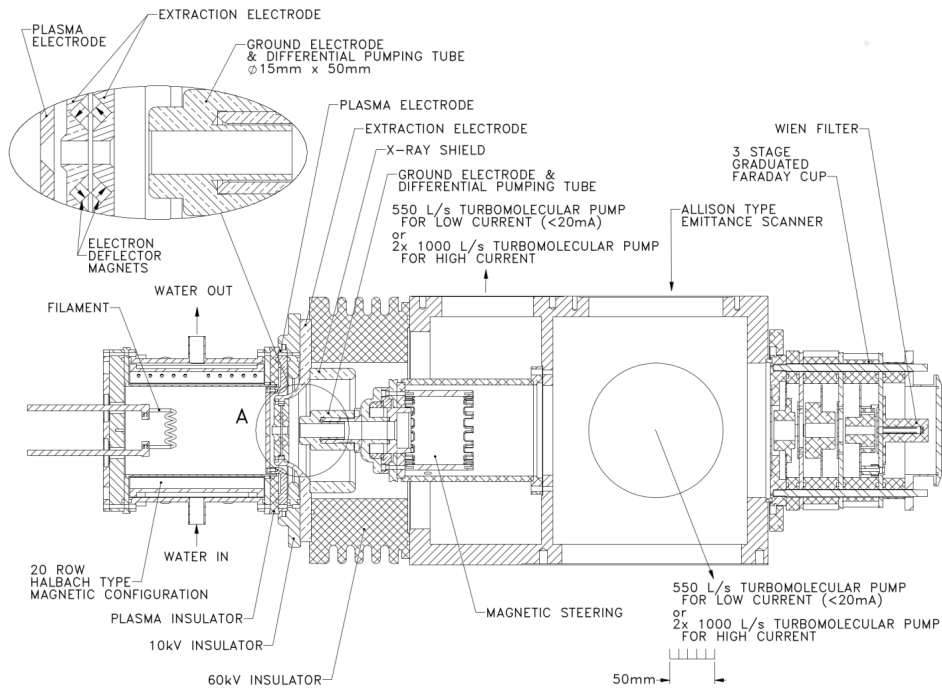


Figure 2a. Schematic view of the source setup with 3 electrode extraction system. The distance between the plasma electrode and the extraction electrode is 2.8 mm and the distance between the extraction electrode and the ground electrode is 14 mm.

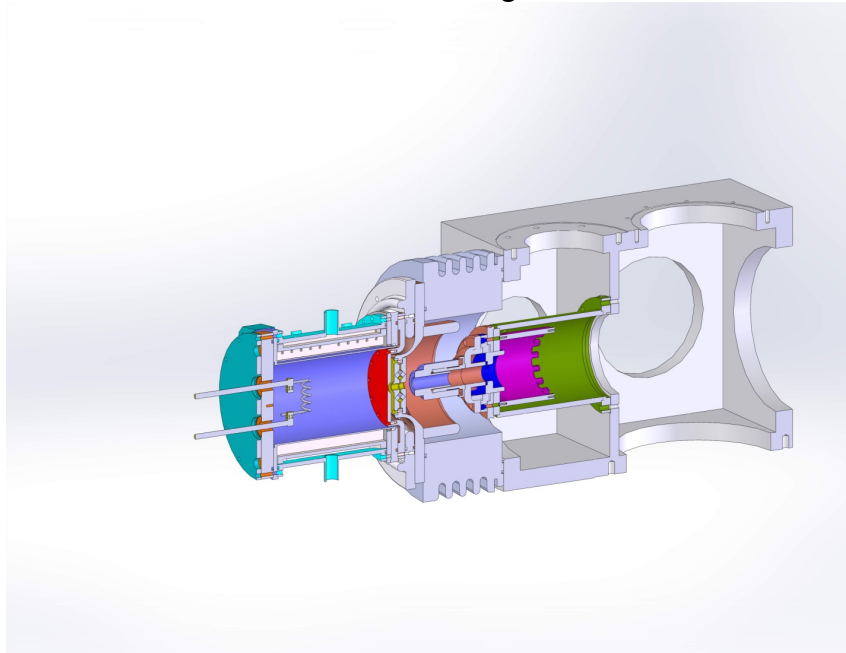


Figure 2b. A 3D cross-section of the ion source and extraction system with three electrodes. See the adjustable differential tube at the ground electrode front nozzle end.

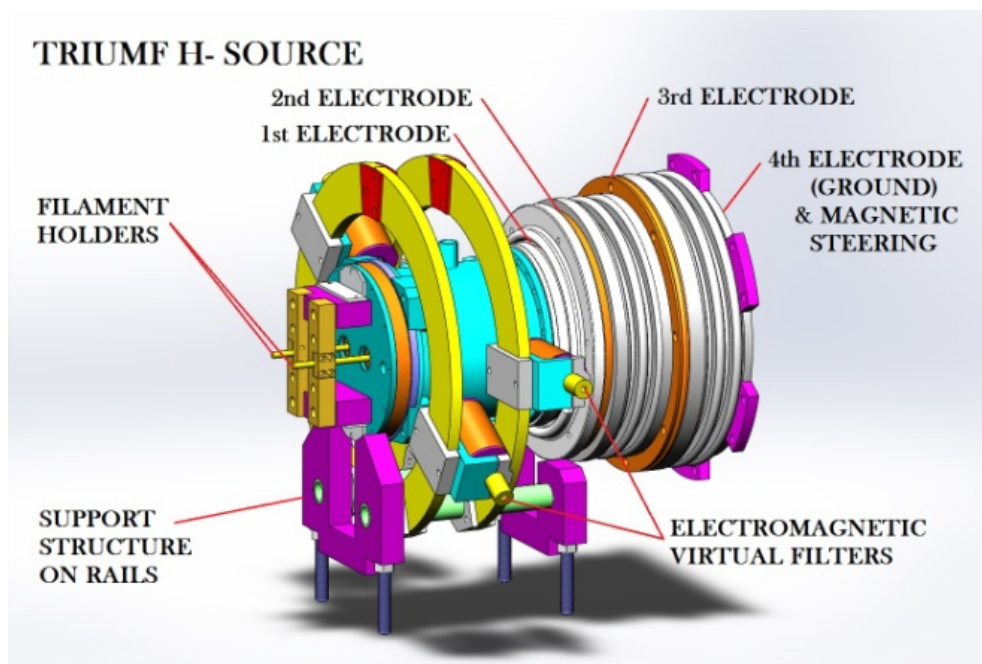


Figure 3. A 3D view of a four-electrode extraction system (accel-accel-decel) with adjustable electromagnetic virtual filters.

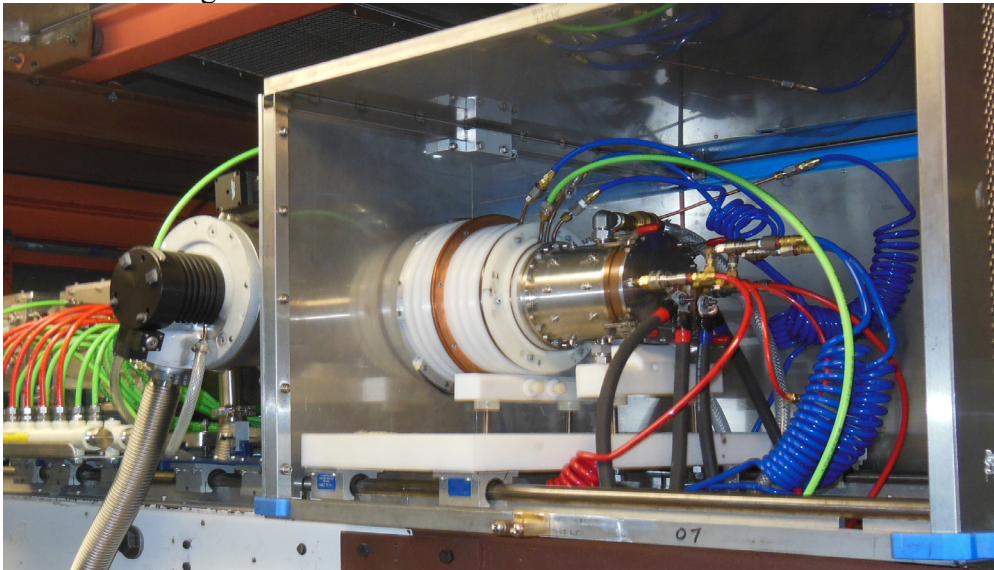


Figure 4. Ion source with four electrodes (accel-accel-decel). External coils were removed in this photograph.

2.14.6 Electron filters

Two electron filters are necessary as described above for H^- production. By reversing 10 short magnets in the cusp at selected places (see Figure 5) at the horizontal axis, a small dipole field (virtual filter) was created. It filters the high-energy electrons from the low-energy electrons [11]. An IV curve from a movable Langmuir probe (Figure 6) along the axis of the source determined the optimum values of the electron filters [14]. Measured positive ion density along the axis is shown in figure 7. Four electromagnetic filters are also installed (Figure 3 Orange) in order to optimize the virtual filter created by the permanent magnets dipoles for various arc conditions [13]. Near the extraction

aperture where the majority of H^- is created, the electron temperature must be around 0.5 eV for dissociative attachment of vibrationally excited hydrogen molecules. Everywhere else, high-energy electrons are beneficial for producing as many excited hydrogen molecules as possible in order to maximize H^- production. Therefore optimization of the virtual filter is utmost important for high current H^- output. Even though the multi-cusp ion source is a volume production based ion source, surface produced H^- ions may also be present. They are not affected by those filters.

Another two pairs of small 3 mm x 5 mm x 25 mm magnets are installed in the extraction electrode (see Figure 2a top left) to remove any electrons extracted from the source before gaining full energy. These electrons must be removed from the beam to reduce space charge problems as well as to reduce unnecessary power drainage from the high voltage bias power supply. The majority of the electrons returns back to the plasma electrode because of the filters, but some escape and reach the extraction electrode (second electrode). Due to the strength of these magnetic dipoles no significant amount of electrons were found passing the extraction electrode along the beam path. A Wien filter shows no electrons with the H^- beams but does show negligible amounts of neutrals and negatively charged oxygen ions. Electromagnetic steering placed after the ground electrode (third electrode) corrects the H^- trajectory while removing any leftover electrons in the H^- beam. Figure 8 shows the sum of transverse magnetic fields along the axis from three filters. For very high-current operation, another small transverse magnetic field along the beam path after the extraction is needed to improve H^- beam transmission.

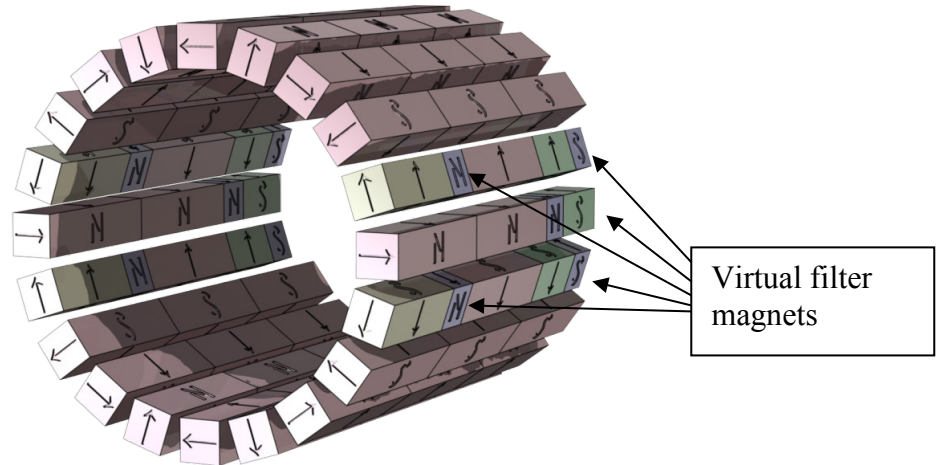


Figure 5. Halbach magnetic configuration used in most of TRIUMF type H^- ion sources, including the test stand and the main ion source at the 500 MeV cyclotron.

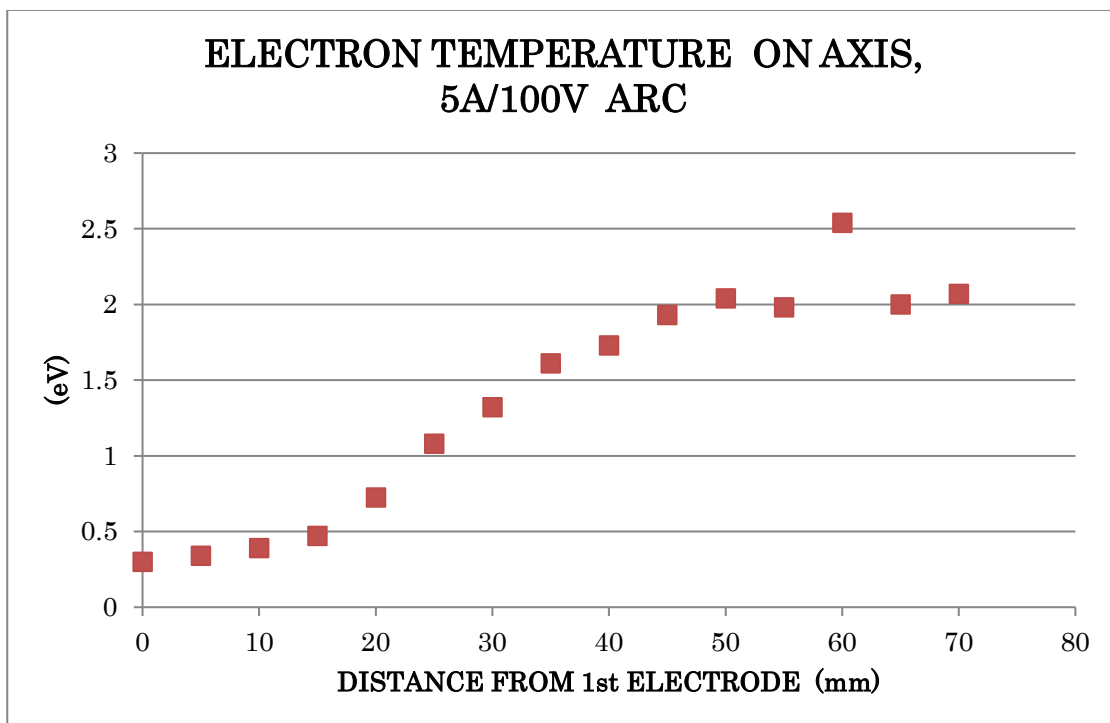


Figure 6 shows the electron temperature on axis with 5 A 100 V arc measured with a Langmuir probe. An aberration near the 60 mm is due to the filament interference to the probe measurements.

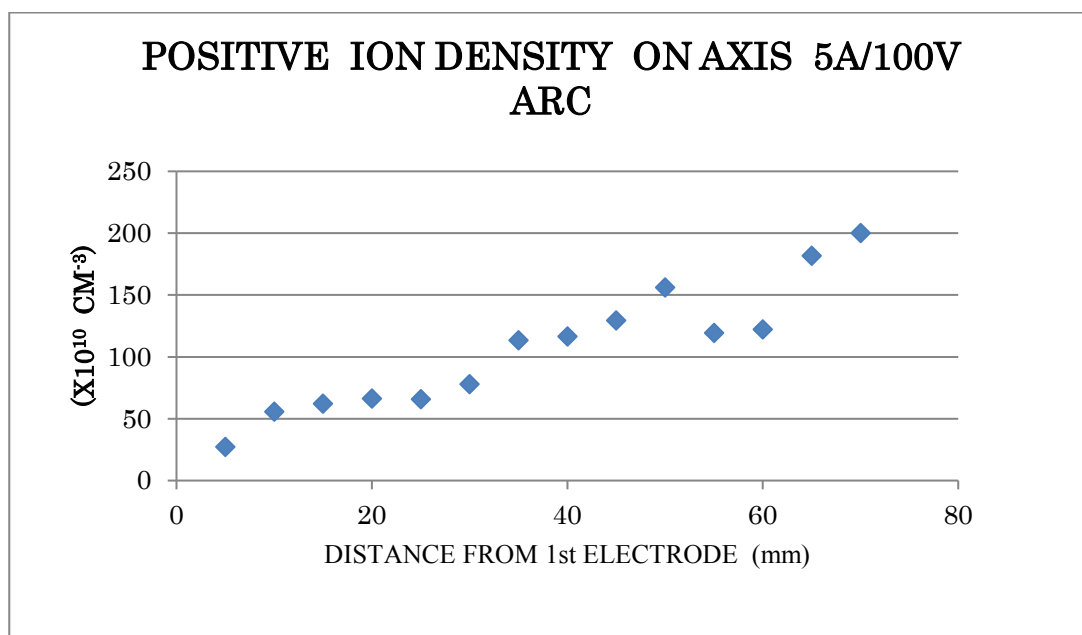


Figure 7 shows the positive ion density on axis with 5 A 100 V arc measured with a Langmuir probe. Above aberration near the 60 mm is due to the filament interference to the probe measurements.

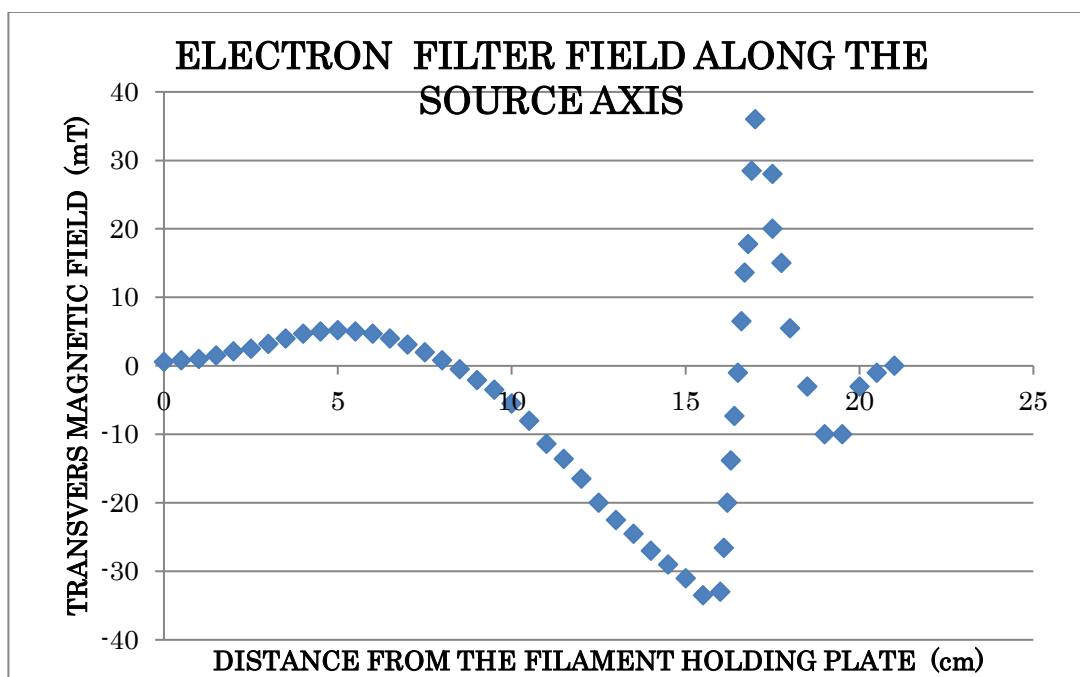


Figure 8 Filaments are located at the 5 cm position and the plasma electrode is at the 16 cm mark. Most electrons return to the plasma electrode and the erosion is visible at the back of the plasma electrode after a long run. Any electrons that escaped from the plasma electrode will accelerate and curve into the second electrode.

2.14.7 Beam line and diagnostics

A set of steerers is used to steer and center the beam to the three stage graduated Faraday cup. Two Allison type emittance scanners [24] for vertical and horizontal directions are installed in the beam line to complete the test stand.

2.14.8 Extraction system

The test setup is designed to operate the source high voltage terminal at a potential of up to -60 kV. An electrical schematic is shown in figure 9. AC power to supply a 10 V, 1000 A filament power supply and a 100 A, 150 V arc power supply and other necessary power supplies for the extraction potentials is fed in via a 45 kV·A transformer with 75 kV isolation. A -60 kV, 50 mA power supply is used to study higher extraction voltages and a -20 kV, 500 mA is used to study higher H^- currents at voltages below 20 kV. We use two high voltage power supplies because of availability and the power constraints of the system. For the extraction electrode, a 10 kV, 400 mA power supply is installed. Another 100 kV, 1 kV·A transformer is utilized to supply uninterrupted power to controls and the safety devices. Each electrode and power supply is connected via protective circuits with varistors (GEMOVs), capacitors, ferrite toroid coils and bleeding resistors. Figure 9. Electrical schematics of the H^- ion source system with an einzel lens as the third electrode. For fixed beam energy studies this electrode was removed and only a three-electrode system was used. Toroid rings, varistors and capacitors were installed for protection where necessary. Bleeding resistors are also installed to minimize damage to the equipment in case of sparking occurring during the vigorous testing.

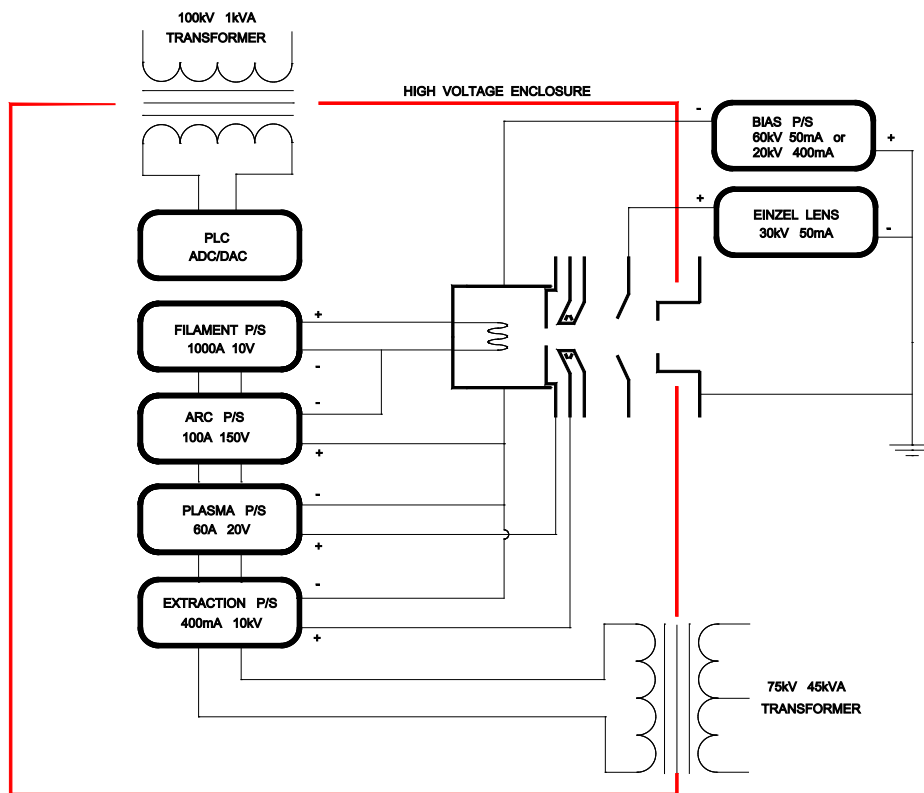


Figure 9. Electrical schematics of the H^- ion source system with an einzel lens as the third electrode. For fixed beam energy studies this electrode was removed and only a three-electrode system was used. Toroid rings, varistors and capacitors were installed for protection where necessary. Bleeding resistors are also installed to minimize damage to the equipment in case of sparking occurring during the vigorous testing.

2.14.9 Vacuum System

The vacuum system consists of four 1000 L/s turbo molecular pumps (for hydrogen), two for the source box and two for the diagnostic box. A low current ($H^- < 20\text{mA}$) version needs only two 550 L/s turbo molecular pumps, one for the source box and one for the diagnostic box. Two 600 L/min dry pumps back each section of the beam line. A 15 mm diameter and 50 mm long tube is installed between the source box and the diagnostic box in order to achieve the required differential pumping, (see Figure 1). The differential pumping is necessary for transporting the H^- beam with minimum stripping losses. Optimum H^- production at the source is ~ 0.4 Pa therefore removing gas as early as possible from the beam path is essential for efficient beam transmission.

Two gas flow controllers with flow rates of 0.1-10 cm^3/min STP and 3-100 cm^3/min STP are utilized for low and high current studies. Two controllers are used because the higher capacity flow controller does not have enough resolution for fine-tuning when the gas flow is below 3 cm^3/min . Also for very low H^- current with brighter beam studies, a smaller plasma aperture and a very low hydrogen flow is needed. Without hydrogen gas flow, the background pressure for both the source chamber and the diagnostic chamber is $\sim 2 \cdot 10^{-7}$ Pa. When the gas flow is 2 cm^3/min STP, the source box and the diagnostic box pressure is $2 \cdot 10^{-5}$ Pa and $2 \cdot 10^{-6}$ Pa respectively. The pressure of both boxes rises

linearly with the hydrogen gas flow. For higher H^- currents, hydrogen gas flow as high as $66 \text{ cm}^3/\text{min}$ STP is needed.

2.14.10 Results and discussions

2.14.10.1 H^- Beam current studies

The results up to 20 mA were published previously [21]. This paper describes the higher current studies and summary of filament lifetime studies. While increasing the H^- output current, many components needed to be upgraded or modified. A 50 A, 200 V arc power supply was replaced with 100 A, 150 V unit. A 50 mA, 60 kV bias power supply was replaced with a 500 mA, 20 kV unit. An extractor power supply was also replaced with a 400 mA, 10 kV unit. A 20 row Halbach type cusp configuration with the virtual filter also went through several iterations in order to be optimized to the desired output requirement. The gaps of the extraction system also went through a few iterations.

H^- beam current was studied with respect to various other parameters. Figure 10 shows the H^- beam current versus arc current. While these measurements were taken, all other parameters including hydrogen flow, plasma electrode voltage and extraction electrode voltage were adjusted to both maintain manageable electron currents on the extraction electrode and maximize the output. The system limitations become visible above 80 A and 140 V arc. The water temperature at the source reached the critical limit to operate. Water flow is limited by the input and output pressure $5.5 \cdot 10^5 \text{ Pa}$ and $1.4 \cdot 10^5 \text{ Pa}$ respectively. The copper plasma chamber collapses if pressure above $5.5 \cdot 10^5 \text{ Pa}$ is used. Also, the space charge effect began seriously affecting the beam performance. H^- beam current started limiting at the Faraday cup even though the high voltage power supply current kept rising with the arc power. Most likely the reason behind this is when the beam increases in size at very high currents and subsequently it is cut geometrically by the ground electrode aperture. Arc power became a major source of filament heating therefore arc current stabilizing proportional integral derivative (PID) loop parameters needed to be adjusted accordingly. It is not clear what is the dominating factor limiting the beam current at 60 mA.

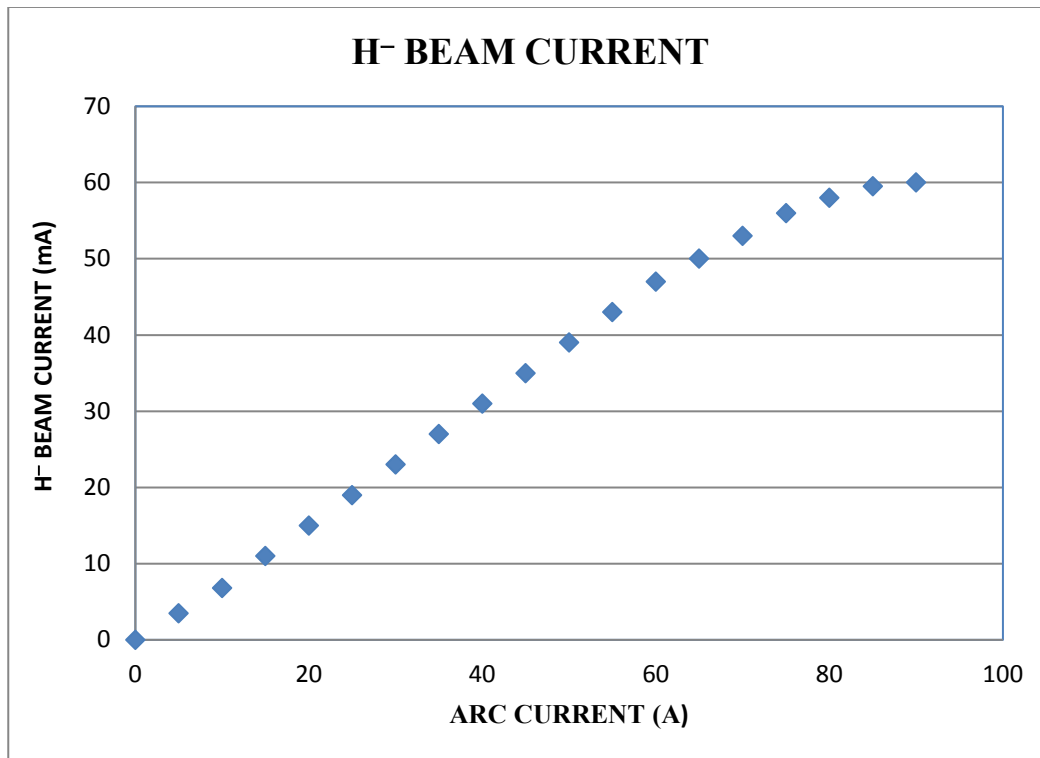


Figure 10: Throughout the high current test arc voltage was kept at 140 V. All other parameters including hydrogen flow, PE and EE voltages were adjusted to optimize the Faraday cup current.

Measured 4rms emittance for 30mA was about $60 \pi \cdot \mu\text{rad}$ at 20kV and it is shown in figure 11. An accurate emittance above 30 mA of H⁻ current was difficult to measure due to power related slit opening (0.025mm) deformation issues of the emittance scanner. An emittance scanner able to handle H⁻ current above 30 mA is being assembled. Apertures were opened up to eliminate beam cutting issues. A pepper pot was installed in order to measure emittance values with reduced beam power. Detailed emittance results will be published separately.

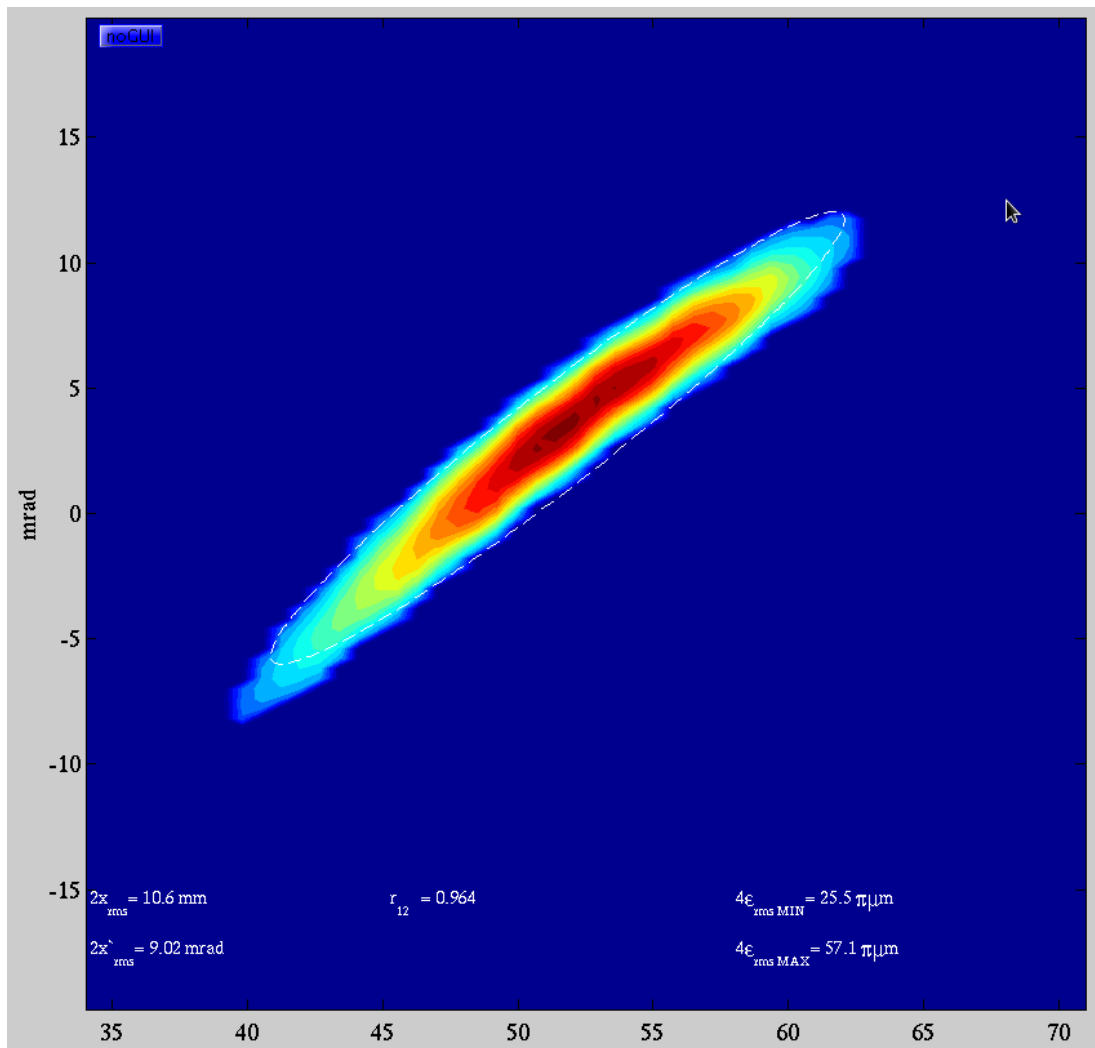


Figure 11. An emittance measurement of a 30mA H⁻ beam at 20kV

2.14.11 Filament lifetime studies

Tantalum and tungsten filaments with various sizes and shapes were studied. Tantalum filaments produced H⁻ beams that were both brighter and of higher current but degraded faster than tungsten at higher arc currents. Detailed discussion regarding filament shapes and sizes is beyond this paper's scope.

Since the filament lifetime is measured in months, it is difficult to measure each filament precisely. The lifetime of the filament can be estimated by the decrease in heater current while keeping a constant arc current using software (PID) loop. It is presented as amperes per day with the usable filament current range (see Figure 12). From these numbers, the filament lifetime can be extrapolated with reasonable accuracy. The filament used for highest H⁻ current (60 mA) is shown in Figure 13. In this case, over 800 A of filament current is needed to initiate plasma with an arc current and voltage at 90 A and 140 V respectively. After the plasma is ignited the filament current has to be reduced to less than 400A due to additional filament heating by the arc power. In order to produce 20 mA of H⁻, a single filament (blue in figure 12 – TRF200-20) is sufficient. Up to 5 A of arc current none of the filaments showed any measurable decay while the largest

filament did not show any measurable decay when tested with up to 15 A arc current. The results obtained can be applied to medical cyclotrons as well as other H^- machines with filament based ion sources and reduce maintenance time significantly.

The smallest filament tested is now installed in the TRIUMF 500 MeV cyclotron and has been running for over 6 months with 7 A arc current and 100 V arc. This is the first time in the cyclotron's history that the filament could last from shutdown to next shut down without replacing it. Filament decay of the main cyclotron H^- ion source is shown in Figure 14. Note the beam off time in the plot is for cyclotron shutdown activity related work and not related to the source.

The same filament was installed in the TR13 cyclotron and running nearly a year at 4A and 100V arc without seen any noticeable filament degradation.

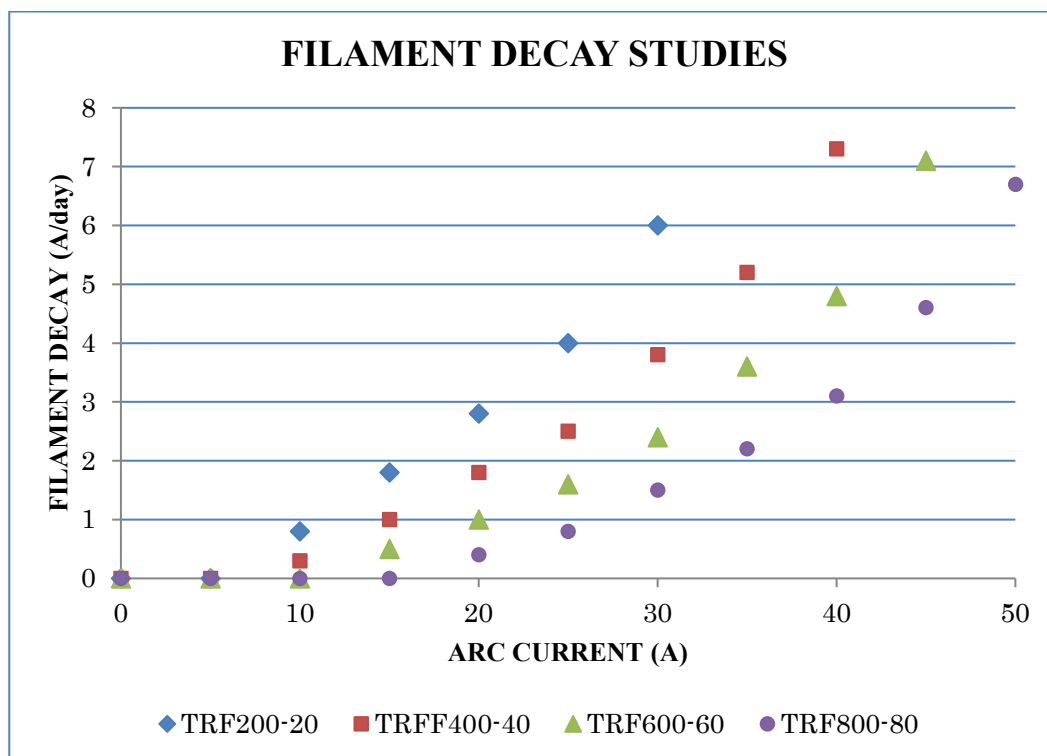


Figure 12: Four different filaments were developed for different arc currents and characterized. TRF200-20 a single filament is suitable for up to 20 A arc and the filament usable current range is 200 A. Filament lifetime calculated by usable filament current divided by filament decay at required arc current. Larger the filament, the longer the filament life but compromise must be made depending on the current available for the filament at the source terminal.



Figure 13: Cathode (TRF800-80) capable of producing up to 90 A at 140 V arc is made of four 2.5 mm diameter Tungsten filaments. Note the cone loss cusp lines from each filament on the back plate.

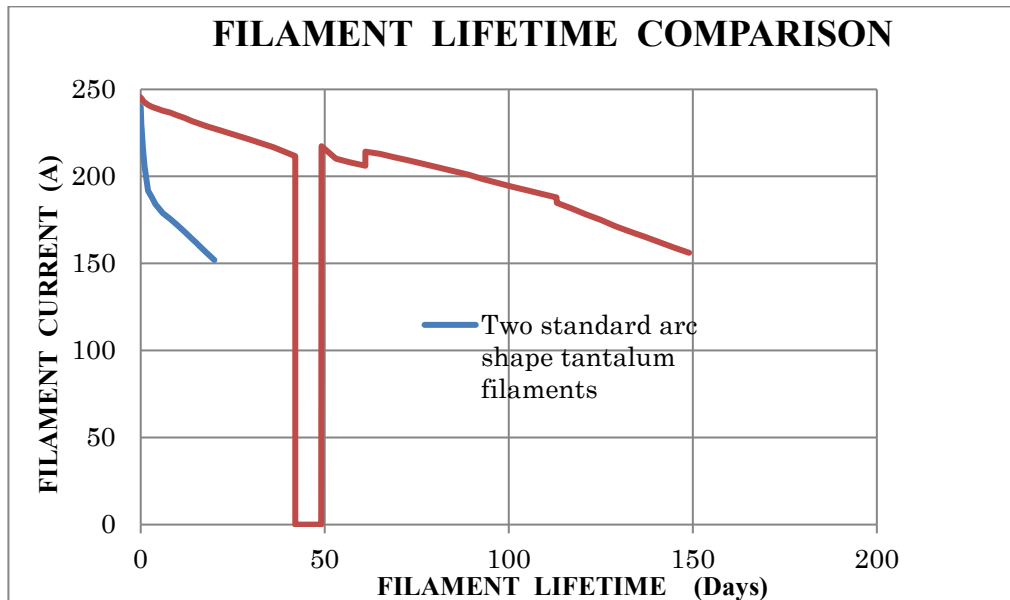


Figure 14. Superimposed filament decay data from the TRIUMF 500 MeV cyclotron ion source. The blue line indicates the standard two of 2 mm diameter arc shaped filaments. The red indicates the newly developed single tungsten filament of 2.5 mm diameter. In both cases the arc current and arc voltage are 7 A and 100 V respectively. The extracted H^- current in this case was 1.2 mA at 12 kV.

2.14.12 Conclusion

With the installation of a new high power filament in the H^- ion source the output current has been increased up to 60 mA with 90 A at 140 V arc. Four different filament configurations were tested for four different arc current ranges and their decay is presented. The new filament design allows operation of the main H^- ion source at the 500

MeV cyclotrons for more than 6 months at 7 A arc current, compared to 3 weeks with the old design. The same filament was installed in TR13 cyclotron and is running nearly a year without noticeable degradation. The results will benefit machines with filament based H⁻ ion sources including medical cyclotrons. To achieve the high output current the magnetic field configuration and extraction optics of the source had to be upgraded as well. Filament lifetime studies and high current H⁻ beam studies have been concluded. Low current (up to several mA) and high brightness beam studies, which are more important for the operation of the TRIUMF cyclotron will continue.

2.14.13 Acknowledgment

TRIUMF receives federal funding via contribution agreement through the National Research Council of Canada.

2.14.14 References

- [1] S. Korenev, Proceedings of Cyclotrons Vancouver, TUPPT018, (2013)
- [2] D. Yuan, AIP Conference Proceedings 210p, 323 (1990)
- [3] G. Dutto, RSII Volume 65 Issue 4, (1998)
- [4] F Benard, Journal of Nuclear Medicine 55 1017p, (2014)
- [5] B. Milton, Particle Accelerator Conference V28 N19, (1995)
- [6] G. Cojocaru, Proceedings of Cyclotrons, Vancouver BC, Canada, 446(2013)
- [7] M. Bacal, Applied Physics Reviews 2, 021305 (2015)
- [8] J. M. Wadehra and J. N. Bardskt Phys. Rev. Let. Vol. 41 1078p (1975)
- [9] H. Tawara Journ. Physical Chemistry Reference Data Vol. 19 No.3 (1990)
- [10] K. Jayamanna, 1987 PhD Thesis, UDN Press, Moscow, No: YDK 621.039.643
- [11] K. Jayamanna, Proceedings of Second EPAC, Nice 647p (1990)
- [12] T. Kuo, Review of Scientific I 67-3 1314p (1996)
- [13] K. Jayamanna, Proceedings of Cyclotrons (2013), Vancouver BC Canada, 198p (2013)
- [14] P. W. Allison, IEEE Trans. Nucl. Sci Ns 30, 2204 (1983)
- [15] D. Yuan, AIP conference proceedings 210, 603 (1990)
- [16] K. Jayamanna, Review of Scientific Instruments, Volume 67, Issue 3, (1996)

2.15 Laser Ion Source

Masahiro Okamura

Mail to: okamura@bnl.gov

Brookhaven National Laboratory, Upton NY 11973 USA

(Style:BNL)

2.15.1 Introduction

Laser ion source (LIS) is a simple, powerful and high brightness pulsed ion source. Some people may think that a LIS is uncontrollable and could have poor emittance without good reproducibility, since the initial plasma is created by an unpredictable

explosion. But this opinion is incorrect. A LIS has many advantages and is potentially being adopted by many accelerator facilities. Due to its very simple configuration, a LIS matches not only to large scale facilities but also to small accelerators. A LIS has several advantages listed below.

1. Ionizing energy is given only by a laser light. We don't need to have power source at a high voltage terminals. A LIS can be mounted at the terminal easily including static electric accelerators.

2. Ionization occurs in nanoseconds range and the plasma cannot expand much within the ionization period. This means that we don't need to provide any plasma confinement forces.

3. Beam current can easily reach more than 100 mA with a table top laser system. Probably it is the most powerful heavy ion source at a reasonable budget.

4. Very high charge state can be effortlessly achieved from light to medium mass species.

5. Ionizing plasma's volume is very small and far away from the extraction electrode. Thus, we can obtain very uniform beam from well cooled expanded plasma. This feature enables us to extract a minimum emittance beam with a great uniformity.

6. Due to the plasma's moving velocity, we can extract more intense beam than that predicted by the static three halves law.

7. Direct plasma injection scheme (DPIS) can be applied.

Of course, there are some drawbacks.

1. Beam pulse duration is from one to hundred microseconds only. Only pulsed ion beams can be delivered.

2. In case of high charge state production mode, the ion beam has momentum spreads. (But this can be compensated.)

3. To achieve high charge state ions from very heavy materials, a powerful laser system is demanded.

Since the first idea of an ion source using laser ablation plasma arose, almost fifty years has already passed. However, LIS has not widely spread out yet. We hope that this article will encourage more scientists and engineers to become familiar with Laser Ion Sources.

In this article, we only discuss about laser ablation plasma ion source. A selective LIS, which uses resonant ionization process, and a target normal sheath acceleration (TNSA) LIS are excluded.

2.15.2 Basic principle of LIS

A typical laser ion source consists of a laser system, a target and an extraction electrode like shown in Fig.1. Here we assume that laser pulse duration is from 5 ns to 10 ns range with highly focused condition. The spot size is typically from 10 to 100 microns to obtain highly charged ions. In the very early part of the laser irradiation period, the laser energy is not absorbed efficiently. Once an initial plasma is formed, however, the laser energy is started to be converted to the electron temperature by classical absorption process and then plasma is rapidly heated. Due to the collisions with ions and electrons, stepwise ionization occurs. Simultaneously, the plasma starts to expand. At the end of laser irradiation period, the front end of the plasma reaches a few mm for the target surface, which is larger than the laser spot size. After finishing laser irradiation period, the plasma

still keeps expanding three dimensionally and becomes colder and colder. The entire expanding plasma moves away from the target surface. In case of highly charge state ion production, the velocity of the plasma front reaches around 100 eV/u. When one prefers to have lower charge state ions, the laser spot size can be increased up to a few mm size by changing the laser focusing condition and the plasma temperature is lowered. The heating stage plasma's shape may be very thin, because the plasma expansion becomes slower and the plasma front proceeds less than 1 mm. If the plasma is optimized to provide singly charged ions, the velocity of the plasma front reaches approximately 1 eV/u.

Now we pay attention to the trajectory of each ion. At the plasma heating stage, the size of the formed plasma can be assumed as a pin point, because its size is negligible compared to the drift length shown in the figure. So that, in the plasma expansion stage, all the ions start from the identical point in the space at the surface of the laser target. Then, each ion moves straight with constant velocity while drifting, and the expansion occurs in a three-dimensional space. The difference in arrival times of the fastest and slowest ions at the extraction point defines the ion beam pulse width. Although the laser irradiation is very short (~ 10 ns), the pulse width of the extracted ion beams can be extended to the microsecond scale.

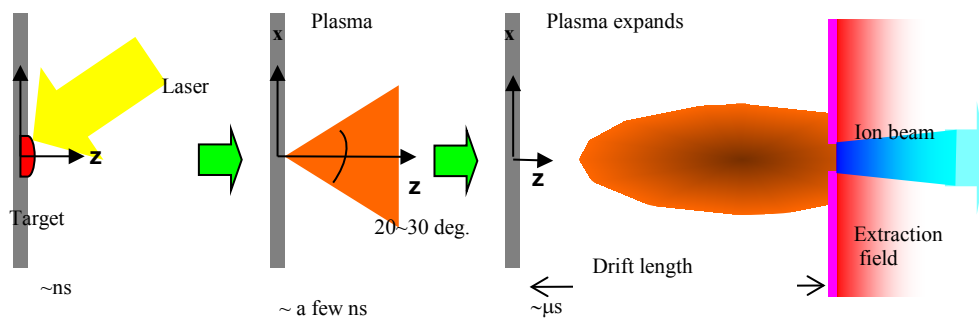


Figure 1: Principle of a laser ion source.

2.15.3 General Description

2.15.3.1 Laser System.

Historically, CO_2 lasers have been used in many institutes. The advantage of the CO_2 laser is its high energy output and cooling capability. It can be operated even in CW mode and widely used in the industrial machining field. An example of the most powerful CO_2 LIS was demonstrated in 2003 by CERN and ITEP group. They developed a gigantic 100 J laser [1] system, which could deliver lead ions with charge states from 19+ to 32+ and the charge states 26+ and 27+ showed the highest yield.

A typical wavelength of a CO_2 laser is about 10 micrometers, which is in the infrared spectral region. Therefore, a vacuum window made from zinc selenide or salt crystal is

used, which is transparent for the wavelength. A CO₂ laser has a medium gas mixture and requires a discharge to obtain a population inversion. Due to the discharge process, special attention is required to obtain good stability. The pulse length is typically more than a few tens of nanoseconds. Within this relatively long laser pulse period, the laser is continuously transferring the energy to the plasma at near the target's surface, so that the plasma is not heated evenly. Therefore, the momentum distribution of the ions in the plasma does not represent a shifted Maxwell-Boltzmann distribution. A CO₂ laser is one of the candidates of driver lasers.

We have used Q-switched Nd-YAG lasers for ion source application for more than ten years. Many reliable models in a reasonable cost range are available in the market. The fundamental wavelength and typical pulse duration are 1064 nm and 6~10 ns respectively. The laser energy can be controlled easily by changing the interval between flash lamp trigger and Q-switch timing or the flash lamp's excitation voltage. To minimize undesired target damage, a contrast value of the Q-switch is important so that a laser leakage before opening the Q-switch may heat the target before starting the main laser pulse. The major optics parts including lenses, mirrors and Faraday isolator can be obtained at reasonable costs. Figures 2 and 3 show typical ion beam profile and charge state distribution of aluminum plasma using 6 ns, 1064 nm, 840 mJ Nd-YAG laser. The beam corrector with 5 mm aperture was placed 300 mm away from the target surface. We have tested shorter pulse length lasers including a sub nanosecond laser system, which

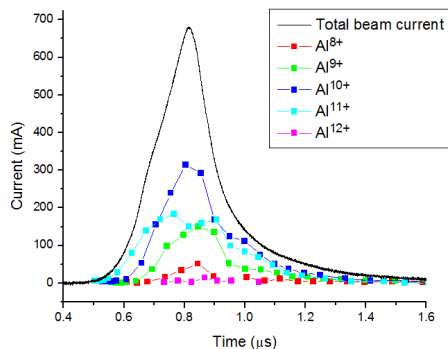


Figure 2: Current profile.

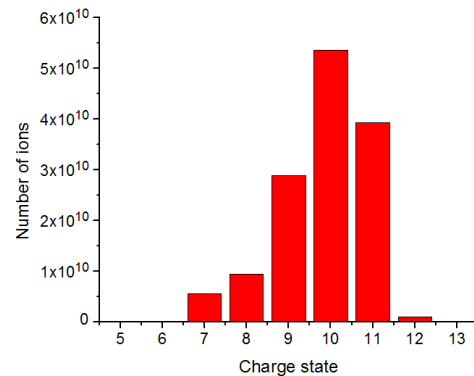


Figure 3: Charge state distribution.

has a stimulated Brillouin scattering (SBS) cell. Some reports indicate that the laser power density around 10^{14} W/cm² may be able to provide very high charge state ions [2, 3] and the sub nanosecond laser was supposed to provide a close value to the singular working point. Unfortunately, so far, we did not find yet significant advantages comparing to a typical Nd-YAG laser. We could observe small amount of higher charge state ions but total quantity of the plasma reduces one order less than that of the plasma created by typical nanosecond lasers. We suppose that the laser pulse length may be not enough to achieve temperature equilibrium condition in the plasma heating stage.

2.15.3.2 *Target*

Unlike other ion sources, a LIS can provide very versatile species except helium. All solid material can be ionized by laser irradiation. In Brookhaven National Laboratory

(BNL), we regularly provide Li, B, C, O, Al, Ca, Si, Ti, Fe, Zr, Nb and Au to the user facilities from a LIS. Proton and Oxygen beam can be easily obtained from Zr-hydride and alumina targets. We have also demonstrated how to obtain good beams from frozen Ne and Ar targets using a cryocooler head.

Due to laser ablation, the material at the target surface is consumed. In case of high charge state production mode, we need to focus laser beam at the surface. The material contributes to create high temperature plasma is at only the surface layer of the target which is typically less than 500 nm on thickness. However, heat from the plasma induces subsequent ionization and evaporation of the material from the deeper layer and crater is formed which may reach down to 200 μm of depth. Once a crater is formed, we cannot apply second laser shot on the crater since the focal spot of the laser is in the empty space in the crater and the effective laser power density is decreased. It also influences on the beam stability. To avoid these negative effects, target needs to be scanned to provide a fresh target surface for every laser shot.

For the low charge state production mode, laser power density on the target surface should be controlled to have desired charge state in the plasma. For example, if we like to have 1+ charge state beam, the laser power density should be adjusted between 2×10^8 and 10^9 W/cm^2 for the efficient ion production. The laser spot size on the target surface would be several mm in diameter, when we use a several hundred mJ of laser energy. In that case, the damage on the target surface caused by a single laser irradiation is minor and we can apply multiple shots on the same spot up to several hundred times. After many irradiations, the surface becomes damaged by ablation. The remaining melted surface layer after the laser irradiation is rapidly resolidified. During the very short time that the target material is liquefied, surface tension causes blisters formation. To minimize the effect of the blisters, the target can be slowly scanned for long term maintenance-free operation.

2.15.3.3 *Plasma Drift Length*

As mentioned above, an ablation plasma plume expands in three dimensions in the space. When the head of the plasma plume reaches the extraction voltage gap, ion beam formation occurs. Ion beam generation continues until the end of the plasma plume reaches the extraction electrode. If the distance from the target to the extraction point is extended, the plasma expands more. Therefore, more distance makes longer ion pulse and thinner ion density. We call the distance as “plasma drift length.” The plasma drift length is important parameter to characterize the ion beam properties. The ion pulse width is proportional to the length and peak current amplitude is inversely proportional to the cube of this value. Figure 4 shows sample relationships of peak currents and pulse widths as a function of the distance.

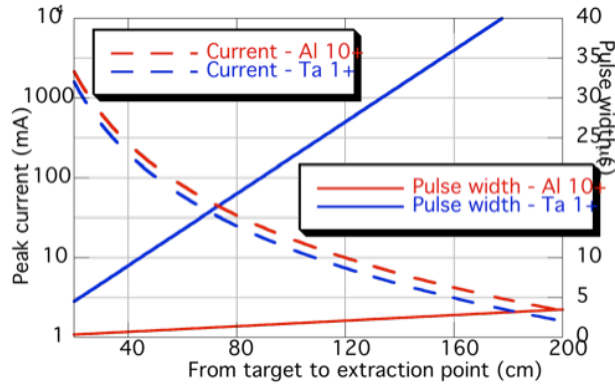


Figure 4: Ion beam peak currents and ion beam pulse width vs. plasma drift length.

2.15.3.4 Ion Beam Extraction

The expanded plasma moves to the beam extractor and the strong electric force pulls the ions out from the plasma at the extractor. It is well known that the maximum beam current is limited by the space charge [5,6]. For a static plasma, the space charge limit is expressed by the famous three halves law as,

$$J = \frac{4}{9} \varepsilon_0 \sqrt{\frac{2q}{m}} \frac{V_a^{3/2}}{d^2} \quad (1).$$

In the formula, J , q , m , V_a and d are the limiting current density, charge of a particle, mass of a particle, applied voltage between the extraction electrodes and the distance of the electrodes, respectively. This formula is derived from the Poisson's equation with zero initial velocity of the charged particles. In case of a LIS, the ions already have velocity toward the extraction region and this makes a slight difference in the formula as [4,5,6],

$$J = \frac{4}{9} \varepsilon_0 \sqrt{\frac{2q}{m}} \frac{(\sqrt{V_0} + \sqrt{V_0 + V_a})^3}{d^2} \quad (2),$$

where V_0 is the voltage corresponding to the initial velocity of an ion in the sheath at the starting electrode. In case of high charge state ion production, the V_0 goes up to a significant value and the maximum beam current can be increased several times.

For rapid cycling beam extraction, the evacuation system at the extractor needs to be carefully designed to achieve and maintain good vacuum condition. In addition to the main plasma pulse, a neutral vapor reaches the extraction area those may cause electron recombination of ions and also may trigger discharges. A sample design of the LIS extraction system is illustrated at Fig. 5. This is being used to provide low charge state ion beams in BNL and the measured typical emittance is 0.043π mm mrad (RMS normalized, Au^{1+} beam).

Here, we like to emphasize that LIS does not have a background magnetic field. This condition helps to minimize beam emittance from a LIS.

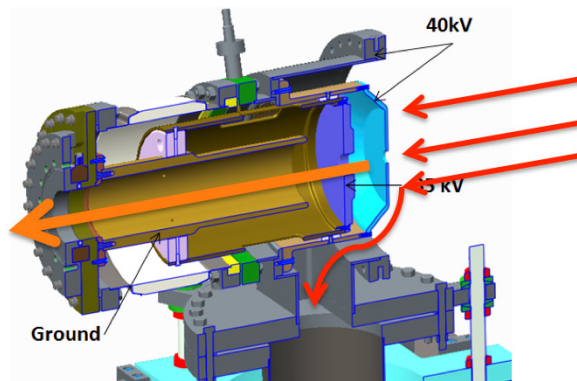


Figure 5: Ion beam extractor used in the low charge state LIS in BNL. The system consists of three electrodes. The first gap determines the extraction voltage and the second gap is used to achieve required platform voltage. This source is not equipped with backstreaming electron suppression electrode.

2.15.3.5 *Direct Plasma Injection Scheme*

We have originally developed a unique technique called direct plasma injection scheme (DPIS) since 2001 [7]. A LIS can provide exceptionally intense beam, nevertheless the beam loss at the beam transport line between the LIS and first stage accelerator restricts usable beam currents. This is due to strong space charge force with high current and low velocity transport condition. DPIS can overcome this issue. The DPIS consists of a LIS and radio frequency quadrupole (RFQ) linear accelerator. As we know, ablation plasma has an initial velocity normal to the laser target surface. This means that we don't need to extract ion beams to transport the beam to an RFQ, which is commonly used as a first stage accelerator. Since plasma travels by itself, the ions contained by the plasma can be transported as neutral state. Then, the plasma is directly injected into the RFQ cavity and the ion beam is extracted at the entrance of the RFQ.

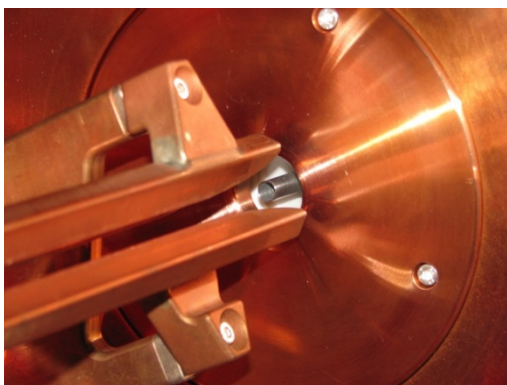


Figure 6: Plasma injection point.

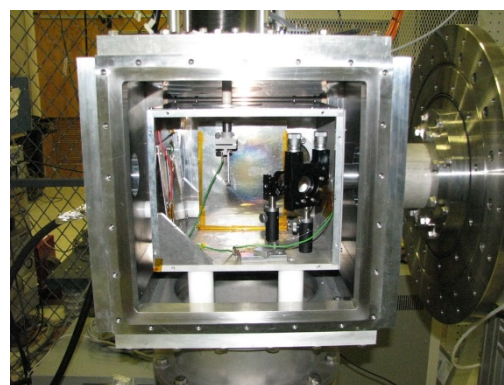


Figure 7: Laser illumination box.

Figure 6 shows the inside of the RFQ cavity. The stainless steel nozzle is located at the beam axis of the RFQ. The nozzle is isolated and an injection voltage is applied to it. The beam emission surface is slightly inside of the nozzle. The nozzle is mechanically and electrically connected to the high voltage box, which is surrounded by the grounded

vacuum vessel as shown in Fig. 7. The laser light is guided and is focused on the target material in the high voltage box and the induced plasma expands in the space enclosed by the same potential metal wall up to the end of the nozzle. The applied high voltage is not exposed to the outside of the ion source. So that neither safety cage nor platform is required.

As mentioned, the DPIS eliminates space charge effect at the low energy beam transport line and high brightness beam can be effortlessly transferred to an RFQ which has strong transverse focusing force. DPIS has another advantage to handle high current beams. Figure 8 shows equipotential lines in an RFQ with DPIS. The intervals of the equipotential lines are very dense at the edge of the nozzle. Therefore, the electric field strength at the beam extraction region is much enhanced than orthodox parallel plate shape electrodes. Using DPIS, peak current after the RFQ can be achieved more than 50 mA easily.

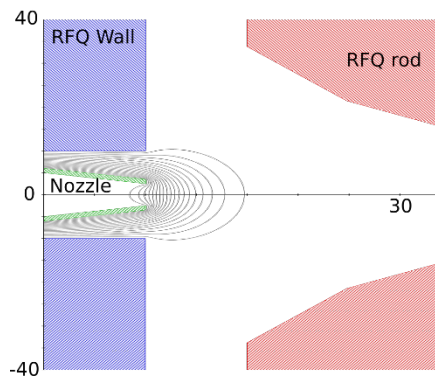


Figure 8: Cross-sectional view of typical DPIS setup with equipotential field lines.

2.15.3.6 *Beam current manipulation*

A LIS has very simple structure. In other words, it does not have many knobs to adjust the ion beam property. The charge state distribution can be adjusted by the focal condition of the laser light or laser energy. For instance, defocusing the laser or reducing the laser energy can lower the most abundant charge state. There had been not much adjustment procedures in a LIS, when the system is in operation.

In 2009, we established a beam current enhancement technique by applying weak solenoid field on the plasma drift section [8]. When the plasma is in expanding stage, it spreads three dimensionally. However, by overlaying an axial magnetic field on the expanding space, the transverse expansion of the plasma can be restricted.

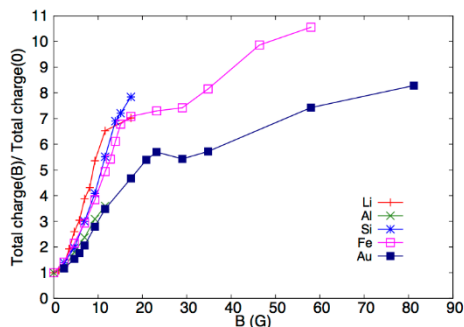


Figure 9: Total charge enhancement.

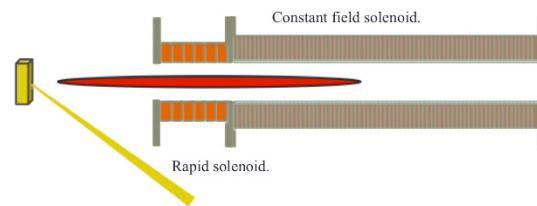


Figure 10: Schematic view of solenoids

Figure 9 shows the effect of a static solenoid field, which is being used in the low charge state LIS of BNL. The solenoid was wound around the plasma drift pipe, which has 76 mm of I.D. and 3.0 m in length. This is a very convenient knob to adjust the current of the entire beam pulse. In the LIS, another short solenoid was recently installed to control the beam current profile as shown in Fig. 10. This short solenoid is ramped up to 60 Gauss in 10 μ s. The I.D. and length of the short rapid solenoid are 75 mm and 56 mm respectively. This solenoid can enhance only within a certain time slice of an ion beam pulse. So, this is another convenient knob to tailor a beam current profile [9,10].

Figure 11 shows a setup of a long solenoid for DPIS acceleration test using a 1.0 J 6 ns 1064 nm Nd-YAG laser. We tested carbon beam production. The I.D. of the solenoid is 76 mm and other dimensions are indicated in the figure. At 900 Gauss of solenoid field, C^{4+} and C^{6+} were accelerated up to 100 keV/u. A single laser shot provided 36 mA at peak, 2.1 μ s of pulse width 1.2×10^{11} particles C^{4+} [11] and 33 mA at peak, 1.6 μ s of pulse width 5.2×10^{10} particles C^{6+} after the RFQ. The total accelerated beam current could be easily adjusted by changing the solenoid field strength. The charge state switching was done by finely adjusting the target position.

Solenoid is a very effective tool to control the plasma expansion in the LIS.

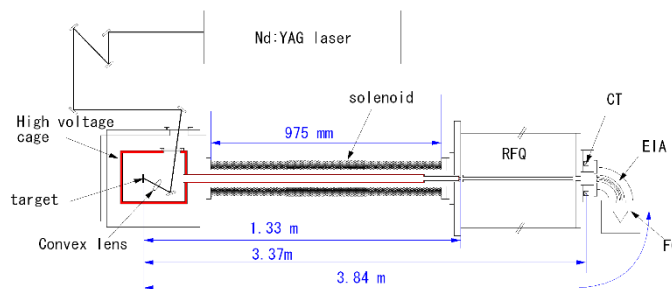


Figure 11: DPIS set up for carbon acceleration with solenoid.

2.15.3.7 Summary

A LIS can provide high current, high brightness beams with wide variety of charge state from many species. The structure of the LIS is simple and the illumination chamber is easily isolated electrically. Therefore, a massive safety fence can be eliminated. In BNL, we are regularly operating both low charge state source and high charge state source with DPIS with good stabilities. Solenoid plasma manipulation was established and a LIS has improved flexibility. When you consider building a LIS don't hesitate to contact us.

2.15.4 Acknowledgement

This work was performed under contract DE-AC02-98CH1-886 with the auspices of the DoE and National Aeronautics and Space Administration. The author thanks to colleagues in BNL, RIKEN and TITech.

2.15.5 References

1. B. Sharkov and R. Scrivens, “Laser Ion Sources”, IEEE Plasma Science, 33-6(2005), 1778.
2. L. Laska et al., “Charge-state and energy enhancement of laser-produced ions due to nonlinear processes in preformed plasma”, APPLIED PHYSICS LETTERS 86, 081502 2005.
3. L. Laska et al., “Review of laser ion sources developments in Prague and production of q over 50+ ions at Prague Asterix Laser System (invited)”, RSI, 75-5(2004), 1546.
4. G. Jaffe, “On the Currents Carried by Electrons of Uniform Initial Velocity”, Phys. Rev. 65 (1944) 91.
5. M.S. Benilov, “The Child–Langmuir law and analytical theory of collisionless to collision-dominated sheaths”, Plasma Sources Sci. Technol. 18 (2009) 014005.
6. Liu and R.A. Dougal, “Initial velocity effect on space-charge-limited currents”, S J. Appl. Phys. 78 (1995) 5919.S.
7. M. Okamura, T. Katayama, R. A. Jameson, T. Takeuchi, T. Hattori, N. Hayashizaki, “Carbon beam acceleration using a simple injection method into an RFQ”, Nuclear Instruments and Methods in Physics Research B 188 (2002) 216–220
8. M. Okamura et al., “Magnetic plasma confinement for laser ion source”, RSI 81, 02A510 (2010)
9. M. Sekine et al., “Plasma shape control by pulsed solenoid on laser ion source”, Nuclear Instruments and Methods in Physics Research A 795 (2015) 151–155
10. M. Okamura et al., “PERFORMANCE OF THE LOW CHARGE STATE LASER ION SOURCE IN BNL”, Proceedings of NAPAC2016, Chicago, IL, USA MOA4IO01
11. T. Kanesue, Y. Fuwa, K. Kondo, and M. Okamura, “Laser ion source with solenoid field”, Applied Physics Letters 105, 193506 (2014)

2.16 Sources for Low Charge State Radioactive Ions

Friedhelm Ames

Mail to: ames@triumf.ca

TRIUMF, 4004 Wesbrook Mall, Vancouver BC, V6T 2A3, Canada

2.16.1 Introduction

There are several other methods to produce beams of radioactive ions. However, the following will concentrate mainly on the ISOL (Isotope Separation On Line) technique. Here a high energy particle beam hits a solid (or sometimes liquid) target to induce nuclear reactions in the target material. The target is kept at a high temperature to allow the reaction products to diffuse out and they can enter an ion source. Requirements for the ion source have been summarized nicely in an early review article published 1996 by R. Kirchner [1]. The main difference to ion sources for stable ions is the “feed material”. Its supply is limited and often short lived. That means the ionization process must be efficient and fast. Depending on the target and driver beam in general many elements with several stable and radioactive isotopes are produced at the same time and released

from the target. The release can be in atomic or molecular form as neutrals or sometimes already as ions. As most experiments require pure beams either the ionization process should be element selective or the beam quality of the extracted beam should allow for a good mass resolution in the following mass separator. In most cases both are necessary to achieve the required purity. Purity still remains one of the main challenges for radioactive beam facilities. Typical intensities for the desired isotopes range from a few ions per second to several nA with half-lives from ms to years. The lower limit is mainly determined by the diffusion out of the target. The source is operated in an environment of high radiation fields and high temperature on a high voltage terminal usually at several 10 kV. It has to be directly connected to the production target to allow the delivery of short lived species. That means it must be robust and reliable as it cannot be accessed after the start of the target irradiation. A typical lifetime is several weeks. It is determined by the lifetime of the target and experimenters need for a specific beam. After removal the source and the target have to be disposed together as radioactive waste.

As there is no universal source which can yield to a high efficiency and selectivity for all elements several different types are in use or under development at radioactive beam facilities. A hot cavity surface ion source works very well for elements with an ionization energy up to about 6 eV. All other elements can in principle be ionized by sources using some kind of electron impact. Most commonly are FEBIAD (Forced Electron Bombardment Arc Discharge) ion sources or ECR (Electron Cyclotron Resonance) ion sources. Both sources work well for gaseous elements or volatile molecular compounds. Although they can be optimized to reach a high efficiency, it is on the expense of a limited selectivity. Resonance laser ionization of the neutral atom can achieve high element, or in some cases even isotopic selectivity. The efficiency is mainly determined by the availability of suitable lasers for a specific element. It is used both in combination with a hot cavity or a radiofrequency quadrupole to confine and guide the ions. Basic principles of those ion sources have been developed already around 1980 mainly at GSI and modifications have been implemented at different facilities worldwide since then.

2.16.2 Surface ion sources

Surface ionization in a hot cavity has been described in detail by R. Kirchner in [2,3]. The efficiency for the ionization on a hot surface can be described by the Langmuir equation. In a sufficiently hot cavity in thermal equilibrium it can be increased due the formation of a thermal plasma. The wall potential formed by this plasma repels ions and thus the efficiency for extracting them is enhanced. The enhancement factor depends on the ratio of the number of wall collisions of the neutral atoms and ions in the cavity, which is given by the temperature and geometry. Atoms are not affected by the wall potential and thus can make more wall collisions where they can be ionized. As an example, an enhancement factor up to 150 has been reported in [3].

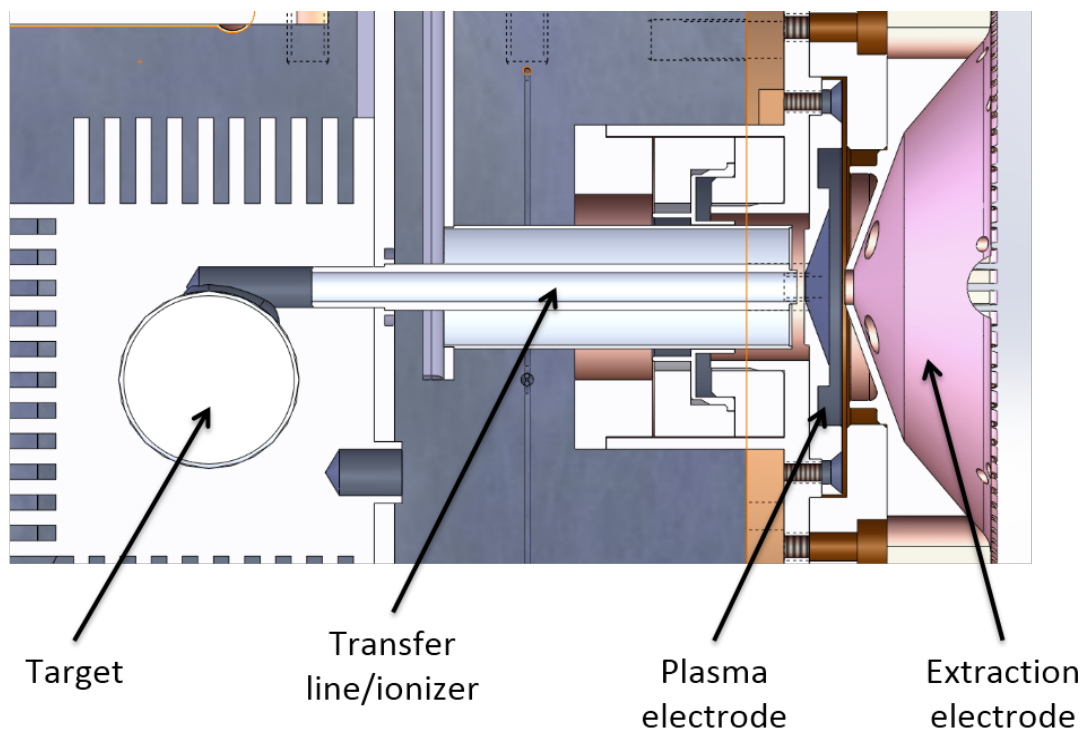


Figure 1: Surface ion source design as implemented at the ISAC facility at TRIUMF, ground electrode not shown.

In most on-line installations the geometry of such a source has been simplified to just a tube which can be heated by passing a high current through it. On one side it is connected to the target to allow the reaction products to enter. On the other side an extraction electrode provides an electric field to extract ions and eventually they can be accelerated to the desired energy. The ionization efficiency is enhanced by either coating the inside of the tube with a high work function material or inserting a Re or W foil. The design can reach close to 100% ionization efficiency for alkaline elements and several % for elements with an ionization energy around 6 eV. Figure 1 shows a design how it is used at the ISAC facility at TRIUMF.

2.16.2.1 *FEBIAD ion sources*

The principle of operation of a FEBIAD ion source has been described already in [2] and [4] for the sources used at the on-line facility at GSI. It is an arc discharge ion source based on a Nielson type ion source, which has been used in early ISOL facilities like for example at LISOL in Louvain-La-Neuve [5]. Here the target material was inside the plasma chamber of the source. For the FEBIAD the filament of the original Nielson source was replaced by a cathode with an acceleration grid in front of it. Electrons are accelerated to about 200 eV into the plasma chamber, which acts as the anode. The source is embedded in the field of a solenoid to confine the resulting plasma. The source is operated at a low gas pressure, which is provided either by the products evaporating out of the target or an additional gas feed. Aspects concerning the operation at different gas loads are discussed in [6]. For the first installations at GSI the target was again placed directly inside the source. For the coupling to a thick target like at ISOLDE or TRIUMF the radioactive isotopes diffuse out of the target through a transfer tube. The end of this

transfer tube then acts as the cathode. The implementation of the source at the ISOLDE facility at CERN especially the coupling of the source to the target can be found in [7] and the implementation at TRIUMF in [8]. The design from TRIUMF is shown in figure 2. For noble gases efficiencies up to several 10% have been reported.

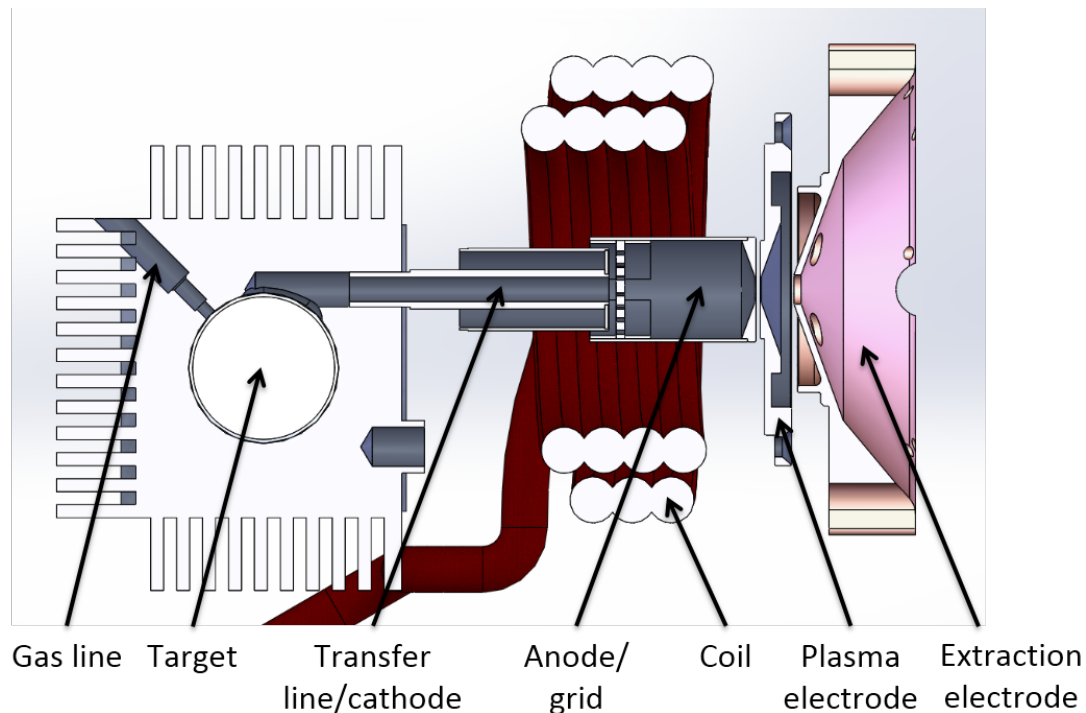


Figure 2: FEBIAD ion source design as implemented at the ISAC facility at TRIUMF, ground electrode not shown.

The separation of the target and the ion source allows the implementation of additional purification methods. The temperature of the tube can be controlled to allow only volatile species to reach the source. The material may be chosen to act as a chemical suppressor for certain species.

2.16.3 ECR ion sources

Electron cyclotron resonance ion sources have been proven to produce high intensity beams of many mainly gaseous species and different charge states. The on-line operation requirements do not allow very complicated designs. Together with the high and often variable gas pressure, which may be dominated by the outgazing of the target, the source is limited to the production of singly or low charged ions. Therefore, the first on-line tests have been done with sources operating at relatively low frequency at 2.45 GHz. The main challenge in the design is the limited space available for the creation of the magnetic confinement fields. The first on-line application used permanent magnets and was based on the Minimono source developed at GANIL [9]. It was adapted to the ISOLDE target design [10]. At higher driver beam power, the resulting neutron fields reduce the lifetime of permanent magnets and coils must be used. Designs have been developed for ISOLDE [11] TRIUMF [12]. Although some experiments could be done with radioactive noble

gas isotopes from those sources, the efficiency which could be achieved on-line was low. The main reason is that due to limited space and available power for the coils confinement of the plasma had to be compromised. The relatively high operating pressure range increased the transit time [13] so that short lived isotopes could not be observed. For the SPIRAL I facility at GANIL a source based on the NANOGUN III design has been used. The source is built with permanent magnets and operated at 10 GHz [14,15]. It can directly produce higher charge states, which can be post-accelerated. Beams from radioactive isotopes of the noble gases He, Ne, Ar and Kr and of N, O and F have been produced with this source. Parts of the source magnets are reused after a cooldown period of about 2 years after irradiation. Although, some degradation of the permanent magnets due to the neutron fields during operation has been observed.

Several design studies and tests have been done in recent years to reduce the volume of the source and thus increase the efficiency for short lived isotopes. The magnetic field configuration has been changed from the "standard" ECR design. Two sets of coils are used to provide radial confinement without the use of additional multipoles. At GANIL the design is for a 2.45 GHz source [16], whereas at TRIUMF the source can be equipped with different cavities to allow operation in the range of about 3.5-5.6 GHz [7,17]. Off line test with those sources have demonstrated the ability of reaching high efficiency for volatile species.

2.16.4 Resonance ionization laser ion sources

Using resonance ionization with lasers for ion sources for radioactive ion beams at ISOL facilities has been first proposed in [18] and the principle is described in detail in [19]. Laser light is used to ionize atoms via stepwise excitation of atomic states. The final ionization step yields either non-resonantly into the continuum above the ionization energy or to increase the cross section for this process excitation into an autoionizing state or a high-lying Rydberg state can be used. In the latter case the electron is removed either via collisions, black body thermal photons or field ionization in sufficiently high electric fields. With up to 3 atomic resonances used the process is highly selective for the desired element and thus significantly increases the purity of the beam compared for example to ionization processes using electron impact, like in gas discharge and ECR ion sources. The ionization process occurs in a hot cavity. Atoms are confined and thus have a higher chance to interact with the lasers before they are extracted through a small extraction hole. High repetition rate (~10kHz) pulsed lasers are used to provide enough power especially for the last ionization step. With enough laser power to saturate all excitation steps, the efficiency is mainly limited by the laser repetition rate. Several 10% can be reached. In some cases, the thermal population of low lying atomic states or a large hyperfine structure splitting exceeding the doppler broadening of the lines in the hot cavity, can reduce the efficiency as not all atoms can be excited. However, in case of a large hyperfine structure splitting or isotope shift it can be used to further purify the beam by having an isotope or isomer selective ionization. Laser ionization has been implemented at most of the radioactive ion beam facilities over the past years. The development was mainly driven by the progress in laser technology to provide lasers with sufficient average power and high repetition rate. The originally used copper vapor and dye laser systems, which has been used for example at ISOLDE, have been replaced by fully solid state laser systems, which are more reliable and easier to operate. Similar designs have been developed for TRIUMF, ISOLDE and GANIL and latest results are summarized in [20],

[21] and [22]. In both cases the surface ion source design is used, and the lasers are introduced into the end of the transfer line.

Although the ionization process with the laser is very selective, background ions can still be produced, mainly by surface ionization in the hot cavity. This background can be reduced by making use of the pulsed structure of the laser ionized ions either by installing a fast beam gate after the source or synchronizing the data acquisition at the experiment with the laser pulses. The typical ion pulse length after extraction depends on the geometry of the source. For example, at TRIUMF it is about 10 μ s. Thus, with a repetition rate of 10 kHz a background suppression up to a factor of 10 can be achieved. To further improve the ratio of the desired ions to the background the ionization process cannot any longer take place inside the hot cavity. A solution for this the laser ion source trap (LIST) has been first proposed by Blaum et al. in 2003 [23]. Ions originating from the target or transfer tube are repelled by a positively charged repeller-electrode and the laser ionization of neutrals takes place in a cold environment in front of it. The laser ionization region is inside a radiofrequency ion guide to confine the ions and guide them to the extraction. The proposal included a gas filled ion guide, but due to the difficulty of implementing this in the vicinity of the hot target this was not implanted so far. The first prototype was installed at ISOLDE [24] and a further improved one at TRIUMF [25]. It was demonstrated that in the case of laser ionized Al isotopes the isobaric surface ionized Na could be suppressed by a factor up to 10^6 , whereas the reduction in yield for the Al, due to reduced overlap of the laser beam with the neutral atoms, was less than an order of magnitude.

2.16.5 Summary and outlook

Ion sources for radioactive ions at ISOL facilities have been in use for more than 4 decades. Depending on the isotope of interest and the application several different sources have been developed. The main sources are surface ion sources, gas discharge and plasma ion sources and resonant laser ion sources. Due to its high efficiency and selectivity laser ion sources are now used for example for about 50% of the delivered beams at TRIUMF and to a similar extend at other facilities. As a side effect it has been found that the laser ion sources can also be used for direct measurements of atomic properties of the rare isotopes as for example isotope shifts and hyperfine structure in the atomic levels. Especially for elements, with no stable isotope fundamental quantities like the ionization potential and atomic levels can be determined as was demonstrated for example for Astatine [26]. Recent ongoing developments are mainly aiming to improve the FEBIAD operation. At ISOLDE tests are being done to combine the advantages of laser ion sources with a plasma source by applying resonant ionization in a FEBIAD source to further increase the efficiency [27]. At the ALTO facility a new design has been developed. It uses a coaxial geometry and no magnetic field [28]. Results with ionization efficiencies for noble gases about 40% higher than with the standard design are reported in [29].

With the increase of primary beam intensities at ISOL facilities, as it is planned at several locations, the sources will have to handle higher beam current by keeping or improving the efficiency of the existing sources. Even with improved selectivity of the source, high purity beams may only be achieved by high resolution mass separation to reduce isobaric contamination. This will require high beam quality with low transversal emittance and energy spread. As an example, at TRIUMF a high-resolution mass

separator aiming for a resolution $M/\Delta M = 20,000$ is being set up [30]. It requires a transversal emittance of $\varepsilon_{rms} = 3 \mu\text{m}$ and an energy spread of about 1 eV. This is at the limit of the presently used ion sources. Further developments will be needed to achieve this goal reliable at higher intensities.

2.16.6 References

1. R. Kirchner, "Ion sources for radioactive beams and related problems", *Rev. Sci. Instrum.*, 67, 928-933 (1996)
2. R. Kirchner, "Progress in ion source development for on-line separators", *Nucl. Instr. Methods* 186, 275-293, (1981)
3. R. Kirchner, "On the thermoionization in hot cavities", *Nucl. Instr. Methods A292*, 203-208, (1990)
4. R. Kirchner and E. Roeckel, "Investigation of gaseous discharge ion sources for isotope separation on-line", *Nucl. Instr. Methods* 133, 187-204, (1976)
5. G. Dumont, H. Pattyn, M. Huyse, L. Lhersonneau, J. Verplancke, J. van Klinken, J. de Raedt and D.L. Sastry, "LISOL, the Leuven isotope separator on-line at the "CYCLONE"-cyclotron", *Nucl. Instr. Methods* 153, 81-92, (1978)
6. L. Penescu, R. Catherall, J. Lettry, T. Stora, "Numerical simulations of space charge effects and plasma dynamics for FEBIAD ion sources", *Nucl. Instr. Methods B266*, 4415-4419, (2008)
7. S. Sundell, H. Ravn and the ISOLDE collaboration, "Ion sources with combined cathode and transfer line heating", *Nucl. Instr. Methods B70*, 160-164, (1992)
8. P. G. Bricault, F. Ames, M. Dombisky, P. Kunz, J. Lassen, "Rare isotope beams at ISAC – target & ion source systems", *Hyperfine Interactions* 225, 25-49, (2014)
9. G. Gaubert, C. Baru, C. Canet, J. Cornell, M. Dupuis, W. Farabolini, J.L. Flambard, P. Gorel, P. Jardin, N. Lescenene, P. Leherissier, F. Lemagnen, R. Leroy, J.Y. Pacquet, M.G. Saint-Larent, A.A.C. Vilari, "Minimono: An ultracompact permanent magnet ion source for singly charged ions", *Rev. Sci. Instrum.* 74, 956-960 (2003)
10. F. Wenander, W. Farabolini, G. Gaubert, P. Jardin, J. Lettry, "First ECR-ionized noble gas radioisotopes at ISOLDE", *Nucl. Phys. A* 746 659c-662c, (2004)
11. F. Wenander, J. Lettry and the ISOLDE collaboration, "MECRIS: A compact ECRIS for ionization of noble gas radioisotopes at ISOLDE", *Rev. Sci. Instrum.* 75, 1627-1629 (2004)
12. K. Jayamanna, D. Yuan, M. Olivo, R. Baartman, G. Dutto, M. McDonald, A. Mitra, P. Schmor and G. Stanford, "Commissioning the TRIUMF/ISAC electron cyclotron resonance ion source for radioactive ion beams", *Rev. Sci. Instrum.* 75, 1621-1623 (2004)
13. K. Jayamanna, D. Yuan, F. Ames, P. Bricault, R. Baartman, V. Hanemaayer, C. laforge, A. Mitra, M. McDonald, J. McKinnon, M. Olivo and P. Schmor, "Efficiency and transit time studies performed with the electron cyclotron resonance ion source dedicated to the radioactive ion beam production at ISAC/TRIUMF", *Rev. Sci. Instrum.* 77, 03A709 (2006)
14. G. Gaubert, C. Barué, C. Canet, J. C. Cornell, M. Dubois, M. Dupuis, C. Eleon, J. L. Flambard, R. Frigot, P. Jardin, C. Leboucher, N. Lescene, P. Leherisser, F. Lemagnen, R. Leroy, and J.Y. Pacquet, "Status report of stable and radioactive ion beam production at GANIL", *Rev. Sci. Instrum.* 79, 02A309 (2008)

15. P. Jardin, C. Barué, O. Bajeat, C. Canet, C. Clément, J. C. Cornell, P. Delahaye, M. Dubois, M. Dupuis, J. L. Flambard, H. Frånberg, R. Frigot, C. Leboucher, N. Lescene, P. Lecomte, P. Leherisser, F. Lemagnen, R. Leroy, L. Maunoury, A. Méry, F. De Oliveira, A. Pichard, J. Y. Pacquet, M. G. Saint-Laurent, and J. C. Thomas, “Latest development at GANIL for stable and radioactive ion beam production”, *Rev. Sci. Instrum.* 81, 02A909 (2010)
16. C. Huet-Equilbec, P. Jardin, P. Gorel, J. Y. Pacquet, G. Gaubert, J. Cornell, M. Dubois, N. Lecesne and R. Leroy, “MONOBOB: A radiation-hard and efficient 2.45 GHz ECRIS dedicated to radioactive ion production”, *Nucl. Instr. Methods B240*, 752-761, (2005)
17. F. Labrecque, N. Lescene, and P. Bricault, “MISTIC: Radiation hard ECRIS”, *Nucl. Instr. Methods B266*, 4407-4410, (2008)
18. H. -J. Kluge, F. Ames, W. Ruster, K. Walmeroth, “laser ion sources”, Proceedings of the “Workshop of Accelerated Radioactive Beams” Parksville, Canad, 1985, editors: I. Buchmann, J.M. d’Auria, TRIUMF, CANADA, TRI-85-1, 119 (1985)
19. F. Ames, T. Brumm, K. Jäger, H.-J. Kluge, B. M. Suri, H. Rimke, N. Trautmann, and R. Kirchner, “A high temperature laser ion source for trace analysis and other applications”, *Appl. Phys.* B51, 200-206, (1990)
20. J. Lassen, R. Li, S. Raeder, X. Zhao, T. Dekker, H. Heggen, P. Kunz, C.D.P. Levy, M. Mostanmand, A. Teigelhöfer and F. Ames, “Current developments with TRIUMF’s titanium-sapphire laser based resonance ionization laser ion source”, *Hyperfine Interactions* 238, 33, (2017)
21. V. Fedosseev, K. Chrysalidis, T. Day Goodacre, B. Marsh, S. Rothe, C. Seiffert and K. Wendt, “Ion beam production and study of radioactive with the laser ion source at ISOLDE”, *J. Phys. G: Nucl. Part. Phys.* 44, 084006, (2017)
22. N. Lecesne, R. Alvès-Condé, E. Coterreau, F. De Oliveira, M. Dubois, J. L. Flambard, H. Franberg, T. Gottwald, P. Jardin, J. Lassen, F. Le Blanc, R. Leroy, C. Mattolat, A. Olivier, J. Y. Pacquet, A. Pichard, S. Rothe, M. G. Saint-Laurent, and K. Wendt, “GISELE: A resonant ionization laser ion source for the production of radioactive ions at GANIL”, *Rev. Sci. Instrum.* 81, 02A910 (2010)
23. K. Blaum, C. Geppert, H.-J. Kluge, M. Mukherjee, S. Schwarz, and K. Wendt, “A novel scheme for a highly selective laser ion source”, *Nucl. Instr. Methods B204*, 331-335, (2003)
24. D.A. Fink, S.D. Richter, B. Bastin, K. Blaum, R. Catherall, T.E. Cocolios, D.V. Fedorov, V.N. Fedosseev, K.T. Flanagan, L. Ghys, A. Gottberg, N. Imai, T. Kron, N. Lecesne, K.M. Lynch, B.A. Marsh, T.M. Mendonca, D. Pauwels, E. Rapisarda, J.P. Ramos, R.E. Rossel, S. Rothe, M.D. Seliverstov, M. Sjödin, T. Stora, C. Van Beveren, and K.D.A. Wendt, “First application of the Laser Ion Source and Trap (LIST) for on-line experiments at ISOLDE”, *Nucl. Instr. Methods B317*, 417-421, (2013)
25. S. Raeder, H. Heggen, J. Lassen, F. Ames, D. Bishop, P. Bricault, P. Kunz, A. Mjøs, and A. Teigelhöfer, “An ion guide laser ion source for isobar-suppressed rare isotope beams”, *Rev. Sci. Instrum.* 85, 033309 (2014)
26. S. Rothe, A. N. Andreyev, S. Antalic, A. Borschevsky, L. Capponi, T. E. Cocolios, H. De Witte, E. Eliav, D. V. Fedorov, V. N. Fedosseev, D. A. Fink, S. Fritzsche, L. Ghys, M. Huyse, N. Imai, U. Kaldor, Yuri Kudryavtsev, U. Köster, J. F. W. Lane, J. Lassen, V. Liberati, K. M. Lynch, B. A. Marsh, K. Nishio, D. Pauwels, V. Pershina, L. Popescu, T. J. Procter, D. Radulov, S. Raeder, M. M. Rajabali, E.

- Rapisarda, R. E. Rossel, K. Sandhu, M. D. Seliverstov, A. M. Sjödin, P. Van den Bergh, P. Van Duppen, M. Venhart, Y. Wakabayashi, and K. D. A. Wendt, “Measurement of the first ionization potential of astatine by laser ionization spectroscopy”, *Nature communications* 4, 1835 (2013)
27. T. Day Goodacre, J. Billowes, R. Catherall, T.E. Cocolios, B. Crepieux, D.V. Fedorov, V.N. Fedosseev, L.P. Gaffney, T. Giles, A. Gottberg, K.M. Lynch, B.A. Marsh, T.M. Mendonça, J.P. Ramos, R.E. Rossel, S. Rothe, S. Sels, C. Sotty, T. Stora, C. Van Beveren, and M. Veinhard, “Blurring the boundaries between ion sources: The application of the RILIS inside a FEBIAD type ion source at ISOLDE”, *Nucl. Instr. Methods B376*, 39-45, (2016)
 28. C. Lau, M. Cheikh Mhamed, and S. Essabaa, “Status of ionization by radial electron neat adaptation ion source research and development for SPIRAL2 and EURISOL-DS”, *Rev. Sci. Instrum.* 79, 02A903 (2008)
 29. S. Essabaa, N. Barré-Boscher, M. Cheikh Mhamed, E. Cottureau, S. Franchoo, F. Ibrahim, C. Lau, B. Roussi re, A. Sa id, S. Tusseau-Nenez, and D. Verney, “The radioactive beam facility ALTO”, *Nucl. Instr. Methods B317*, 218-222, (2013)
 30. J.A. Maloney, R. Baartman, and M. Marchetto, “New design studies for TRIUMF’s ARIEL High Resolution Separator”, *Nucl. Instr. Methods B376*, 135-139, (2016)

2.17 Ion sources for therapy accelerators

Atsushi Kitagawa

Mail to: kitagawa.atsushi@qst.go.jp

National Institutes for Quantum and Radiological Science and Technology (QST),
4-9-1, Anagawa, Inage, Chiba 263-8555, Japan

2.17.1 Introduction

Ion beam technology is a powerful tool for radiotherapy. Applications of ion accelerators for radiotherapy are classified into three categories: charged particle radiotherapy, boron neutron capture therapy (BNCT), and targeted radionuclide therapy (TRT). Charged-particle radiotherapy is an important treatment method; in it the accelerated ion beam itself is being used for patient treatment. The good localized physical dose distribution given by charged particles. Two distinctly different radiotherapy methods are being applied: proton radiotherapy (P-RT) or heavy-ion radiotherapy (HI-RT). The basic difference between the two methods is the biological effectiveness on tumors. The relative biological effectiveness (RBE) of proton beam is nearly 1, it is almost same as RBE of X-rays. On the other hand, the RBE of a heavy-ion beam is increased to 2-4 around the stopping point of the particles. This advantage comes from the high linear energy transfer (LET) of heavy ions.

BNCT also gives a good localized dose distribution through a unique process. A patient receives the injection of a drug that contains boron atoms in its chemical formula. The drug has a special characteristic that it concentrates in a tumor, a so-called drug delivery system. When the patient is irradiated with neutrons from outside, the boron atom captures a neutron and decays to alpha and ${}^7\text{Li}$ particles. Since these particles have a short range, they give a large dose only near the concentration point of the drug.

Neutrons were formerly produced by reactors, but it is recently realized that reactors are replaced with proton accelerators.

TRT is another treatment method use in drag delivery systems. Radiations emitted from radiopharmaceuticals irradiate target tissues. In addition, TRT is expected to give an opportunity to get a diagnosis image during treatment. P-RT and HI-RT are available for a localized tumor only. On the other hand, BNCT and TRT can treat nonlocalized tumors. So these methods are complementary.

2.17.2 Charged particle radiotherapy

2.17.2.1 *Proton radiotherapy*

The first P-RT application was carried out at the Lawrence Berkeley National Laboratory (LBNL) in 1954. In the first 30 years, nine institutes carried out clinical trials with proton beams; Uppsala University since 1957, the Harvard Cyclotron Laboratory in Boston since 1961, the Joint Institute for Nuclear Research (JINR) in Dubna since 1967, the Institute for Theoretical and Experimental Physics (ITEP) in Moscow since 1969, the Nuclear Physics Institute in St. Petersburg since 1975, the National Institute of Radiological Sciences, National Institutes for Quantum and Radiological Science and Technology (NIRS-QST) in Chiba since 1979, the High Energy Accelerator Research Organization (KEK) in Tsukuba since 1983, and the Paul Scherrer Institute (PSI) in Villigen since 1984. Treatments done at almost all of these facilities were based on using accelerators for fundamental physics research. Their ion sources were of various styles and were originally designed for non-medical use.

In 1991, Loma Linda University (LLU) started the operation of the first hospital-specified P-RT facility [1]. This epoch-making facility consists of a medical dedicated accelerator, multiple treatment rooms, and a beam delivery system with a flexible irradiation angle, a so called rotating gantry. The accelerator is based on a design made by the Fermi National Accelerator Laboratory and has the ability to accelerate protons up to 250 MeV. A combination of an RFQ linac and a duo-plasmatron ion source is utilized as an injector for a synchrotron. The injection energy into the linac is 30 kV to suppress the space charge effect at the entrance. The operational output current of the ion source is 70 mA. The injector system is operated with a pulse length of 50 ms and a repetition rate of 2 s.

In 1998, Ion Beam Applications s.a. (IBA) and Sumitomo Heavy Industry, Co. (SHI) jointly developed a facility at the National Cancer Center in Kashiwa. A 235 MeV cyclotron was fully designed as a medical dedicated accelerator [2]. A standard Livingston-type PIG ion source is utilized as an internal H⁺ ion source for the cyclotron. The maximum beam current is 10mA at an arc voltage of 140 V and an arc current of 500 mA. Typical lifetimes of the tantalum filament and the tungsten anti-cathode are 100 hours and 2 years, respectively.

At present, over 60 facilities are under operation worldwide. The 7 types of machines supplied by 8 vendors share the world market. Accelerators for the proton radiotherapy are classified into two categories: synchrotrons and cyclotrons.

Hitachi Ltd. developed a 250 MeV synchrotron in 2001. The microwave ion source realizes a typical output H⁺ current of 30mA [3]. Mitsubishi Electric Co. Ltd. (MELCO) developed a 250 MeV medical synchrotron in 2003. A 2.45 GHz electron cyclotron resonance ion source (ECRIS) has a typical H⁺ output current of 25mA [4]. However,

MELCO agreed with Hitachi to transfer their business concerning the charged-particle radiotherapy in 2018. ProTom is a new vendor and is developing a 330 MeV synchrotron.

The PSI started operation of their medical dedicated cyclotron in collaboration with the National Superconducting Cyclotron Laboratory and Kernfysisch Versneller Institute in 2007. It has a 250 MeV cyclotron which is the first medical accelerator to apply superconducting magnet technology; it was manufactured by Varian (formerly Accel Co.). A cold cathode PIG ion source has been developed by the National Superconducting Cyclotron Laboratory [5]. Mevion Medical Systems is another vendor and developed a synchrocyclotron mounted on a rotating arm to omit a large rotating gantry in 2013.

2.17.2.2 *Heavy-ion radiotherapy*

In order to treat a deep-seated tumor with the good localized dose distributions, carbon ion was predicted as a good candidate for heavy-ion radiotherapy by Robert R. Wilson in 1946 [6]. Based on physics, lighter ion species cause larger multiple scattering in the deep side, and heavier ion species give unexpected dose over the end-point due to the projectile fragmentation. In addition, the biological dose distribution depends on the depth and thickness of a tumor. In the case of ten and several cm depth and several cm thickness, the linear energy transfer of neon ions is too high than that of carbon ions shown by Lawrence Berkeley Laboratory, University of California in 1980's. Although heavier ions shows other biological advantages like oxygen enhancement ratio, NIRS-QST chose carbon ions for the clinical trial at the Heavy-Ion Medical Accelerator in Chiba (HIMAC) in 1994 [7]. By HIMAC's clinical success [8], the existing and almost all the planned heavy-ion radiotherapy facilities require a carbon beam. At present, all existing facilities utilize an ECRIS. The ECRIS is well known for its long lifetime and good performance for highly-charged ions; however it is no exception to this limitation.

The 10GHz NIRS-ECR ion source was developed to supply carbon ions for clinical treatments at HIMAC. Although the original design was to produce C^{2+} , it has been able to provide C^{4+} ions for daily clinical treatments. Experience with this source led to designing a more compact injector for the next facility. CH_4 gas was used in order to obtain enough C^{4+} ions. In the case of the NIRS-ECR, its record intensity reached 430 e mA for C^{4+} under good conditions, just after a cleaning; then the beam intensity decreased to about 300 e μ A due to rapid carbon deposition after several days. As a result, the source has been able to produce about 240 e μ A for several years without any cleaning maintenance [9].

In 1997, the Gesellschaft für Schwerionenforschung (GSI) in Darmstadt started their clinical trial with carbon beam treatment. The heavy ion synchrotron (SIS) at the GSI was constructed for fundamental experiments and was modified for medical applications to accelerate the carbon beam with a pulse-to-pulse energy change towards the operation pattern determined by the treatment planning and to automatically control the accelerator complex. C^{2+} ions were produced from CO_2 gas by the 14.5 GHz CAPRICE ECRIS. CO_2 suppresses carbon deposition on the wall and keeps the wall relatively clean [10]. This is because oxygen carries away deposited carbons due to reformation of CO_2 . On the other hand, the intensity of the highly charged ions is decreasing.

In 2001, the Hyogo Ion Beam Medical Center (HIBMC) was constructed as the first commercial HI-RT facility manufactured by MELCO with the support of NIRS. The ion sources, ECR1 and ECR2, at HIBMC are close copies of the NIRS-ECR. ECR1 and ECR2 have exactly the same structure, and they produced H_2^+ and C^{4+} beams,

respectively [11]. Since 2006, the Heavy Ion Research Facility in Lanzhou (HIRFL) has carried out a clinical trial. An ECRIS, LECR3, which was originally designed for the production of highly charged ions for atomic physics, was installed [12].

In 2009, construction of the Heidelberg Ion Therapy Center (HIT) was completed as the first medical dedicated HI-RT facility in Europe; it was based on the developments at GSI. The clinical trial in GSI was terminated due to completion of HIT. In 2010, the Gunma University Heavy Ion Medical Center (GHMC) began operated as a carbon dedicated demonstration facility. In order to reduce size and cost of ion sources, it was expected that permanent magnets could be utilized. HIT and GHMC utilize permanent magnet ECRISs.

The ECRISs, SUPERNANOGUN, are commercially delivered by Pantech S.A. of Caen, France. The original source was developed by GANIL in the 1990's. It was reported that the sources were modified to fit medical applications. The sources at HIT, the National Centre for Oncological Hadrontherapy (CNAO), the Shanghai Proton and Heavy Ion Center (SPHIC), PTC-Marburg, and MedAustron are now being operated [13,14].

NIRS-Kei2 was developed for hospital-specific facilities by NIRS. NIRS-Kei2 is an all-permanent magnet ECRIS, and its magnetic configuration was designed to match that of the NIRS-ECR, being optimized for the production of C^{4+} . The performances and some special technical issues of NIRS-Kei2 have been described in detail. The sources at GHMC, the Heavy Ion Medical Accelerator in Tosu (SAGA-HIMAT), the Ion-beam Radiation Oncology Centre in Kanagawa (i-ROCK) are now being operated [15]. The sources at the Osaka Heavy Ion Therapy Center (HIMAK) and the Yamagata University Hospital are under commissioning.

Presently eleven HI-RT facilities are situated worldwide. Five are under construction and many projects are planning. New ECRISs are also under development .

2.17.2.3 *Future prospects for charged particle radiotherapy*

In order to reduce the size of the injector into the synchrotron, a combination of an electron beam ion source (EBIS) and a linac has been developed. Since C^{6+} ions are produced, the acceleration voltage can be decreased and the charge stripper after the injector is not necessary. However, these trials have not been utilized for a treatment.

If the acceleration voltage is high enough from the ion sources, it is not necessary to install an injector. Or, in more fanciful plans, carbon ions are directly accelerated up to the high energy required by medical applications. A completely different style of facility will require a new noble ion source. Revolutionary developments are necessary for the future. Laser ion acceleration is expected to realize such a revolution. QST started the new project to combine a laser ion injector and a superconducting synchrotron for heavy ion radiotherapy which is called the 'Quantum scalpel' project. This 'scalpel' has a size of 20 x 10 m [16]. The Kansai Photon Science Institute (KPSI-QST) has a high-intensity laser system (J-KAREN-P) which is one of the 1 PW laser systems in the world and can deliver laser pulses with energy of up to ~30 J with the duration of ~30 fs by 0.1 Hz. One of the research activities using J-KAREN-P laser system is a laser-driven ion acceleration. The research activities are now carried out at KPSI aiming at understanding the laser-driven ion acceleration mechanism and controlling the accelerated ion beam parameters. It demonstrated to produce highly charged energetic iron beam with the energies of 0.56 to 0.89 GeV (from 10 to 16 MeV/u) [17,18].

2.17.3 Boron neutron capture therapy

Although fast neutron radiotherapy has been deserted as a possible treatment method due to its bad dose distribution, BNCT is anxiously expected as a treatment method with neutrons. Use of CP-RT is anticipated for localized tumors. On the other hand, BNCT is expected to be applicable for scattered tumors. Both methods are fully complementally. BNCT has a longer history than charged particle radiotherapy. The treatment method was proposed in the 1930's, and the first clinical trial was carried out at BNL in 1951. However, there are several problems for the promotion of BNCT worldwide; it is difficult to deliver drugs into tumors and to produce or to control neutron beams. One of the most important reasons is the need for a reactor to produce neutrons. In the present clinical trials, thermal neutrons are used with craniotomy mainly in Japan, and epithermal neutrons are used in other countries. The beam energy of the neutrons should be between 4 eV and 40 keV. This is because almost all neutrons of too low energy are stopped and cannot penetrate into the tumors, and neutrons of too high energy produce secondary proton particles which give an undesirable dose on normal tissues. The typical beam intensity of 1×10^9 particle/cm²/s is necessary.

An accelerator is expected to replace the reactor to produce the above conditions. Several production reactions have been proposed: ${}^7\text{Li}(p,n){}^7\text{Be}$, ${}^2\text{H}(d,n){}^3\text{He}$, ${}^3\text{H}(d,n){}^4\text{He}$, and protons irradiated on metal targets. The Kyoto University Research Reactor Institute constructed a 30 MeV 2 mA proton cyclotron for the reaction of $\text{Be}(p,xn)$ in a collaboration with SHI [19] and started the clinical trial in 2012. A multi-cusp ion source originally developed by TRIUMF was installed [20]. The typical H^- output current is 15 mA. An epithermal neutron flux of $1.2 \times 10^9/\text{cm}^2/\text{s}^1$ is obtained under the proton beam condition of 1 mA on a target. This value was reported to be about twice as large as that obtained by their research reactor [21].

There are several accelerator-based BNCT projects in Japan. The Ibaraki Neutron Medical Research Center (INMRC) collaborated with KEK, Tsukuba University, Japan Atomic Energy Agency and so on and developed a BNCT facility. The system consists of a 3 MeV RFQ linac and a 5 MeV DTL linac. An ECRIS is expected to produce 50 mA peak current with a pulse width of 1 ms [22]. The National Cancer Center (NCC) installed a 2.5 MeV RFQ linac with a current of 20 mA. Nagoya University developed a 2.8 MeV dynamitron with a current of 15 mA. These projects are under commissioning.

2.17.4 Targeted radionuclide therapy

The targeted radionuclide therapy is not common yet, but new radioactive compounds are expected to be developed. For example, an alpha particle emitting targeted radiotherapeutic, Meta[²¹¹At]astatobenzylguanidine (²¹¹At-MABG) recently demonstrated a promising effect on malignant chemodectoma. Cyclotrons are historically utilized as accelerators for radioisotope production. These are mainly utilized for diagnosis like PET, however these are also available for the targeted radionuclide therapy.

There were several manufacturing company like The Cyclotron Corporation, Scanditronix, or Japan Steel Works; however few companies remain on the market now, most have been acquired by large medical companies. A combination of a source for negative ions, usually H^- and or D^- , and a cyclotron was developed by CTI, and it is generally used today. Systems like the IBA CYCLONE series or SHI HM series are well

established and in use all over the world. Such compact cyclotrons install negative penning ion sources. A typical beam intensity of H^- and D^- is several tens of mA. Routine maintenance for ion sources is necessary a few times per year. These performance values have satisfied medical requirements and there has been no large change in the past ten years.

2.17.5 References

1. J.M. Slater et al., *Int. J. Radiation Oncology, Biology and Physics* 22, 383 (1992).
2. Y. Jongen, A. Laisne, W. Beeckman, J.P. Dufour, H. Marie, R. Verbruggen, H. Wollnik, N. Takahashi, S. Satoh, M. Sano, T. Takayama, *Nucl. Instrum. Meth.* B79, 885 (1993).
3. T. Iga, T. Seki, and S. Hara, *Proceedings of the International Particle Accelerator Conference 2010, Kyoto, 2010*, p.85.
4. Mitsubishi Gihou 84, 56 (2010) (in Japanese).
5. E. Forringer and H. G. Blosser, *Proceedings of the 16th International Conference on Cyclotrons and Their Applications, 2001*, p.277.
6. R. Wilson, *Radiology* 47(5), 487 (1946).
7. Y. Hirao, H. Ogawa, S. Yamada, Y. Sato, T. Yamada, K. Sato, A. Itano, M. Kanazawa, K. Noda, *Nucl. Phys. A* 538, 541c (1992).
8. H. Tsujii and T. Kamada, *Jpn. J. Clin. Oncol.* 42, 670 (2012)..
9. A. Kitagawa, M. Muramatsu, N. Sasaki, W. Takasugi, et al., *Rev. Sci. Instrum.* 79, 02C303 (2008).
10. K. Tinschert, R. Iannucci, and R. Lang, *Rev. Sci. Instrum.* 79, 02C505 (2008).
11. K. Sawada, J. Sawada, T. Sakata, K. Uno, K. Okanishi, H. Harada, A. Itano, A. Higashi, T. Akagi, S. Yamada, K. Noda, M. Torikoshi and A. Kitagawa, *Rev. Sci. Instrum.* 71, 987 (2000).
12. H.W. Zhao, Z.M. Zhang, W. He, X. Zhang, X.H. Guo, Y. Cao, P. Yuan, L.T. Sun, L. Ma, M.T. Song, W.L. Zhan, and B.W. Wei, *Rev. Sci. Instrum.* 75, 1410 (2004).
13. T. Winkelmann, R. Cee, T. Haberer, B. Naas, A. Peters, and S. Scheloske, *Rev. Sci. Instrum.* 81, 02A311 (2010).
14. G. Ciavola, S. Gammino, L. Celona, F. Maimone, A. Galata, M. Pullia, C. Bieth, W. Bougy, G. Gaubert, O. Tasset, and A.C.C. Villari, *Proceedings of EPAC08*, p.415 (2008).
15. M. Muramatsu, A. Kitagawa, A.G. Drentje, S. Hojo, T. Ueda, H. Miyazaki, K. Yusa, M. Tashiro, K. Torikai, M. Sakama, T. Kanai, and S. Yamada, *Rev. Sci. Instrum.* 81, 02A327 (2010).
16. T. Shirai, Y. Iwata, E. Noda, K. Mizushima, T. Inaniwa, K. Kondo, H. Sakaki, M. Nishiuchi, K. Noda, the *Proceedings of the 14th Annual Meeting of Particle Accelerator Society of Japan, Sapporo, August 2017*.
17. M. Nishiuchi, H. Sakaki, T. Zh. Esirkepov, K. Nishio, T. A. Pikuz, A. Ya. Faenov, I. Yu. Skobelev, R. Orlandi, H.Sako, A. S. Pirozhkov, K. Matsukawa, A. Sagisaka, K. Ogura, M. Kanasaki, H. Kiriya, Y. Fukuda, H. Koura, M. Kando, T. Yamauchi, Y. Watanabe, S. V. Bulanov, K. Kondo, K. Imai, and S. Nagamiya, *Phys. Plasmas* 22, 033107 (2015).
18. M. Nishiuchi, H. Sakaki, T. Zh. Esirkepov, K. Nishio, T. A. Pikuz, A. Ya. Faenov, I. Yu. Skobelev, R. Orlandi, A. S. Pirozhkov, K. Matsukawa, A. Sagisaka, K. Ogura, M. Kanasaki, H. Kiriya, Y. Fukuda, H. Koura, M. Kando, T.

- Yamauchi, Y. Watanabe, S. V. Bulanov, K. Kondo, K. Imai, and S. Nagamiya, *Plasma Physics Report*, (2016).
19. T. Mitsumoto, K. Fujita, T. Ogasawara, H. Tsutsui, S. Yajima, A. Maruhashi, Y. Sakurai, H. Tanaka, the Proceedings of CYCLOTRONS 2010, Lanzhou, China, p. 430.
 20. T. Kuo, D. Yuan, K. Jayamanna, M. McDonald, R. Baartman, P. Schmor, and G. Dutto, *Rev. Sci. Instrum.* 67, 1314 (1996).
 21. H. Tanaka, Y. Sakurai, M. Suzuki, S. Masunaga, T. Mitsumoto, K. Fujita, G. Kashino, Y. Kinashi, Y. Liu, M. Takada, K. Ono, A. Maruhashi, *Applied Radiation and Isotopes* 67, Suppl., P. S258 (2009).
 22. M. Yoshioka, T. Kurihara, S. Kurokawa, H. Kobayashi, H. Matsumoto, N. Matsumoto, H. Kumada, A. Matsumura, H. Sakurai, S. Tanaka, T. Sugano, T. Hashirano, T. Nakamura, F. Hiraga, T. Ohba, N. Nagura, T. Nakamoto, T. Zagar, T. Ouchi, the Proceedings of LINAC2014, Geneva, Switzerland, p. 230 (2014).

3 Workshop and Conference Reports

3.1 7th Low Emittance Rings Workshop

Yannis Papaphilippou
Mail to: ioannis.papaphilippou@cern.ch
CERN, Geneva, Switzerland

CERN has hosted the first general workshop for ultra low emittance rings on January 15th-17th 2018, sponsored by the WP7-RULE of the ARIES European project.

The workshop was attended by 77 delegates, with representing the three accelerator communities working on ultra low emittance rings, i.e. light sources (41 delegates), damping rings and colliders (36 delegates). Delegates were from EU (57), America (10) and Asia (10) representing 21 Institutes. The workshop was organized in four sessions: lattice design, experiments with low emittance rings, collective effects, technology. Summaries were produced at the end of the workshop. While the light source community has recently become predominant driving force in the R&D for low emittance ring, it was pleasant to note the strong participation of the colleagues involved in damping rings and colliders (mostly CLIC and FCC) showing that the cross breeding between these community is still very important.

Ultra low emittance rings constitute one of the cutting edge R&D activities in accelerators of recent years. The R&D effort, originating from the damping rings' and colliders' community is now predominantly in the hands of the light source community with the first operation of a MBA lattice in MAX IV, the upgrade of the ESRF to the ESRF-EBS, the construction of SIRIUS in Brazil, and many other upgrade projects around the world. ARIES is promoting these developments providing support for the networking activity. This workshop was the first of the series and the first milestone of the WP7 RULE. Partners involved were CERN and UOXF. The presentations are collected in the indico page

<https://indico.cern.ch/event/671745/overview>

The sessions were organized to allow 30 minutes talks and some discussion at the end of the day. The talks were split in the following way

- lattice design – 16 talks
- collective effects – 8 talks
- experiments towards low emittance rings – 5 talks
- technology for ultra-low emittance rings – 7 talks

About 40 high quality presentations gave a clear overview of the main activity in the various aspects of physics and technology of low emittance rings.

In the lattice design it was interesting to see that new projects are continuously proposed, namely the SLRI upgrade in Thailand and the South-Eastern initiative in Montenegro. Such project benefit from the work already being discussed in the low emittance rings within the EuCARD2 project. The Hybrid Multibend Achromat (HMBA) lattice is the clear highlight and many projects are trying to extend it by using reverse bends and more advanced forms of longitudinal gradient bends. The latter technology is also driven by studies and technological developments for the CLIC damping rings.

In the field of collective effects, a strong numerical and analytical activity is focusing on understanding the limitation in current for such rings. In particular the impact of high harmonic cavities in the instability threshold was discussed extensively.

On technology, significant advances were presented in the understanding of the behavior of NEG coating in terms of impedance, vacuum performance and secondary electron yield emission. Noticeable progress in the operation of efficient klystrons was also presented. These technological advancements will benefit the whole set of communities and are example of the multidisciplinary nature of the R&D carried out in this field.

It is likely that the success and the interest aroused by this general meeting will deserve another general workshop in 2019.

3.2 Topical Workshop on Emittance Measurements for Synchrotron Light Sources and FELs

Ubaldo Iriso

Mail to: ubaldo.iriso@cells.es

ALBA-CELLS, C. de la Llum, 2-26, Cerdanyola del Vallès (Spain)

(Style: author_affiliation)

3.2.1 Introduction

The Topical Workshop on Emittance Measurements for Synchrotron Light Sources and FELs held at ALBA-CELLS in January 2018 brought together experts working on emittance measurements for electron machines, including Synchrotron Light Sources (SLS) and Free Electron Lasers (FEL). The workshop presented the status of the present techniques and discussed the challenges that this community is facing for the next generation of ultra-low emittance machines.

The workshop did not include paper proceedings, but all the presentations are available at the workshop website [1]. Interested readers can find not only presentations from the diagnostics side, but also from the beam dynamics requirements and challenges that this kind of machines will pose to the diagnostics community (see contributions from M.Boege and E. Prat from PSI).

3.2.2 Emittance Measurements Techniques for Synchrotron Light Sources

In the case of SLS, the preferred techniques to infer the beam size are based on the analysis of the synchrotron radiation due to its non-destructive nature. But for small beam sizes as the ones in low emittance machines, direct imaging techniques are limited by the so-called “diffraction limit”, especially when using the visible part of the radiation spectrum. In order to overcome this limit, techniques like pinhole cameras or Compound Refractive Lenses (CRL) do not use the visible range of the synchrotron radiation, but the x-ray part. These techniques were reviewed and compared by L. Bobb (Diamond) and F. Ewald (ESRF), and it was concluded that they can be used to measure beam sizes down to the $\sim 4\mu\text{m}$ level.

Other SLS like KEK or Max-IV use techniques based on the analysis of the synchrotron light coherence, like the double-slit interferometry presented by T. Mitsuhashi (KEK), or the polarization methods shown by A. Andersson (Max-IV). There is even a variable of this technique, presented by L. Torino (ESRF), in which a rotating mask is used to even reproduce the transverse beam profile including beam tilts. These techniques analyze the visible part of the synchrotron light, but the workshop showed that in order to measure beam sizes below the $\sim 2\mu\text{m}$ level, the system should be adapted to smaller wavelengths, like ultra-violet or even x-rays. This would imply larger setups (i.e. beamlines), and an example of that is the design shown by B. Yang for the APS upgrade, whose emittance measurement is foreseen to be performed in a complex beamline which allows to accommodate both x-ray pinhole cameras and x-ray interferometry. Further details about these techniques were reviewed by A. Snigirev (IKBF), who also presented the challenges of performing diffraction in the x-rays regime, and showed few tests done in the past.

3.2.3 Emittance Measurements Techniques for FELs

On the other hand, the beam sizes in FELs are measured through the interaction of obstacles in the electron beam trajectory, which often detrimentally affect the electron beam (and whence the name “destructive” techniques). One of these techniques (reviewed by L. Sukhik from TPU) is based on the Optical Transition Radiation (OTR) screens, which are used for direct beam imaging after the beam impinges on the screen. On the other hand, E. Chiadroni (INFN) showed also how beam size measurements in a non-destructive way can be done using Optical Diffraction Radiation, and how it can be used produce Diffraction Radiation Interferometry, with the benefit of clearly separating the contributions of the beam size and the angular divergence.

Other obstacles like Wire Scanners (reviewed by K. Wittenburg from DESY) are nowadays getting thinner (down to the $1\mu\text{m}$ level) using lithography and electroplating, which improves the method resolution and which has been used to measure beam sizes down to the 500nm level (S. Borrelli, SLS). This type of resolution can also be achieved using a laser wire, where as shown by P. Karataek (JAI) the electron beam does not interact with a solid (metallic) object, but a “light pencil”. However, this solution involves a significant degree of complexity and it requires an important team of experts to maintain and properly operate the whole system.

3.2.4 Summary and Other Techniques

The workshop also presented techniques which are not used widely in SLS or FELs but that can potentially improve the emittance measurements in the near future. Figure 1 shows two examples of these techniques: Fig. 1 a) shows an example of the power spectra produced by the Heterodyne Near Field Speckle technique presented by M. Siano (Univ. of Milano), which is able to measure the horizontal beam size in an ALBA beamline; and Fig. 1 b) shows the image produced by the Cherenkov Diffraction Radiation shown by M. Bergamaschi (CERN), which is nowadays able to measure beam sizes in the order of $\sim 2\text{mm}$ at CESR.

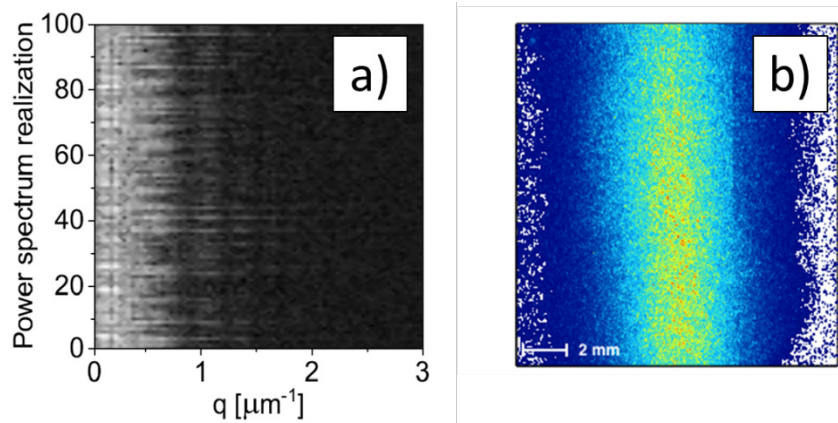


Figure 1: a) power spectra obtained using the Heterodyne Near Field Speckle technique at BL11 at ALBA, from which a horizontal beam size of $135\ \mu\text{m}$ is inferred. b) image produced by the Cherenkov Diffraction Radiation of a positron beam at 5.3GeV interacting with the radiator.

The Workshop ended with a review of the methods used in other accelerators like hadron colliders or Laser Plasma Accelerators. Nowadays, the proton beam at LHC (CERN) is measured using the synchrotron radiation interferometry technique, which was only used in electron machines until few years ago. Perhaps techniques based on Ionization Profile Monitor (IPMs, widely used in hadron machines) can be used in electron machines in a mid-term future, as shown by M. Sapinsky (GSI). Certainly, the diagnostics experts on emittance measurements will benefit from the synergies between the different communities.

3.2.5 References

Topical Workshop on Emittance Measurements for Synchrotron Light Sources and FELs, website at <https://indico.cells.es/indico/event/128/overview>

3.3 ICFA Mini-Workshop on Beam-Beam Effects in Circular Colliders

Ji Qiang, LBNL, Berkeley, U.S.A.

Mail to: jqiang@lbl.gov

Beam-beam effects due to electromagnetic interactions of two oppositely moving charged particle beams present strong limit to the final achievable luminosity in high energy colliders. With a number of future machines, such as an electron-ion collider, under consideration, as well as upgrades such as the High-Luminosity LHC, an ICFA Mini-Workshop on Beam-Beam Effects in Circular Colliders was held in Berkeley, CA, USA from February 5 to 7, 2018 (<https://indico.physics.lbl.gov/indico/event/586/>) and was attended by 42 participants representing institutions from Asia, Europe and USA. This workshop is a successor and follows up to similar workshops held at CERN in April 1999, at Fermilab in June 2001, in Montauk 2003, and at CERN in March 2013.

The scientific program of the workshop was set up by the International Organizing Committee, chaired by J. Qiang and J. Vay (LBNL). The workshop was hosted by the Accelerator Modeling Program of the Accelerator Technology and Applied Physics Division of the Lawrence Berkeley National Laboratory. The Local Organizing Committee M. Condon, Lucky Cortez and J. Chew helped make local arrangements.

Thirty-six talks were presented during the three-day workshop and covered six topics of the scientific program. The first day of the workshop focused on the future collider topic (part I) and the beam-beam experience topic. The studies of beam-beam effects related to the future electron-ion colliders were presented in the morning session and the experience with the current colliders such as BEPC, KEK-B, LHC and RHIC was presented in the afternoon session. The second day of the workshop focused on the future collider topic (part II) and the coherent and incoherent beam-beam effect topic. The beam-beam effects in FCC, LHeC, CEPC, and laser plasma driven collider were discussed in the morning session talks and the coherent beam-beam instabilities in LHC and FCC and incoherent beam-beam effects in LHC and HL-LHC were discussed in the afternoon session. The third day of the workshop focused on the theory and simulation topic and the beam-beam compensation topic. Some numerical issues such as noise in strong-strong beam-beam simulation and long-term simulation on GPUs, and a theoretical model using the renormalization group theory were discussed in the morning session and various methods such as electron lens and conducting wire to compensate the head-on and the long-range beam-beam effects were discussed in the afternoon session. The workshop also included a time slot each day for discussions.

The detail program and talks are available via the workshop website.

ICFA Mini-Workshop on Beam-Beam Effects in Circular Colliders



<https://indico.physics.lbl.gov/indico/event/586/>
 February 5 – 7, 2018, Berkeley, CA

Organization:

Workshop Chairs:
 Ji Qiang (BNL)
 Jean-Luc Vay (LBNL)

International Organizing Committee:
 Yunhai Cai (SLAC)
 Yong Ho Chin (KEK)
 Wolfram Fischer (BNL)
 Elias Meier (CERN)
 Kazuhiro Ohmi (KEK)
 Fulvia Pilat (JLab)
 Ioannis Papaphilippou (CERN)
 Tattana Pieloni (EPFL)
 Qing Qin (HEP)
 Vladimir Shiltsev (FNAL)
 Ferdinand Willeke (BNL)
 Yuhong Zhang (JLab)

Local Organizing Committee:
 Joseph Chew
 Lucky Condon
 Lucky Cortez




U.S. DEPARTMENT OF
ENERGY

Office of
Science

ACCELERATOR TECHNOLOGY &
APPLIED PHYSICS DIVISION



Fig. 1: Beam-Beam 2018 workshop poster.



Fig. 2: Participants of the Beam-Beam 2018 workshop.

3.4 Accelerator-Industry Co-Innovation Workshop: Tools and strategies to enhance industry-academia cooperation in the particle accelerator community

Maurizio Vretenar

Mail to: Maurizio.Vretenar@cern.ch

CERN, Geneva, Switzerland

The particle accelerator community is increasingly engaged with industry, for the development of the critical components that will power the next generation of accelerators and in a joint effort to bring down to society the benefits from the technologies developed for the past generation of accelerators.

To define instruments and tools to structure and foster industry participation to accelerator development programmes, a Workshop was organized by three institutions engaged in the development of particle accelerators: the TIARA consortium of European research institutions in the Particle Accelerator Research Area, the ARIES Integrating Activity project for accelerator R&D, and the AMICI project for support to accelerator and magnet technological infrastructures.

The main objectives of the Workshop were to foster discussion on most effective ways to develop co-innovation with industry in Europe, to identify sustainable structures, possible funding schemes and financing mechanisms, to contribute to the definition of new EC instruments to boost co-innovation and to provide a communication platform to all relevant stakeholders: policy makers, academia, industry and scientific management.

A Committee that included representatives from the three organizing institutions and from industry set up the programme for the Workshop. Its members were Roy Aleksan (CEA/TIARA), Jean-Luc Lancelot (SigmaPhi/PIGES), Sylvie Leray (CEA/AMICI), Marcello Losasso (CERN/ARIES), Mauro Morandin (INFN/AMICI), Mark Plesko (Cosylab), Toms Torims (RTU/ARIES), Maurizio Vretenar (CERN/ARIES). The poster is shown in Figure 1.



Figure 1: Workshop poster.

The Workshop was well attended, with 90 participants coming from 18 countries. 37 participants were from industry, 36 from research centres, 9 from Universities, and 9 from the European Commission. The attendance data are summarized in Figure 2.



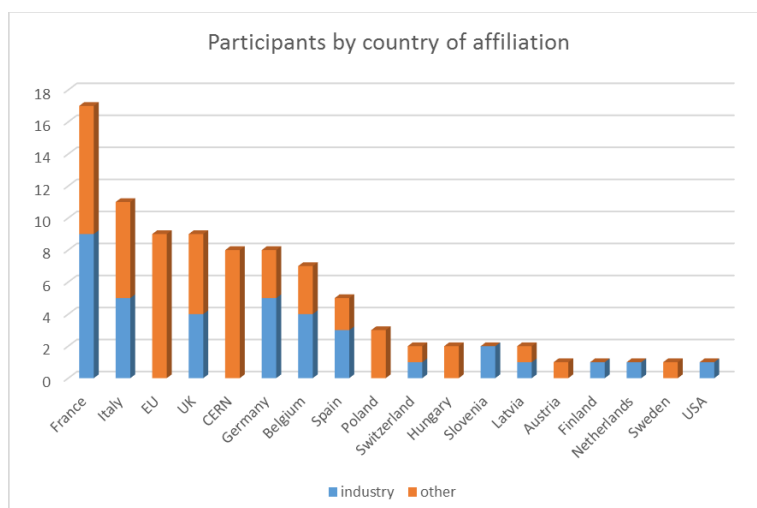


Figure 2: Workshop attendance.

The Workshop gave the opportunity to people coming from different horizons and experiences to discuss issues and to develop a common language, with the goal of creating a community around the main actors of the development of accelerator technology and of the related technology infrastructure.

During the meeting, many presentations highlighted the long way that we have come through to reach the present status of accelerator technologies. The collaboration between European research infrastructures and the industry has been seminal for the realization of unprecedented scientific endeavours. J. M. Perez on behalf of the TIARA consortium stressed the importance of developing a consistent collaborative programme for Accelerator Science and Technologies as well as the need to further integrate the industrial partners from the beginning onwards of the design of research infrastructures. In the following talk M. Vretenar, ARIES project coordinator, highlighted the broader goals for this event. He emphasized that a project like ARIES promotes accelerator R&D but at the same time will create an academia-industry community around common R&D activities, contribute in developing novel applications for accelerators and finally help the research community to meet the market needs and come closer with the industry. An additional dimension was brought in by O. Napoly, AMICI project coordinator, who highlighted the importance for industry and for the accelerator community of the vast technological infrastructure of the accelerator laboratories, whose sustainability is a priority goal for Europe.

Successful projects in the framework of FP6, FP7 and H2020 have enabled to integrate the European expertise for collaborative accelerator R&D. P. Froissard, Deputy Head of the EC Research Infrastructures (RI) Unit, discussed some of the lessons gained from H2020. Industries through involvement in public RIs can validate and produce reliable and standardized results while public procurement for RIs should be used to boost innovation in industry. Innovation ecosystems can be developed around RIs and is important to think of efficient mechanisms to facilitate knowledge and technology transfer. Finally, he stressed the need to “set roadmaps in key technologies for the construction and upgrade of the pan European network of research infrastructures in order to maximize the benefits for the research community and society as a whole”.

On the second day of the event, representatives from industry shared lessons and their thoughts on how joint R&D projects could be a win-win opportunity for industry. Representatives from ASG, Bruker, Oxford Instruments, SigmaPhi and Elytt, key companies developing magnets for accelerators, shared their experience of collaborating with different research centres. Working with research centres offers unique opportunities for R&D and innovation but also certain challenges given the discontinuity in R&D projects. Designing long-term large-scale research infrastructures represent the best chance for setting a new frame of co-innovation.

Finally, R. Wichmann, head of the XFEL Project Office in DESY discussed the lessons learned from XFEL. The challenging technology of superconductivity required a strong collaborative effort between researchers and the industry while knowledge transfer has been challenging and often more time-consuming than expected.

An animated debate took place at the end of the Workshop, with the participants engaged in identifying the limitations to industry participation in R&D and co-innovation with academia, in giving their opinion on the existing instruments and schemes for co-innovation, and in addressing possible new instruments.

One of the main subjects treated in the debate was IP protection and licensing (“a tool of the last century”) and modalities for sharing IP in common projects. Another important topic was how to transfer the positive experience gained in low TRL projects to higher TRL initiatives. Funding of projects is of course and issue, as well as education and training that is considered a priority by industry as well as by the accelerator laboratories.

In general terms, this Workshop indicated that, with the active support from the European Commission, accelerator laboratories and projects are now willing to join efforts with industry to consolidate the European accelerator research and innovation community and propel accelerator technology into the next decade. This was only the first in a series of events that aim to advance a rigorous collaboration with industry and consequently maximise the impact that accelerators have for science and society.

3.5 The 1st ICFA Mini-Workshop on Machine Learning Applications for Particle Accelerators

Xiaobiao Huang, Chris Mayes, Daniel Ratner, Tor Raubenheimer

Mail to: dratner@slac.stanford.edu

SLAC National Accelerator Laboratory

The 1st ICFA workshop on machine learning for particle accelerators (ML18) was held at SLAC National Accelerator Laboratory from February 28 to March 2, 2018. Approximately 65 attendees from over 20 institutes spanned fields of accelerator physics, controls, operations, computer science, and industry. The goal of the workshop was to establish the current state of machine learning in accelerator physics, discuss opportunities and needs for machine learning, and promote inter-laboratory collaboration going forward.

Prior to the workshop, a one-day tutorial covered introductory topics in machine learning as well as the Ocelot simulation/optimization package. The three-day workshop itself was split into five sessions:

- a) Facility needs
- b) Optimization and online tuning
- c) Simulations and modeling
- d) Prognostics
- e) Data analysis

Given the early stage of the field, talks were kept short to allow substantial time for discussion after each session. Approximately 25 posters were hung throughout the workshop to serve as a basis for discussion during breaks. The final afternoon was reserved for general discussion and to begin the process of writing a summary white paper.

Discussions covered a number of challenges for existing and future accelerators, along with potential machine learning solutions. Applications included colliders, cyclotrons, synchrotron light sources, and free electron lasers. Work reported included preliminary application of machine learning techniques in accelerator tuning, simulations, fault detection, and analysis of large data sets. There was a general optimism in realizing the potential of machine learning for accelerators, although some barriers, such as lack of funding, administrative support, and computer science expertise, were also recognized and possible solutions discussed. More details will be included in the summary white paper to be published later this year.

More information and slides can be found at <https://conf.slac.stanford.edu/icfa-ml-2018/>. The next workshop is planned for March, 2019, to be hosted by the Paul Scherrer Institute, Switzerland.



Figure 1: Participants of the machine learning for accelerators workshop

3.6 The 60th ICFA Advanced Beam Dynamics Workshop on Future Light Sources, FLS2018

Zhentang Zhao

Mail to: zhaozhentang@sinap.ac.cn

SINAP, Shanghai, China

The 60th ICFA Advanced Beam Dynamics Workshop on Future Light Sources, FLS2018, was held on 5-9 March, 2018 at Hotel Equatorial Shanghai, China. There are 148 participants representing institutions from Asia, Europe and America. After a lapse of 6 years, FLS2018 restarts the Future Light Sources series.

The scientific program of the workshop is set up by the International Organizing Committee, chaired by Yong Ho Chin (KEK), and the conference is chaired by Zhentang Zhao (SINAP). The workshop is hosted by SINAP - the Shanghai Institute of Applied Physics, CAS. Its Local Organizing Committee is chaired by Zhengchi Hou (SINAP). 86 talks are presented during the plenary and parallel working group (WG) sessions, including 8 plenary, 45 invited and 33 contributed talks. They cover a wide spectrum of topics on accelerator and laser based light sources and related key technologies during the past six years since the last FLS workshop gathering at JLab, USA, in 2012. These talks are well researched, highly informative and well received by the audience.

The four working groups are themed as follows: WG1: Linac based light source convened by T. Raubenheimer (SLAC), L. Giannessi (Elettra) and W. Decking (DESY); WG2: Ring based light source convened by R. Walker (DLS), Y. Li (BNL) and Q. Qin (IHEP); WG3: Compact light source convened by Chunguang Jing (Euclidtechlabs), M.E. Couprie (SOLEIL) and H. Zen (Kyoto University), and WG4: Key technologies convened by John Byrd (ANL), Joachim Pflueger (European XFEL) and Y.B. Leng (SINAP). The four topics have generated heated interests in all breakdown sessions and the WG conveners have showed strong leadership to engage all participants in the discussions.

The poster session is also a huge success with 38 posters presented. The detail program and talks are available via the workshop website (<https://indico.sinap.ac.cn/e/fls2018>). The workshop proceedings will be published at JACoW.



4 Recent Doctorial Theses

4.1 Development of direct measurement techniques for the in-situ internal alignment of accelerating structures

Natalia Galindo Munoz

Mail to: nataliagalindomunoz@gmail.com

Graduation date: 13 March 2018

Institutions: CERN, Geneva, Switzerland
IFIC, Valencia, Spain

Supervisors: PhD Nuria Catalan Lasheras (CERN)
PhD Angeles Faus Golfe (LAL, Univ. Paris-Sud, CNRS/IN2P3,
Université Paris-Saclay, Orsay, France).
PhD Vicente Enrique Boria Esbert (UPV)

Abstract

In the Compact Linear Collider (CLIC), challenging 10 μm alignment tolerances are required in the positioning of the components focusing, accelerating and detecting the beam over the accelerator length in order to achieve the maximum machine performance.

This PhD concerns the investigation, development and implementation of a new non-destructive intracavity technique, referenced here as “the perturbative method”, to determine the electromagnetic axes of accelerating structures by means of a stretched wire, acting as a reference of alignment. Of particular importance is the experimental validation of the method through the 5.5 mm iris-mean aperture CLIC prototype known as TD24, with complex mechanical features and difficult accessibility, in a dedicated test bench. The feasibility study of the method, carried out with extensive electromagnetic fields simulations, gived as a result, the knowledge of the theoretical 7.5 μm accuracy expected in the measurement of the electromagnetic axes and facilitated the development of a measurement algorithm. The conceptual design, manufacturing and calibration of the automated experimental set-up, integrating the solution developed to measure the electromagnetic axes of the TD24, were covered. The most significant results obtained from an extensive experimental work were presented, analysed and compared with simulations. The proof-of-principle was completed, the measurement algorithm was optimised and the electromagnetic centre was measured in the TD24 with a precision less than 1 μm and an estimated error less than 8.5 μm . Finally, the future lines of research and developments of the perturbative method were also explored, and the impact of the achievements were analysed.

4.2 Understanding the plasma and improving extraction of the ISIS Penning H^- ion source

Scott Lawrie

Mail to: scott.lawrie@stfc.ac.uk

Graduation date: 30 September 2017
Institutions: ISIS Neutron and Muon Facility, STFC Rutherford Appleton Laboratory, UK
 John Adams Institute for Accelerator Science, University of Oxford, UK
Supervisors: Prof. Andrei Seryi (JAI)
 Dr. Dan Faircloth (STFC)
 Mr. Alan Letchford (STFC)

Abstract

A Penning-type surface-plasma negative hydrogen (H^-) ion source has been delivering beam at the ISIS pulsed spallation neutron and muon facility for over thirty years. It is one of the most powerful and well-renowned H^- sources in the world. Although long-term experience has allowed the source to be operated reliably and set up in a repeatable way, it is treated as something of a 'black box': the detailed plasma physics of why it works has always been unclear.

A vacuum Vessel for Extraction and Source Plasma Analyses (VESPA) has been developed to understand the ISIS ion source plasma and improve the beam extracted from it. The VESPA ion source is operated in a completely new regime whereby the analysing sector dipole magnet housed inside a refrigerated 'cold box', presently used on ISIS, is replaced by an on-axis extraction system. The new extraction system incorporates a novel einzel lens with an elliptical aperture. This is the first demonstration of an elliptical einzel being used to focus an asymmetric H^- ion beam.

With the dipole magnet removed, the ion source has been shown to produce 85 mA of H^- beam current at normal settings; of which 80 mA is transported through the new einzel lens system, with a normalised RMS emittance of 0.2π mm mrad. Optical emission spectroscopy measurements have shown a plasma density of 10^{19} m^{-3} , an H_2 dissociation rate of 70%, an almost constant electron temperature of 3.5 eV and an atomic temperature which linearly increases above the electron temperature.

In support of these principal measurements, rigorous particle tracking, electrostatic and thermal simulations were performed. In addition, a suite of new equipment was manufactured by the author. This includes a fast pressure gauge, a temperature controller, a high voltage einzel lens circuit, a fast beam chopper and a caesium detection system.

4.3 Fast Luminosity Monitoring Using Diamond Sensors for SuperKEKB

Dima El Khechen
 Mail to: scott.lawrie@stfc.ac.uk

Graduation date: December 16, 2016
Institutions: Laboratoire de l'Accélérateur Linéaire (LAL), Université Paris Sud, CNRS/IN2P3, Université Paris-Saclay, Orsay, France
Supervisors: Dr. Philip Bambade (LAL) and Dr. Cécile Rimbault (LAL)

Abstract

SuperKEKB is a very high luminosity collider dedicated to the Belle II experiment, it consists of a Low Energy Ring (LER) of 4 GeV positrons and a High Energy Ring (HER) of 7 GeV electrons. The commissioning of this machine is split into three phases: phase 1 (single-beam phase) is dedicated to vacuum scrubbing, where beams circulate without focusing at the collision point. Phase 2, for which the major part of the Belle II detector will be installed, will enable the tuning of the final focus system to achieve a luminosity of $10^{34} \text{ cm}^{-2} \text{ s}^{-1}$. During phase 3, Belle II physics runs will start with an aimed luminosity up to $8 \times 10^{35} \text{ cm}^{-2} \text{ s}^{-1}$.

In this context, the aim of my thesis is to develop and install a fast luminosity monitoring system, which is required for online correction of beam instabilities and maintenance of optimal luminosity. To reach the aimed relative precision of 10^{-3} in 1 ms, the measurement will be based on the radiative Bhabha process at zero photon scattering angle, whose cross-section is large and well-known. These particles will be detected using diamond sensors, resistant to radiation and enabling very fast signal acquisition, to be placed outside of the beam-pipe and downstream of the interaction point.

The first part of this work is dedicated to the investigation of the best locations for the diamond sensor positioning in both rings. Using detailed simulations, we studied the dynamics of Bhabha particles during their tracking in the rings and their interaction with the beam pipe material. This led to the identification of two positions, at 11.9 m in LER and at 30 m in HER, and to considering a new geometry for the vacuum pipe in the LER.

The second part is related to the phase 1 of the SuperKEKB commissioning and concerns the measurements performed with the diamond sensors that were installed. Single beam loss processes (Bremsstrahlung, Touschek, beam-gas Coulomb scattering) were studied in detail with respect to the LER beam and ring parameters (current, pressure, transverse beam sizes). The results of this study were then compared to the data collected from February to June 2016. We found good qualitative and quantitative agreement between our simulations and measurements. From this we could estimate that the level of background to be expected during luminosity monitoring will be two orders of magnitude smaller than the rate of the radiative Bhabha scattering signal.

5 Forthcoming Beam Dynamics Events

5.1 Mechanical Engineering Design of Synchrotron Radiation Equipment and Instrumentation (MEDSI)

The 10th edition of this conference, MEDSI 2018, will take place from June 25 to 29, 2018 at Paris, France. MEDSI is the main biannual event for the engineers from worldwide synchrotrons and light sources to showcase and exchange cutting-edge developments in mechanical design and engineering of synchrotron-based instrumentation.

MEDSI 2018 is hosted by Synchrotron SOLEIL and supported by French Society of Physics (SFP). The program covers beamline and accelerator technology, theoretical aspects and numerical simulation, precision mechanics and core technology developments including vacuum, cryogenics, mechatronics, etc.

The conference will be held in the historical Cité Internationale Universitaire of Paris which is a multicultural space built in the 1930's. It was conceived as a place where students of all nationalities could meet. Its style, inspired by the Château de Fontainebleau, gives it a monumental air. Inside, some of the lounges are in Art Deco style. The conference website is regularly updated to include the latest information:

<http://www.meds2018.org>

Keihan Tavakoli, MEDSI 2018 Chair

5.2 International Beam Instrumentation Conference (IBIC2018)

The 7th International Beam Instrumentation Conference (IBIC 2018) will take place from September 9th to 13th, 2018 hosted by the Shanghai Institute of Applied Physics, Chinese Academy of Sciences (SINAP, CAS) in Shanghai, China.

The International Beam Instrumentation Conference has a long and healthy history, dating back to 2012. The conference takes place every year with the most recent events being held in Grand Rapids, MI, USA (2017) and Barcelona, Spain (2016). The 2018 edition will be hosted by Shanghai Institute of Applied Physics. Like its predecessors, this conference is also dedicated to exploring the physics and engineering challenges of beam diagnostics and measurement techniques for charged particle beams.

The conference will be held in the Parkyard hotel at Shanghai. Shanghai, located on China's central eastern coast at the mouth of the Yangtze River, is mainland China's center for commerce and finance. The city is also an emerging tourist destination renowned for its historical landmarks such as the Bund, Xintiandi, Yu Garden and the Oriental Pearl Tower. Shanghai Institute of Applied Physics is located about 1.5km from the venue and participants of the conference will have the opportunity to visit the accelerator facilities at SINAP, including two large scale facilities: SSRF and SXFEL. The conference website

<https://indico.sinap.ac.cn/event/3/>

will be regularly updated to include the latest information as it becomes available.

Zhentang Zhao, Conference Chair IBIC 2018

5.3 23rd International Workshop on ECR Ion Sources

The 23rd Workshop on ECR Ion Sources will take place from September 10th to 14th, 2018 in Catania, Italy. The ECRIS conference series have a long history dating back to the 70's (recently: 2012 Sydney, Australia; 2014 Nizhny Novgorod, Russia; 2016 Busan, South Korea), promoting stimulating discussions and new collaborations. The 2018 edition will be hosted by the Istituto Nazionale di Fisica Nucleare – Laboratori Nazionali del Sud and it is aimed to highlight the state of the art in ECR Ion Sources Science & Technology, and to reinforce the common ground and synergies among the different experts in this field.



The baroque-style Duomo square of Catania with the Cathedral and the Clerics's seminary housing the Diocesan Museum.

The programme covers all the different issues concerning to the production and transport of singly and highly charged ion beams, the fundamental processes related and the industrial applications to new technologies.

The venue, placed at the foot of the Etna Volcano – the highest and most active of Europe – in a city that is now experiencing its third millennium of history, since its establishment in 730 BC, will hopefully encourage fertile cultural discussions.

The workshop will take place in the halls of the Catania Diocesan Museum, located in the heart of the old city; the location will permit an easy access to the major archaeological and cultural attractions of the city, a real baroque gem, midway between the two ancient cities of Syracuse and Taormina.

The workshop website (<http://ecris18.lns.infn.it>) will be regularly updated with the detailed workshop programme including the registration, accommodation and touristic information.

Luigi Celona, ECRIS 2018 Chair

5.4 eeFACT2018, 24-27 September 2018

Following the successful eeFACT2016 ICFA workshop in Daresbury, UK, HF2014 in Beijing, and HF2012 at FNAL, the 2018 workshop on e^+e^- factories, **eeFACT2018**, will take place in Hong Kong, from 24 to 27 September 2018, at the Hong Kong University of Science and Technology, Institute for Advanced Study. eeFACT2018 is the 62nd beam dynamics workshop organized under the auspices of ICFA. It is co-sponsored by the HKUST IAS, CERN, IHEP, KEK, and by the EU's Horizon2020 ARIES project.

Since more than 50 years lepton colliders have been the most widely used collider species, always pushing the frontiers of science. Present efforts range from existing or planned low-energy factories like DAFNE, BEPC-II, two super-tau-charm factory designs, and BINP's compact collider for dimuonium production, to record-luminosity machines such as SuperKEKB, and the proposed high-energy future circular electron positron colliders CEPC and FCC-ee. Despite the long history of circular lepton colliders, many recent novel ideas promise further dramatic increases in their performance.

By the summer of 2018, the commissioning phase 2 of SuperKEKB will be completed. At the same time both FCC-ee and CEPC will finalize, or publish, their conceptual design reports. Accelerator-design breakthroughs combined with physics prospects have also sparked a renewed interest in super tau-charm factories. Many design challenges of e^+e^- colliders are common with the ever more ambitious plans for storage-ring light sources.

ICFA is encouraging the global coordination of, and joint research on, factory-like circular colliders. The eeFACT2018 workshop held in Hong Kong, from 24 to 27 September 2018, will cover the full scope of circular lepton colliders over a wide range of energies, and address the complementary physics goals. Topical working groups including contributions from the light-source community are foreseen.

Like its predecessors, eeFACT2018 will address all aspects of present and future e^+e^- factories, through plenary talks and dedicated working groups covering physics landscape and motivations, design concepts, optics issues, interaction region and machine detector interface, beam-beam issues, injectors and beam injection, impedance issues and beam instabilities, emittance control, polarization, beam instrumentation and beam diagnostics, superconducting RF, other technologies, and energy efficiency.

The goals of the eeFACT18 workshop are: (1) Reviewing and documenting the state of the art in e^+e^- factory design. (2) Reviewing and drawing lessons from SuperKEKB phase 2 commissioning. (3) Catalyzing further contributions to the SuperKEKB, FCC, CEPC & tau-charm design efforts. (4) Fostering synergies and new collaborations across communities, in particular with the low-emittance light sources and between continents. (5) Jointly developing novel solutions to outstanding problems.

The workshop organizers are:

Andrew Cohen (Local Committee Chair, IAS, HKUST)

Frank Zimmermann (CERN)

Qing Qin (IHEP)

Yoshihiro Funakoshi (KEK)

The workshop secretary is:

Miss Prudence Wong

HKUST Institute for Advanced Study

E-mail: eefact2018@ust.hk

Tel: +852-2358-5061

A program committee is being formed. Further information can be found on the conference website: <http://eefact2018.ust.hk/>

6 Announcements of the Beam Dynamics Panel

6.1 ICFA Beam Dynamics Newsletter

6.1.1 Aim of the Newsletter

The ICFA Beam Dynamics Newsletter is intended as a channel for describing unsolved problems and highlighting important ongoing works, and not as a substitute for journal articles and conference proceedings that usually describe completed work. It is published by the ICFA Beam Dynamics Panel, one of whose missions is to encourage international collaboration in beam dynamics.

Normally it is published every April, August and December. The deadlines are 15 March, 15 July and 15 November, respectively.

6.1.2 Categories of Articles

The categories of articles in the newsletter are the following:

1. Announcements from the panel.
2. Reports of beam dynamics activity of a group.
3. Reports on workshops, meetings and other events related to beam dynamics.
4. Announcements of future beam dynamics-related international workshops and meetings.
5. Those who want to use newsletter to announce their workshops are welcome to do so. Articles should typically fit within half a page and include descriptions of the subject, date, place, Web site and other contact information.
6. Review of beam dynamics problems: This is a place to bring attention to unsolved problems and should not be used to report completed work. Clear and short highlights on the problem are encouraged.
7. Letters to the editor: a forum open to everyone. Anybody can express his/her opinion on the beam dynamics and related activities, by sending it to one of the editors. The editors reserve the right to reject contributions they judge to be inappropriate, although they have rarely had cause to do so.

The editors may request an article following a recommendation by panel members. However anyone who wishes to submit an article is strongly encouraged to contact any Beam Dynamics Panel member before starting to write.

6.1.3 How to Prepare a Manuscript

Before starting to write, authors should download the template in Microsoft Word format from the Beam Dynamics Panel web site:

<http://icfa-bd.kek.jp/icfabd/news.html>

It will be much easier to guarantee acceptance of the article if the template is used and the instructions included in it are respected. The template and instructions are expected to evolve with time so please make sure always to use the latest versions.

The final Microsoft Word file should be sent to one of the editors, preferably the issue editor, by email.

The editors regret that LaTeX files can no longer be accepted: a majority of contributors now prefer Word and we simply do not have the resources to make the conversions that would be needed. Contributions received in LaTeX will now be returned to the authors for re-formatting.

In cases where an article is composed entirely of straightforward prose (no equations, figures, tables, special symbols, etc.) contributions received in the form of plain text files may be accepted at the discretion of the issue editor.

Each article should include the title, authors' names, affiliations and e-mail addresses.

6.1.4 **Distribution**

A complete archive of issues of this newsletter from 1995 to the latest issue is available at

<http://icfa-usa.jlab.org/archive/newsletter.shtml>.

Readers are encouraged to sign-up for electronic mailing list to ensure that they will hear immediately when a new issue is published.

The Panel's Web site provides access to the Newsletters, information about future and past workshops, and other information useful to accelerator physicists. There are links to pages of information of local interest for each of the three ICFA areas.

Printed copies of the ICFA Beam Dynamics Newsletters are also distributed (generally some time after the Web edition appears) through the following distributors:

John Byrd	jmbyrd@lbl.gov	North and South Americas
Rainer Wanzenberg	rainer.wanzenberg@desy.de	Europe++ and Africa
Toshiyuki Okugi	toshiyuki.okugi@kek.jp	Asia**and Pacific

++ Including former Soviet Union.

** For Mainland China, Jiu-Qing Wang (wangjq@mail.ihep.ac.cn) takes care of the distribution with Ms. Su Ping, Secretariat of PASC, P.O. Box 918, Beijing 100039, China.

To keep costs down (remember that the Panel has no budget of its own) readers are encouraged to use the Web as much as possible. In particular, if you receive a paper copy that you no longer require, please inform the appropriate distributor.

6.1.5 Regular Correspondents

The Beam Dynamics Newsletter particularly encourages contributions from smaller institutions and countries where the accelerator physics community is small. Since it is impossible for the editors and panel members to survey all beam dynamics activity worldwide, we have some Regular Correspondents. They are expected to find interesting activities and appropriate persons to report them and/or report them by themselves. We hope that we will have a “compact and complete” list covering all over the world eventually. The present Regular Correspondents are as follows:

<i>Liu Lin</i>	<i>Liu@ns.lnl.br</i>	<i>LNLS Brazil</i>
Sameen Ahmed Khan	Rohelakan@yahoo.com	SCOT, Middle East and Africa

We are calling for more volunteers as Regular Correspondents.

6.2 ICFA Beam Dynamics Panel Members

Name	eMail	Institution
Rick Baartman	baartman@lin12.triumf.ca	TRIUMF, 4004 Wesbrook Mall, Vancouver, BC, V6T 2A3, Canada
Marica Biagini	marica.biagini@lnf.infn.it	INFN-LNF, Via E. Fermi 40, C.P. 13, Frascati, Italy
John Byrd	jbyrd@anl.gov	Accelerator Systems Division Argonne National Laboratory 9700 S. Cass Ave Building 401-C4263, Argonne, IL 60439, U.S.A.
Yunhai Cai	yunhai@slac.stanford.edu	SLAC, 2575 Sand Hill Road, MS 26 Menlo Park, CA 94025, U.S.A.
Swapan Chattopadhyay	swapan@fnal.gov	Northern Illinois University, Dept. of Physics, DeKalb, Illinois, 60115, U.S.A.
Yong Ho Chin	yongho.chin@kek.jp	KEK, 1-1 Oho, Tsukuba-shi, Ibaraki-ken, 305-0801, Japan
Jie Gao	gaoj@ihep.ac.cn	Institute for High Energy Physics, P.O. Box 918, Beijing 100039, China
Ajay Ghodke	ghodke@cat.ernet.in	RRCAT, ADL Bldg. Indore, Madhya Pradesh, 452 013, India
Eliana Gianfelice-Wendt	eliana@fnal.gov	Fermilab, Mail Station 312, PO Box 500, Batavia IL 60510-5011, U.S.A.
Ingo Hofmann	i.hofmann@gsi.de	High Current Beam Physics, GSI Darmstadt, Planckstr. 1, 64291 Darmstadt, Germany
Sergei Ivanov	sergey.ivanov@ihep.ru	Institute for High Energy Physics, Protvino, Moscow Region, 142281 Russia
In Soo Ko	isko@postech.ac.kr	Pohang Accelerator Lab, San 31, Hyoja-Dong, Pohang 790-784, South Korea
Elias Metral	elias.metral@cern.ch	CERN, CH-1211, Geneva 23, Switzerland
Toshiyuki Okugi	toshiyuki.okugi@kek.jp	KEK, 1-1 Oho, Tsukuba-shi, Ibaraki-ken, 305-0801, Japan
Peter Ostroumov	Ostroumov@frib.msu.edu	FRIB, National Superconducting Cyclotron Laboratory, Michigan State University, 640 S. Shaw Lane East Lansing, Michigan 48824, U.S.A.
Mark Palmer	mpalmer@bnl.gov	Brookhaven National Lab, Upton, NY 11973, U.S.A.
Chris Prior	chris.prior@stfc.ac.uk	ASTeC Intense Beams Group, STFC RAL, Chilton, Didcot, Oxon OX11 0QX, U.K.
Yuri Shatunov	Yu.M.Shatunov@inp.nsk.su	Acad. Lavrentiev, Prospect 11, 630090 Novosibirsk, Russia
Jiu-Qing Wang	wangjq@ihep.ac.cn	Institute for High Energy Physics, P.O. Box 918, 9-1, Beijing 100039, China
Rainer Wanzenberg	rainer.wanzenberg@desy.de	DESY, Notkestrasse 85, 22603 Hamburg, Germany
Zhentang Zhao	zhaozhentang@sinap.ac.cn	SINAP, Jiading campus: 2019 Jia Luo Road, Jiading district, Shanghai 201800, P. R. China Zhangjiang campus: 239 Zhang Heng Road, Pudong New District, Shanghai 201203, P. R. China

The views expressed in this newsletter do not necessarily coincide with those of the editors.

The individual authors are responsible for their text.